Process Intensification of liquid phase and gas-liquid precipitation of calcium carbonate in narrow channel reactors

Giuliana Trippa

Thesis submitted in partial fulfilment of the requirements for the Degree of Doctor of Philosophy

School of Chemical Engineering and Advanced Materials
Faculty of Science, Agriculture and Engineering

University of Newcastle upon Tyne

January 2006

Acknowledgements

I am extremely grateful to my supervisor, Professor Keith Scott, for the interest in my work, the time spent with me discussing it and for giving me the opportunity of learning so much during the writing of the thesis. I would also like to thank Professor Julian Morris, Head of School, for the financial support during my writing-up period.

I would like to thank Professor Roshan Jachuck, my supervisor in the first two years, for giving me the opportunity of carrying out this work and for the funding for my studentship and the project. Thanks to Dr John Burns for machining the channels and for the help with the conductivity study set-up and to Protensive Limited for letting me use their particle size analyzer.

I would like to thank Dr Kath Liddell for carrying out the X-ray diffraction on my samples and for the time spent answering my questions.

I am extremely grateful to all the technical staff in the School of Chemical Engineering and Advanced Materials. I could have done very little without their contribution and I have really enjoyed working with all of them. Thanks to Mr Stewart Latimer, Mr Ian Strong, Mr Jimmy Banks and Mr Brian Grover for manufacturing the reactors and all the help whenever I asked. Thanks to Mr Rob Dixon and Mr Paul Sterling for all their help with the lab equipment and the chemicals.

Thanks to all the people I have had the opportunity to meet and to get to know in the School during the last three years. They contributed in making this experience very valuable and enriching for me. Special thanks should go to my colleagues and friends Mr Eddie McCarthy and Mr Ryan McGlen for sharing the time in the lab and in the office with me. I would also like to thank my other friends for their interest in my work and for their ability in not making me think about it at times.

Last, but not least, I would like to thank my mother and my sister for their interest in what I do and for their constant support.

Abstract

A fundamental study of liquid phase and gas-liquid precipitation of calcium carbonate in narrow channel reactors is presented. Precipitation is strongly dependent on transport rates, as the final product properties are determined by local values of the concentrations during the reaction. The high transport rates available in narrow channels provided the intensification of a precipitation process in this type of equipment.

Liquid phase precipitation of calcium carbonate was studied in two square cross section reactors with diagonal lines of 1 and 2 mm. Flow rates ranging between 0.15 and 1 cm^3/s were used. Mixing efficiency in the narrow channels was characterized with the iodide-iodate reaction scheme. The results showed that mixing efficiency increased with Reynolds number. The mean particle size of calcium carbonate precipitate was found to range between 3 μm and 8 μm approximately. The narrow channels allowed production of particles similar or smaller in size than in a well stirred batch reactor. Liquid phase precipitation was further characterized by monitoring the change in electrical conductivity, during precipitation, in a narrow channel reactor with embedded electrodes. This system allowed a preliminary study of precipitation rate and limited data on scaling by solid deposits were also obtained.

Gas-liquid precipitation of calcium carbonate was studied in a square cross section 2 mm diagonal line narrow channel reactor. The carbonation reaction between a calcium hydroxide solution or suspension and CO_2 gas was considered. Liquid flow rates between 0.35 and 1.48 cm^3/s and carbon dioxide flow rates between 1 and 8.22 cm^3/s were used. Flow patterns for the water-carbon dioxide system were visually characterized. The experimental volumetric mass transfer coefficients for precipitation from a calcium hydroxide solution were found to vary between 0.33 and 0.8 s^{-1}. Particle size and morphology were characterized on selected calcium carbonate samples obtained in both cases from a calcium hydroxide solution and suspension.

<u>Key words:</u> Calcium carbonate, Mixing, Mass transfer, Narrow channel reactors, Particle size, Precipitation, Process Intensification.

Table of contents

List of Figures

List of Tables

Notation

A absorbance

A_{mt} (m^2) mass transfer area

A_{TP} two-phase dimensionless parameter

[A] (mol/m^3) concentration of A

a (m^2/m^3) specific interfacial area

a+ activity of the cation

a- activity of the anion

B ratio between the average and the standard deviation (percentage)

c (mol/m^3) generic concentration

c_{bg} (mol/m^3) concentration of the liquid in equilibrium with the bulk of the gas

c_L (mol/m^3) concentration of the reagent in the liquid phase

C constant

d (m) narrow channel diagonal line

d_e (m) distance between electrodes

d_h (m) hydraulic diameter

d_i (*generic unit*) deviation from the average for the generic measurement

$D_{G,L}$ (m^2/s) diffusivity of the gas in the liquid

D_i (m) generic definition of particle size

D[1,0] (m) number based average particle size

D [3,2] (m) surface area moment mean

D [4,3] (m) volume moment mean

D_{10} (m) diameter correspondent to 10% of the cumulative size distribution

D_{50} (m) median diameter

D_{90} (m) diameter correspondent to 90% of the cumulative size distribution

De Dean dimensionless number

E transmittance

E_f enhancement factor

$E_{f,inf}$ enhancement factor for infinitely fast chemical reaction

f friction factor

Fr Froude dimensionless number

g (m/s^2) acceleration due to gravity

G (m^{-1}) geometric factor

h_G gas hold-up

H (atm m^3/mol) Henry's constant

Ha Hatta number

J (nuclei/m^3 s) homogeneous nucleation rate

J_o (nuclei/m^3 s) pre-exponential factor for the homogeneous nucleation rate

k (J/K) Boltzmann constant

k_G (mol/(s m^2 atm)) gas side mass transfer coefficient

k_L (m/s) liquid side mass transfer coefficient

k_La (s^{-1}) volumetric mass transfer coefficient

k_n (units) primary nucleation constant

k_r (m^3/(mol s)) kinetic constant (units for a second order reaction)

K (dm^3/mol) equilibrium constant

K_a (mol^2/m^6) activity solubility product

K_G (mol/(s m^2 atm)) overall gas side mass transfer coefficient

K_L (m/s) overall liquid side mass transfer coefficient

K_{SP} (mol^2/m^6) solubility product

K_1 (mol/m^3) first dissociation constant

l (m) optical path length

L (m) length of reactor in the Perspex chip

L_{UC} (m) unit cell length

L_Y (m) length of the Y mixer

$\dot{m}_{tot}$ (Kg/(m^2 s)) total mass flux

M (mol/dm^3) molar concentration

n primary nucleation order

n (A) (mol) number of moles for species A

n_{CO_2} (mol) carbon dioxide number of moles

N (mol/s) molar flow rate, absorption rate

p (atm) pressure

p_{bl} (atm) pressure of the gas in equilibrium with the bulk of the liquid

P (W) transmitted power

P_o (W) power of the incident beam

Q (m^3/s) flow rate

Q_{H^+} (m^3/s) sulphuric acid flow rate

Q_{in} (m^3/s) inlet flow rate

Q_{out} (m^3/s) outlet flow rate

Q_{sol} (m^3/s) iodide-iodate-borate solution flow rate

r (m) nucleus radius

(-r) mol/(s m^3) reaction rate

r_c (m) critical nucleus radius

R result

Re Reynolds dimensionless number

R_b best approximation of the result

R_p (Ω) resistance during precipitation

R_s (Ω) resistance of the solution

R_v ratio between solution and acid volumetric flow rates

S supersaturation ratio

S_{NCR} (m^2) cross sectional area of the narrow channel reactor

T (K) temperature

t (s) time

t_{ind} (s) induction time

t_i (s) time of formation of the critical nucleus

t_g (s) time of growth of the nucleus to visible size

u (m/s) fluid velocity

v (m^3/kg) molecular volume

V (m^3) internal volume of the narrow channel reactor

V_c (m^3) collected volume

V_{HCl} (m^3) volume of hydrochloric acid

V_{H_2O} (m^3) volume of deionised water

V_r (m^3) reference volume

w_i uncertainty of the generic experimental variable

w_R uncertainty of the result

W_p (m) wetted perimeter

We Weber dimensionless number

x number of positively charged atoms in the salt molecule

x_i generic experimental variable

x_m arithmetic mean

X_s segregation index

Y selectivity

Y_s selectivity in the case of total segregation

y number of positively charged atoms in the salt molecule

z^+ valence of the cation

z^- valence of the anion

Greek symbols

χ gas mass fraction

Δc (mol/m^3) concentration gradient

ΔG (J) change in Gibbs free energy

ΔG_c (J) change in Gibbs free energy at the critical nucleus size

ΔG_v (J/m^3) specific change in Gibbs free energy associated with the phase change

ΔG_{hom} (J) change in Gibbs free energy for homogeneous nucleation

ΔG_{het} (J) change in Gibbs free energy for heterogeneous nucleation

Δp (Pa) pressure drop

ε (W/kg) specific power input

ε_M (m^2/mol) molar absorptivity

ε_G gas injection ratio

Φ^2_{Lo} all liquid two-phase flow multiplier

γ_+ activity coefficient for the cation

γ_- activity coefficient for the anion

$\gamma_\pm$ mean activity coefficient

φ generic function

κ^* dimensionless conductivity

κ_p (S/m) conductivity during precipitation

κ_s (S/m) conductivity of the solution

λ (m) Kolmogorov microscale

Λ (S m^2/mol) molar conductivity

Λ_o (S m^2/mol) molar conductivity at infinite dilution

μ (Pa s) fluid viscosity

θ (rad) contact angle

ρ (Kg/m^3) fluid density

ρ_c (m) radius of curvature

ρ_s (Ω m) resistivity of the solution

σ (N/m) surface tension

σ_d standard deviation

τ (s) residence time in the narrow channel reactor

τ_c (s) residence time in the Perspex chip

τ_Y (s) residence time in the Y mixer

Superscripts

bg - bulk gas

bl - bulk liquid

f - final

i - initial

tot - total

* - chemical reaction

Subscripts

Abs - absorbed

CO_2 - carbon dioxide

First - first electrode

G - gas

GS - gas, superficial velocity

i - interface

in - inlet

last - last electrode

L - liquid

LS - liquid, superficial velocity

out - outlet

TP - two-phase

Abbreviations

CFD computational fluid dynamics

GCC ground calcium carbonate

ID inside diameter

LALLS low angle laser light scattering

LIGA lithographie, galvanoformung, abformung

NCR narrow channel reactor

OD outside diameter

OFR oscillating flow reactor

PCC precipitated calcium carbonate

PSD particle size distribution

PTFE Poly Tetra Fluoro Ethylene

PVC poly vinyl chloride

RPB rotating packed bed

SDR spinning disc reactor

SEM scanning electron microscopy (or microscope)

SFTR segmented flow tubular reactor

SOP standard operating procedure

XRD X-ray (powder) diffraction

CHAPTER 1

Introduction

Precipitation processes are widely used for the production of organic and inorganic chemicals used in form of particles and slurries. Examples of the application of solids produced by precipitation include their use as fillers, pigments and pharmaceutical products. The use of the precipitates often has to meet with strict requirements in terms of particle size, particle size distribution (PSD), morphology and chemical purity.

Process conditions greatly affect the formation of supersaturation of the precipitating species and local values of supersaturation in the precipitation equipment determine the kinetics of the different stages of precipitation. The final properties of the precipitates are then greatly dependent on phenomena that influence local values of supersaturation.

Precipitation from two miscible liquids occurs when the two reagents mix and react, creating a supersaturation of the final product. Local concentration values of the reagents depend on the efficiency of their mixing and this reflects in the local values of the precipitating species concentration. Mixing efficiency is then one of the main factors affecting final properties in liquid phase precipitation.

In gas-liquid precipitation, local concentration values depend on the way gas is supplied to the liquid and on the rate at which the reagents are consumed. Particle properties are influenced both by the efficiency of mass transfer and by the extent of the contact area between the phases. This parameter influences the level of depletion of the reagent concentrations in the liquid phase. As for the relevance of the knowledge of mixing phenomena in liquid phase precipitation, information on mass transfer performance and on the extent of the contact area between the phases are fundamental in the characterization of a gas-liquid precipitation process.

The concept of Process Intensification has evolved from its initial perception, a few decades back, of a drive for miniaturization for reducing investments costs in chemical plants, to the idea of carrying out unit operations more efficiently, with real advantages in terms of product quality, when compared to the performance given by traditional equipment.

One of the main routes for achieving intensification of chemical processes is through the use of equipment that guarantees high transport rates. In recent years the use of microreactors has proved to lead to enhanced product properties, higher yields and more efficient and lower cost operation for a number of processes. Microreactors usually have characteristic dimensions ranging from tens to hundreds of microns and have shown to provide high heat and mass transfer efficiency, together with good mixing properties and high contact areas between the phases.

The demonstrated advantages in using micro scale reactors for improving mixing and mass transfer efficiency provided motivation and interest in using and investigating small scale systems for precipitation. The presence of a solid phase product, which can lead to greater scaling problems than in other reacting systems, was one of the factors which determined the choice of characteristic dimensions of the reactors used in this investigation. The main concept that determined this choice was that of operating with relatively high fluid velocities in the channels so as to limit phenomena of local solid build-up that can constitute the first stage of the scaling process. In order to be able to work with acceptable pressure drops, the reactors used were chosen to have characteristic dimensions in the millimetre scale. In each of the studies carried out reactors had hydraulic diameters of approximately 0.7 or 1.4 mm.

Microreactors owe their high transport properties to their characteristic dimensions of the order of tens or few hundred of microns, at which diffusion is the controlling mechanism. The choice of characteristic dimensions of narrow channels closer to the mm scale could have led to losing some of the benefits associated with the use of microreactors. However, before the work was started, it was considered that the chosen length scale would guarantee a good compromise in terms of transport properties, scaling problems, acceptable pressure drops and the possibility of working with higher fluid velocities than those normally used in microreactors. This last property was considered to possibly be beneficial in terms of guaranteeing good

mixing of the reagents in the liquid phase system and an efficient surface renewal process and improved mass transfer in the gas-liquid system. Particularly, it was thought that a better performance in respect to traditional stirred vessels could be achieved.

As the dimension chosen for the reactors was higher than that commonly adopted for what are usually identified as microreactors, the chosen terminology in this case was narrow channel reactors (NCRs). This term is adopted in several of the heat transfer studies carried out in millimetre scale reactors, which usually focus on two-phase systems.

Calcium carbonate occurs naturally as the main constituent of various minerals and it is also produced industrially by precipitation from the carbonation of concentrated calcium hydroxide suspensions. Calcium carbonate can also be precipitated from a liquid phase reaction; reacting two aqueous solutions of various salts containing calcium and carbonate ions respectively. The selection of calcium carbonate precipitation as a system to study was related to the fact that it allowed working with both a liquid phase and a gas-liquid system and hence investigating narrow channel reactors both with a one phase and a two-phase system.

Calcium carbonate can be found in different polymorphs, different crystalline structures which correspond to various particle morphologies. The considerable amount of work reported in the literature on the influence of process conditions on particle size and morphology as well as other more specific studies on chemical or physical aspects of calcium carbonate precipitation constituted the background for this study.

An introduction to precipitation processes and to the theoretical aspects used to describe them is presented in the first part of Chapter 2. The last part of this chapter presents a description of the production methods and uses of precipitated calcium carbonate. Some of the characteristic properties of precipitated calcium carbonate particles for industrial applications are reported.

Chapter 3 presents a review of the literature covering research areas related to this work. The different sections focus on Process Intensification, microreactors,

precipitation of calcium carbonate and new equipment for precipitation. Other more specific reviews are presented in the context of the description of the single studies. An example of this is a review of chemical reaction methods to characterize mixing efficiency which is presented in Chapter 4 as an introduction to the study on mixing efficiency in narrow channel reactors.

Chapter 4 focuses on the application of narrow channel reactors for liquid phase precipitation of calcium carbonate. The reaction used was between aqueous solutions of calcium nitrate and sodium carbonate. Characterizing mixing with a chemical reaction method was considered as a complementary investigation to the precipitation study. A module with two narrow channel reactors was used for this investigation and results of particle size and morphology as well as of benchmarking tests with a stirred vessel are presented.

Chapter 5 describes the investigation of gas-liquid precipitation of calcium carbonate from the carbonation of calcium hydroxide solution and suspensions. It includes a study on gas-liquid flow patterns for the water-carbon dioxide system and characterization of the absorption of carbon dioxide in water by reacting the water-CO_2 mixture with a sodium hydroxide solution at the reactor outlet. Absorption rates of carbon dioxide for the precipitation of calcium carbonate were quantified and data on particle size and morphology are presented.

Chapter 6 describes the development and testing of a narrow channel reactor with embedded electrodes for monitoring the change in electrical conductivity associated with the liquid phase reaction studied. Results of the change in conductivity at varying distances from the mixing point of the reagents in the narrow channel reactor are presented.

Chapter 7 summarizes the main findings for each study and formulates general conclusions. General guidelines on areas that could be further investigated are also presented.

Some of the information that is not directly relevant to the main description of the work is presented in the appendices. This includes experimental errors and uncertainty, particle size analysis by laser diffraction, the X-ray diffraction patterns obtained for

the calcium carbonate samples in this investigations and data on the conductivity of sodium carbonate solutions.

CHAPTER 2

Precipitation processes and production and uses of precipitated calcium carbonate

2.1 Introduction

The first part of this chapter describes the fundamental aspects of precipitation processes. The influence of operating conditions, such as reagents concentration and hydrodynamic conditions, on the various stages of precipitation is outlined in order to define their influence on product properties. Details of the theoretical aspects used to describe precipitation are provided as a general background for this study.

The second part of the chapter describes the production and uses of calcium carbonate. The aim of this work was to characterize narrow channel reactors for the production of particulate materials of industrial interest by precipitation. In this respect information on the desired properties of calcium carbonate particles for different applications in industry is provided.

2.2 Precipitation

2.2.1 Fundamental aspects

The term precipitation is normally used to describe the appearance of a solid phase in the form of particles as a consequence of chemical reaction. It is also referred to as reactive crystallization, to distinguish it from the crystallization processes in which the concentration of the compound to be obtained in solid form is increased above its solubility limits with other methods. These processes are cooling of the solution, evaporation, vacuum (adiabatic cooling) and salting out (Mullin, 2002). Another main factor characterizing precipitation and differentiating it from crystallization is the usual relative insolubility of the solid. This influences the rate of the process, as in fact precipitation is much faster than cooling crystallization, and the characteristics of the final product. The relative insolubility of precipitating systems means working with relatively high levels of supersaturation in the reaction environment; this determines high nucleation rates and low particle size, usually in the range 0.1 μm-10 μm (Söhnel and Garside, 1992, p.1). Particle size is one of the main parameters influencing the use of the final product and usually the main objective of a precipitation process is to produce particles with sizes in a definite range. Other important characteristics of precipitation products are chemical purity and particle morphology. The studies described in this work focus on particle size and morphology, which are the usual main properties that can be affected by the characteristics of the process.

Precipitation is widely used in industry for the production of both inorganic and organic compounds. The products obtained by this process find use as fillers, pigments, dyes and pharmaceutical compounds. Usually inorganic products are produced from precipitation from aqueous solution, whereas organic chemicals usually involve the use of solvents different from water.

The following sections describe the different steps involved in a precipitation process and the main parameters and equations used to define them are reported. Furthermore, the main problems arising when designing a precipitation process are described in order to delineate the context in which the studies on precipitation in narrow channels were carried out.

2.2.2 Solubility of the solid phase and definitions of supersaturation

When considering aqueous systems, the solubility of a sparingly soluble electrolyte in water is usually expressed with its solubility product. Considering the general electrolyte M_xA_y that dissociates into x cations and y anions:

$$M_xA_y \leftrightarrow xM^{z+} + yA^{z-} \tag{2.1}$$

where z^+ and z^- are the valences of the metal cation M and the anion A respectively, then for a solution that is saturated:

$$[M^{z+}]^x[A^{z-}]^y = \text{constant} = K_{SP} \tag{2.2}$$

where K_{SP} is the solubility product of the salt. The equilibrium concentration $[M_xA_y]^*$ can then be calculated (Mullin, 2002):

$$[M_xA_y]^* = \left[\frac{K_{SP}}{x^x y^y}\right]^{1/(x+y)} \tag{2.3}.$$

The difference between the concentration of the precipitating species and its solubility in water is the driving force for the formation of the solid phase and the supersaturation ratio can be defined as follows:

$$S = \left(\frac{[M^{z+}]^x[A^{z-}]^y}{K_{SP}}\right)^{(1/x+y)} \tag{2.4}.$$

A more rigorous definition of solubility and supersaturation requires the introduction of the activity coefficients of the species in solution. The activity solubility product is defined by the equation (Mullin, 2002):

$$(a_+)^x(a_-)^y = \text{constant} = K_a \tag{2.5}$$

where a_+ and a_- are the ionic activities or by:

$$\left([A^{z+}]\cdot\gamma_{+}\right)^{x}\left([M^{z-}]\cdot\gamma_{-}\right)^{y}=K_{a} \tag{2.6}$$

where γ_+ and γ_- are the activity coefficients.

Equation 2.6 can also be written:

$$K_{a}=K_{SP}\left(\gamma_{\pm}\right)^{x+y} \tag{2.7}$$

where $\gamma_\pm$ is the mean activity coefficient.

K_a and K_{SP} may be assumed equal for concentrations up to 10^{-3} M (Mullin, 2002), but above this value the interactions between different ions can greatly influence the solubility of a salt.

2.2.3 Nucleation

Different processes occur during precipitation: particle nucleation, growth and secondary changes which can be the agglomeration of the precipitates or the change in their size distribution by ripening.

Particle nucleation can be classified into primary and secondary nucleation (Söhnel and Garside, 1992, p.42), where primary nucleation indicates the formation of the precipitate without the presence of the solid phase being formed and secondary nucleation describes the formation of the solid on pre-existing particles of the precipitating material itself. Usually precipitation processes do not involve secondary nucleation, which is instead often encountered in cooling crystallization, where for example seed crystals are used to promote the formation of the solid phase. Primary nucleation can be further classified into homogeneous and heterogeneous nucleation; in the first case the formation of the solid phase occurs only due to the conditions which make this possible thermodynamically and in the second case the formation of the particles is promoted by the presence of a foreign solid phase.

The mechanism of homogeneous nucleation is the most studied theoretically as it is more understood and easier to model than heterogeneous nucleation. The formation of particles by homogeneous nucleation can be represented from the analogy with the formation of liquid droplets in a supersaturated vapour. The change of Gibbs free energy associated with the formation of a new particle of radius r in a supersaturated fluid is given by the expression (Mullin, 2000):

$$\Delta G = 4\pi r^2 \sigma + (4\pi/3) r^3 \Delta G_v \qquad (2.8)$$

where σ (N/m) is the interfacial tension between the crystal and its surrounding supersaturated fluid and ΔG_v (J/m^3) is the specific free energy associated with the phase change.

In this case a spherical geometry for the nucleus being formed is assumed. The first term on the right-hand side of equation 2.8 is positive and it represents the surface contribution. The second term is negative and it represents the volume contribution. The overall change of Gibbs free energy goes through a maximum, as shown in Figure 2.1, which corresponds to the size of the critical nucleus. At this size the probability of growth and disappearance of the new crystal are equal. The radius of the critical nucleus, r_c (m) can be obtained setting the derivative of equation 2.8 to zero (Myerson and Ginde, 1993, p.44):

$$\frac{d(\Delta G)}{dr} = 8\pi r_c \sigma + 4\pi r_c^2 \Delta G_v = 0 \qquad (2.9)$$

which gives:

$$r_c = -\frac{2\sigma}{\Delta G_v} \qquad (2.10).$$

Substituting the value given for ΔG_v by equation 2.10 in equation 2.8, the change in Gibbs free energy for the critical nucleus size is obtained:

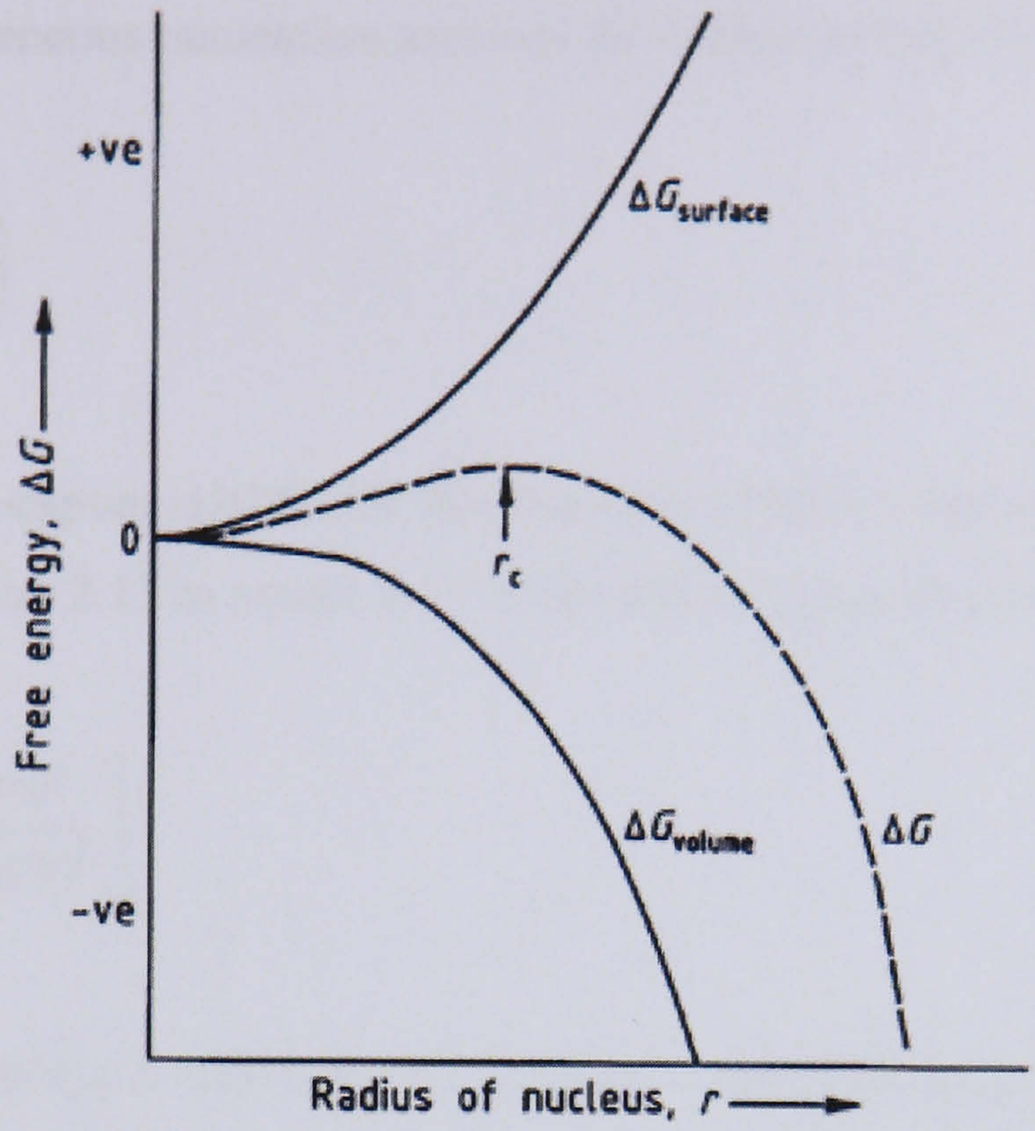

Figure 2.1. Change of Gibbs free energy for the formation of a nucleus (from Mullin, 2002).

$$\Delta G_c = \frac{4\pi r_c^2 \sigma}{3} \qquad (2.11).$$

The relationship between particle size and solubility is given by the Gibbs-Thompson equation, applied to solid-liquid systems by Ostwald and Freundlich:

$$\ln S = \frac{2\sigma v}{kTr} \qquad (2.12)$$

where v (m^3/kg) is the molecular volume, T (K) is the temperature and k (J/K) is the Boltzmann constant.

Substituting r_c from equation 2.12 in equation 2.11 the following expression is obtained:

$$\Delta G_c = \frac{16\pi\sigma^3 v^2}{3(kT\ln S)^2} \qquad (2.13).$$

The rate of homogeneous nucleation assumes an Arrhenius type of expression:

$$J = J_o \exp\left(-\frac{\Delta G_c}{kT}\right) \tag{2.14}$$

where J_o is the pre-exponential factor that has a theoretical value of 10^{30} nuclei /cm^3 s. Substituting equation 2.13 in equation 2.14 the following expression is obtained:

$$J = J_o \exp\left[\frac{-16\pi\sigma^3 v^2}{3k^3T^3(\ln S)^2}\right] \tag{2.15}$$

which indicates that the nucleation rate increases with increasing supersaturation and temperature and decreases with an increase in surface tension.

A foreign substance present in solution reduces the energy required for nucleation, this process is called heterogeneous nucleation and it occurs at lower supersaturations than homogeneous nucleation, as the energy barrier is lower in the case of a heterogeneous system. Volmer (1939, cited by Myerson and Ginde, 1993, p.46) found that the decrease in Gibbs free energy depends on the contact angle between the foreign solid phase and the liquid:

$$\Delta G_{hom} = \left(\frac{1}{4}(2+\cos\theta)(1-\cos\theta)^2\right)\Delta G_{het} \tag{2.16}.$$

If the solid phase is not wetted by the liquid, that is if $\theta = \pi$ then $\Delta G_{hom} = \Delta G_{het}$ and in this case the nucleation is not influenced by the solid phase. In practice, a displacement towards lower values of supersaturation of the curve representing homogeneous nucleation is obtained, as reported in Figure 2.2.

The above theoretical expressions are of limited applicability for industrial crystallizers. The expressions that are most commonly used for representing primary nucleation rates are of the following type:

$$J = k_n S^n \tag{2.17}$$

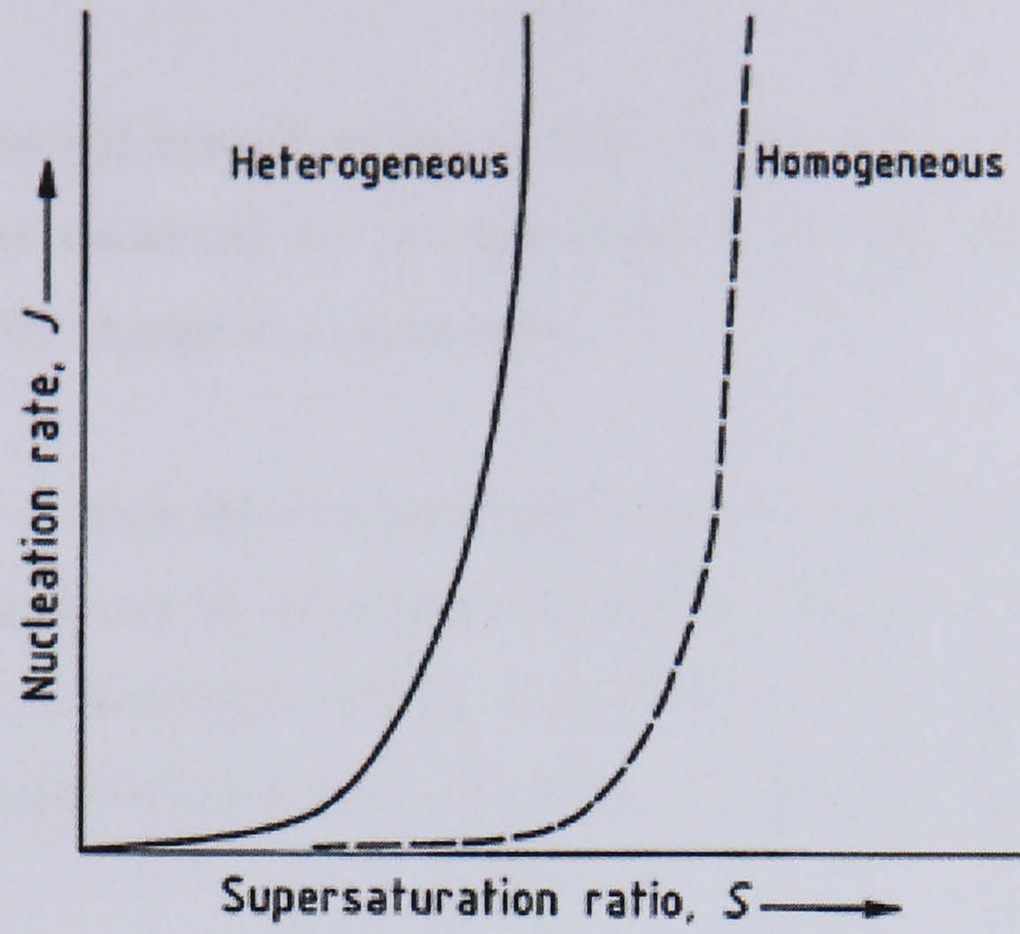

Figure 2.2. Qualitative trends for heterogeneous and homogeneous nucleation rates (from Mullin, 2002).

where k_n is the primary nucleation constant and n is the order of the nucleation process, which depends on the physical properties and the hydrodynamics of the system. Values of n are usually greater than 2 (Mullin, 2002).

2.2.4 Induction time

The time that elapses between the establishment of supersaturation and the first changes in the system physical properties, due to the formation of the solid phase, is called the crystallization induction time (Söhnel and Garside, 1992, p.67). Depending on the physical property being monitored, the induction time will change and its determination will be relative to the specific technique used. Induction periods before precipitation are usually followed either visually, turbidimetrically or taking into account the change in concentration or in conductivity.

The induction time determined visually represents the sum of the time necessary for the critical nucleus to be formed, t_i and the time that is necessary for the nucleus to grow to a visible size, t_g;

$$t_{ind} = t_i + t_g \qquad (2.18).$$

If the induction time is instead measured from a change in concentration, then t_g will represent the time necessary for enough solute to be deposited on the nucleus to determine a specific change in concentration.

If the assumption is made that the induction time is essentially related to the formation of the nuclei, then it can be considered inversely proportional to the nucleation rate. Following classical nucleation theory, the following functional dependence of the induction time on the surface tension, temperature and supersaturation is obtained:

$$\ln t_{ind} \propto \frac{\sigma^3}{T^3 (\ln S)^2} \qquad (2.19).$$

For a given temperature, a plot of the induction time versus $(\ln S)^{-2}$ should therefore give a straight line, from which, in real conditions of homogeneous nucleation, the interfacial tension can be calculated.

2.2.5 Crystal growth

After the nucleation process, particles grow larger by the addition of solute molecules, this process is called crystal growth. Crystal growth may be considered a two step process involving (1) mass transport, either by diffusion or convection from the bulk solution to the crystal face, followed by (2) a surface reaction in which the growth units are integrated into the crystal lattice (Mullin, 2002). Either step may control the overall growth process, although convective mass transport is unimportant for crystals smaller than 10 μm as, in this size range, diffusion is the prevailing transport mechanism; this is what usually happens for crystal growth in reactive crystallization (Estrin, 1993, p.137). The two most known surface reaction models are the Spiral Growth model (also known as the BCF, Burton, Cabrera and Frank model) and the Polynuclear model (Mullin, 2002). The first model considers that screw dislocations on the crystal surfaces can constitute the preferential location on which molecules are adsorbed forming a new dislocation on which growth continues with a spiral structure. Growth proceeds at a relatively low supersaturation with a rate proportional to the

square of the supersaturation (Mullin, 2002). The second model describes the growth process as nuclei developing on the edges, corners and faces of a crystal. These surface nuclei spread across the crystal face and further nuclei develop on them. This mechanism is sometimes referred to as the Birth and Spread model. Polynuclear growth is related to supersaturation by an exponential relationship. Further details and theoretical description of these models can be found in Söhnel and Garside (1992, p.85).

In the case of sparingly soluble systems, as encountered in precipitation processes, descriptions of crystal growth mechanisms, taking into account the chemistry of electrolytes have been proposed and are generally more accepted (Estrin, 1993, p. 137). Chiang and Donohue (1988) proposed three models for crystal growth in ionic systems in which the growth at the surface is represented by chemical reactions. For systems that can grow by more than one mechanism, the fastest mechanism determines the growth and the slowest step in that mechanism controls the growth rate. Adsorption of ionic species on the crystal surface is described with Langmuir, Freundlich and Temkin isotherms. The modelling carried out in this way is similar to the one normally used to represent reversible chemical reactions on the catalyst surface in heterogeneous catalysis. The three mechanisms proposed by Chiang and Donohue are (1) the Surface-Reaction/Molecule-Integration mechanism (SR/MI), (2) the Sequential-Ionic-Integration mechanism (SII) and (3) the Molecular Growth mechanism. The authors found that the SR/MI model with a Langmuir type isotherm explained different sets of experimental data very well. An example of this was the growth rate of calcium carbonate which usually is described with a parabolic dependence on supersaturation. Power law type of expressions usually adopted to describe growth rates found theoretical justification in the mechanisms introduced by Chiang and Donohue (1988).

2.2.6 Agglomeration and ripening

After nucleation and growth, particles can undergo different processes which can greatly affect their morphology, size and size distribution. The two main processes that can cause secondary changes on the particles are agglomeration and ripening.

The term agglomeration describes the process consisting of several particles sticking together to form larger particles. This process is usually favoured by the presence of supersaturation. To obtain agglomerates, three successive steps have to occur (Klein and David, 1995, p.372): (a) the collision of two particles, (b) a sufficient period during which the two particles stay together and (c) adherence of the two particles with the help of supersaturation. Several parameters influence these steps, one of the most important is the hydrodynamics in the precipitator. Two main mechanisms of particle collision and agglomeration can be distinguished depending on the hydrodynamic conditions (Mersmann, 1995, p.162): (1) perikinetic agglomeration, caused by Brownian motion of primary particles subjected to (diffusion-controlled) collisions in a solution at rest and (2) orthokinetic agglomeration, for which the collisions are induced by the shear rate in a solution in motion. Agglomeration normally concerns particles in the submicron to micron size range and it is therefore usually more important in precipitation rather than other crystallization processes. Agglomeration is usually negligible for particles larger than 50 μm (Mersmann, 1995, p.160). Orthokinetic agglomeration is the most important mechanism in agitated precipitators (or where the fluid is in motion), its relevance increases with increasing shear rate and particle size (Mullin, 2002). More details on the kinetic expressions used to describe the two mechanisms can be found in Mersmann (1995, p.163).

Other primary factors affecting agglomeration are the properties of the solvent, the size of the particles and their concentration. Small particles agglomerate more than large ones as they tend to reduce their surface energy. A greater number of particles per unit volume of suspension gives higher probabilities of collision. Supersaturation is also very important, as it provides the material for the formation of the crystalline bridges that keep the agglomerate together. In the absence of supersaturation, aggregation and flocculation can occur. In these cases the bonding forces between the particles, such as Van der Waals forces, are weaker (Mersmann, 1995, p.159). A flocculate is a group of particles that consists of primary particles connected by weak cohesive forces. For aggregates, the strength of the bonding forces is intermediate between agglomerates and flocculates. Agglomerates and flocculates can occur in saturated or undersaturated solutions and can readily be destroyed.

Ripening, or as it is best known Ostwald ripening, is caused by the difference in solubility between small and large particles and it is a process that determines the dissolution of the smaller particles and the deposition of the resulting excess solute on the larger particles. The particle size distribution tends to shift to larger dimensions and ultimately it should theoretically become monodisperse (Mullin, 2002). The system tends in this way to achieve a minimum of surface free energy. The size-solubility relationship is given in equation 2.12, however the effect of this process only becomes significant for particle sizes smaller than 1 μm. Ripening usually occurs at very low supersaturation and for this reason its kinetics tends to be controlled by surface reaction rather than by diffusion.

2.2.7 Particle size and morphology

From a physical point of view, precipitates are characterized by their size and morphology. These properties are determined by the different mechanisms involved in the precipitation process and by their relative rates. Size and size distribution determine the use of the precipitated solid, together with chemical purity, as they influence the reactivity of the solid as well as its optical, mechanical and bulk properties.

At low supersaturations, heterogeneous nucleation dominates and the number of nuclei formed is determined by the number of active heteronuclei within the solution. As previously illustrated, nucleation is followed by crystal growth, this process strongly influences crystal shape. If surface reaction controlled growth takes place at low supersaturations, crystals of compact shapes such as cubes and octahedra are formed (Söhnel and Garside, 1992, p.165). If the growth rate is anisotropic, shapes like needles, rods and plates may be formed. At high supersaturations diffusion might become the controlling step for crystal growth. The crystal faces become surrounded by areas of depleted solutions as the growth rate is so high that the solute can not be supplied with sufficient velocity. This can cause the formation of so called dendrites, which have a ramified structure. When heterogeneous nucleation is predominant, if the supersaturation is increased, the amount of mass available to the precipitate is also increased. Assuming that the activity of heterogeneous nuclei does not greatly depend on supersaturation, then the number of particles formed in the system is essentially constant and independent of supersaturation. A higher supersaturation does therefore

supply more solute to the system for crystal growth and it determines a higher final average crystal size.

Increasing the initial supersaturation, the concentration values at which homogeneous nucleation is dominant are attained and this determines a sudden increase of the number of particles formed. As a result, their final size begins to decrease and the crystals become more isometric. A precipitate formed by homogeneous nucleation often appears initially as amorphous and converts to a crystalline structure only after some time.

The relation between supersaturation, nucleation and growth mechanisms and particle morphology has been summarized by Walton (1967, p. 184) and the main conclusions are reported in Table 2.1 which contains some general guidelines. In practice, the prevailing mechanisms for nucleation and growth and the final properties of the particles can depend on many factors; first of all the hydrodynamics in the reaction environment which influences the local values of supersaturation.

Table 2.1. General guidelines on nucleation mechanisms and product morphology depending on initial supersaturation and interfacial energy (from Walton, 1967).

Initial supersaturation ratio	Interfacial energy	Nucleation	Morphology
1-2	High	None	-
	Low	Heterogeneous	Discrete, well formed crystals
2-5	High	Heterogeneous	Discrete, well formed crystals
	Low	Heterogeneous	Poorly formed discrete crystals
10-50	High	Heterogeneous	Poorly formed discrete crystals
	Low	Homogeneous	Agglomerated particles
> 1000	High	Homogeneous	Agglomerated particles
	Low	Homogeneous	Colloidal system

2.2.8 Influence of hydrodynamics and mixing

Mixing and the hydrodynamic characteristics of the reaction environment greatly influence the rates of the different processes which determine the precipitate final size and morphology. Several processes need to be taken into account when precipitation results from mixing two separate reacting solutions: mixing of the reagents, formation of the precipitating solid by chemical reaction, nucleation of the solid phase and growth of the particles. As discussed, agglomeration or aggregation can follow these steps. Usually the influence of mixing on the kinetics of the single stages cannot be neglected.

Mixing of two liquids can be considered to take place in three consecutive (or sometimes parallel) stages (Villermaux and David, 1983, cited by Söhnel and Garside, 1992, p.175):

1. One liquid is dispersed in another so as to achieve a uniform average composition. On the microscale, however, the mixture consists of segregated parts of the two liquids and therefore local concentration differences persist.
2. The size of the segregated regions of uniform composition increases and the contact area between the regions of different composition grows.
3. Mixing by molecular diffusion occurs to such an extent that segregated area disappears and total homogeneity is attained.

The first stage is the so called "macromixing", whereas the last two stages are termed "micromixing". This description is particularly representative of the mixing process in stirred tanks, where macromixing is determined by the main convective flow pattern imposed by the stirrer. The flow is divided into different circulation loops or zones created by the main flow field. The material is exchanged between zones, increasing homogeneity (Hemrajani, 1995). Micromixing takes place through two mechanisms, laminar stretching of the segregated regions and their turbulent erosion. The characteristic length scale at which micromixing occurs is called the Kolmogorov microscale λ:

$$\lambda=\left[\frac{\mu^3}{\rho^3\varepsilon}\right]^{1/4} \tag{2.20}$$

where μ (Pa s) is the fluid viscosity, ρ (Kg/ m^3) is the fluid density and ε (W/Kg) is the local value of the specific power transferred to the fluid, usually called specific power input.

Precipitation rates in agitated systems can in some cases be influenced by the feed tubing diameter and by the feed flow rate (Barresi et al., 1999) and mixing effects due to these parameters are described with the term mesomixing.

Prediction of the rates of the different phenomena involved in precipitation would require the knowledge of local values of supersaturation for the duration of the process. Moreover, theoretical approaches require the knowledge of the different kinetic expressions, on which often no closure has yet been found. Experimental studies have the great advantage of offering real information on the final properties of the particles. This work is concerned with the acquisition of fundamental knowledge on the precipitation in narrow channels and the different factors affecting the final properties of the particles.

2.3 Calcium carbonate

2.3.1 Production and properties

Calcium carbonate occurs in nature as the principal constituent of limestone, marble and chalk. Calcium carbonate occurs naturally in three crystal structures: calcite, aragonite and, although rarely, vaterite. A single substance can in fact crystallize in different crystalline structures, this implies that crystals can have different shapes, but also that the bulk properties of the material can vary. A substance that crystallizes in more than one form is said to exhibit polymorphism. Polymorphs may be "enantiotropic" (interconvertible) or "monotropic" (incapable of transformation) (Mullin, 2002). The polymorphs of calcium carbonate are enantiotropic. Calcite is the thermodynamically stable form, aragonite is metastable and irreversibly changes to calcite when heated in dry air to about 400° C (Carr and Frederick, 2003). Vaterite is a metastable form as well and tends to convert to calcite at ambient conditions, especially when moist. Vaterite is mostly found in precipitated calcium carbonate (PCC), as it is metastable to calcite and aragonite in geological conditions. Many forms of calcite crystals have been reported, however the most common shapes are cubic, rhombohedral and scalenohedral. Aragonite usually has an acicular shape, whereas vaterite can be normally found as spherical or disc like crystals.

Calcium carbonate particles used in the industry are produced either by grinding the naturally occurring mineral or by precipitation from the carbonation of dissolved calcium hydroxide. For the production of ground calcium carbonate the best deposits for most industrial applications are those containing minerals with a high content (> 90%) of $CaCO_3$ and a high brightness. The ore is usually taken to a primary crusher for size reduction and then into the processing plant (Carr and Frederick, 2003). The plant process depends on the grade of the material being made. Typically, coarse products that do not require high purity, 90-98% $CaCO_3$, go to secondary crushing. Final grinding for products down to approximately 5 μm median particle size can be done in a roller mill or ball mill. Products finer than 10 μm often involve additional processing, usually in a dry ball mill circuit with air classification.

For final products with a high degree of purity the process is different. In this case the secondary crushing should reduce the ore to a size where mineral impurities are liberated (< 100 μm) without producing an excess of fines. The particles might then be further purified by flotation. At the end of this process the material obtained usually has a calcium carbonate content higher than 98%. The product is then subjected to more grinding stages to obtain the required final particle size.

Production route for precipitated calcium carbonate usually involves the calcination of a mineral containing calcium carbonate to give carbon dioxide and calcium oxide. The calcium oxide is then mixed with water to give a calcium hydroxide suspension (milk of lime). Carbon dioxide is then bubbled through the calcium hydroxide suspension to give precipitated calcium carbonate. The precipitation stage is usually carried out in stirred tanks and the operating conditions of the process determine the final properties of the particles, such as shape, size and size distribution. Products having mean particle sizes between approximately 0.03 μm and several microns are available. The precipitation stage is usually followed by evaporation or drying, depending on whether the final application will require a slurry or dry powder. Calcium carbonate slurries are primarily used in the paper industry, as described in more detail in the following section. The solids content of these slurries is typically higher then 70 % by weight for ground products and between 20 % and 50 % for precipitated calcium carbonate (Carr and Frederick, 2003).

2.3.2 Applications

Ground and precipitated calcium carbonate (respectively indicated as GCC and PCC) find their widest fields of application in the paper and in the plastics industries. Calcium carbonate particles (usually as very fine product) are used in the paper industry as fillers in the papermaking process and as a part of the coating on paper (Carr and Frederick, 2003). The benefits of using calcium carbonate in papermaking include higher brightness for the paper, greater resistance to yellowing and ageing and the economic advantage of substituting pulp with the less expensive calcium carbonate. Depending on the paper grade, calcium carbonate can constitute 25% or more of the sheet. Both ground and precipitated calcium carbonate are used for this application.

Calcium carbonate is also used as the pigment in paper coatings to improve paper brightness, ink receptivity and smoothness, with particle sizes lower than 1 μm. This size range also guarantees the enhancement of the rheological properties of coating formulations. In coating applications the use of ground natural calcium carbonate exceeds that of the precipitated material.

In terms of weight, ground calcium carbonate is the most important filler used in plastics (Bosshard and Schlumpf, 1987, p.408). Ultrafine ground chalks are frequently employed, particularly in poly vinyl chloride (PVC). The inert filler calcium carbonate is important in keeping a low cost for the plastic material, while this retains or improves its mechanical properties. Both ground and precipitated calcium carbonate have to present a number of physical and chemical properties in order to constitute a suitable filler. Particles are in some cases surface coated to improve their handling properties and dispersability in plastics. Precipitated grades usually allow a greater control of particle size and surface treatment, giving therefore superior properties to the final plastic material. Table 2.2 lists some of the properties of different grades of calcium carbonate used as filler for plastics (Murphy, 1996, p.439).

Table 2.2. Properties of different grades of calcium carbonate used as a filler for plastics (from Murphy, 1996).

Property	**Unit**	**Typical grades**			
Chemical analysis	CaCO3 %	97.9	97.9	97.9	97.9
Specific gravity	g/cm^3	2.7	2.7	2.7	2.7
Mohs hardness		3			3
pH value		9.1	8.5	8.5	9.0
Specific surface	m^2/g	2.2	2.2	3.2	2.2
Part. size distr.	μm	0.8-20	0.8-25	0.8-10	0.8-20
Loose bulk density	kg/m^3	550-600	1790	1200	600

CHAPTER 3

Literature review

3.1 Introduction

This chapter provides a description of the studies reported in the literature on subjects related to the investigation on calcium carbonate precipitation in narrow channel reactors. The review focuses on Process Intensification, microreactors, calcium carbonate precipitation and new equipment for precipitation.

The aim of the present work was Process Intensification of a process for the production of powders and/or slurries. Details of the original perception of Process Intensification and of the evolution of this concept are given together with the description of some of the applications of the different types of novel equipment that are relevant to this study.

The second part of the review focuses on a description of the main advantages encountered in the use of small scale and microstructured systems. A description of the main applications that microreactors have found in recent years is provided. The studies described mostly refer to examples of high efficiency of mixing and mass transfer, as these are the most relevant aspects for liquid phase and gas-liquid precipitation processes respectively. The review on microreactors concludes with two sections on micromixers and the use of micro scale systems for particle synthesis.

The third part of the review describes the studies reported about liquid phase and gas-liquid precipitation of calcium carbonate. A description of the work carried out in recent years on novel type of equipment for the production of precipitates concludes the chapter.

3.2 Process Intensification

Process Intensification has had in time various definitions. It was traditionally described as a strategy for reducing plant size by means of substituting traditional types of equipment such as stirred vessels with modules which are smaller in size and more efficient. This concept started being developed at the end of the 1970s in ICI, with the main aim of reducing the impact of civil engineering work and piping on plant investment costs (Ramshaw, 1993). The reduction in the initial investment seemed the greatest advantage of intensified equipment at the time. However, in fact, the possibility of capital cost reduction has not produced an extensive introduction of intensified modules in the chemical industry.

Research work on Process Intensification has in the meantime continued and followed different paths and it is now a general belief that an intensified module has to present a whole series of advantages compared to traditional equipment to justify its use for industrial production. However, the decisive reason for switching from conventional to novel equipment would depend on the possibility of performing the process in a completely different way, with real advantages in terms of process performance. Examples of this would be the capability of an intensified module of giving a performance in terms product quality and/or selectivity that cannot be obtained with traditional equipment. These advantages would, in the general case, bring reductions of investment and/or operating costs.

One of the first steps for developing a process with intensified equipment is the acquisition of fundamental knowledge on the process itself in the new equipment. The use of centrifugal acceleration to enhance heat and mass transfer efficiency has in recent years showed potential for many applications. The spinning disc reactor (SDR) is, in its simplest configuration, a rotating surface on which the reagents are fed to the centre of the disc. Rotation of the disc leads to the formation of thin films of liquid, depending on flow rate, rotational speed and viscosity, of the order of hundreds of microns. The hydrodynamic characteristics of films generated on the rotating surface make the SDR suitable for applications in which high heat transfer rates and/or high contact areas between a gas and a liquid system are required. This last property is achieved by creating a gas pressure in the part of the reactor above the liquid film generated on the rotating surface or by having a continuous flow of gas through it. A

schematic of a spinning disc reactor with several of the possible design options is shown in Figure 3.1.

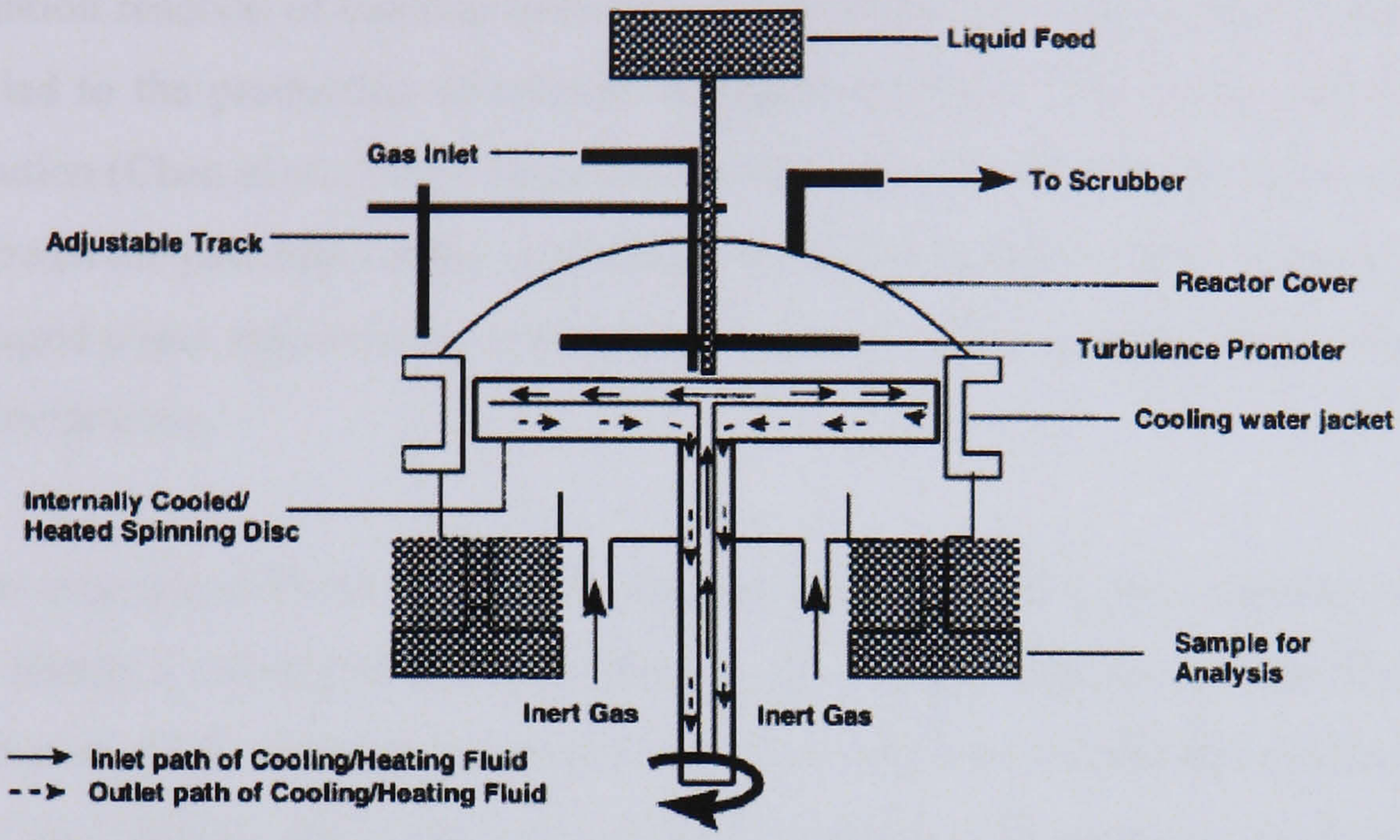

Figure 3.1. Schematic of a spinning disc reactor (from Jachuck, 2002).

Benchmarking tests between stirred tank reactors and the spinning disc reactor showed that the SDR presents great advantages in terms of reduction of reaction times in the polymerization of unsaturated polyester (Jachuck et al., 1997) and in the solution free radical polymerization of styrene (Boodhoo and Jachuck, 2000). In this last case the SDR also gave better molecular weight distribution of the polymer, compared to that obtained in a batch reactor.

Studies on gas-liquid mass transfer (Moore, 1986, Burns and Jachuck, 2005) have demonstrated that thin films generated on rotating surfaces can provide relatively high mass transfer coefficients. These characteristics and the relatively high specific interfacial area obtained in the SDR proved to be beneficial in the gas-liquid precipitation of calcium carbonate. In fact, a study on the carbonation of calcium hydroxide solutions showed that better product properties of particle size and size distribution can be obtained in a SDR rather than in a conventional stirred vessel (Trippa et al., 2002).

Centrifugal acceleration in rotating packed beds (RPBs) can produce advantages in terms of mass transfer efficiency. The flow configuration usually is characterized by the presence of liquid droplets and rivulets, which influence the contact area between the phases (Burns and Ramshaw, 1996). It was shown that, when using the carbonation reaction of calcium hydroxide suspensions, the mass transfer intensity in RPBs led to the production of calcium carbonate particles with narrow particle size distribution (Chen et al., 1997). High mixing efficiency obtained in this type of reactor has showed the potential for the production of pharmaceuticals with small particle size from liquid phase reactions, as reported by Chen et al. (2004) in their study on benzoic acid precipitation.

Another example of Process Intensification is in the oscillatory flow reactor (OFR), in which transport properties are improved by imposing oscillation on the fluid. The main feature of this reactor is that mixing efficiency does not depend on the overall flow of the reagents and it can be controlled by altering the frequency and amplitude of the oscillations (Harvey et al., 2001). As an example of its application, it has been shown that the OFR can be used for the production of biodiesel with acceptable conversions in times lower than in a batch reactor (Harvey et al., 2003).

Vibration of the liquid phase has also been used in gas-liquid mass transfer in a bubble column (Ellenberger and Krishna, 2003). It was shown that the use of vibration in the liquid produced an increase in the gas hold-up and in the volumetric mass transfer coefficients compared to the absence of vibration.

The design and characterization of high efficiency gas-liquid contactors are amongst the most relevant examples of Process Intensification for mass transfer processes. For examples, Zhu et al. (1992) looked into the mass transfer performance of different types of static mixers for their use as gas-liquid reactors.

Gaddis and Vogelpohl (1992) developed a novel impinging stream reactor (Figure 3.2) with good mass transfer characteristics. Gas hold-up was characterized for impinging stream reactors of different volumes in a later study (Mudimu et al., 2000). In the impinging stream reactor the gas and liquid are pre-mixed in two nozzles, the two homogeneous gas-liquid mixtures are then forced into an impinging zone of the reactor. The mass transfer efficiency can be further enhanced with recirculation of the

streams. Kleingeld et al. (1999) also characterized mass transfer performance for impinging stream reactors with various configurations. Cramers et al. (1993) characterized local values of mass transfer coefficients in the different zones of gas-liquid ejectors.

Vandu et al. (2005a) have investigated mass transfer performance of an upflow monolith loop reactor. This contactor is constituted by a cordierite monolith, with square cross section cells, with approximately 3 mm sides. The monolith is contained in a column which is filled with the liquid. Gas bubbles are formed in a gas distributor and flow upwards in the monolithic structure. The top of the column contains a gas-liquid separator and the liquid is recirculated between the separator and the reactor. Figure 3.3 shows a schematic of a set-up for hydrodynamic and mass transfer characterization of an upflow monolith reactor (Vandu et al., 2004). Results showed that that the monolith reactor gives better mass transfer performance than an airlift reactor or a bubble column.

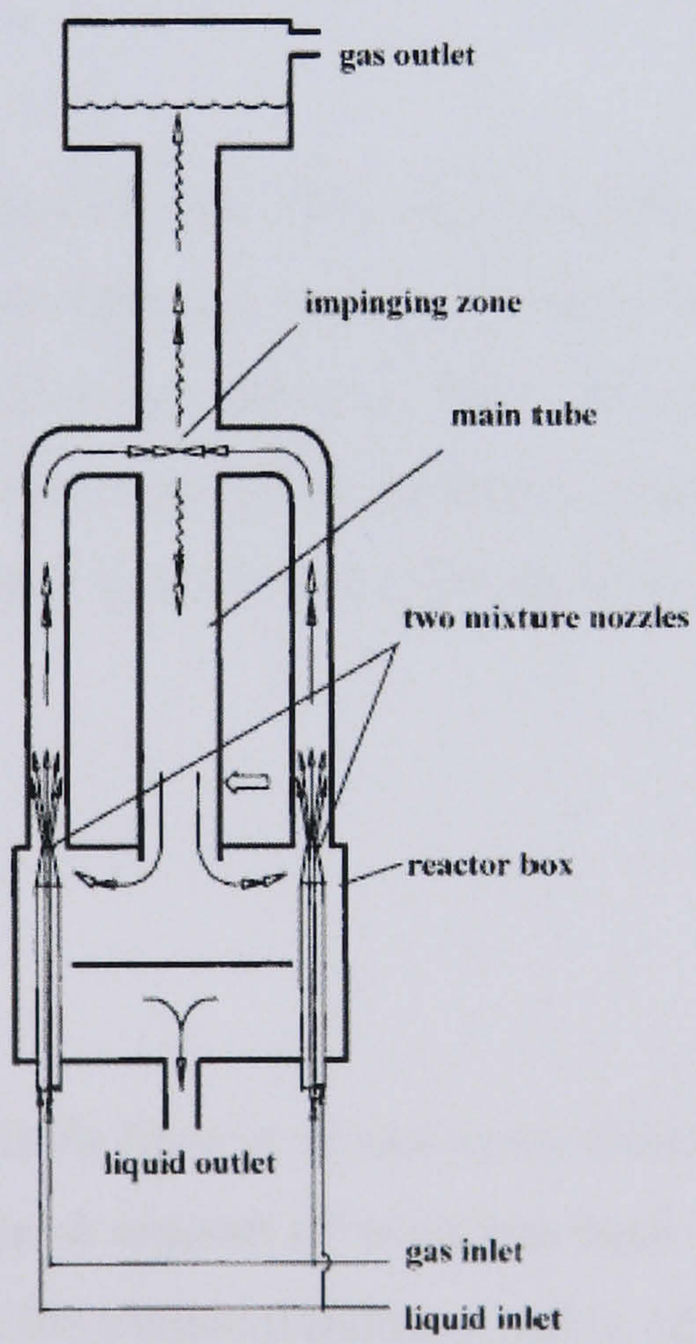

Figure 3.2. Schematic of an impinging stream reactor (from Mudimu et al., 2000).

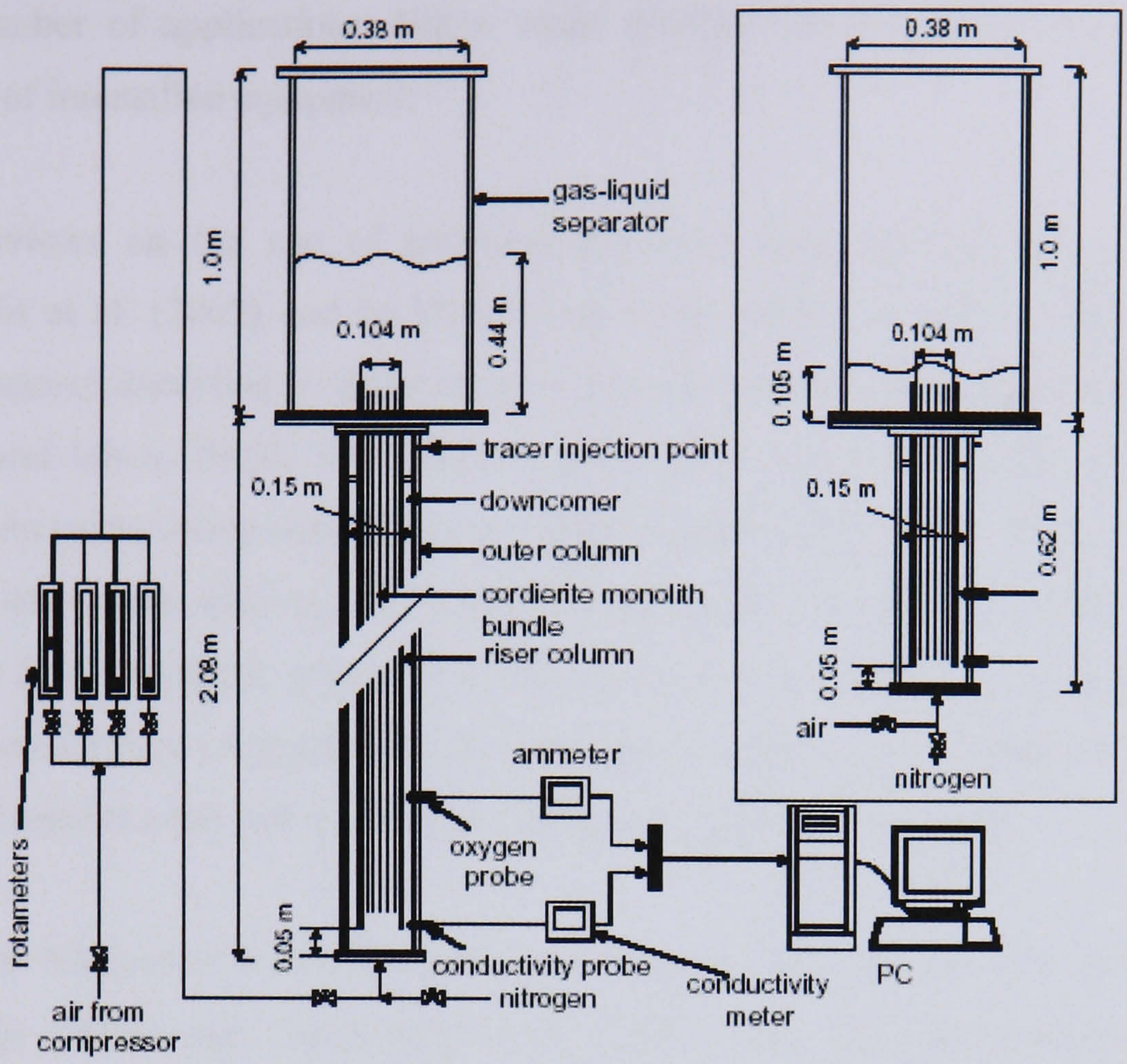

Figure 3.3. Schematic of upflow monolith reactors for hydrodynamic and mass transfer studies (from Vandu et al., 2004).

One of the more recent areas of interest of Process Intensification is related to the use of micro scale systems. In the following section the main advantages encountered in the use of micro scale channels are outlined. This will contribute to defining the background that motivated this investigation on narrow channel reactors for calcium carbonate precipitation and the context in which the work was carried out.

3.3 Microreactors

3.3.1 Introduction

Microreactors and microchannels have in recent years shown to be useful for a large number of processes and a great amount of work has been carried out to investigate their potential applications in the chemical industry and in other fields. The basic ideas for their use in chemical processes are linked to the intrinsically high transport properties found at the micro scale that have shown to give better product properties

for a number of applications. Micro scale systems can then be considered as an example of intensified equipment.

Many reviews on the use of microreactors have been written, for example by Gavriilidis et al. (2002) and by Hessel and Löwe (2003a, b and c). Microreactors, more precisely identified with the terms microstructured or microengineered reactors (Hessel and Löwe, 2003a, Gavriilidis et al., 2002), are novel reactors with internal dimensions in the micro scale. They are usually machined by using at least, partially, methods of microtechnology and precision engineering (Löwe and Ehrfeld, 1999) in materials such as metals, glass and various polymers. The choice of material usually depends on the type of application, for example in relation to chemical compatibility with the reagents used, and on the manufacturing techniques available.

The main fabrication methods used for microstructured reactors are reviewed by McCreedy (2000) and Gavriilidis et al. (2002) who also describe the bonding techniques used and the methods employed to immobilize catalysts on the surfaces of the microreactors. Photolithography and etching techniques have been used for silicon and glass substrates. X-ray lithography and electroforming are used in the LIGA (acronym for the German words lithographie, galvanoformung, abformung, which mean lithography, electroforming and moulding) technique (Löwe and Ehrfeld, 1999). Other fabrication routes include the extension of traditional techniques to a very small scale with high precision, such as precision milling.

3.3.2 Applications of microreactors

The main general characteristics of microreactors are related to their large surface to volume ratio, increasing with decreasing linear dimension. This provides a very high heat transfer area per unit volume of the reactor and of the fluid used. Low characteristic dimensions also lead to small characteristic lengths for mixing and to high contact areas between the phases in multiphase systems. These features explain the main type of applications microreactors have had and the advantages they can bring in terms of process performance.

Many highly exothermic reactions have been carried out in microstructured reactors with immobilized catalysts. Near isothermal operation was obtained in a

microstructured reactor, with immobilized silver catalyst, for the oxidation of ethylene to ethylene oxide (Löwe and Ehrfeld, 1999). This was possible even without using an integrated heat exchanger.

The high specific heat transfer areas obtained in microreactors have lead to better conversions and less catalyst damage by hot spots in the oxidation of ammonia (Rebrov et al., 2001). Different microreactors with various designs, both with and without integrated heat exchanger were studied. Manufacturing techniques and operating conditions could be chosen to achieve near isothermal operation of the reaction, leading to a very high selectivity in the desired product.

Wörz et al. (2001) carried out the dehydrogenation of an alcohol to an aldehyde in a 1 cm^3 volume microreactor fabricated in silver, the catalytically active material. The choice of the cross section of the reactor was a compromise between the need to have a high specific heat transfer area and to limit channel blockages. The cross section was 0.32×0.40 mm^2. The microreactor allowed a lower maximum operating temperature without hot-spots; a hot-spot of 160° C was obtained in a traditional pan-like reactor commonly used for the production of formaldehyde. Selectivity in the microreactor reached values up to 96% against the 40% value obtained in the traditional reactor.

The use of microstructured reactors has proved to give increased yields and selectivities in liquid-liquid reaction systems. Burns and Ramshaw (1999, 2002) studied the nitration of benzene and toluene in capillary tubes of various internal diameters between 127 and 300 μm and lengths between 30 and 180 cm. Reaction was practically carried out under isothermal conditions, due to the high heat transfer area provided by the capillaries. This, together with mass transfer efficiency obtained with the use of the narrow channels, lead to limited concentrations of unwanted by-products at the end of the reaction.

Wörz et al. (2001) also reported improved yields in the desired product using a microstructured reactor with 32 reaction channels surrounded by cooling channels. A schematic of the microreactor used for this study can be seen in Figure 3.4. Reaction occurred between a reactant dissolved in hexane and sulphuric acid, which constituted

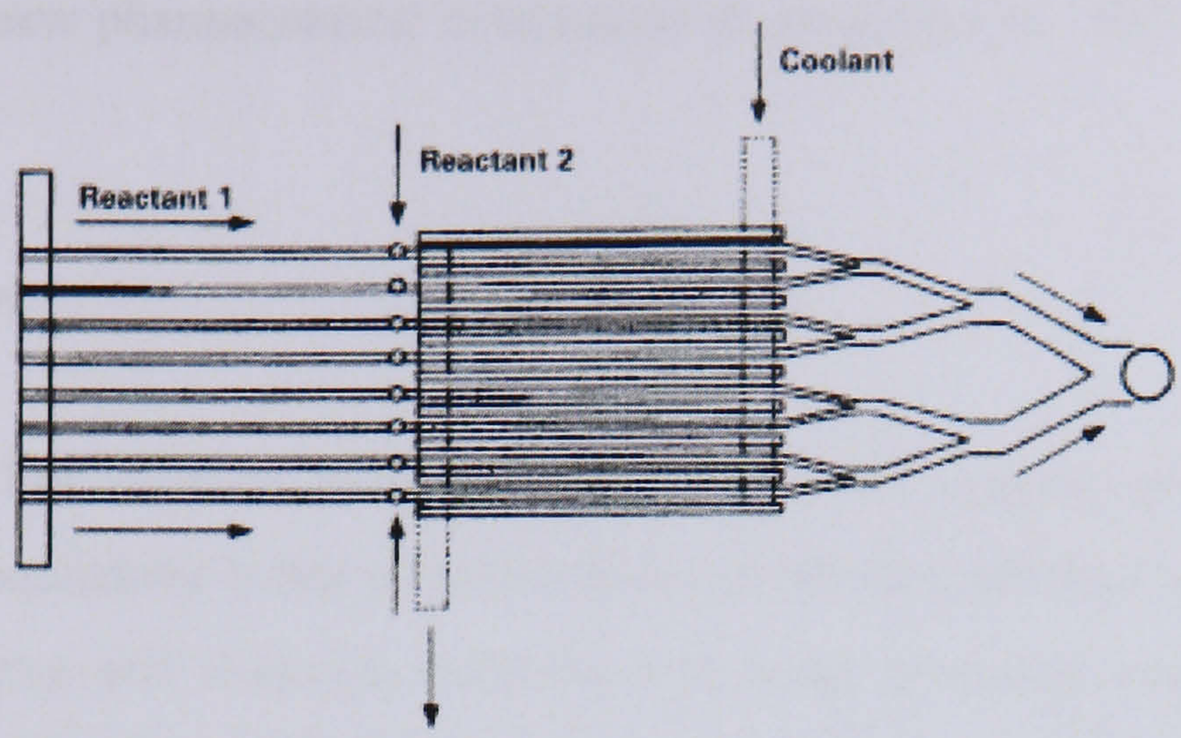

Figure 3.4. Schematic of a liquid-liquid microreactor (from Wörz et al., 2001).

the second phase. This configuration allowed a low temperature increase with the exhotermic reaction and very short contact times, of the order of a few seconds, which provided a very high final yield.

Research on microstructured reactors in the last few years has been mostly focused on demonstrating that different reactions can be carried out in these systems in a more efficient way than in traditional reactors. This has lead to a consistent build up of knowledge on the characteristics of processes carried out at the micro scale. An aspect more recently investigated has been the integration of micro scale systems with detecting methods that could allow monitoring of the processes carried out. A recent development has been reported by Ferstl et al. (2004) who designed and built an automated reaction system with integrated microstructured sensors and analytical interfaces for the monitoring of various process parameters. The pressure and mass flow sensors were especially built for this application using silicon microstructures. The reaction system with integrated sensors was tested by using the nitration of 2-(4-chlorobenzoyl-) benzoic acid.

Microreactors have also been used as a tool for discovery of new compounds. The ability to control mixing conditions and operating temperatures has proved to lead to improved yields and selectivity, as reported earlier. These properties can be applied to the discovery of new products reducing the time for the development of optimized processes. As an example, combinatorial chemistry can be used for the discovery and

development of new pharmaceutical compounds as suggested by Watts and Haswell (2003).

3.3.3 Micromixers

An area which has received particular attention in the context of the study of microstructured equipment is that of micromixers. Achieving efficient mixing is often critical for carrying out chemical reactions and other processes and a consistent amount of work has been devoted to the design and fabrication of micro scale equipment that could perform mixing operations more efficiently than traditional mixers.

Kakuta et al. (2001) presented one of the first reviews on different manufacturing methods used to provide high mixing efficiency in microengineered reactors. One of the techniques used for achieving efficient mixing in micro scale equipment is referred to as multilamination and is based on a design that forces the fluid path to be split and then recombined so as to reduce the characteristic length for mixing. A picture of a multilamination based mixer can be seen in Figure 3.5 (Ehrfeld et al., 1999).

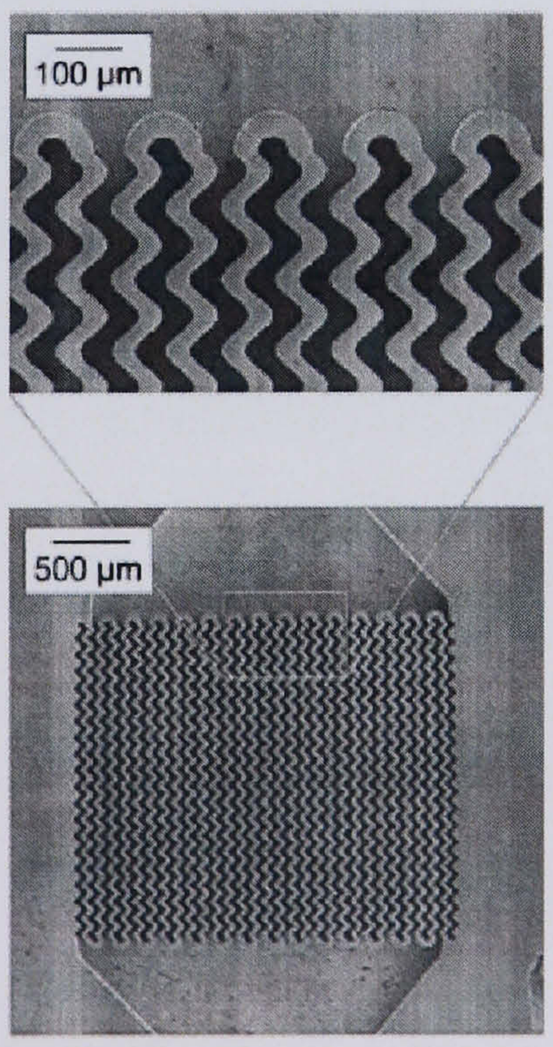

Figure 3.5. SEM micrograph of a multilamination mixer (from Ehrfeld et al., 1999).

The idea behind the multilamination concept is that mixing occurs mainly by diffusion at the length scales of microreactors and that reducing the characteristic length of diffusion and increasing the contact area between the phases improves mixing. Hessel et al. (2003) characterized flow patterns in different interdigital micromixers by using visual techniques. The mixers used were fabricated in glass and had three different mixing chamber geometries, slit-shaped, rectangular and triangular. In each case the fluid stream was fed to the mixing chamber by the interdigital flow distribution zone operating with the multilamination principle. The authors observed that for the slit-shaped configuration when the fluid lamellae recombined in the mixer, some complex phenomena such as lamellae tilting occurred, giving rise to an enhancement to diffusion mixing.

Hessel et al. (2005) recently reviewed the main techniques for enhancing mixing in microscale systems in respect to the diffusion driven process. The methods used can be divided in two main categories: active and passive principles. The first group includes all the techniques that imply an external energy input, such as the use of ultrasound, vibration or pulsation of the flow. The passive methods include all the techniques used to affect the fluid path by way of special designs of the micromixers. Multilamination belongs to this category. Other designs include different variations of the splitting of the fluid stream into smaller lamellae, such as repeated fluid division and recombination structures.

Various geometric designs can be used to generate local recirculations in the fluid path and enhance mixing in respect to a purely diffusive process. An example of this is the use of zig-zag shaped microchannels for which a deviation from laminar flow profile was observed above a critical Re approximately equal to 80 (Mengeaud et al., 2002). Another application of this method was reported by Keoschkerjan et al. (2004) who developed a microreaction unit with a mixing section composed of a 3-dimensional structure made of cavities to force the fluid to continuously change direction.

3.3.4 Microreactors for particle synthesis

Recent years have seen an increasing number of applications of micro scale systems for particle synthesis. The fluid dynamic characteristics of microreactors have proved

to be beneficial for the generation of particles with controlled size and narrow size distributions. A short review on the production of nanoparticles in microreactors elucidating the advantages of using microfluidic system for particle synthesis has been written by deMello and deMello (2004). The authors identified the main advantages of using micro scale systems for particle generation in the possibility of easily controlling and reproducing process variables such as temperature, flow rate and reagents concentrations.

Shestopalov et al. (2004) carried out the synthesis of CdS and CdS/CdSe core-shell particles by using a droplet based microfluidic device. The microreactors had a 50 μm × 50 μm cross section and were fabricated in polydimethylsiloxane. Aqueous solutions of $CdCl_2$, Na_2S and Na_2Se constituted the reagent systems and an oil phase immiscible with the solutions was used to segment the aqueous phase and generate a droplet system. The oil formed a layer around the liquid plugs containing the reacting system and this prevented the formed particles from building up on the reactor walls.

Wagner et al. (2004) studied the growth of 12 nm gold seeds in a microreactor and produced larger nanoparticles with diameters ranging from 15 to 24 nm. They took into account the effect of changing concentrations of the reagents, their flow rate and their order of addition on the size and size distribution of the particles. They used flow rates between 10 and 50 μl/min and observed that all the parameters taken into account affected the size distribution of the particles. Particularly, larger particles were obtained by decreasing the flow rates of the reagents.

Zhang Lin et al. (2004) carried out the synthesis of silver nanoparticles in a microreactor by using the thermal reduction of silver pentafluoropropionate. Their reactor was constituted by a 20 cm long, 0.84 mm ID stainless steel coil. The authors found that they could change the size and size distribution of the silver particles by varying the reaction temperature and the flow rate of the silver precursor. Another system requiring heating of the reagents was studied by Sue et al. (2004), who carried out the hydrothermal synthesis of ZnO nanocrystals. They mixed potassium hydroxide and zinc sulphate solutions in a narrow T mixer (with diameters of a few mm or lower) and used microreactors with 0.15 or 0.59 mm ID. Particle size as low as 9 nm was achieved when using a T mixer with a 0.3 mm ID.

Takagi et al. (2004) prepared titanium dioxide particles from the hydrolysis of titanium tetraisopropoxide in a microreactor system. The reaction was carried out by contacting two immiscibile phases, one containing the titanium complex and the other one water. The reaction occurred at the interface between the phases which was established between the aqueous solution which flowed in the outer part of the microchannel and the organic phase with the titanium tetraisopropoxide which occupied the inner part of the microreactor. The two phases generated an annular flow pattern and this mode of operation presented the advantage of preventing particle build-up on the walls of the channels. The reactors used had internal diameters equal to 307, 607 and 877 μm. The particles produced were mono-modal in size distribution and the lowest mean size obtained was 45 nm, correspondent to the use of the smallest channel.

3.4 Calcium carbonate precipitation

In the last part of Chapter 2 the most relevant industrial applications of precipitated calcium carbonate were described. This section will outline the information available in the literature on calcium carbonate precipitation both from liquid phase and gas-liquid systems.

Calcium carbonate precipitation has been and still is widely studied. The various studies on precipitation usually focus on the effect of process parameters on particle properties such as particle size, particle size distribution and morphology. This requires the understanding of the various phenomena affecting the precipitation process described in Chapter 2 and firstly of the hydrodynamic conditions in the reaction environment.

Hostomský and Jones (1991) studied the precipitation of calcium carbonate from reacting solutions of calcium nitrate and sodium carbonate in a continuous stirred crystallizer. They found that particle morphology depended on the concentration of the reagents, pH and residence time. Particle size was greatly affected by agglomeration at high concentrations.

Zauner and Jones (2000) further studied the liquid phase precipitation of calcium carbonate in a semi-batch crystallizer. They used the reaction between calcium chloride and sodium carbonate solutions in reactors of different volumes and took into account the influence of process conditions on particle size. Moreover they developed an hybrid mixing-CFD (computational fluid dynamics) model which gave predictions that were in reasonable agreement with the experimental data. Particle size was found to generally decrease with increasing specific power input.

Kotaki and Tsuge (1990) studied precipitation of calcium carbonate both from a liquid phase system and from the carbonation of calcium hydroxide solutions and suspensions. The equipment used was a continuous flow crystallizer and they interpreted their results in terms of nucleation and growth rates.

Wachi and Jones (1991a) modelled the gas-liquid precipitation of calcium carbonate from the carbonation reaction of calcium hydroxide solutions in a stirred tank reactor with the liquid operated in batch mode and the gas continuously flowing over the surface of the liquid phase. They represented gas-liquid mass transfer with the film theory, and used power law equations to describe nucleation and growth rates. The authors found that both mass transfer rates and the specific unit volume of liquid influenced the particle size, as they both affected how the supersaturation profiles would develop in the liquid phase. Wachi and Jones (1991b) characterized particle size dependence on stirring intensity in experimental work with the same type of equipment. Results showed that lower stirring speeds, and therefore lower mass transfer coefficients, gave smaller particles in the early stages of precipitation; particle size being then controlled by agglomeration. This was due to the fact that lower stirring speeds allowed a greater build up of supersaturation close to the gas-liquid interface, due to the contact method used between the two phases. In a later study, Hostomský and Jones (1995) developed a model of precipitation based on the penetration theory of mass transfer.

More recently, Hamid and Jones (2002) studied the precipitation of calcium carbonate from calcium hydroxide solutions in laboratory and pilot scale draft tube bubble columns. Characterization of mean particle size at varying gas flow rates showed that smaller particles were produced in the pilot scale reactor. This was attributed by the authors to high local supersaturation values generated because of the lower mass

transfer efficiency in the pilot scale reactor. This influence of mass transfer performance on particle size is similar to that reported for precipitation in a flat interface stirred vessel. Particle size distributions were found to be relatively broad or bimodal for both the laboratory scale and the pilot scale reactor.

Hoon Kang et al. (2003) studied the effect of operating conditions, such as calcium hydroxide concentration and liquid and gas flow rates, in the precipitation of calcium carbonate from calcium hydroxide solutions in a Couette-Taylor reactor. In this type of equipment, fluid is subjected to the shear generated between an inner cylinder, which is rotating, and an outer cylinder concentric to the first one, which is stationary. Beyond a critical rotational speed, the radially oriented axisymmetric laminar flow (Couette flow) becomes unstable and turbulent (Taylor) vortices are formed. A schematic of a Couette-Taylor reactor can be seen in Figure 3.6. Hoon Kang et al. found the occurrence of needle like particles at high pH and cubic shape particles at low pH. The change in shape was attributed by the authors to a change in the excess Ca^{2+} ions concentration present in solution. No identification of the polymorphs by X-ray diffraction was carried out.

García Carmona et al. (2003a) studied the effect of changes in the solution electrical conductivity in the gas-liquid precipitation of calcium carbonate in a stirred tank reactor. Experiments were carried out at 30, 45 and 60°C and the conductivity was

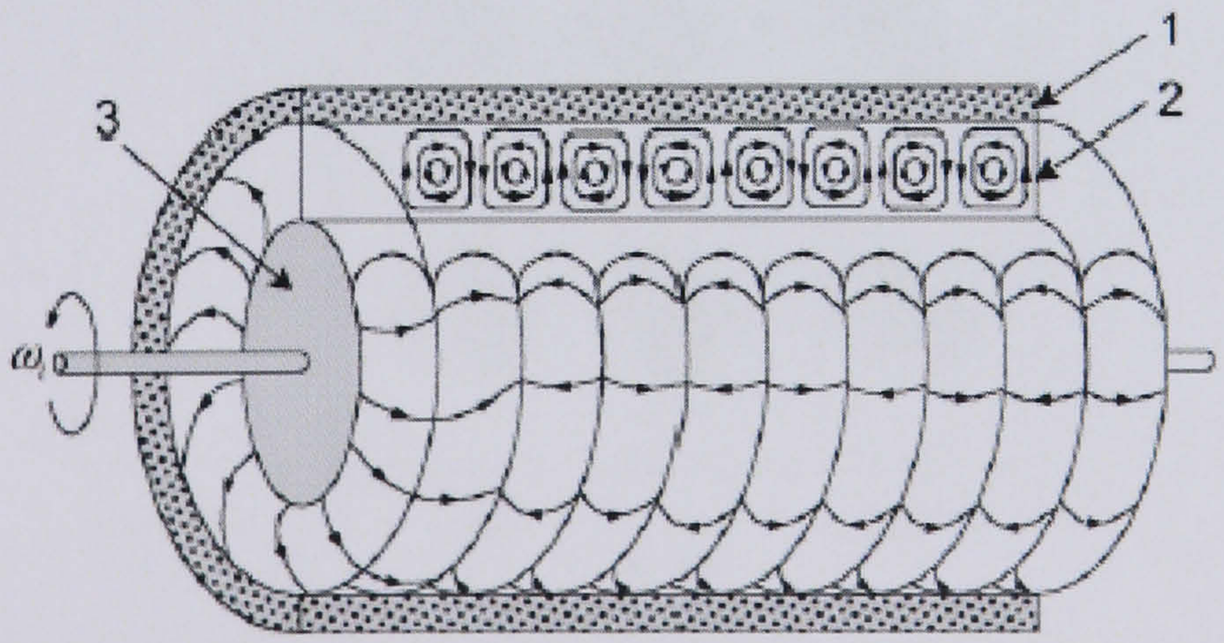

Figure 3.6. Schematic of flow patterns in a Couette-Taylor reactor. 1:outer stationary cylinder, 2: Taylor vortices, 3: inner rotating cylinder (from Hoon Kang et al., 2003).

controlled by manipulating the feed flow rate of the reagent calcium hydroxide suspension. The authors found that the precipitates corresponded to pure calcite in all cases. Both temperature and conductivity influenced particle morphology. The change in conductivity was reflected in the change of the ratio between the total calcium and the total carbonate charged species, with this ratio increasing with increasing conductivity. Morphology of the single particles changed from generally rhombohedral (or cubic type) to scalenohedral (with a more elongated shape) with increasing conductivity. The transition stages are summarized in Figure 3.7. The change in shape was of the same type reported by Hoon Kang et al. (2003) for the Couette-Taylor reactor.

García Carmona et al. (2003b) also studied the use of various additives to control particle morphology in the gas-liquid precipitation of calcium carbonate. They found that additives like citric acid, sucrose or triethanolamine as examples, could affect the morphology, the size and the aggregation behaviour of precipitated calcite particles.

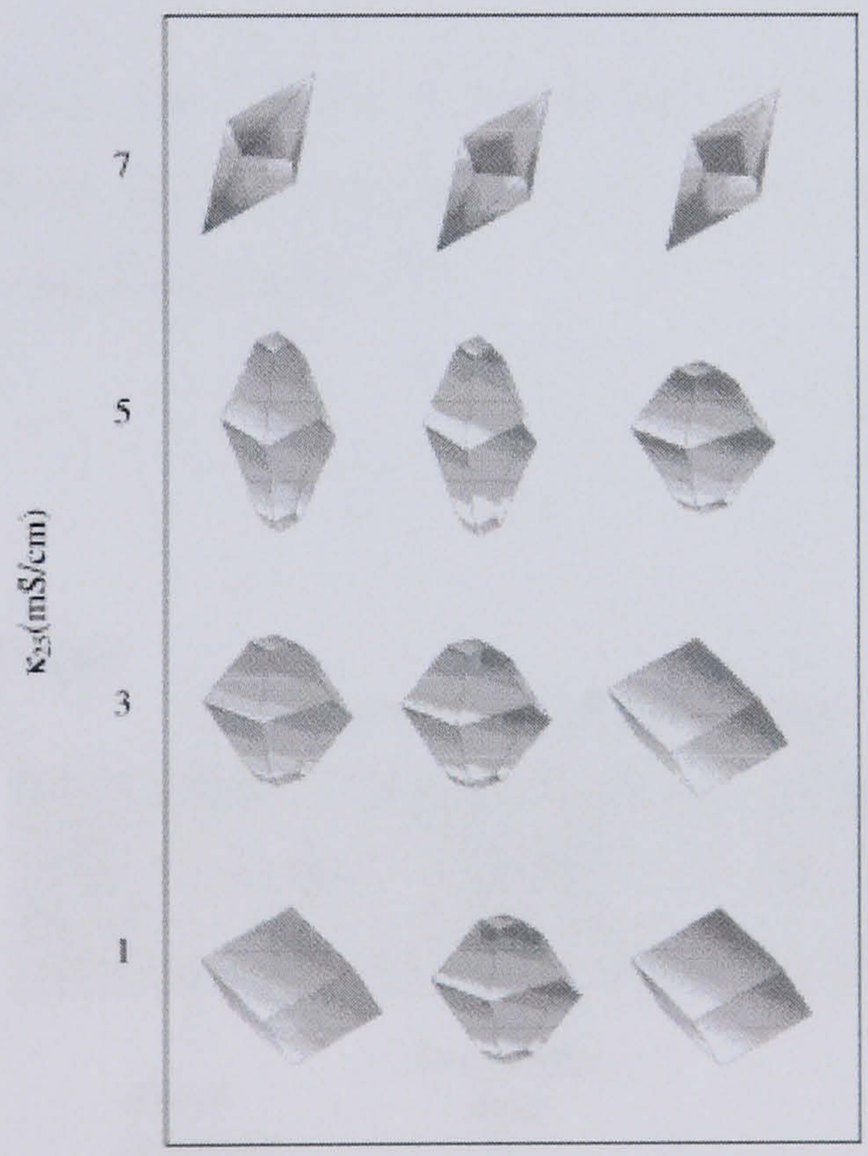

Figure 3.7. Calcite particles morphology at various temperatures and conductivities for the precipitation from a $Ca(OH)_2$ suspension (from García Carmona et al., 2003b).

3.5 New equipment for precipitation

As anticipated in the sections relative to Process Intensification and calcium carbonate, recent years have seen various applications of novel types of equipment for precipitation processes. The drive for this type of investigation is to define precipitation processes that can be carried out more efficiently than in traditional vessels and that can give improved product properties.

Vacassy et al. (2000) designed and characterized the segmented flow tubular reactor (SFTR), a novel type of reactor for the production of high quality powders. The reactor was made from flexible tubing with 4 mm ID and 10 m or 20 m long (Guillemet-Fritsch et al., 2004). Several microreactors were generated in the tubing by separating limited volumes of reaction mixture (typically lower than 1 cm^3) with a segmenting fluid which was immiscible with the reaction mixture itself. A schematic of the operating principle is shown in Figure 3.8 and a picture of the SFTR can be seen in Figure 3.9.

The design of the SFTR was based on producing confined volumes of reacting systems in which uniform levels of supersaturation can be attained very rapidly, to obtain particles with controlled properties.

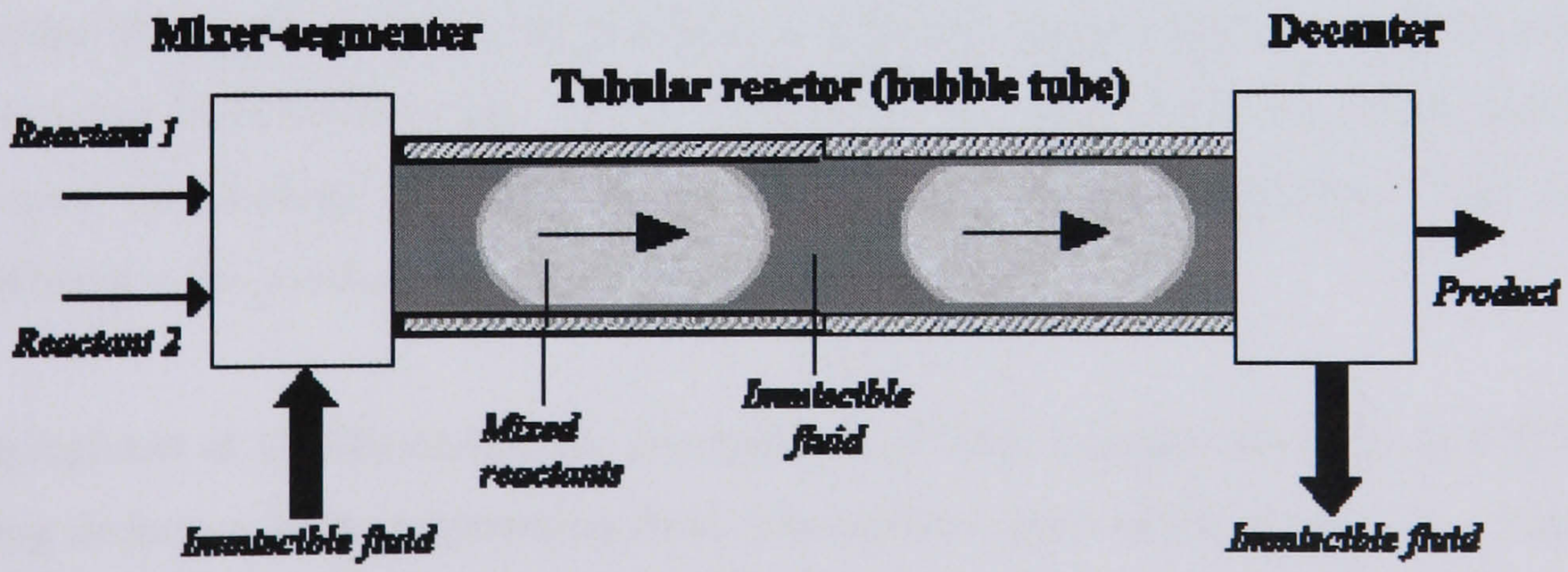

Figure 3.8. Schematic of the segmented flow tubular reactor (from Guillemet-Fritsch et al., 2004).

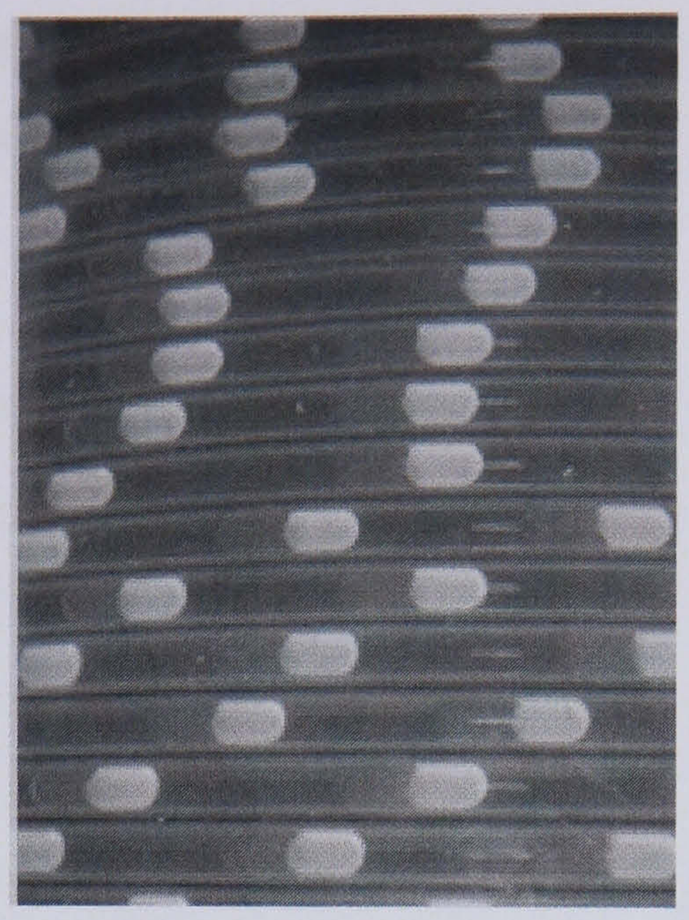

Picture 3.9. Picture of the segmented flow tubular reactor (from Guillemet-Fritsch et al., 2004).

Vacassy et al. (2000) investigated the precipitation of calcium carbonate by reacting aqueous solutions of calcium chloride and ammonium carbonate. Two configurations of a mixer were used to feed the phases to the reactor, a Y mixer and a cross mixer. The precipitated calcium carbonate was found to correspond to pure vaterite in both cases.

Donnet et al. (2000) studied the reaction between sodium oxalate and calcium nitrate solutions in a 40 cm long, segmented flow tubular reactor. Air was used as the segmenting fluid. The authors found that the main phase to precipitate was calcium oxalate trihydrate, with a small fraction of calcium oxalate monohydrate. The most interesting result of the study was that the trihydrate obtained, in the SFTR, had an unusual morphology characterized by a high degree of organization. This was attributed to the mixing conditions obtained in the SFTR.

Buscaglia et al. (2002) studied the precipitation of barium titanate particles in a SFTR using dodecane as the segmenting fluid. The authors reported the production of nano sized particles of $BaTiO_3$ with narrow particle size distributions.

Donnet et al. (2002) carried out seeded precipitation of calcium carbonate in a SFTR by using calcite seeds to control the final morphology of the precipitate. Solutions of calcium nitrate and potassium carbonate were used as reagents and limited concentrations of polyacrilic acid were added to one of the solutions. This additive

influenced the final properties of the precipitate, giving higher specific surface area and lower particle size. Calcite particles with narrow particle size distribution were obtained.

Guillemet-Fritsch et al. (2004) reported the precipitation of high quality mixed nickel manganese oxalate powders in the SFTR. Benchmarking tests carried out with a batch stirred reactor showed that the segmented flow tubular reactor gave particles with a more homogeneous morphology and a narrower particle size distribution.

Bénet et al. (2002) described the operating principles of two novel types of precipitators, the two-impinging-jets mixing device and the sliding surface mixing device. Both devices were developed to overcome problems related to high concentration gradients produced by the mixing characteristics of stirred tank reactors. In the two-impinging-jets mixing device, shown in Figure 3.10, the two reagent solutions are forced through narrow feed tubes, as in a T-mixer. Unlike this case though, the impinging of the two solutions occurs not within a third tube, but within the liquid itself, inside a reactor. This design has the advantage of limiting scaling problems connected to industrial operations.

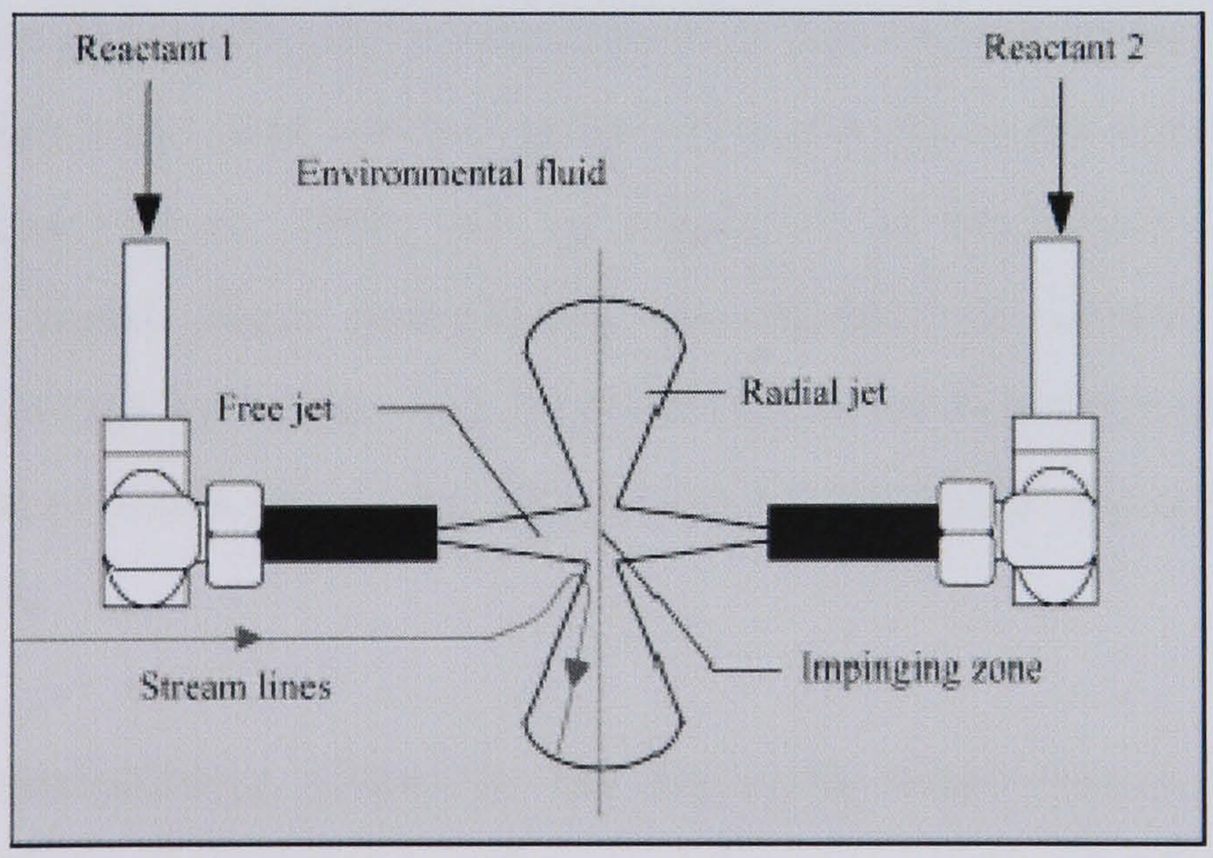

Figure 3.10. Two- impinging-jets mixing device and impinging zone (from Bénet et al. 2002).

The sliding surface mixing device provides stirring in a reactor of standard configuration. The disc has a diameter approximately 80-90% of the diameter of the vessel which is situated a few millimetres from the bottom of the tank. With this configuration the zone below the sliding surface mixing device provides intense mixing. The zone above the disc is characterized by moderate mixing in which slower processes like particle growth can take place.

3.6 Conclusions

A review of the literature on liquid phase and gas liquid precipitation of calcium carbonate in narrow channel reactors has been presented. The aims of Process Intensification have been described together with examples of its application to various types of processes. The main characteristics of microstructured reactors have been presented and specific cases in which their use has shown to bring improvement to various processes have been described. The literature on calcium carbonate precipitation and new equipment for precipitation was also described.

The following chapters describe the investigation on liquid phase and gas-liquid precipitation of calcium carbonate in narrow channel reactors. Some of the studies cited in the literature were presented as a general background, whereas others will be referred to more specifically in the description of the various studies. Results of the work on the segmented flow tubular reactor for liquid phase precipitation of calcium carbonate (Vacassy et al., 2000) will be referred to in describing the particle size results of the liquid phase precipitation investigation in narrow channels. The information collected by Zauner and Jones (2000) on calcium carbonate morphology will be referred to when examining this aspect for the liquid phase precipitation in narrow channels.

Mass transfer performance offered by the impinging stream reactor (Gaddis, 1999) will be referred to when discussing the mass transfer results obtained for a narrow channel reactor. Particle size for the gas-liquid precipitation will be compared to the results obtained in a Couette-Taylor reactor (Hoon Kang et al., 2003).

CHAPTER 4

Characterization of mixing efficiency by a chemical reaction method and liquid phase precipitation of calcium carbonate in a narrow channel reactor system

4.1 Introduction

Production of particles by reactive crystallization is greatly influenced, as seen in the previous chapters, by mixing conditions in the reaction environment. The time scales involved in the mixing of the reagents and their final degree of mixing determine how the local values of supersaturation are distributed in the equipment used to carry out the reaction. As seen from the theory of precipitation, supersaturation values determine the rate at which nucleation and growth and the secondary phenomena in precipitation take place and therefore greatly influence the final properties of the product in terms of size and size distribution.

The understanding of the mixing conditions in the reaction environment constitutes one of the fundamental aspects for the design of reactors to be used for carrying out liquid phase precipitation. The main aim of a study on the mixing efficiency for a reactive crystallization process is characterization of the mixing efficiency as a function of the size and size distribution of the product. This constitutes a design tool for the evaluation of an optimized configuration of the equipment.

In the first part of this chapter the application of a set of parallel competing reactions, the iodide-iodate reaction system, to the narrow channel reactors used for carrying out liquid phase precipitation of calcium carbonate is described. In the second part, the work on calcium carbonate precipitation in the narrow channel system by reacting aqueous solutions of calcium nitrate and sodium carbonate is presented. Results are discussed in terms of flow characteristics in the narrow channel reactor system and of the findings of the mixing study.

4.2 Chemical reactions for characterizing mixing efficiency

Mixing characterization in relation to precipitation reactions can allow the understanding of the influence of operating parameters on the product final properties. Experimental methods can prove to be effective in providing information on the influence of operating conditions on mixing. The method used should be adaptable to different types of equipment and present good sensitivity and reproducibility. Chemical reactions have proved to be particularly useful in this sense, as the mixing efficiency can be directly related to the concentration of reaction products which can be analyzed using relatively easy techniques. Different reactions might be considered or concentrations of the reagents might be adjusted in order to characterize equipment that provide various degrees of efficiency in mixing. The reactions used to characterize mixing efficiency usually fall into three categories: single reactions (A + B $\rightarrow$ C), consecutive competing reactions (A + B $\rightarrow$ R, R + B $\rightarrow$ S) and parallel competing reactions (A + B $\rightarrow$ R, C + B $\rightarrow$ S). Fournier et al. (1996a) presented a review of some of the reactions that have been used to characterize mixing for all the three types of scheme.

Meyer et al. (1988) used a set of consecutive competing reactions to characterize mixing in a static mixer and in an empty tube. The reactions used in this case lead to the precipitation of barium sulphate, the concentration of which can be related to mixing efficiency in the equipment. The selective iodination of the aminoacid l-tyrosine was used by Bourne and Rohani (1983) to characterize mixing in a batch reactor. This is again a set of consecutive competitive reactions.

The most used reaction systems are the diazo coupling of 1-naphtol developed by Bourne and co-workers and the iodide-iodate system introduced by Villermaux and co-workers. The first scheme is a set of consecutive competing reactions, whereas the iodide-iodate reaction system is a scheme of parallel competing reactions. A detailed study on the kinetics of the diazo coupling of 1-naphtol with diazotized sulfanilic acid has been described by Bourne et al. (1990). An improved reactions system, capable of characterizing mixing equipment with higher energy dissipation is based on the simultaneous reactions between 1-naphtol and 2-naphtol and sulfanilic acid and has been introduced by Bourne et al. (1992).

In this study the iodide-iodate set of reactions was adopted because it is an entirely inorganic system based on the use of aqueous solutions and therefore closer to the reagent system chosen for the precipitation study in terms of physical and transport properties. The following section reports a description of the characteristics of the iodide-iodate system and of the previous studies carried out with this reaction scheme.

4.3 The iodide-iodate reaction system

The iodide-iodate reaction system consists of the two parallel competing reactions:

$$H_2BO_3^- + H^+ \leftrightarrow H_3BO_3 \qquad (4.1)$$

$$5I^- + IO_3^- + 6H^+ \leftrightarrow 3I_2 + 3H_2O \qquad (4.2).$$

Reaction 4.1 can be considered as quasi-instantaneous and reaction 4.2 is fast but much slower than 4.1. The iodine formed from reaction 4.2 reacts according to the equilibrium:

$$I_2 + I^- \leftrightarrow I_3^- \qquad (4.3)$$

and the concentration of the triiodide ion formed can be detected by UV-vis spectrometry at 352 nm.

Knowledge of the equilibrium constant for reaction 4.3 allows the calculation of the final concentration of iodine, which is a measure of the mixing state of the fluid. In fact, if the fluid is perfectly mixed, adding acid to a mixture of borate, iodide and iodate ions will cause only reaction 4.1 to occur, as it is much faster than reaction 4.2. Conversely, if the fluid is not perfectly mixed, local values of acid concentration will vary and the excess of acid left after completion of reaction 4.1 will react with the iodide and iodate ions to form iodine. Increasing concentrations of iodine in the final product distribution will then indicate less efficient mixing.

Following on the description of mixing phenomena given in Chapter 2, when a fluid is perfectly mixed, usually it is referred to as a fluid with no segregation, indicating that no single units of fluid with inhomogeneous concentrations are present. The opposite

case is referred to as the case of total segregation. The mixing efficiency characterization, that is carried out with the iodide-iodate system, usually is quantified with the definition of a segregation index, as shown, for example by Villermaux et al. (1992). The segregation index is given by the ratio of the selectivity of iodine in the general case and the one in conditions of total segregation:

$$X_S = \frac{Y}{Y_{TS}} \tag{4.4}$$

where $X_S = 0$ for perfect mixing and $X_S = 1$ for total segregation.

In conditions of total segregation, both reactions will appear instantaneous compared to the mixing and the selectivity of iodine will depend only on the initial concentrations of the reagents, Y_{TS} will then have the expression:

$$Y_{TS} = \frac{6[IO_3^-]^i}{6[IO_3^-]^i + [H_2BO_3^-]^i} \tag{4.5}.$$

In the general case the selectivity will be given by the ratio of the total amount of iodine formed and the amount of acid fed to the system:

$$Y = \frac{2(n(I_2) + n(I_3^-))}{n^i(H^+)} \tag{4.6}$$

where n represents the number of moles for the single species.

The iodide-iodate method has been used to characterize mixing efficiency in different types of equipment. Fournier et al. (1996a) applied the iodide-iodate method to two stirred tanks of 1 dm^3 and 20 dm^3 nominal volume respectively. In this case the reactors were filled with the iodide-iodate-borate solution and sulphuric acid was subsequently fed to the system. The authors studied the influence of different pipe diameters, feed times and feed locations for the addition of the acid on the segregation index. Schaer et al. (1999) used the iodide-iodate system to characterize mixing efficiency provided by impinging jets submerged in a stirred tank at varying feed time,

feed flow rate, location and stirring speed. Liu and Lee (1999) used the method to characterize mixing in a Couette flow reactor at varying rotating velocities of the inner cylinder while Fang and Lee (2001) studied mixing efficiency in a Kenics static mixer at varying Reynolds numbers. Judat et al. (2004) applied the iodide-iodate system to a reactor consisting of a Taylor-Couette reactor and an external circulation loop. This set-up was also used for the precipitation of barium sulphate, where the Taylor-Couette reactor served as a zone of high mixing intensity for nucleation and the loop flow would be used for slower processes like growth and agglomeration.

Ehrfeld et al. (1999) modified the iodide-iodate reaction system to characterize mixing in microchannels, with dimensions of tens of microns. They also studied mixing in arrays of microchannels and carried out benchmarking tests in stirred vessels and tee-mixers. Guichardon and Falk (2000a) presented the experimental methods for using the iodide-iodate system in stirred tanks of different volumes. They also indicated how to extend the procedure to continuous systems with varying reagent flow rate ratios and gave general guidelines on how to solve sensitivity and measurement problems. Guichardon et al. (2000) also carried out a kinetic investigation on the iodide-iodate reaction system.

The following section describes the experimental apparatus and the operating parameters used for the mixing efficiency and the liquid phase precipitation studies. The conditions, in terms of concentrations of reagents and products, that have to be fulfilled in order to have a correct representation of the mixing conditions when using the iodide-iodate system are subsequently illustrated. Starting from the guidelines given by Guichardon and Falk (2000a) for a continuously operated system, the definition of the experimental conditions for the application of the iodide-iodate set of reactions to the narrow channel reactors is described.

4.4 Experimental apparatus and flow rate calibration

The narrow channel reactor system used for precipitating calcium carbonate from two aqueous solutions and for the study on mixing characterization was made from Perspex. For this case, three reactors having the same length and configuration, but different cross sections were manufactured in the same module. Fabrication of each reactor involved precision milling of two channels with triangular cross section on two

sheets of Perspex. The two parts were then bonded giving three reactors with a square cross section forming a 45° angle with the base of the Perspex module. A photograph of the module can be seen in Figure 4.1. The top sheet of Perspex was 5 mm thick, whereas the lower one was 4 mm thick. Diffusion bonding was used to unite the two sheets. This was achieved by placing the two sheets of Perspex in an oven at atmospheric pressure and by slowly heating the reactor to 130°C. About 3 kg of metal weights were placed on top of the reactor to avoid formation of air pockets and to favour the sealing. The temperature set-point was kept for 5 hours after which the oven was switched off and the reactor left to cool. The module was checked for leaks before use.

The three reactors had diagonal lines of 0.5 mm, 1 mm and 2 mm and they are indicated as reactors C, B and A respectively. What follows focuses on the description of reactors A and B. This is due to the fact that a preliminary study on precipitation showed that for the range of concentrations used consistent scaling with consequent gradual reduction in throughput were obtained using reactor C with the available pumping system.

As shown in Figure 4.1, the reactors consisted of the part in the Perspex module and of a stainless steel capillary with an internal diameter (ID) of 1 mm. The same capillary was also used as inlet tubing. Three feed points are visible in the photograph; the intermediate one was closed and was not used in this investigation. It could be used for feeding an additive to the precipitating particles. Holes were drilled in the Perspex to connect the capillary to the channel in the Perspex module. The system was sealed using Araldite, an epoxy adhesive. The capillary at the inlet was connected to a short Y mixer in the Perspex module with the two shortest sides of the Y being 1 cm long. A schematic of reactors A and B can be seen in Figure 4.2. The channels in the Perspex module were formed by three straight segments each 6.5 cm long and two U bends, with mean diameter of 5 mm. The outlet tubing was 17.2 cm long for reactor A and 19 cm long for reactor B, whereas the inlet capillaries were 13 cm long for reactor A and 12 cm long for reactor B. The inlet tubing terminated with Swagelok fittings to which syringes could be connected. A syringe pump (Sage Instruments, model 355) was used, with the syringes, to feed reagents to the narrow channels.

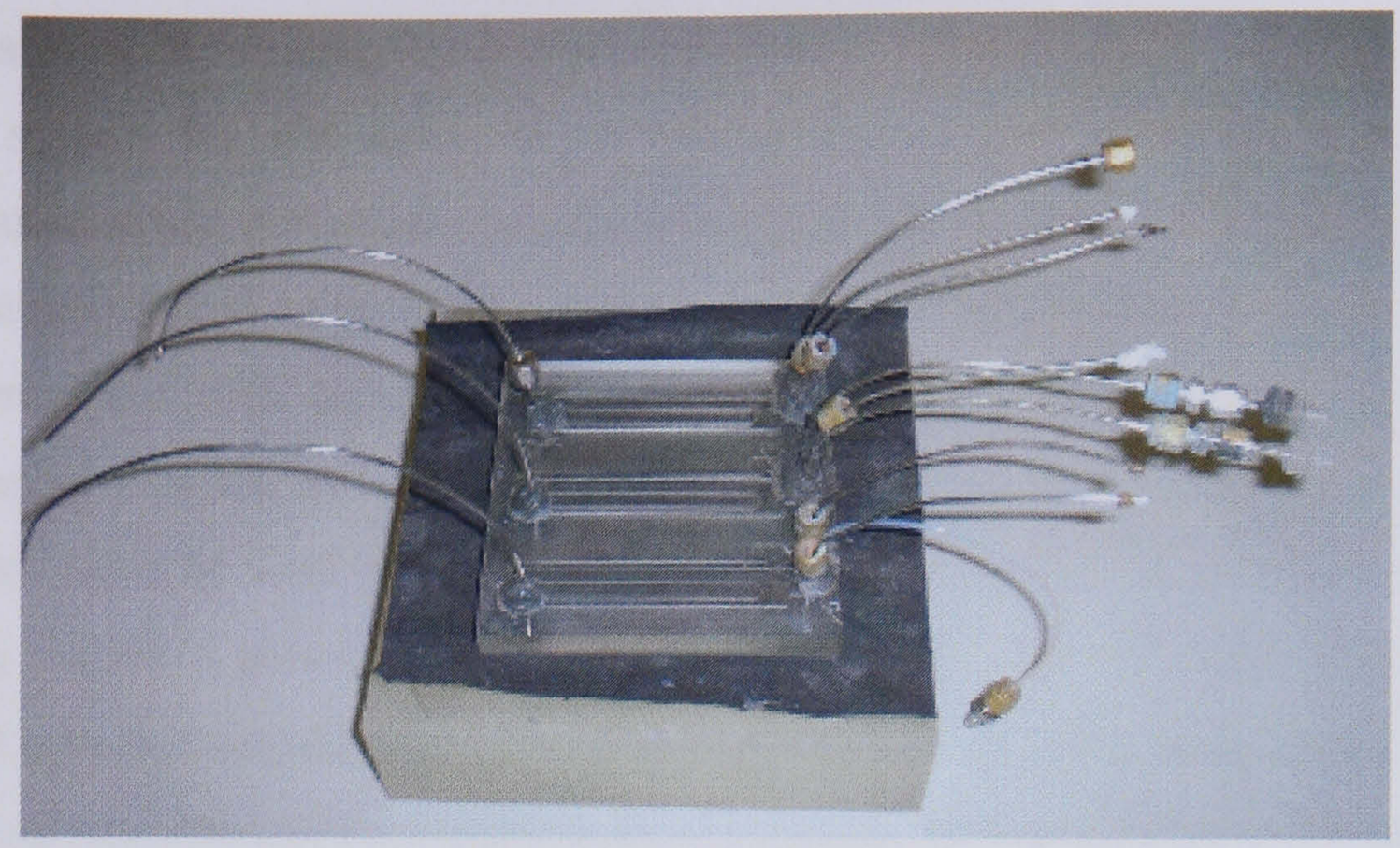

Figure 4.1. Photograph of the narrow channel reactor system.

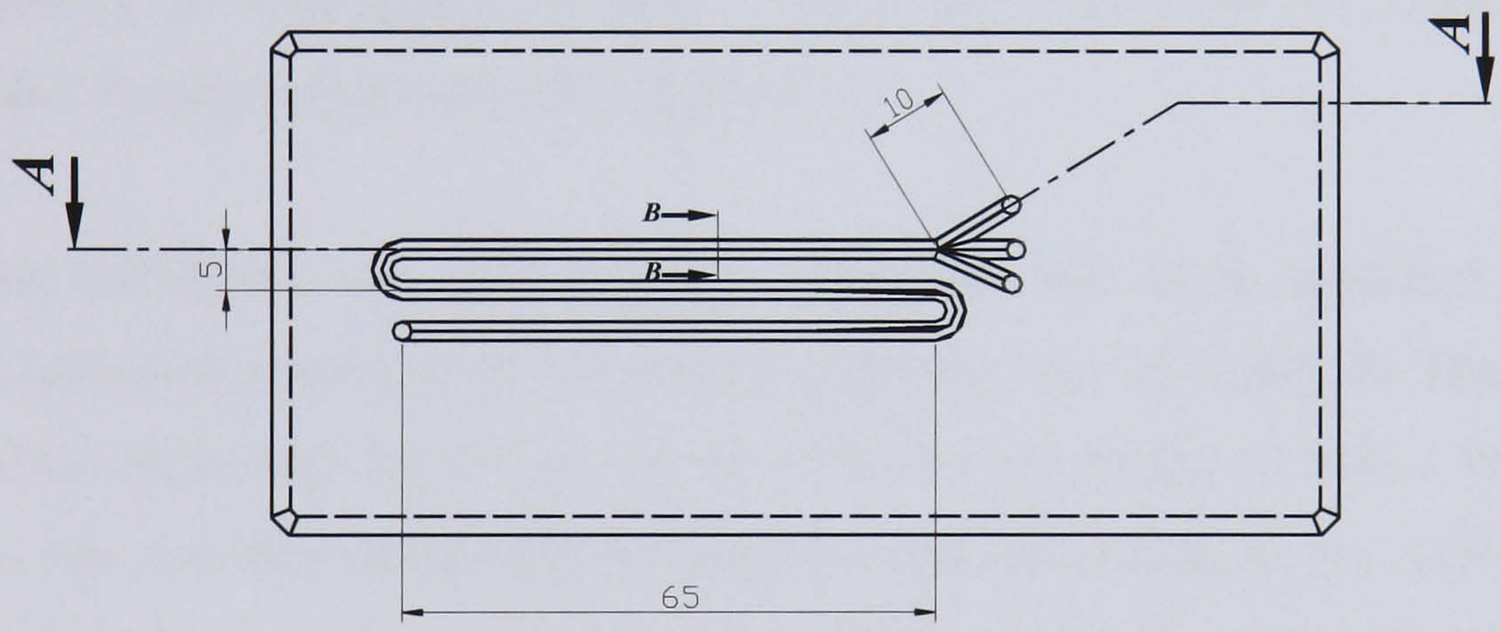

Figure 4.2. Schematic diagram of the narrow channel reactor system.

As the aim of the mixing efficiency study was to characterize the narrow channel reactor system for the same set of hydrodynamic parameters as those of the precipitation study, preliminary precipitation experiments were carried out to find out which range of flow rates could be obtained for both reactors. Flow rate calibration was carried out with different syringes volumes, both using deionised water and precipitating calcium carbonate, at different concentrations to find which range of flow rates could be used without pressure drop effects during precipitation (that is by ensuring that for a given syringe pump speed the trials with deionised water and the ones with the precipitation reaction would give the same flow rate). The tests were carried out with the aim of finding a set of common flow rates for both reactors that could allow comparison on the mixing characteristics and the precipitate properties at total equal throughput. Concentrations for the precipitation runs varied between 0.032 M and 0.38 M for each reagent solution (equimolar feeds were used in each case), corresponding to supersaturation ratios defined in respect to the concentrations (equation 2.4) ranging between 500 and 6000.

Flow rate calibration was carried out by collecting the outlet deionised water or calcium carbonate suspension in a measuring cylinder and recording the time elapsed between the beginning and the end of the collection of the liquid with a stop clock. The flow rate was then calculated dividing the measured volume by the recorded time. As a large number of determinations was carried out for this flow rate calibration (more than 10 for each chosen driver speed), a statistical approach to data analysis was considered in this case to give averages of the results.

The flow rates used both for the mixing characterization study and for the liquid phase precipitation varied between 0.15 and 0.67 cm^3/s for reactor B and between 0.15 and 1 cm^3/s for reactor A. These values refer to the total outlet flow rate, so they should be halved to obtain the inlet flow rate of one of the reagents, assuming a 1:1 ratio between the two feeds. A set of equal flow rates for both reactors was obtained with 5 cm^3 volume plastic syringes, corresponding to the range indicated for reactor B. A wider range of flow rates was obtained for reactor A by using 10 cm^3 plastic syringes. Values of the flow rates used are listed in Table 4.1. Figures 4.3 and 4.4 show the calibration lines for the flow rate versus the speed of the syringe driver and the experimental points for reactors A and B respectively.

Table 4.1. Flow rate values and syringe volumes for the narrow channels.

Reactor	Syringe volume for each reagent (cm^3)	Total flow rates (cm^3/s)
A / B	5	0.15
		0.29
		0.43
		0.59
		0.67
A	10	0.22
		0.41
		0.61
		0.80
		1.00

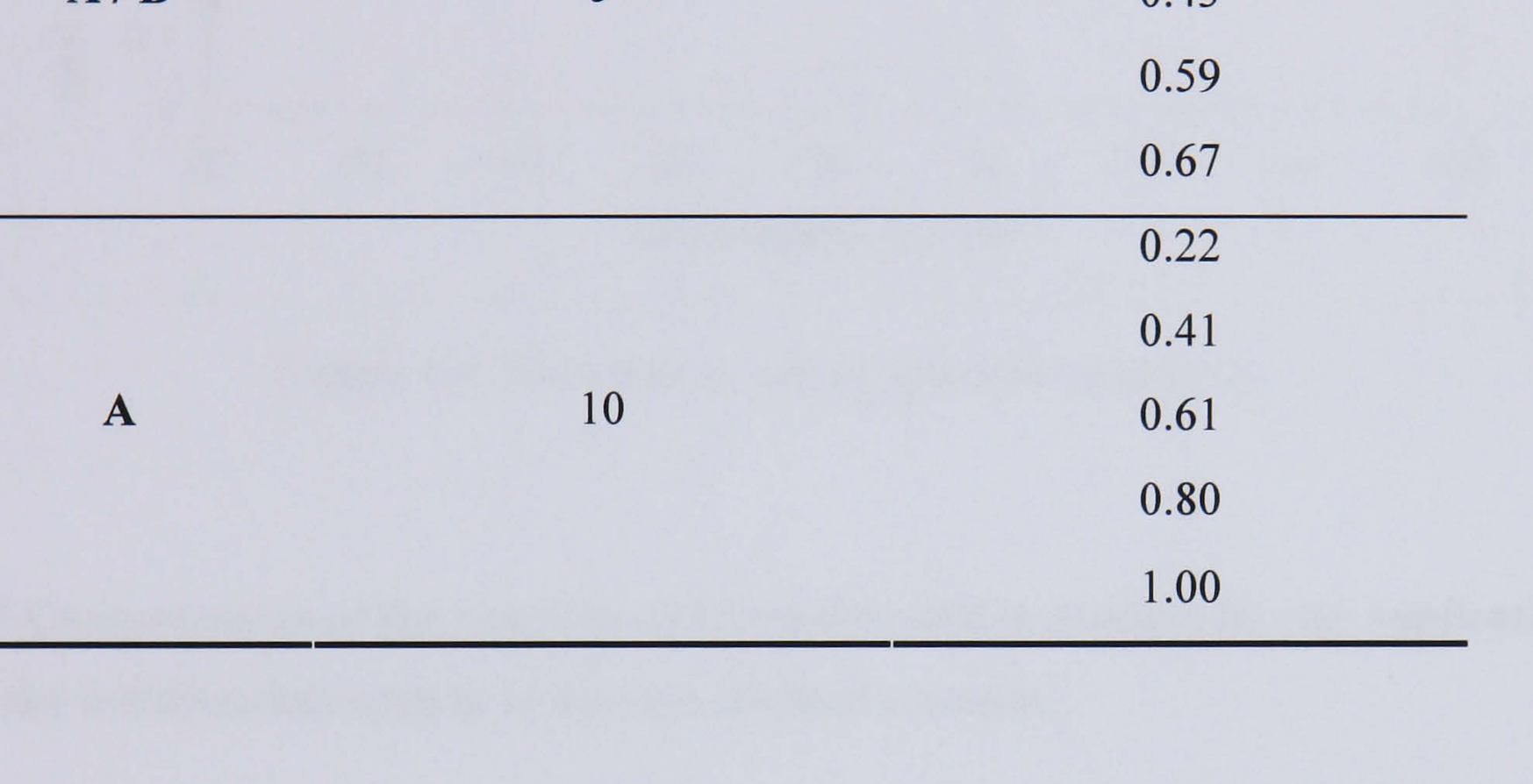

Figure 4.3. Flow rate vs. driver speed for reactor A.

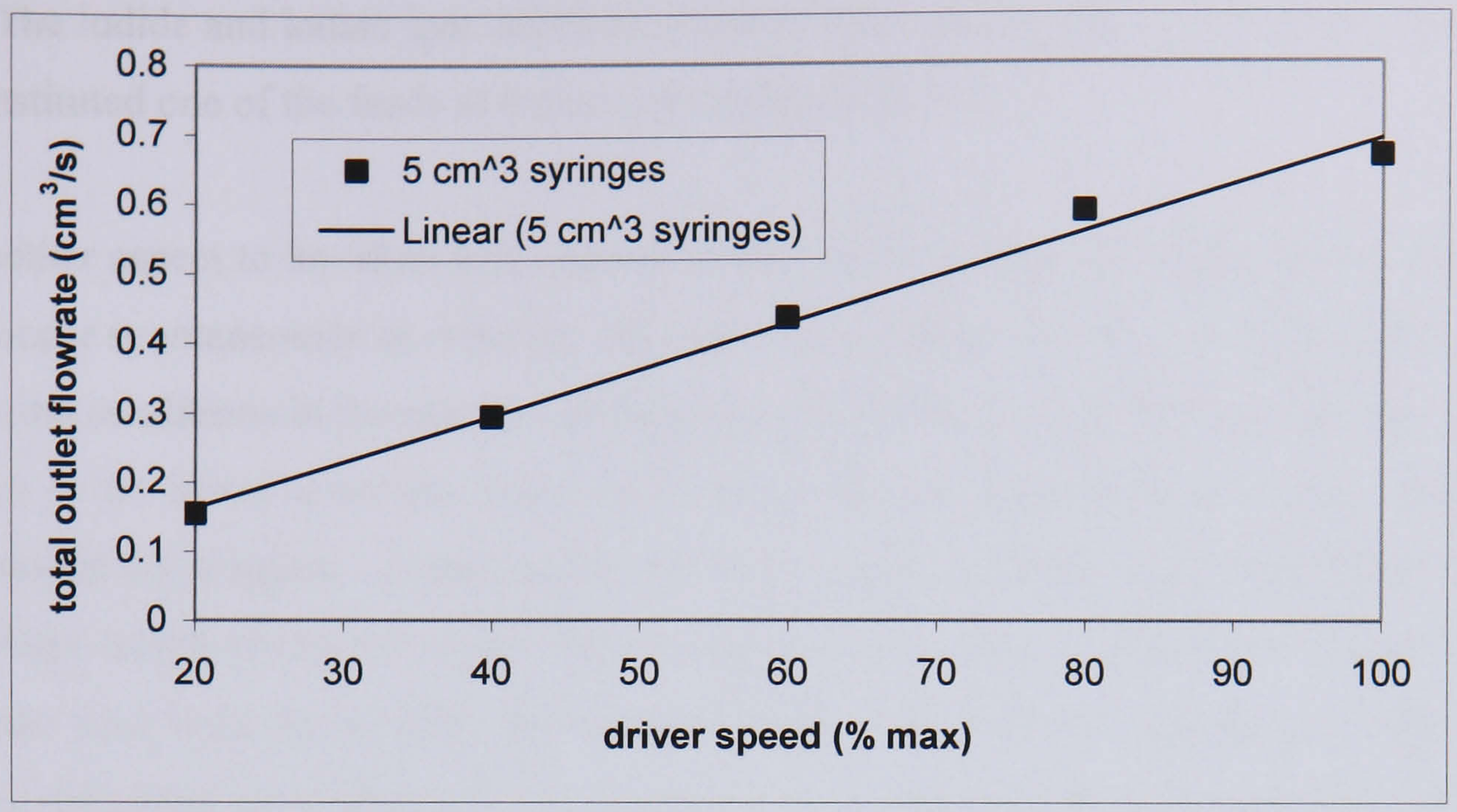

Figure 4.4. Flow rate vs. driver speed for reactor B.

4.5 Concentration of the reagents and experimental procedure for the application of the iodide-iodate system to narrow channel reactors

4.5.1 Definition of the concentrations of the reagents

The iodide-iodate method was originally developed to characterize mixing efficiency in stirred tanks (Villermaux et al., 1992). With this operating mode, the vessel is initially filled with a solution containing the iodide and iodate ions to which a small amount of acid is added. Usually the volume of acid injected is of the order of 10^{-3} times that of the volume contained in the vessel. In the case of the narrow channel reactor system equal volumetric flow rates of the two feeds were used.

Villermaux and co-workers have extensively studied the iodide-iodate system and have reported in various publications the operating parameters that allow a correct application of the reaction scheme, both in relation to the type of equipment used and to the chemistry of the system. The application of the iodide-iodate reaction system requires that the H^+ ions are in less than stoichiometric amount in respect to the borate ions. In addition to this, the spontaneous formation of iodine before the reactions take place must be prevented by controlling the pH of the system. Sodium hydroxide is added to the solution containing borate ions to form a buffer solution with pH around

9. The iodide and iodate ions are then added to this solution. In this case, the solution constituted one of the feeds to the narrow channel reactors.

Another aspect to be taken into account is that the formation of iodine does not have to occur spontaneously in order for the final concentration of iodine to reflect only the mixing conditions in the reaction environment. This implies that the final pH does not have to be below a certain value, pH^*, which can be determined from the electric potential-pH diagram, depending on the total iodine concentration (Fournier et al., 1996a). At pH values below pH^* the spontaneous formation of iodine from iodide and iodate ions becomes possible thermodynamically and therefore operating conditions with pH values lower than pH^* must be avoided. A high limit on pH values also exists, in fact if the final pH is too high, the iodine formed is unstable and no triiodide ion can be detected by UV-vis spectrometry.

Guichardon and Falk (2000a) suggested an operating mode in which the pH of the buffer solution is between 8.5 and 9.5 and the value of pH^* is close to 7. The former condition depends on the concentration of boric acid and sodium hydroxide and the latter on the total concentration of iodine. Respecting these guidelines on the iodide-iodate solution concentrations, the concentration of the acid was adjusted to have sufficient sensitivity for the operating conditions used.

Guichardon and Falk (2000a) first described the procedure for the application of the iodide-iodate method to a stirred tank. For L litres of liquid volume, 10^{-3} L of sulphuric acid with a concentration of $[H^+] = 4$ mol/dm^3 are injected in the tank. The concentrations of the borate-iodide-iodate solution are the following:

$$[I_2]_{potential} = 3[IO_3^-]^i = \frac{3}{5}[I^-]^i = 7 \cdot 10^{-3} \text{ mol/dm}^3$$

$$[H_3BO_3]^{i,\,tot} = 0.1818 \text{ mol/dm}^3 \quad [NaOH]^i = 0.0909 \text{ mol/dm}^3$$

where $[I_2]_{potential}$ is the maximum total concentration of iodine that can be obtained at complete conversion and the concentrations of the iodide and iodate ions follow the stoichiometry of reaction 4.2. As the concentration of sodium hydroxide is half that of orthoboric acid, then H_3BO_3 and $H_2BO_3^-$ are present in equal concentrations:

$$[H_3BO_3]^i = [H_2BO_3^-]^i = 0.0909 \text{ mol/dm}^3$$

with this condition the theoretical pH of the buffer solution (before adding the iodide and iodate ions) is 9.14, where pH = pK_1 and K_1 is the first dissociation constant of orthoboric acid.

For the extension of these conditions to continuous systems, the ratio of the molar flow rates of the reagents should equal the ratio of number of moles for a batch reactor:

$$\left(\frac{n^i\,(I_2)_{potential}}{n^i\,(H^+)}\right)_{batch} = \left(\frac{Q_{sol}[I_2]^i}{Q_{H^+}[H^+]^i}\right)_{continuous} \tag{4.7}$$

$$\left(\frac{n\,(H_2BO_3^-)}{n\,(H^+)}\right)^i_{batch} = \left(\frac{Q_{sol}[H_2BO_3^-]}{Q_{H^+}[H^+]}\right)^i_{continuous} \tag{4.8}$$

where Q_{sol} and Q_{H^+} are the borate-iodide-iodate and acid volumetric flow rates respectively.

Guichardon and Falk give an example of the concentrations that are obtained when the ratio between the solution volumetric flow rate and the acid volumetric flow rate equals 10. In this case, the concentrations of the reagents are:

$$[I_2]_{potential} = 3[IO_3^-]^i = \frac{3}{5}[I^-]^i = 2.1\cdot 10^{-3} \text{ mol/dm}^3$$

$$[H_3BO_3]^{i,\,tot} = 0.5 \text{ mol/l} \quad [NaOH]^i = 0.25 \text{ mol/dm}^3$$

$$[H^+]^i = 0.18 \text{ mol/dm}^3$$

the orthoboric acid and sodium hydroxide concentrations then give:

$$[H_3BO_3]^i = [H_2BO_3^-]^i = 0.25 \text{ mol/dm}^3$$

with the pH of the buffer solution once again equal to 9.14.

For different ratios R_v between the solution and the acid volumetric flow rate:

$$R_v = \frac{Q_{sol}}{Q_{H^+}} \tag{4.9}$$

the following conditions are suggested by Guichardon and Falk:

$$\left(\frac{Q_{sol}[I_2]}{Q_{H^+}[H^+]} \right)^i_{continuous} = \text{constant} \tag{4.10}$$

$$\left(\frac{Q_{sol}[H_2BO_3^-]}{Q_{H^+}[H^+]} \right)^i_{continuous} = \text{constant} \tag{4.11}$$

as defined in case of $R_v = 10$.

In this case, with $R_v = 1$ the conditions on the concentration values became:

$$\frac{[I_2]^i_{potential}}{[H^+]} = 0.11667 \tag{4.12}$$

$$\frac{[H_2BO_3^-]^i}{[H^+]} = 13.8889 \tag{4.13}$$

which, with the same initial concentration of potential iodine used for the case $R_v = 10$ gave:

$$[I_2]^i_{potential} = 2.1 \cdot 10^{-3}\ mol/dm^3$$
$$[H^+]^i = 1.8 \cdot 10^{-2}\ mol/dm^3$$
$$[H_2BO_3^-]^i = 0.25\ mol/dm^3$$

where the concentration of the acid is ten times less than in the case $R_v = 10$.

Choosing $[H^+] = 0.02\ mol/dm^3$, (acid in this concentration was easier to prepare by dilution of a concentrated batch), the following concentrations were obtained:

$$[I_2]^{i}_{potential} = 2.3334 \cdot 10^{-3} \text{ mol/dm}^3$$

$$[H_3BO_3]^{tot,\,i} = 5.5556 \cdot 10^{-1} \text{ mol/dm}^3 \quad [NaOH]^{i} = 2.7778 \cdot 10^{-1} \text{ mol/dm}^3$$

and

$$[H_3BO_3]^{i} = [H_2BO_3^-]^{i} = 2.7778 \cdot 10^{-1} \text{ mol/dm}^3 .$$

4.5.2 Preliminary experiments: tests on the sulphuric acid concentration

The concentrations determined in the previous section were used to carry out a series of preliminary experiments to test the sensitivity of the method for the narrow channel reactors. The borate-iodide-iodate solution was prepared by dissolving the following amounts of solid reagents in deionised water:

27.48 g of H_3BO_3 (from Aldrich, ACS reagent) in 650 cm^3 of deionised water
8.88 g of NaOH (from Aldrich, ACS reagent) in 50 cm^3 of deionised water
516 mg of KI (from BDH, analar reagent) in 50 cm^3 of deionised water
133 mg of KIO_3 (from BDH, GPR) in 50 cm^3 of deionised water.

In this way 800 cm^3 of solution were prepared. The boric acid had to be dissolved in a higher amount of water in order to not go over its solubility limit. The sodium hydroxide solution was added to the orthoboric acid solution to form the buffer solution to which the potassium iodide and the potassium iodate solutions were added. The flow rates used for the preliminary experiments in the narrow channel reactor system are listed in Table 4.2, which also reports the outlet pH and temperatures. The first batch of buffer solution had a pH of 9.28 at a temperature of 23.6°C. The outlet pH was very close to the pH of the buffer solution, therefore indicating that no iodine had formed. Samples at the narrow channels outlet were clear and analysis with the UV-vis spectrometer confirmed that no peak could be detected.

The concentration of sulphuric acid was then gradually increased. For a concentration of $[H^+] = 0.1$ mol/dm^3, no change in colour was detected for one experiment with reactor A in the outlet solution, indicating that the concentration of iodine, if present,

Table 4.2. Preliminary experiments in the narrow channel reactors ($[H^+] = 0.02$ mol/dm^3).

Reactor	Q_{out} (cm^3/s)	pH_{out}	T_{out} (°C)
A	0.15	9.21	20.9
A	0.43	9.23	20.9
B	0.43	9.25	21.3
B	0.43	9.27	20.9

would be very low. In this case the flow rate used was 0.43 cm^3/s and the outlet pH was 8.7 at a temperature of 20.0°C. The sulphuric acid concentration was then increased to 0.1 mol/dm^3 ($[H^+] = 0.2$ mol/dm^3). This concentration proved to give enough sensitivity to represent the change in mixing efficiency obtained between channel size and varying flow rate. With this acid concentration, the H^+ ions were still in less than stoichiometric amount in respect to the borate ions. The outlet pH of the solution was for each set of operating parameters higher then 7, therefore respecting the condition on pH^* given by Guichardon and Falk (this condition was considered as a reference value even if the concentration of potential iodine used in this case was slightly different from the one suggested by them).

4.5.2 Experimental procedure

Once the sulphuric acid concentration was determined, at least three repetitions for each experiment were carried out. The concentrations of orthoboric acid, sodium hydroxide, potassium iodide and potassium iodate used were the same as indicated in the previous section for the preliminary experiments. Fresh solutions were prepared every day and the pH of the buffer solution was in all cases between 9.2 and 9.4 at temperatures between 20°C and 25°C. The addition of the potassium iodide and potassium iodate solutions did not alter the pH and temperatures significantly. The experiments were carried out at ambient conditions at temperatures close to 20°C. The pH of the reaction product varied between 7.06 and 7.31. Reactors were flushed with deionised water after each experiment. The collected product was analyzed in a UNICAM 8700 UV-vis spectrometer using 2.5 cm^3 volume disposable PMMA (poly methyl methacrylate) cuvettes from Kartell. Each sample was analyzed within 2 minutes from the conclusion of the experiment.

4.6 Calculation of the results

4.6.1 Calculation of the triiodide ion and iodine concentration

A UV-vis spectrometer measures the amount of energy in the UV or visible spectrum that a sample subjected to radiation transmits. The radiant power P is defined as the energy of radiation impinging on the unit area of a detector in the unit of time (Skoog et al., 1992, p.518). The fraction of the power transmitted by a sample with respect to the power of the incident beam is called the transmittance, E:

$$E = \frac{P}{P_o} \tag{4.14}$$

The spectrophotometer used gave readings in terms of absorbance A, defined in the following way:

$$A = -\log_{10} E = \log_{10} \frac{P_o}{P} \tag{4.15}$$

where both the transmittance and the absorbance are dimensionless.

From the absorbance value the concentration of the solute can be calculated from the Beer-Lambert law, written for the triiodide ion:

$$[I_3^-] = \frac{A}{\varepsilon_M l} \tag{4.16}$$

where ε_M (m^2/mol) is the molar extinction coefficient or molar absorptivity and l (m) is the optical path length, which corresponds to the length of the side of the cuvette exposed to the radiation.

The Beer-Lambert law adequately describes absorption behaviour of solutions at low concentrations. For concentrations above 0.01 mol/dm^3 (Skoog et al., 1992, p.523), the interactions between the particles of the absorbing species can become significant and the linear relationship between concentration of the absorbing species and

absorbed energy might loose validity. For the measurements carried out, the highest triiodide ion concentrations calculated were of the order of 10^{-5} mol/dm^3 and therefore the Beer-Lambert law was valid.

The concentration of triiodide ion was determined from the intensity of absorption for the peak around 352 nm, as indicated by all authors who studied the iodide-iodate reaction system. In this case $l = 1 \cdot 10^{-2}$ m and the value used for the molar extinction coefficient was 2590 m^2/mol (Custer and Natelson, 1949 cited by Guichardon and Falk, 2000a). Once the triiodide ion concentration was known, the iodine concentration could be calculated taking into account equilibrium 4.3. Palmer et al. (1984) gave the equilibrium constant K as a function of temperature:

$$\log_{10} K = \frac{555}{T} + 7.355 - 2.575 \log_{10} T \qquad (4.17)$$

where K is expressed in dm^3/mol and T in K.

In all cases the value of K obtained for a temperature of 293.16 K was considered. The mass balance of iodine in all its forms, leads to the following second order equation, reported by Guichardon and Falk (2000a):

$$-\frac{5}{3}[I_2]^2 + \left[[I^-]^i - \frac{8}{3}[I_3^-]\right][I_2] - \frac{[I_3^-]}{K} = 0 \qquad (4.18)$$

from which the I_2 concentration can be calculated.

Equation 4.18 has two roots, $[I_2]_+$ and $[I_2]_-$:

$$[I_2]_\pm = \frac{3KD \pm \sqrt{9K^2D^2 - 60K[I_3^-]}}{10K} \qquad (4.19)$$

where D is defined as follows:

$$D = \left[[I^-]^i - \frac{8}{3}[I_3^-] \right] \qquad (4.20).$$

Of the two solutions of the equation, $[I_2]_+$ is chosen because it fulfils the condition $[I_2] < [I_3]$, which implies that the equilibrium is shifted to the right.

As the analysis of the samples by UV-vis spectrometry was carried out after typically 90 seconds from the end of the experiments, the possibility of reactions further continuing between the reactor outlet and the time of analysis was taken into account. It was considered that, as the outlet pH was in all cases very close to 7, most of the $[H^+]$ ions had been consumed and reactions 4.1 and 4.2 would not be significant in these conditions. The triiodide ion concentration could change according to reaction 4.3. Consideration of the kinetics of this reaction, from the data reported by Guichardon et al. (2000), showed that for the iodide ions concentration used in this work (of the order of 10^{-3}M), which is in high excess of the concentrations of I_2 and I_3^-, the reaction rates for the formation and the decomposition of the triiodide ion are of the same order. Moreover it should be considered that the calculation of the segregation index, which was considered as the parameter indicating mixing efficiency, takes into account the total concentration of iodine formed, both as I_2 and I_3^-, as from equation 4.6, so further reaction of iodine to triiodide ion or, vice versa, dissociation of I_3^-, would not change the results.

4.6.2 Calculation of the segregation index

The calculation of the segregation index was carried out according to equation 4.4 and calculating the selectivity in the total segregation and in the general case from equations 4.5 and 4.6 respectively. In applying equation 4.6, the ratio of the molar flow rates rather than the ratio of number of moles was considered, as the system was continuous. The selectivity was calculated with the equation:

$$Y = \frac{2Q_{out}([I_2]+[I_3^-])}{Q_{in}[H^+]^i} \qquad (4.21)$$

where Q_{out} (cm^3/s) is the outlet volumetric flow rate and Q_{in} (cm^3/s) is the inlet one.

As the outlet flow rate is double the inlet value, equation 4.21 becomes:

$$Y=\frac{4([I_2]+[I_3^-])}{[H^+]^i} \tag{4.22}$$

from which the segregation index was calculated.

4.7 Results and discussion

As previously mentioned, each experiment was repeated at least three times, depending on the scatter of the data. In the results reported averages of the segregation index calculated for each repetition were considered. For reactor B the results were satisfactorily reproducible, with a standard deviation lower than 10% of the average value. The results for reactor A were instead less reproducible, with a standard deviation around 20% of the average value. However, since the procedure was exactly the same as for reactor B, any systematic source of error affecting one series of experiments would affect the other. Therefore, averaging the results is sufficient to guarantee valid information, considering that these data are not used to quantify mixing times.

Figure 4.5 shows the segregation index at varying flow rate for both reactors A and B, for all flow rates tested. Improved mixing is achieved at increasing flow rate in both cases and reactor B gives better mixing than reactor A, for the whole range of flow rates common to both reactors. In order to have a complete characterization of the mixing efficiency in the narrow channels, the variation of the segregation index as a function of the parameters that depend on flow rate and channel size was examined. Particularly, the mean velocity, the mean residence time and the Reynolds number in the channel were considered. This characterization, although does not add new information from a fluid dynamics point of view, can prove useful in the design stage to define the desired characteristic dimension taking into account the desired throughput.

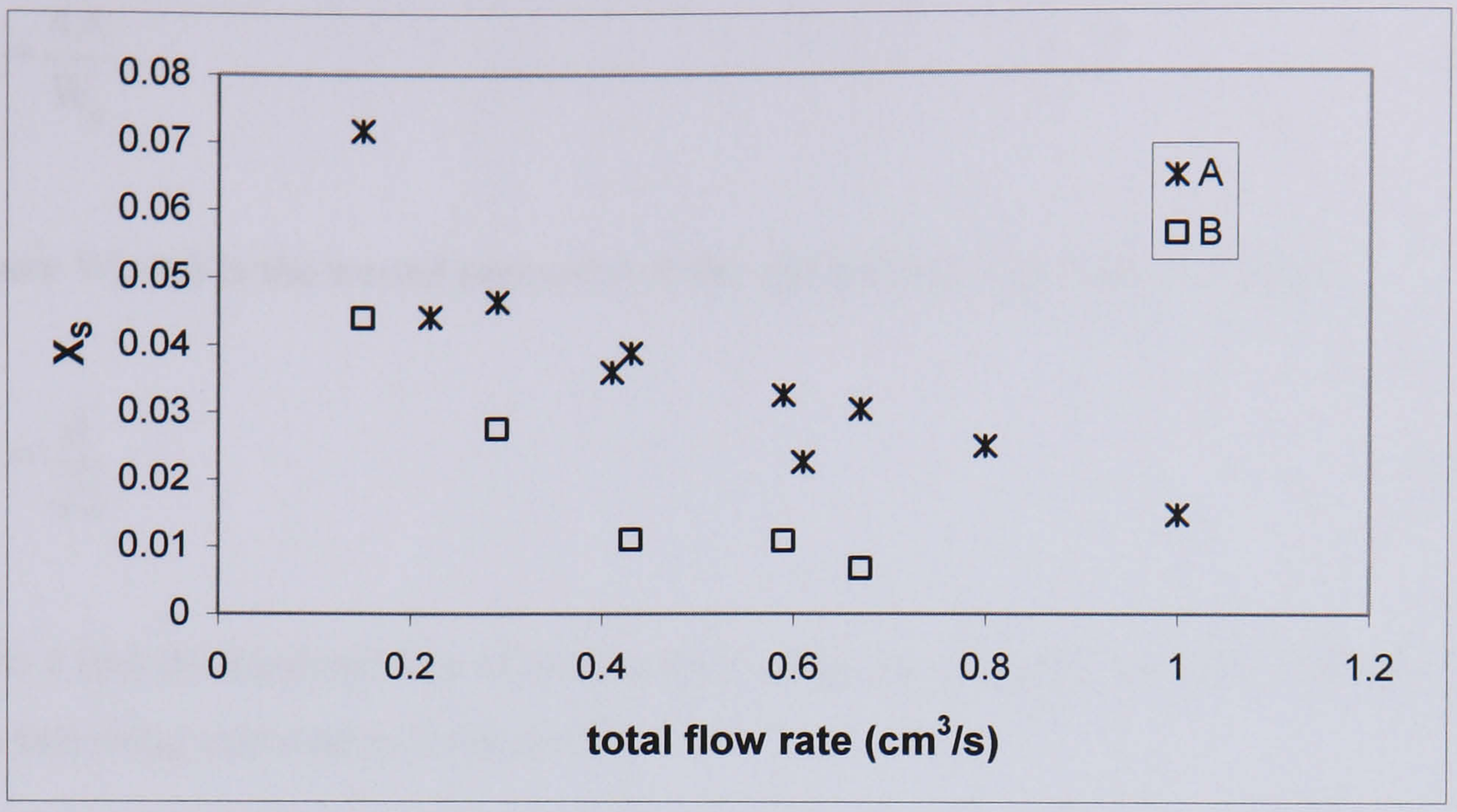

Figure 4.5. Segregation index vs. flow rate for both narrow channels.

The velocity in the channels was calculated from the total outlet flow rate and both the velocity and the Reynolds number refer to the part of the channel in the Perspex module. The mean velocity is given by:

$$u_L = \frac{Q_{out}}{S_{NCR}} \tag{4.23}$$

where S_{NCR} (m^2) is the cross section of the channel reactor.

For a non-circular channel, the Reynolds number is calculated from the following expression:

$$Re = \frac{\rho d_h u_L}{\mu} \tag{4.24}$$

where d_h (m) is the hydraulic diameter of the channel, and ρ (Kg/m^3) and μ (Pa s) are the fluid density and viscosity respectively.

As a first approximation, the density and viscosity of water at 20° C were used. The hydraulic diameter is given by (Darby, 2001, p.195):

$$d_h = \frac{4A}{W_p} \tag{4.25}$$

where W_p (m) is the wetted perimeter of the channel and for a square channel:

$$d_h = \frac{d}{\sqrt{2}} \tag{4.26}$$

with d (m) the diagonal line of the channel. Combining equations 4.23, 4.24 and 4.26 the following expression is obtained:

$$Re = \sqrt{2}\,\frac{\rho}{\mu}\,\frac{Q_{out}}{d} \tag{4.27}$$

in which Reynolds number is expressed as a function of the achieved throughput and the manufacturing characteristic dimension.

Figure 4.6 shows how the segregation index varies with changing mean velocity for both reactors. By considering the data obtained for the two lowest flow rates for reactor B, for which the velocity varies approximately between 0.3 m/s and 0.6 m/s, the segregation ratio for the 2·mm channel is lower than the one for the 1·mm one. These data correspond to flow rates of 0.15 cm^3/s and 0.29 cm^3/s for reactor B and flow rates between 0.61 cm^3/s and 1 cm^3/s for reactor A. The opposite trend to that of Figure 4.6 is obtained reporting the segregation index versus residence time (Figure 4.7).

Residence time in the channel is given by the ratio of the channel volume and the volumetric flow rate:

$$\tau = \frac{V}{Q_{out}} \tag{4.28}.$$

If for the volume only the Perspex block is considered, as the defined mean velocity refers to this part of the channel, then:

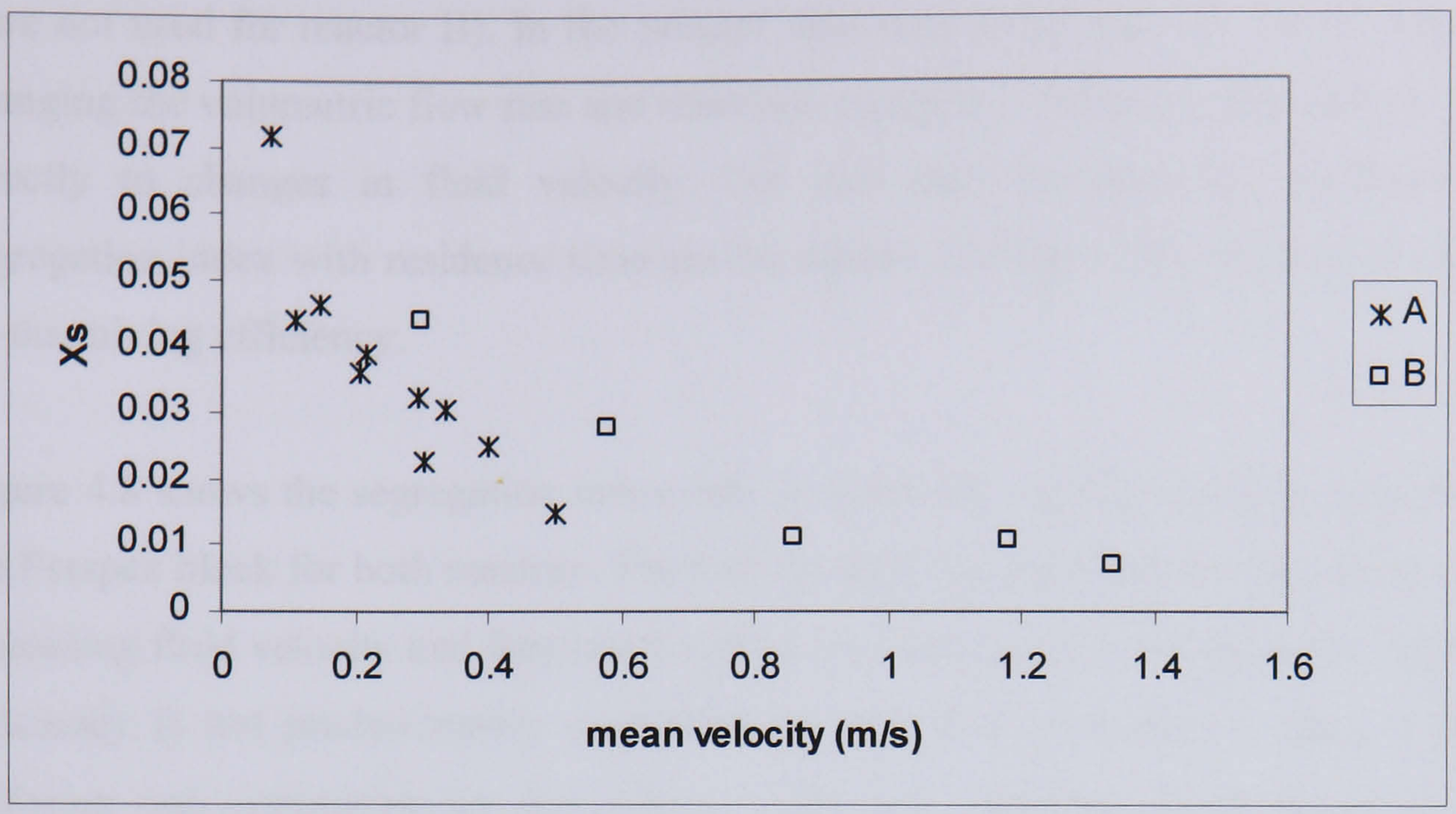

Figure 4.6. Segregation index vs. mean velocity in the channel.

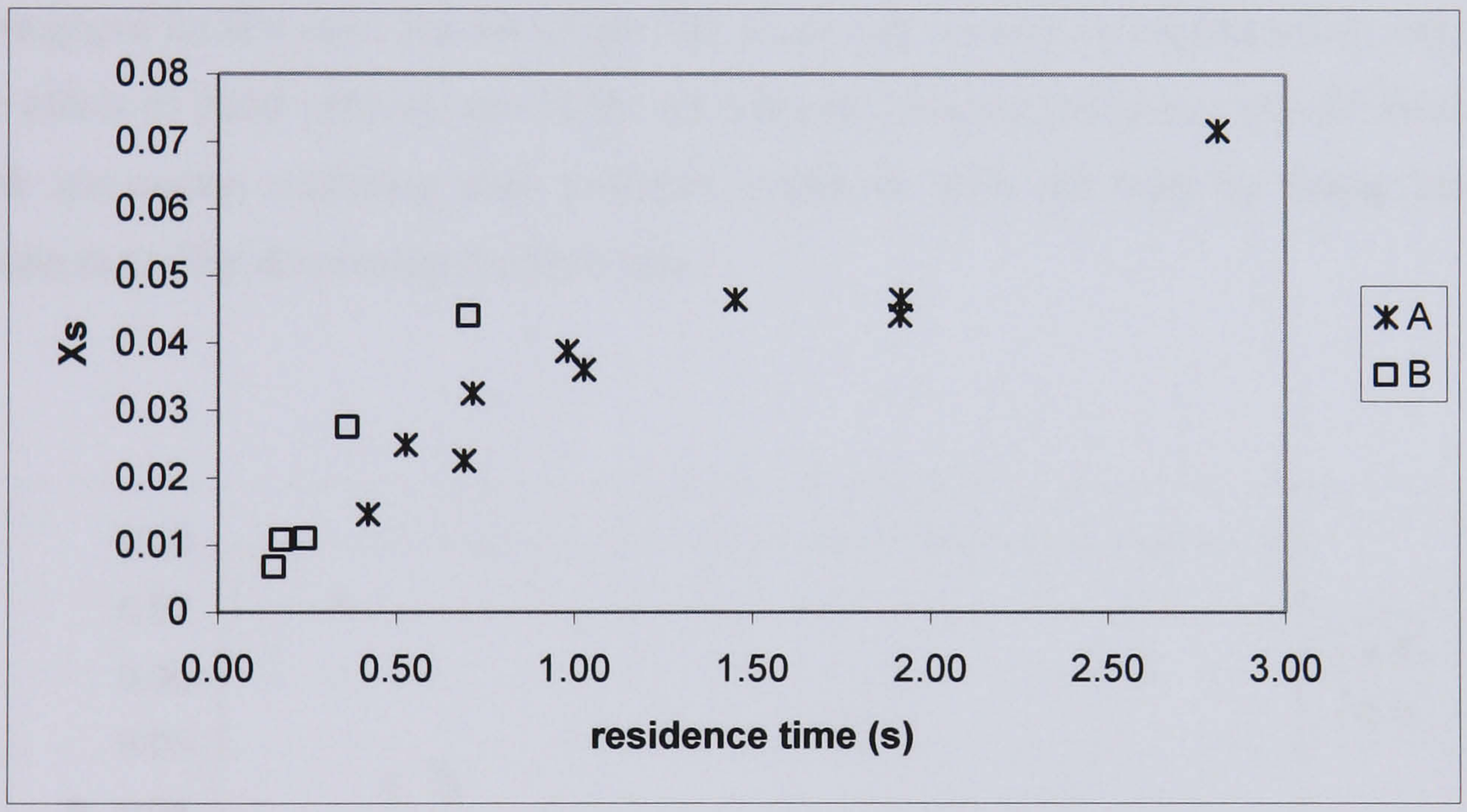

Figure 4.7. Segregation index vs. residence time.

$$\tau_c = \frac{L}{u_L} \tag{4.29}$$

where L (m) is the extension of the channel in the Perspex block. From equation 4.29, it can be seen that residence time in reactor B is 4 times lower than that in reactor A, for the same flow rate through both reactors. This is due to the mean velocity being four times higher in the 1 mm channel. In figure 4.7 the lowest residence times for reactor A are obtained for the highest flow rates used in the 2 mm channel (which

were not used for reactor B). In the present case residence time was varied only by changing the volumetric flow rate and therefore changes in residence time correspond directly to changes in fluid velocity. For this case therefore the variation of segregation index with residence time can be related directly to the effect of velocity on the mixing efficiency.

Figure 4.8 shows the segregation index data as a function of the Reynolds number in the Perspex block for both reactors. The fact that the segregation index decreases with increasing fluid velocity and Reynolds number for both reactors indicates that mixing efficiency is not predominantly controlled by diffusion processes. In fact, if only diffusion was responsible for the mixing of the two solutions, its efficiency would depend only on the diffusion path length, which is a function of channel size (Ehrfeld et al., 1999). In these conditions, increasing the fluid velocity by increasing the throughput for the same reactor should not lead to an increase in mixing efficiency. As the effect of fluid velocity would be not relevant, mixing efficiency should increase with increasing residence time and this could be achieved both by using longer channels and by decreasing the flow rate.

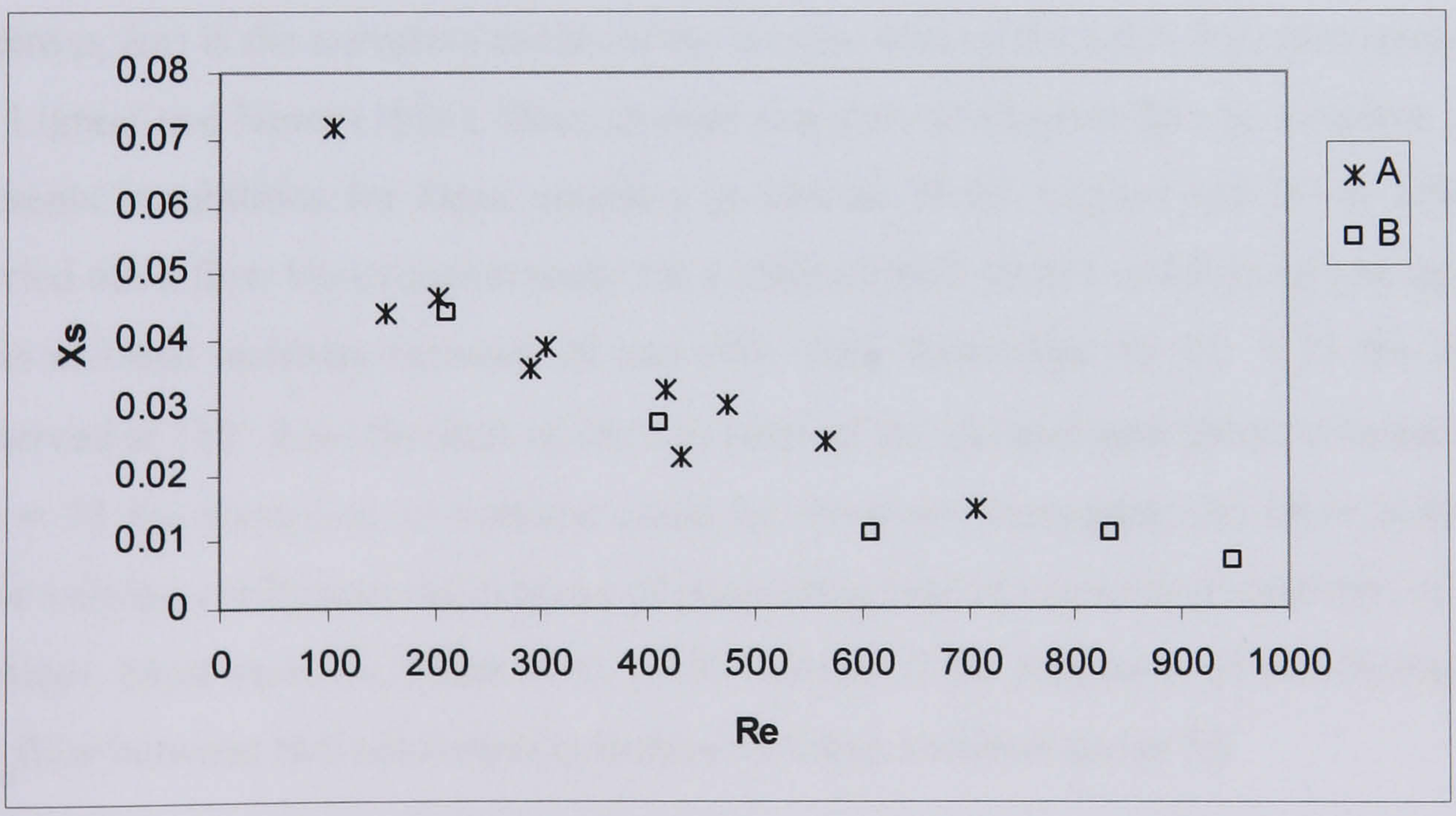

Figure 4.8. Segregation index vs. Reynolds number.

A specific aspect that can be looked at in relation to the effect of fluid velocity on mixing efficiency is the contribution of the flow configuration in the bends of the channel to the mixing process. It has been shown, as reported by Ligrani and Niver (1988), that in many applications curved surfaces can impose instabilities on the flow even at relatively low Reynolds numbers. In the flow trough a channel, if the fluid encounters a bent surface, the fluid layers closer to the concave wall move faster than those close to the convex wall. The fluid is then subjected to centrifugal forces of different intensity in different areas of the channel. This causes the formation of vortices that can affect transport phenomena in the channel and cause a deviation from classical laminar flow behaviour.

The effect of channel curvature on flow configuration is usually studied and quantified using the Dean number, which is proportional to the Reynolds number and to the ratio between centrifugal forces and inertial forces. The Dean number has the following expression:

$$De = Re\sqrt{\frac{d_h}{\rho_c}} \tag{4.30}$$

where ρ_c (m) is the curvature radius of the convex wall of the bend. As again reported by Ligrani and Niver (1988), Dean showed that curved channel flow in a narrow gap presents instabilities for Dean numbers as low as 35.92. Ligrani and Niver (1988) carried out a flow visualization study for a channel with 40 to 1 width to height aspect ratio at Dean numbers between 20 and 500. They found that for $De < 73$ the flow observed at 115° from the start of the curvature of the channel was stable, whereas for $De = 73$ the formation of vortices could be observed. Increasing the Dean number gave varying configurations in terms of geometrical and dynamic characteristics of the vortices. More recently, Aider et al. (2005) observed the formation of instabilities in the flow between two concentric cylinders for Dean numbers above 58.

For this study, Dean numbers varied between 63 and 420 for reactor A and between 84 and 376 for reactor B. The ratio between Reynolds and Dean number was 2.6 for the 1 mm channel and 1.7 for the 2 mm channel. It appears that for most operating conditions, the Dean numbers would lie in the range correspondent to the formation of

vortices, according to the studies reported in the literature. The vortex formation as a consequence of the fluid transiting through the bends, could have a significant influence in determining the final degree of mixing in the narrow channel reactors. The extent of the bends in the channels only constitutes less then 10 % of the entire length, however the vortex formation in a bend would affect the flow configuration in the straight part of the channel following the bend itself, therefore giving rise to instabilities in the flow for a higher portion of the channel. The Reynolds number values obtained for the NCRs, which are on the higher end of the range correspondent to laminar flow, would indicate that instabilities generated in the flow would be less likely to be dampened than in what could be the case at very Reynolds numbers (of the order of a few units for example). It can then be concluded that the enhanced mixing efficiency obtained at increasing velocities in the NCRs can be attributed to the combination of the flow characteristics themselves and to the centrifugal enhancement to mixing provided by the bends in the channels.

4.8 Experimental procedure and operating conditions for the precipitation study

Precipitation of calcium carbonate from reacting two aqueous solutions was carried out using calcium nitrate and sodium carbonate as reagents. This chemical system has been widely reported in the literature and it allows a wide range of supersaturations. As seen earlier, a series of preliminary experiments were carried out at various concentrations in the narrow channel reactor system to evaluate pressure drop effects and for the flow rate calibration. The study on the flow rates was aimed at obtaining the highest flow rates possible in order to have high velocities of the suspension in the channels and therefore limit scaling phenomena.

Once the flow rates were chosen, a large number of experiments were carried out to find the correct procedure for particle size analysis. The principal aim of the investigation on liquid phase precipitation was to evaluate the effect of hydrodynamic parameters on particle size and particle size distribution (PSD). This explains the importance of finding the correct procedure for particle size analysis. The main problem was trying to minimize aggregation and/or agglomeration of the particles between the end of the reaction and the analysis itself. A brief description of the different techniques tested is presented in Appendix B.

After defining the procedure for particle size analysis, experiments were carried out in both channels at two different concentrations S = 2000 and S = 4000, were S is defined by equation 2.4 and, for calcium carbonate, has the expression:

$$S = \left(\frac{[Ca^{2+}][CO_3^{2-}]}{K_{SP}} \right)^{1/2} \qquad (4.31).$$

Reagent solutions were prepared dissolving solid $Ca(NO_3)_2 \cdot 4H_2O$ (GPR, 98% purity) and Na_2CO_3 (GPR, 99% purity), both from BDH, in deionised water. Fresh solutions were prepared each time a new set of experiments was carried out, which usually corresponded to five runs at different flow rates. Experiments were carried out at ambient conditions and temperature of the solutions varied between 16°C and 20°C. In each case, the outlet suspension was collected in a beaker to which 1 cm^3 of 0.1 % weight sodium hexametaphosphate aqueous solution was added to prevent aggregation of the particles before particle size analysis. Sodium hexametaphosphate is a commonly used surfactant and it is recommended by the manufacturer of the particles size analyzer, Malvern Instruments, for dispersing calcium carbonate in water.

Particle size analysis was carried out within 2 minutes from the end of the experiment in a Malvern Mastersizer 2000, which uses laser diffraction characterization. The calcium carbonate suspension was kept in a mixed state during the time between the end of the experiment and the analysis by using a magnetic stirrer. The interval between the run and analysis corresponded to the time in which the instrument aligned the laser and a background reading of the solvent was taken. The procedure for particle size analysis consisted of adding a small amount of slurry (usually a few cm^3) to a vessel contained in the analyzer (the dispersion unit) filled with deionised water. The laser beam then impinged on the slurry and the amount of transmitted energy could be related to the volume distribution of the particles. A measurement was considered acceptable only if an uncertainty parameter returned by the instrument indicated that the difference between the measured and the calculated distribution was lower than 1.5 %. In those cases for which the difference was higher than this value, a new measurement with more sample from the same run was taken until the reading was considered acceptable. If a too long time between the run and the analysis had

elapsed or the sample had been all consumed, a new experiment with the same conditions was repeated immediately and a new measurement was carried out. More details on the principles of particle size analysis by laser diffraction can be found in Appendix B.

The reactors were flushed with 0.1 M HCl and deionised water after each run. They were also emptied of the remaining water before each experiment, so as not to dilute the reacting solutions.

Determination of the conversion of the reaction was carried out for the supersaturation S = 4000. The technique adopted consisted of collecting a certain amount of slurry from the reactor (from more than one experiment), separating the particles from the mother liquor by micro filtration and then drying and weighing the solid. Micro filtration was carried out using 0.45 μm pore size, 47 mm diameter cellulose nitrate filter paper and the particles were dried at 60° C. A precision balance was used to weigh the solid.

Two powder samples (one for each reactor), obtained for a supersaturation ratio of S = 4000 and at a flow rate of 0.43 cm^3/s were analyzed by scanning electron microscopy (SEM) and X-ray (powder) diffraction (XRD) to obtain information about the morphology and the crystalline structure of the precipitated calcium carbonate, respectively. The instruments used in the two cases were a JEOL JSM 5300 and a Philips XPert MPD diffractometer. SEM samples were gold coated prior to analysis. The dry precipitate was obtained as in the case of conversion determination. Some dry powder and slurry samples were also studied by optical microscopy, images of the particles were collected by connecting the microscope to a Philips ToUcam USB PC camera.

Limited benchmarking tests were carried out in small stirred vessels. In this case one of the reagent solutions was placed in the vessel and mixed. The other solution was then added while the liquid was kept in a mixed state. Particle size analysis was carried out at least four times for each batch reaction (at different time intervals from the addition of the two reagents).

4.9 Particle morphology and crystalline structure

As seen in Chapter 2, calcium carbonate is a substance that exhibits polymorphism. When calcium carbonate is obtained by precipitation, all three forms can be found, this is especially valid for the precipitation from two solutions. Many studies on precipitation of calcium carbonate from two solutions carried out at ambient conditions reported the precipitation of an amorphous phase at first, amorphous calcium carbonate (ACC), which then converted into the different crystalline forms or a mixture of them, depending on the operating conditions. Disappearance of the amorphous phase and growth of crystalline phases has been studied by Kawano et al. (2002). The possibility of detecting the different stages of the precipitation process from a crystalline structure point of view depends on the availability of instrumentation with detection times lower than the time scales involved in the transformation. Alternatively, special experimental procedures have to be adopted in order to delay the transformation (Kabasci et al., 1996).

Precipitation of calcium carbonate from two solutions at ambient conditions usually leads to a mixture of calcite and vaterite. The most common shape of calcite crystals is cubic and vaterite usually appears as spherical or disc like crystals. Vaterite tends to convert to calcite and the transformation is generally favoured by contact of the crystals with the original mother liquor. Ogino et al. (1987), found a mixture of vaterite and calcite between 14° C and 30° C and a mixture of calcite and aragonite between 60° C and 80° C when reacting calcium chloride and sodium carbonate solutions. They attributed the transformation of vaterite to calcite to a mechanism of dissolution of the metastable polymorph and growth of the stable one. A mixture of calcite and vaterite in different ratios was observed at varying operating conditions by Kabasci et al. (1996) when mixing calcium nitrate and sodium carbonate solutions in a Tee-Mixer and in a high efficiency Mixing chamber in the batch precipitation of calcium carbonate. These authors also observed the gradual transformation of vaterite to calcite from SEM micrographs of samples taken at different time intervals from the mixing of the reagents. Kitamura (2000) studied the precipitation of calcium carbonate in a stirred tank by reacting solutions of sodium carbonate and calcium chloride. Influence of concentration and addition rate of Na_2CO_3 solution on the amount of vaterite precipitated after disappearance of the amorphous phase was studied and the

presence of magnesium ion was found to inhibit the transformation of vaterite to calcite. Many other studies have been carried out in order to evaluate the influence of different additives on the appearance of the polymorphs of calcium carbonate. Different polymorphs might in fact present different suitability for specific applications.

In this case the slurry at the reactor outlet was collected for more than one experiment, this was in order to have enough powder, both for XRD and SEM, as the two analyses were carried out on the same samples. The collection procedure lasted about 30 minutes in each case. As previously mentioned, the slurry was then filtered and the particles dried. No information can then be gathered in this case on the transformations occurring from the onset of precipitation to the filtering and drying of the samples. X-ray diffraction patterns for the two analyzed samples show a mixture of calcite and vaterite in both cases, particularly 61% calcite and 39% vaterite were found in the sample from reactor A and 82% calcite and 18% vaterite in the one from reactor B. The percentages of the two polymorphs were determined by evaluating the relative intensity of the peaks in each sample and the intensity of the characteristic peaks in the pure phases. The uncertainty of this determination is around 5%. X-ray diffraction patterns for the samples analyzed and the ones used as references for the pure phases are reported in Appendix C.

Figure 4.9 shows an SEM micrograph for the sample relative to reactor A, while Figure 4.10 shows an SEM micrograph for reactor B (both images correspond to a 500 fold magnification). A mixture of spherical and cubic particles can be seen in both images, confirming the presence of calcite and vaterite in the samples. Similar images, showing particles of the two shapes, have been reported by Kabasci et al. (1996) and Zauner and Jones (2000), referring to studies on liquid phase precipitation of calcium carbonate. Zauner and Jones (2000) obtained a mixture of calcite and vaterite in the precipitation of calcium carbonate in a semi-batch reactor. This material was found in the samples collected at the end of the reaction. However, if the particles were left in contact with the original solution for many hours, only cubic crystals could be detected in the final product, indicating that all the particles precipitated as vaterite had converted to calcite.

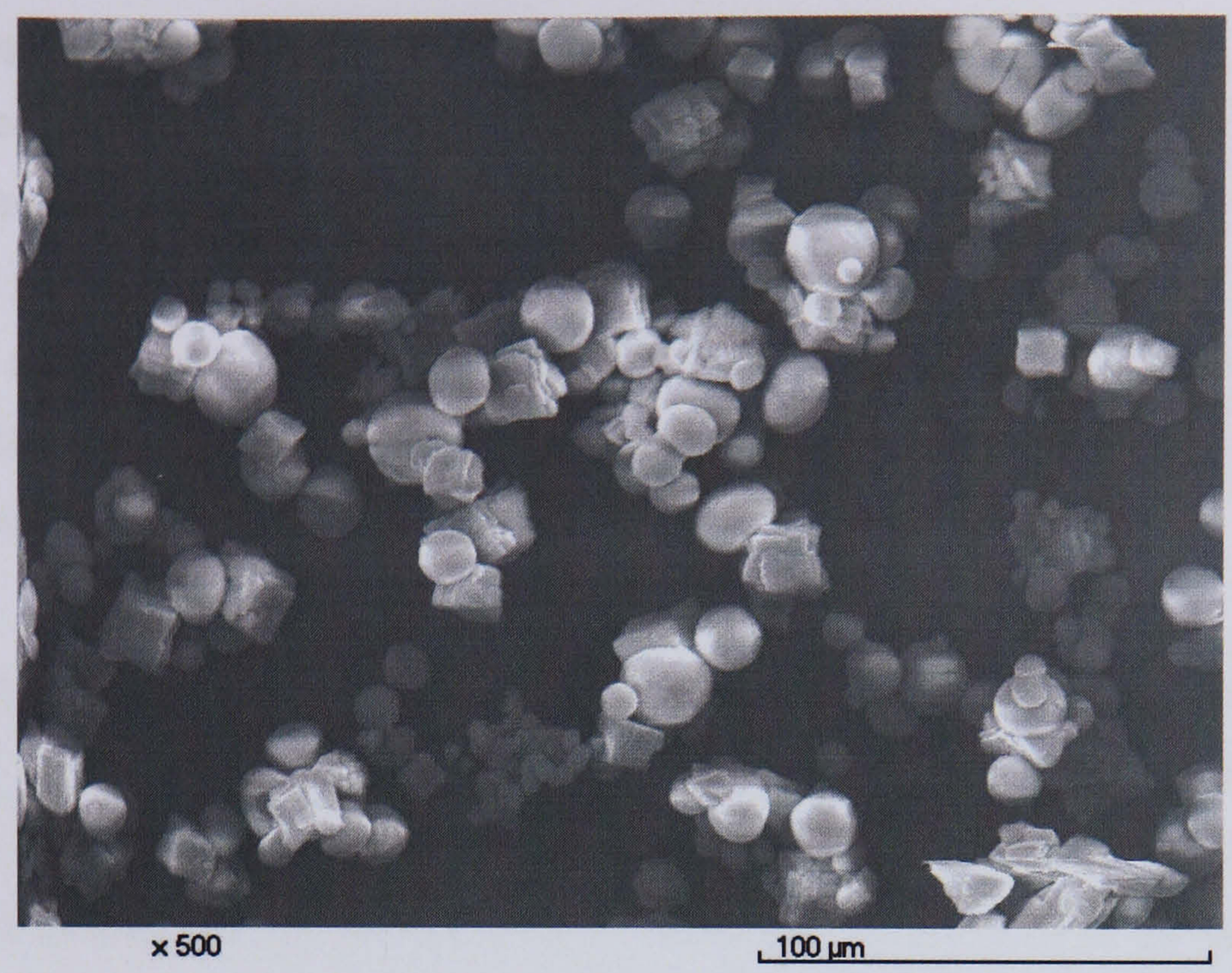

Figure 4.9. SEM micrograph (× 500) for reactor A (Q_{out} = 0.43 cm^3/s).

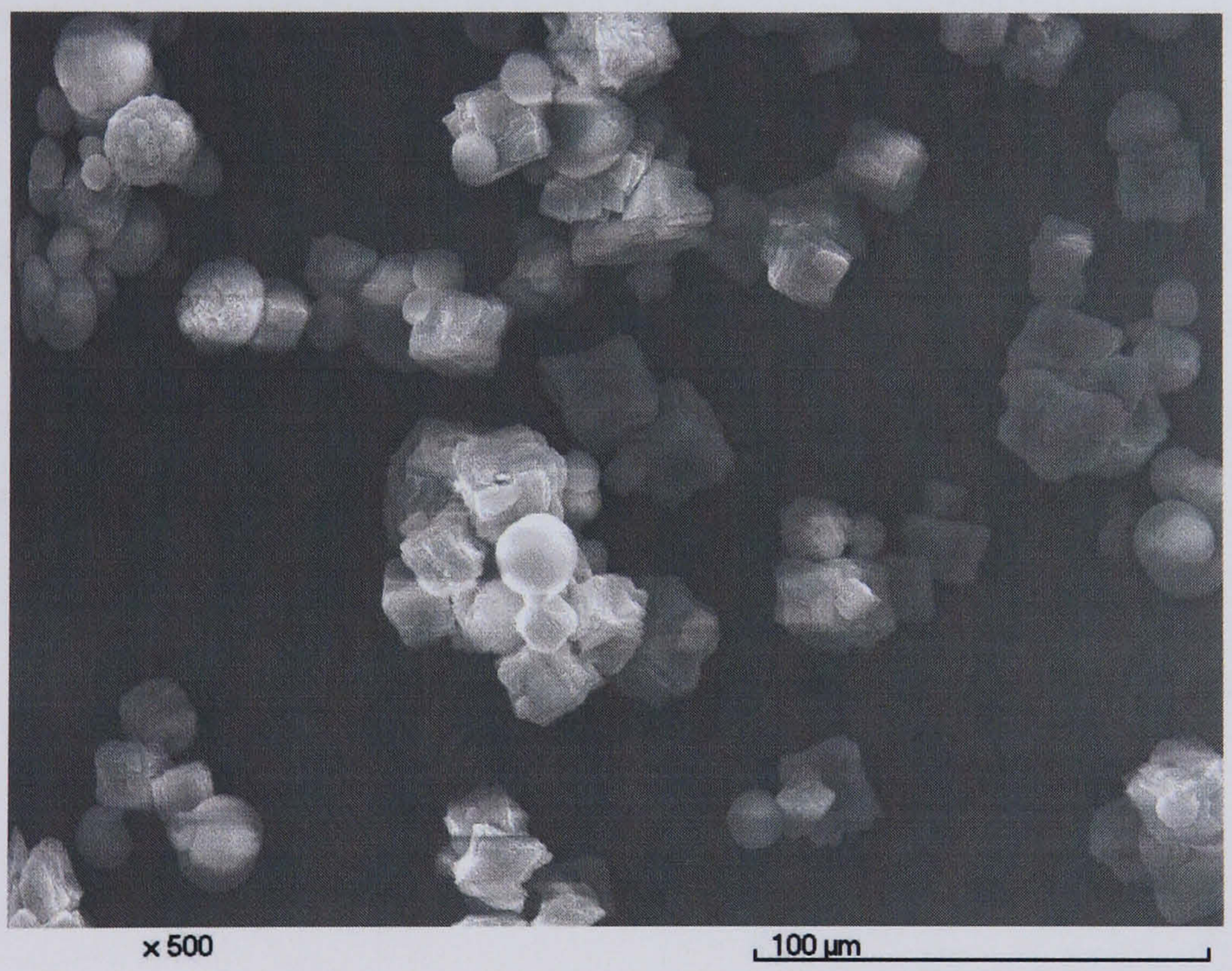

Figure 4.10. SEM micrograph (× 500) for reactor B (Q_{out} = 0.43 cm^3/s).

The two experiments from which powder for SEM and XRD had been prepared were then repeated and the precipitate was left in contact with the original solution from the reaction. Small portions of the slurry were placed on a microscope slide, then dried at 60°C and viewed under the optical microscope at different time intervals from the end of the reaction. This procedure was carried out to try to detect the change in

morphology of the particles. Samples viewed a few minutes after the reaction had taken place appeared to consist mostly of spherical particles. Samples viewed after 24 hours from the end of the experiment seemed to show the presence of cubic and spherical particles. After 48 hours in contact with the mother liquor, the samples appeared to be formed only by cubic particles. An image collected with the video camera after 48 hours from the end of the reaction for the sample relative to reactor B can be seen in Figure 4.11.

Zauner and Jones (2000) observed that the surface of the calcite particles which grew after the dissolution of vaterite was quite irregular. Kinks on the surface were considered sites on which growth of the stable polymorph had taken place. Calcite crystals originally formed in this structure exhibited a very smooth surface. In this case, the calcite particles that can be seen in the samples analysed by SEM appear to have very irregular surface, with a structure that seems to originate by deposition of different layers. This structure is similar to that Zauner and Jones attribute to calcite grown after the dissolution of vaterite and may indicate that all the particles were originally precipitated as vaterite and then converted to calcite. This would confirm what appeared when viewing the precipitate under the optical microscope a few minutes after the reaction. SEM micrographs that show the structure of the cubic particles can be seen in Figure 4.12 (reactor B) and Figure 4.13 (reactor A). More work should be carried out to evaluate the correctness of this hypothesis.

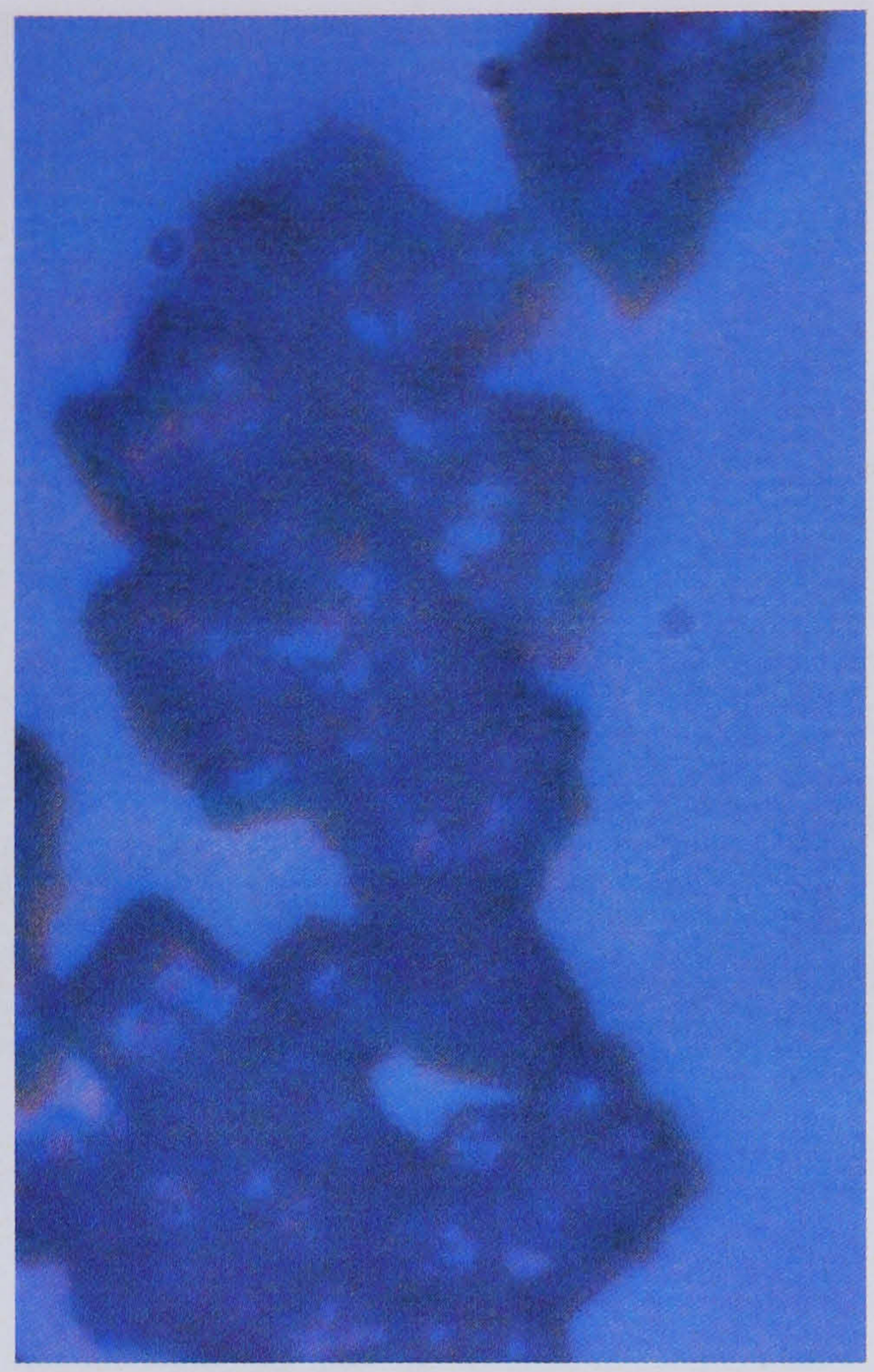

Figure 4.11. Optical microscope image for a sample left in contact with the mother liquor for 48 hours (reactor B, Q_{out} = 0.43 cm^3/s).

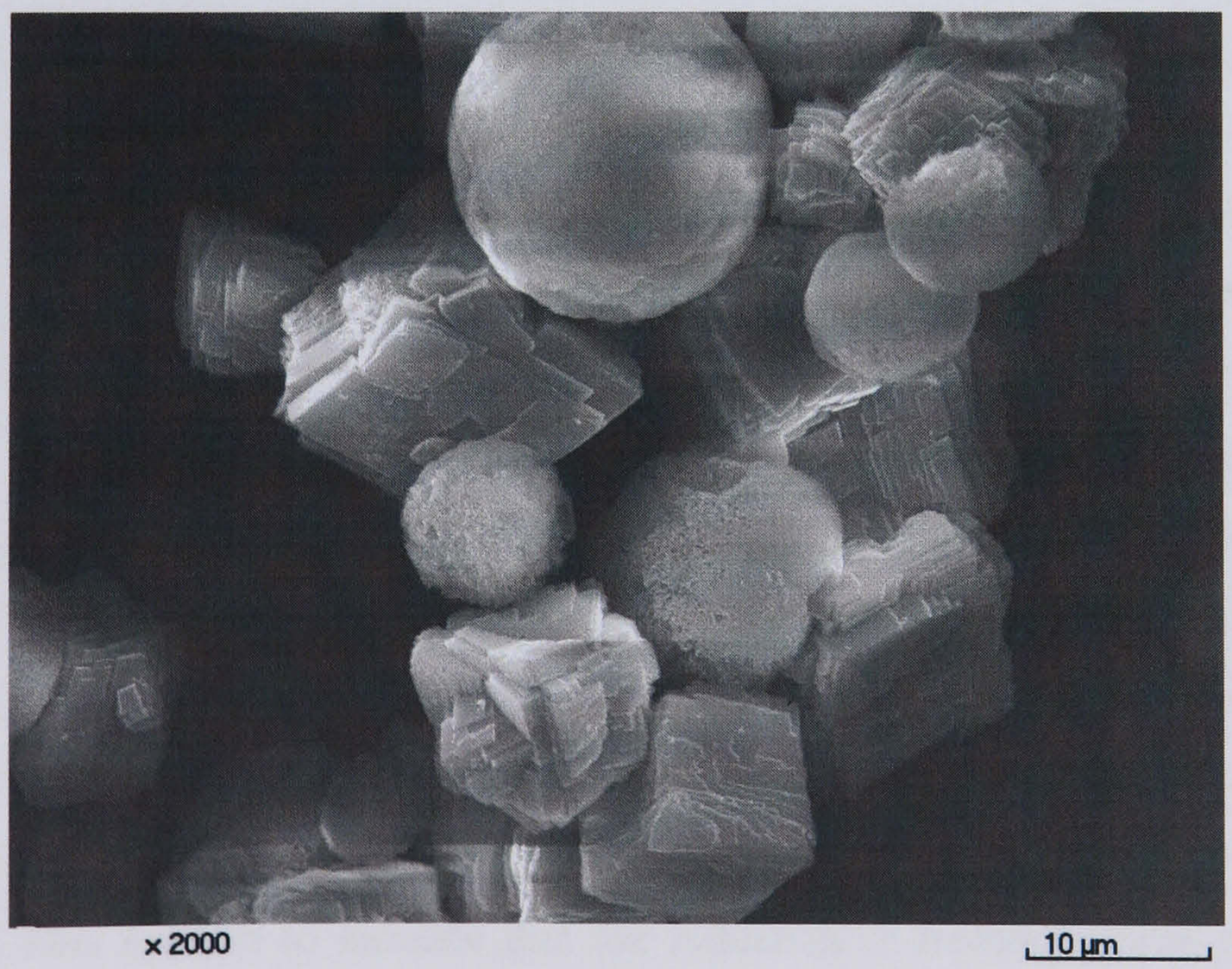

Figure 4.12. SEM micrograph (× 2000) for reactor B (Q_{out} = 0.43 cm^3/s).

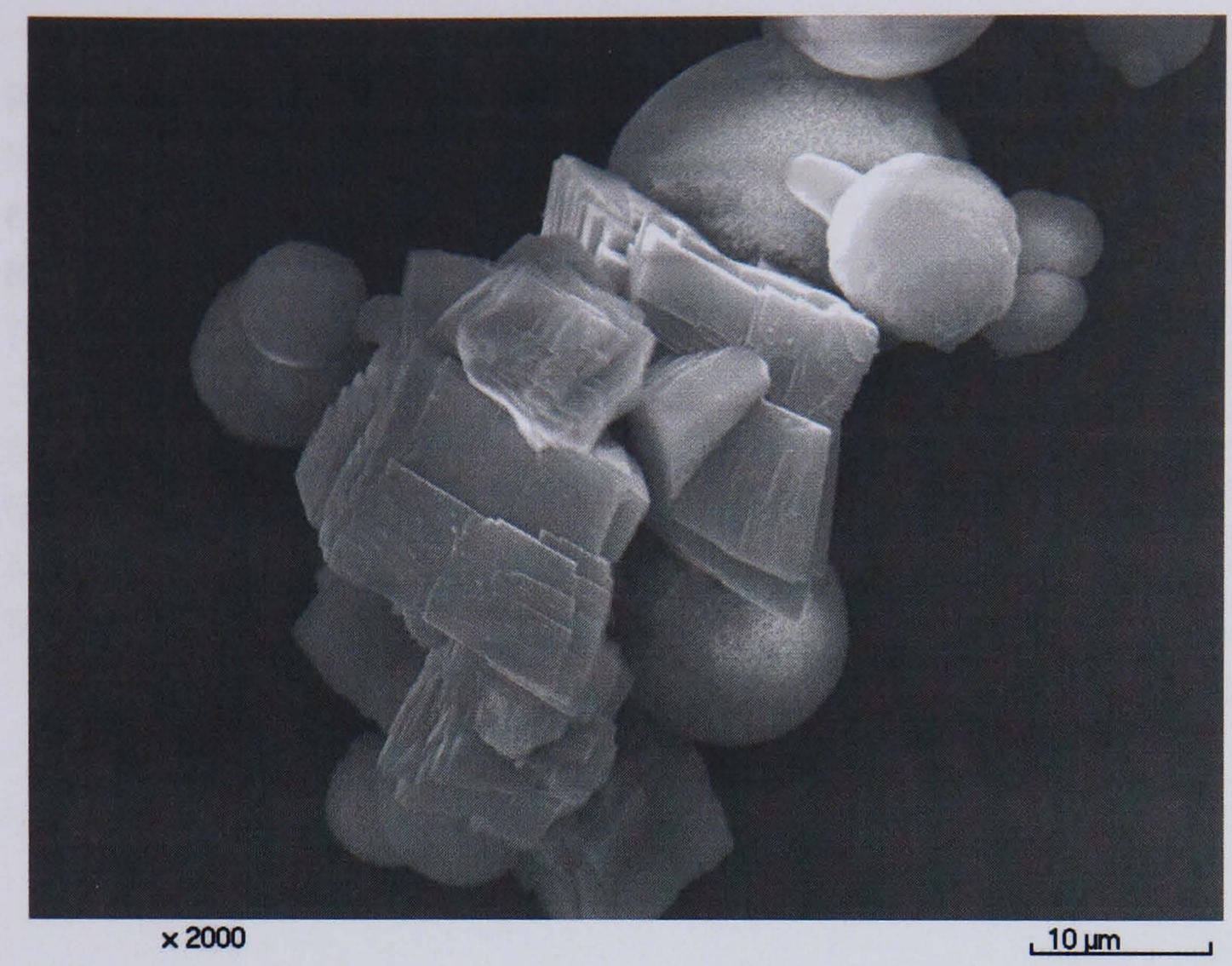

Figure 4.13. SEM micrograph (× 2000) for reactor A (Q_{out} = 0.43 cm^3/s).

4.10 Conversion

The amount of calcium carbonate precipitated per unit volume of collected suspension at varying flow rate was almost constant for the two reactors and conversion was on average close to 80 % for reactor A and to 85 % for reactor B. Three flow rates were considered for reactor B and five for reactor A. In both cases, the maximum and minimum flow rate used for the precipitation reaction were included in the selected values. Accuracy of these data was estimated by uncertainty analysis (described in Appendix A), considering uncertainties on the measurement of the outlet slurry volume and the weight of the dry precipitate. Average uncertainty was estimated to be around 4 % for both series of data relative to the two reactors and a limited number of repetitions of the conversion determinations gave results in the obtained uncertainty range. Figure 4.14 shows a graph with the calculated conversion versus flow rate for both reactors. As already mentioned, conversion is practically constant for increasing flow rate. This appears to indicate that the reduction in residence time obtained at higher flows is compensated by the increase in mixing efficiency. The conversion could then be considered to depend only on the characteristic dimension of the

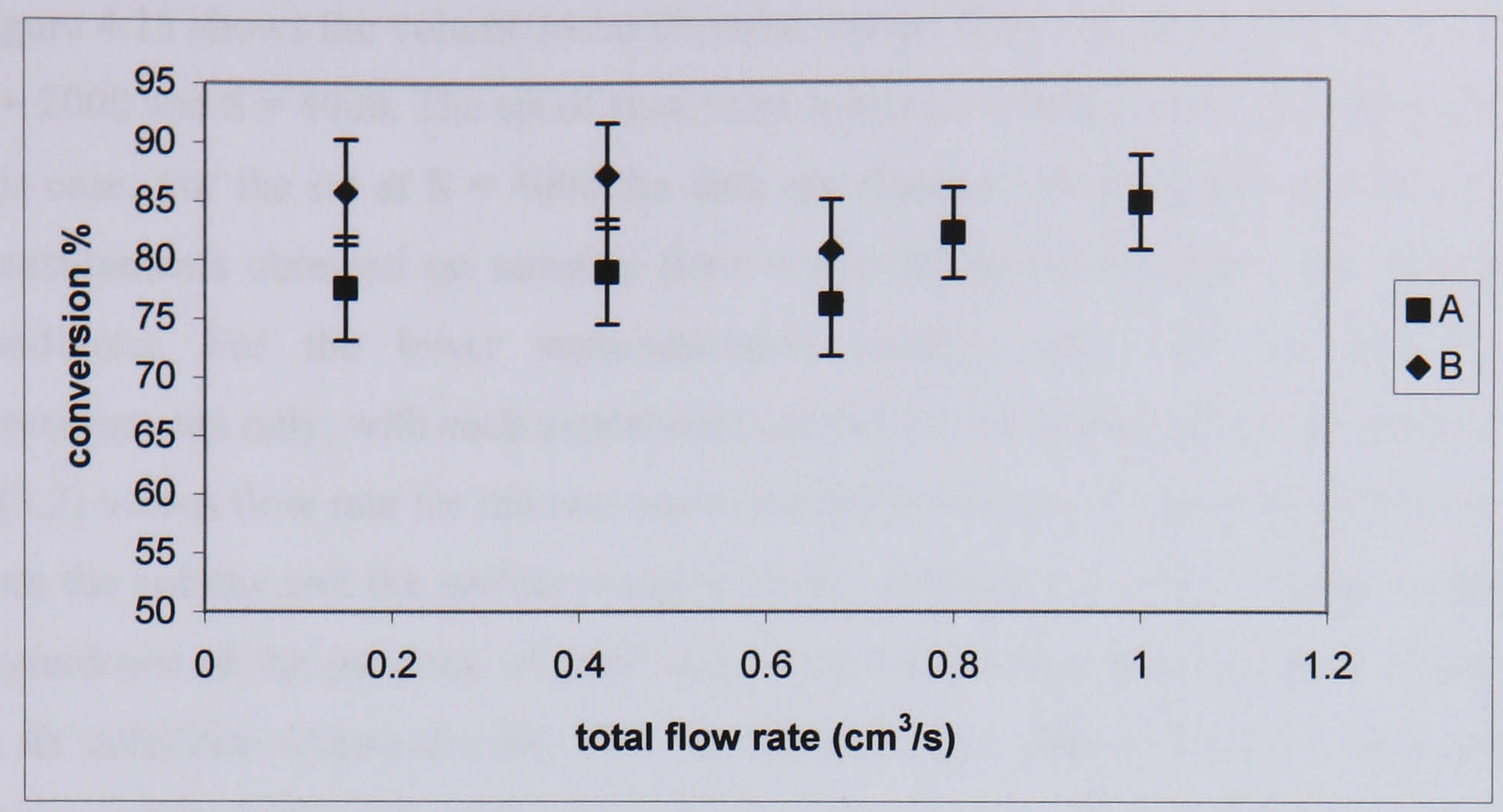

Figure 4.14. Conversion vs. flow rate for both reactors.

channel, even though this particular case does not show significant differences between the two reactors, as not a great difference exists between the two channel sizes.

4.11 Particle size and size distribution

Laser diffraction analysis generates a volume distribution of the particles from which a series of parameters characterizing the product can be evaluated. One of the parameters obtained from a volume distribution measurement is the volume moment mean diameter, D[4,3], the definition of which can be found in Appendix B. Commercial product specifications are often given in terms of D[4,3] and research carried out on particle size usually refers to this parameter. Another parameter often encountered is the surface moment mean diameter or D [3,2]. Both parameters will be referred to within the discussion, with particular attention to D[4,3] which is the parameter commonly accepted to identify mean particle size of a sample.

In this case a relatively large number of repetitions of the experiments was carried out to find a procedure for particle size analysis that could prevent changes between the reaction and the analysis itself, as described in Appendix B. For this reason, most of the tests were not carried out more than once with the final particle size analysis procedure.

Figure 4.15 shows the volume mean diameter versus flow rate for reactors A and B at S = 2000 and S = 4000. The set of flow rates common to both reactors is considered in this case. For the set at S = 4000 the data are obtained averaging the results of two measurements obtained on samples from two experiments with the same operating conditions. For the lower supersaturation instead, data refer to one set of measurements only, with each experiment carried out once. Figure 4.16 shows instead D[3,2] versus flow rate for the two supersaturation values. It is interesting to evaluate both the volume and the surface weighted mean diameters, as the first has a stronger dependence on the presence of small tails in the distribution than the latter, according to its definition (Appendix B). This implies that very limited fractions of particles (down to below 1%) in a relatively high size range, which can be due for example to a not complete dispersion of the sample, can determine a relatively high increase in the particle size and can lead to an incorrect analysis of the results when looking at the effect of process conditions on the particles properties. An example of not complete dispersion of the sample can be seen in Figure 4.17 which shows the particle size distributions for S = 2000 and total flow rates of 0.15 and 0.67 cm^3/s. In this case, for the experiment corresponding to reactor A and a flow rate of 0.15 cm^3/s, a small fraction of particles is found between 30 μm and 150 μm, and corresponds to 2.5 % of the volume in total.

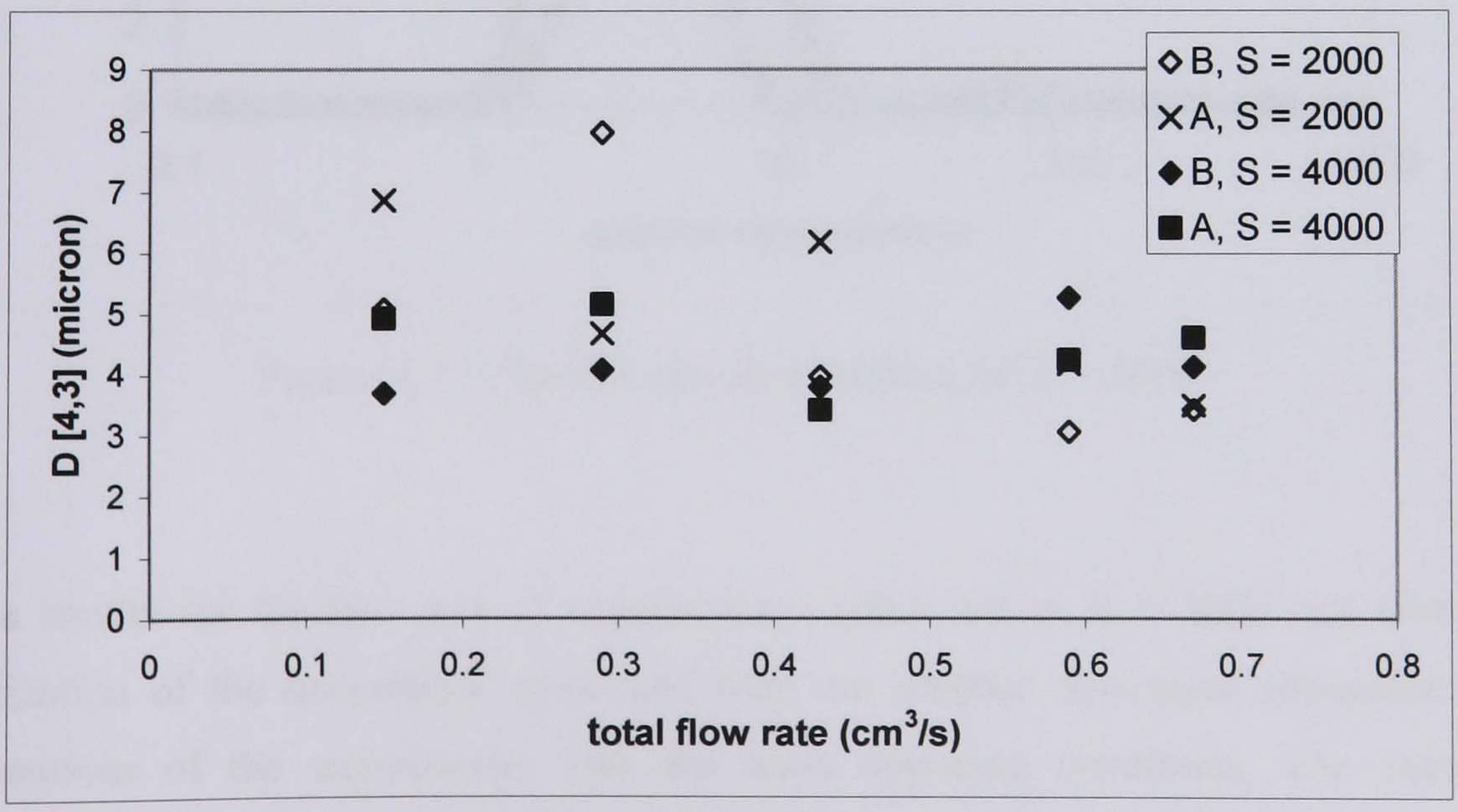

Figure 4.15. Volume weighted mean diameter versus flow rate for both NCRs at two different supersaturation ratios.

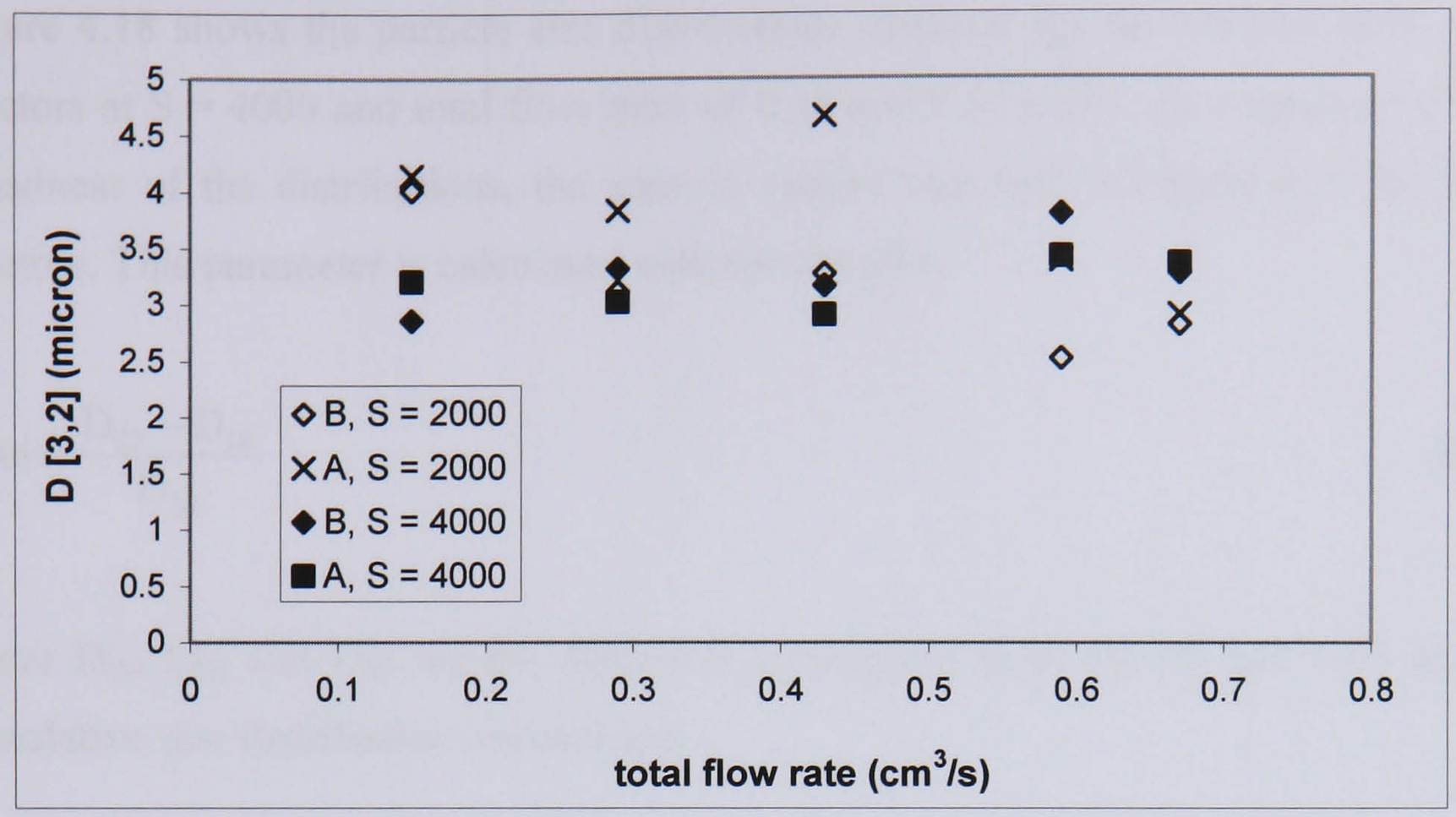

Figure 4.16. Surface weighted mean diameter versus flow rate for both NCRs for two supersaturation ratios.

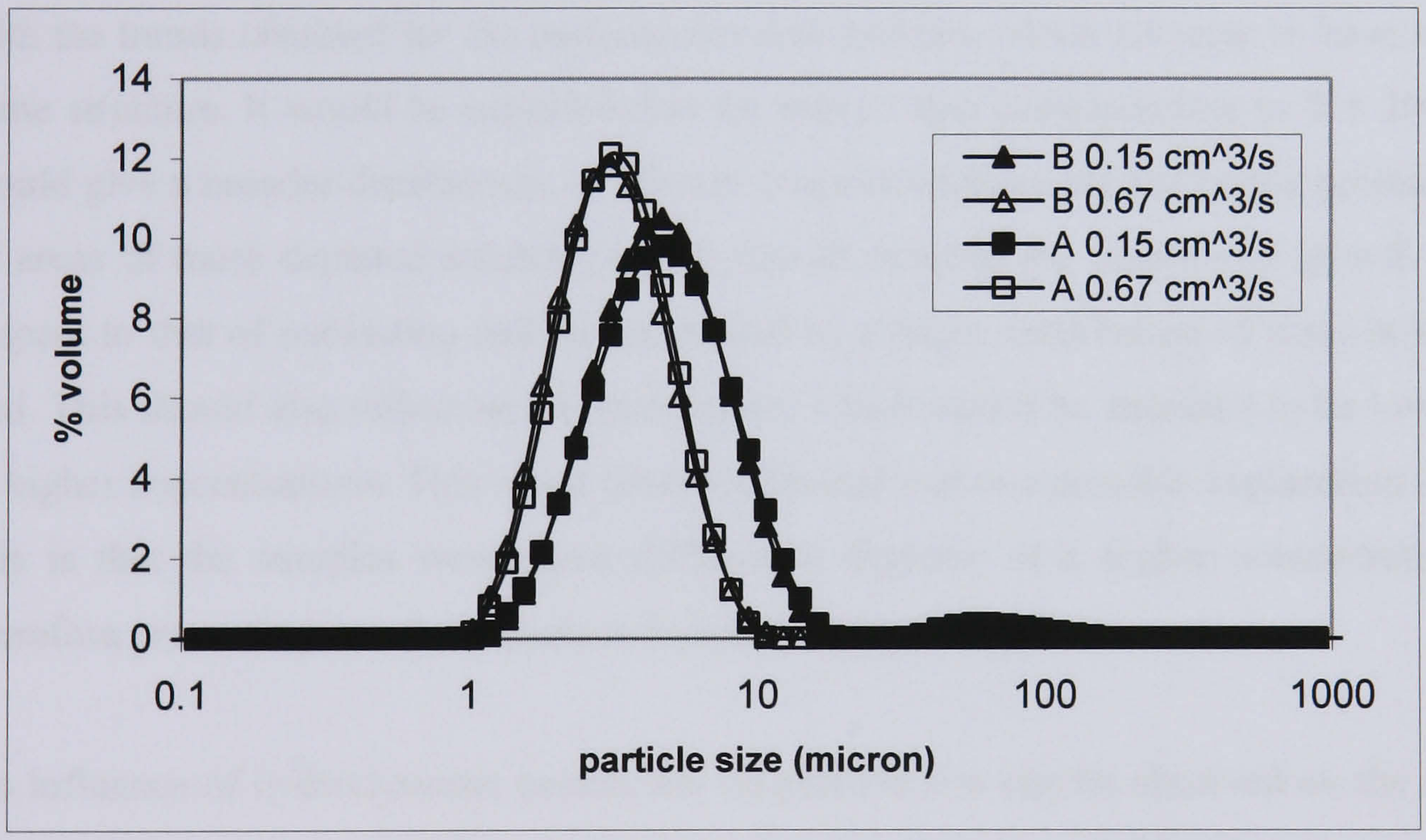

Figure 4.17. Particle size distributions for S = 2000.

The results for the two sets of experiments carried out at S = 4000 can give an indication of the uncertainty associated with the adopted dispersion procedure for repetitions of the experiments with the same operating conditions. The average relative difference between each experiment and the average of the two in terms of D[3,2] was found to be 3.4% for the experiments with reactor A and 10.3% for those with reactor B.

Figure 4.18 shows the particle size distributions obtained for the samples from both reactors at S = 4000 and total flow rates of 0.15 and 0.67 cm^3/s. As a measure of the broadness of the distributions, the span is instead reported in Figure 4.19 for both reactors. This parameter is calculated with the equation:

$$\text{span} = \frac{D_{90} - D_{10}}{D_{50}} \tag{4.32}$$

where D_{10}, D_{90} and D_{50} are the diameters correspondent to 10, 90 and 50% of the cumulative size distribution respectively.

The span varied between 1.1 and 1.7 in all cases, except for one relatively high value obtained for reactor B at S = 2000 which is attributed to a not complete dispersion of the sample. The broadness of the distributions is similar in all cases, this is consistent with the trends obtained for the particle size distributions, which all seem to have the same structure. It would be expected that the sets of data correspondent to S = 2000 would give a broader distribution, as a lower concentration would favour the presence of areas of more depleted solution, which should enhance the kinetics of growth in respect to that of nucleation and therefore lead to a larger distribution of sizes in the end. This should also reflect on the mean sizes, which would be expected to be lower at higher concentrations. This is not observed instead and one possible explanation for this is that the samples were more difficult to disperse at a higher concentration therefore preventing a real comparison between the two conditions.

An influence of hydrodynamic parameters on particle size can be observed on the set of data obtained at S = 2000 for reactor A. The data in terms of D[4,3]are scattered, with particle size varying overall between 3 and 8 μm approximately, but looking at the data in terms of D[3,2] more information can be gathered. A relative distinctive decrease in D[3,2] between the lowest three and the highest two flow rate values can be observed for reactor A and a supersaturation ratio of 2000. As from the results of the mixing study, increasing flow rate was shown to improve mixing efficiency and the decrease in particle size can in this case be attributed to better mixing at higher flow rates. In fact, from the theory of nucleation and from what

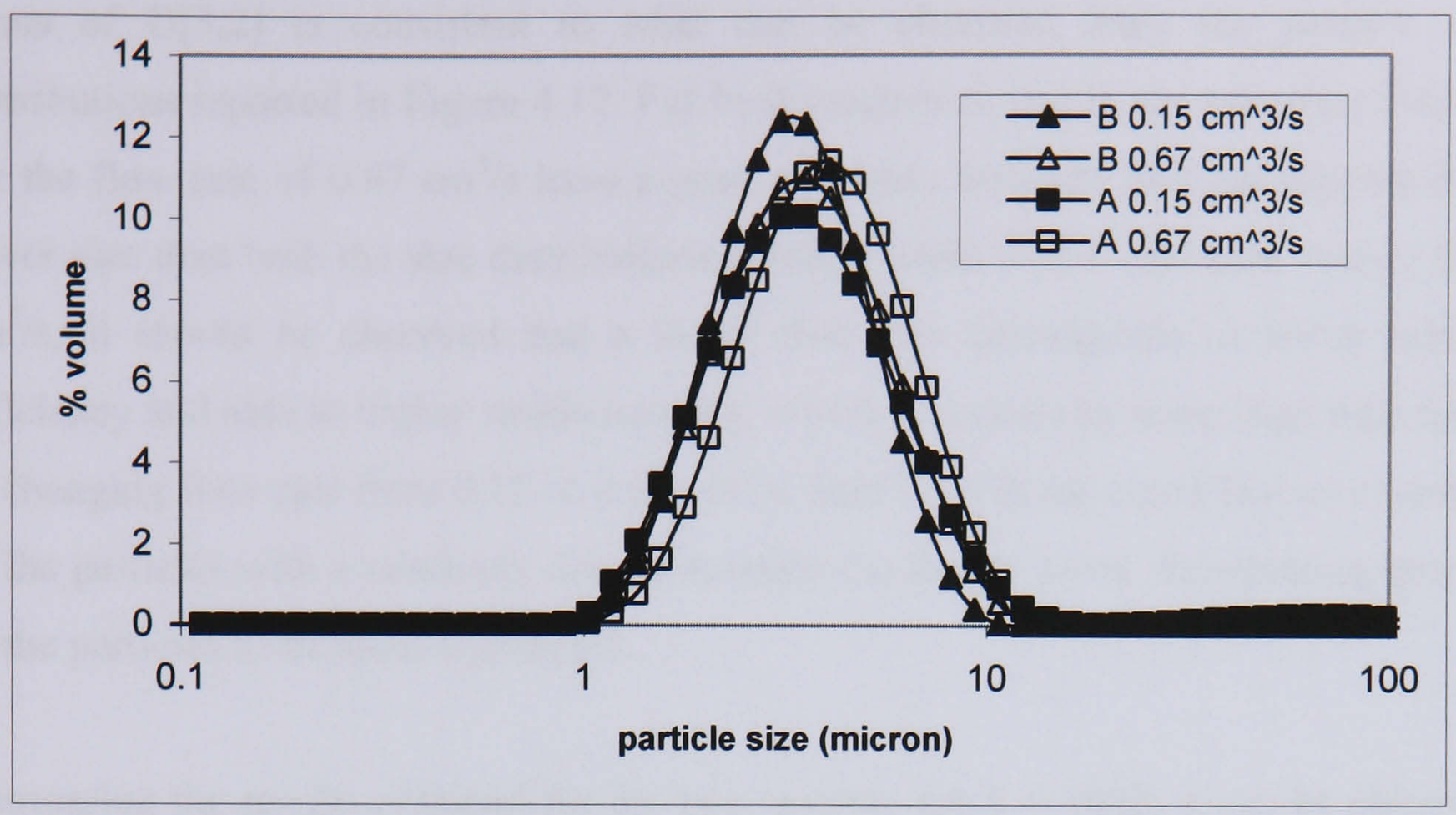

Figure 4.18. Particle size distributions for S = 4000.

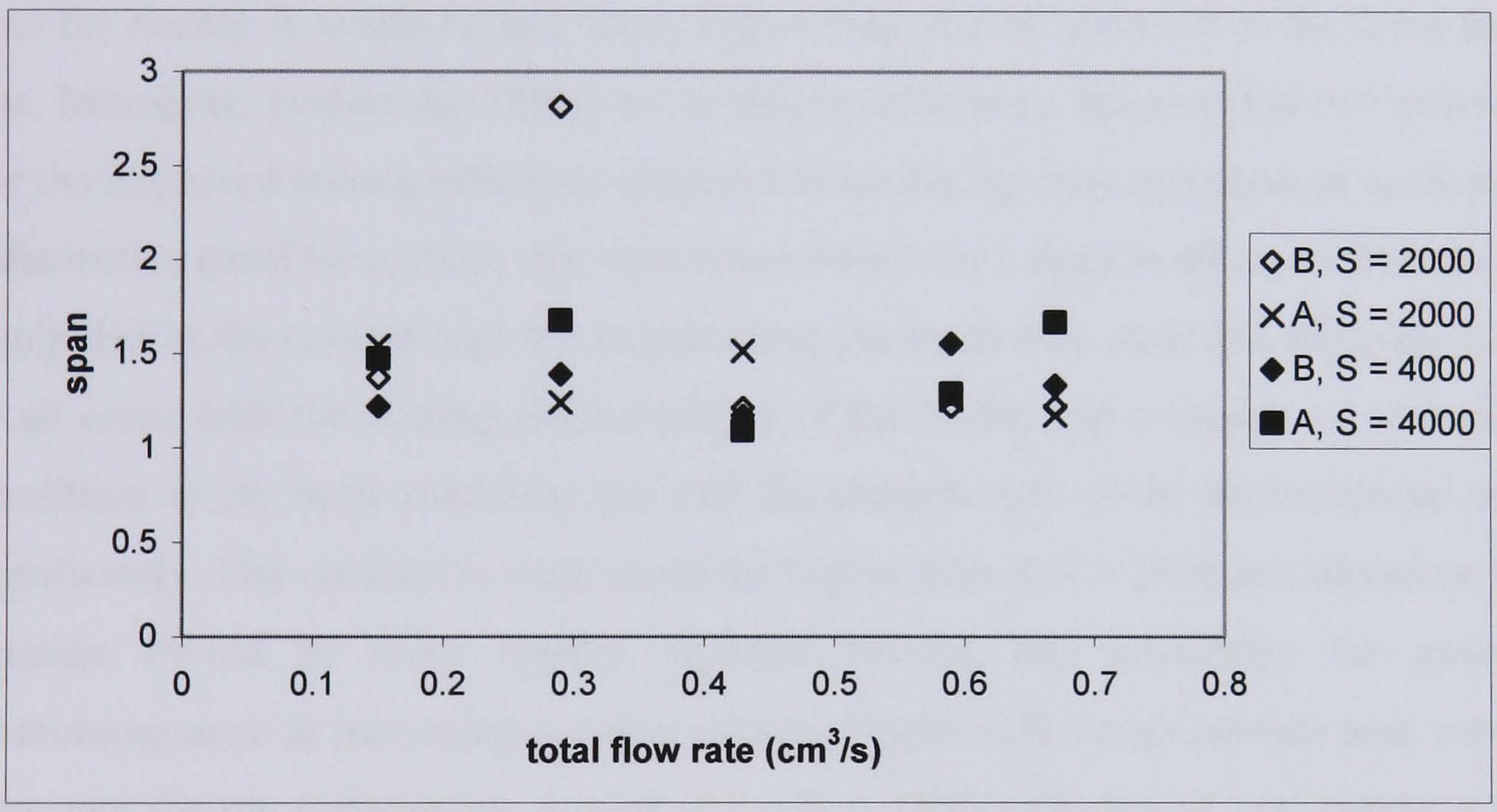

Figure 4.19. Span versus flow rate for both reactors.

reported in experimental studies, high mixing efficiency of the reagents leads to the build up of a relatively uniform high supersaturation of the precipitating species. This causes nucleation rates to be very fast and the supersaturation to be depleted mostly by the nucleation process, making the kinetics of growth less competitive and therefore leading to a final smaller size of the particles. In this perspective, it can be observed that the presence of the bends in the channel, that is considered to enhance the mixing process, can be directly related to the efficiency of mixing of the two reagents and therefore to the characteristics of the precipitation process. The trend obtained in

terms of D[3,2] is consistent to what can be observed from the particle size distributions reported in Figure 4.17. For both reactors A and B, the size distributions for the flow rate of 0.67 cm^3/s have a peak of higher intensity and correspondent to lower size than both the size distributions correspondent to the total flow rate of 0.15 cm^3/s. It should be observed that a lower flow rate corresponds to lower mixing efficiency and also to higher residence time, which decreases by more than four times in changing flow rate from 0.15 to 0.67 cm^3/s. Both conditions could favour a contact of the particles with a relatively diluted solution for longer times, determining growth of the particles to be more significant.

Comparing the results obtained for the two reactors for S = 4000, it can be observed that hydrodynamic parameters do not seem to have a relevant influence on particle size in this case. As observed in the description of the mixing study, the residence time for reactor A would be four times higher than that of reactor B at the same flow rate. Moreover, neither the difference in mixing efficiency between the two reactors nor the improved mixing efficiency obtained at increasing flow rate seem to determine a distinctive trend for particle size, which has very close values in all cases. This could imply that in the case of higher concentrations the nucleation rates are relatively high in all cases with the mixing characteristics of the NCRs and a change of operating conditions in the range used does not alter the characteristic of the nucleation process significantly. The nucleation rates would be higher than at S = 2000 and therefore the solution should be more rapidly depleted leaving less possibility for growth phenomena even at increasing residence times. Figure 4.20 shows particle size versus flow rate for the experiments carried out at S = 4000 with the 10 cm^3 syringes for reactor A. Particle size varies between 3.4 and 5.2 μm and, similarly to the other cases, it does not change substantially with increasing flow rate.

It is interesting to compare the results in terms of particle size obtained in the narrow channels and those obtained in the segmented flow tubular reactor (Vacassy et al., 2000). These authors found that for the liquid phase precipitation of calcium carbonate, a median diameter between 5.0 μm and 5.9 μm was obtained at varying flow rate of the reagents. The median diameter is the diameter corresponding to 50 % of the

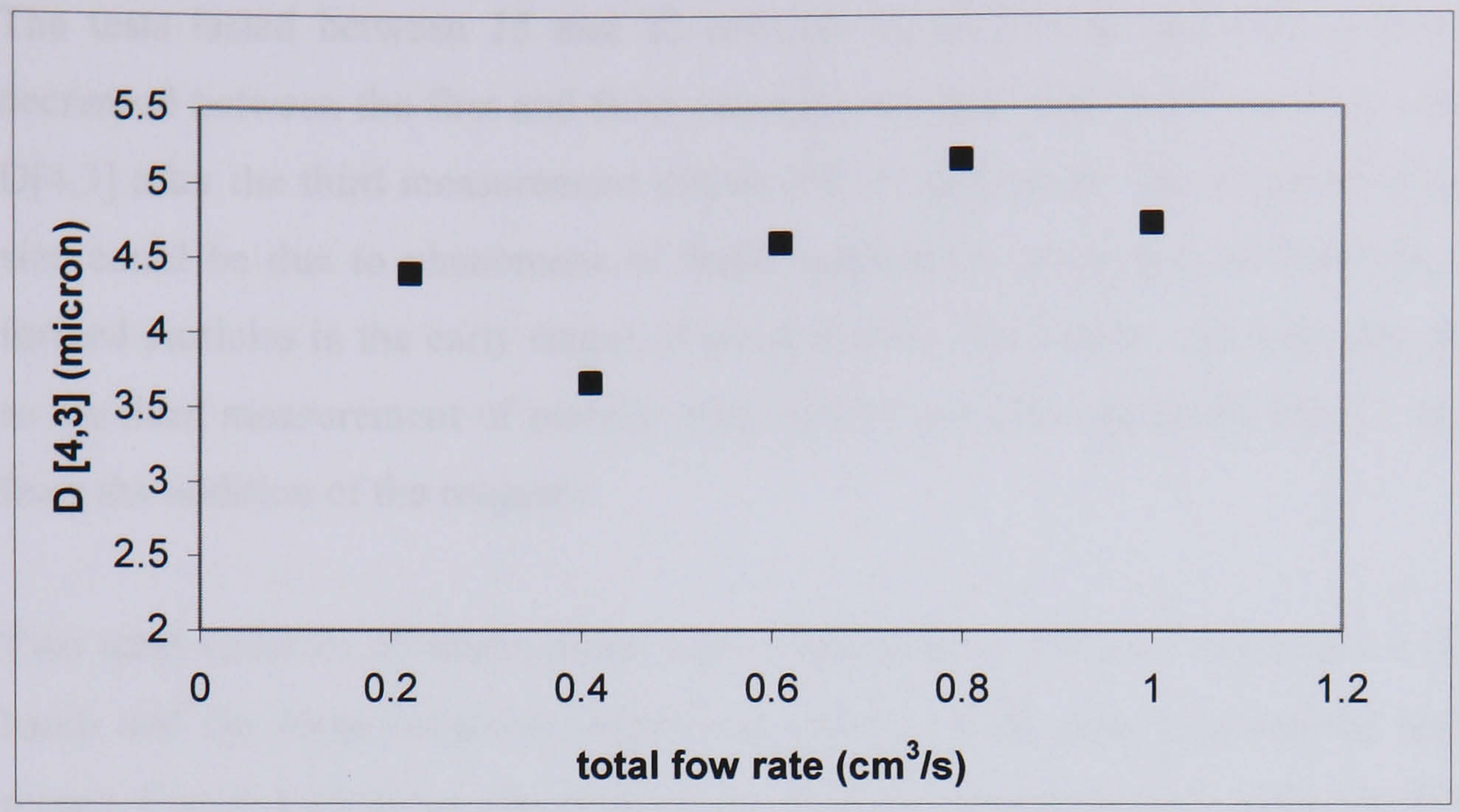

Figure 4.20. Particle size vs. flow rate for reactor A for the 10 cm^3 syringes experiments.

volume distribution and it is lower than D[4,3]. The results of this work give D[4,3] values close to the median diameter in the case of the SFTR, it can be concluded that the performance of the narrow channel reactors matched or was better than that of the SFTR in terms of particle size, according to the reported data. The concentrations of the reagents were of the same order of magnitude in both cases (comparisons were carried out considering S = 4000 for the NCRs).

4.12 Benchmarking

Benchmarking tests were carried out in order to assess the performance of the narrow channel reactors in terms of product quality, i.e. particle size and particle size distribution. The procedure followed for the tests consisted in filling a beaker with a determined volume of sodium carbonate solution and starting stirring the solution vigorously with a lab type magnetic stirrer (Hanna Instruments model HI 190M) operating at the maximum speed (1000 rpm). The calcium nitrate solution was then rapidly added to the beaker while stirring continued. The solutions started changing colour, indicating that precipitation was occurring, almost immediately after the addition of the second solution. For each test, 4 to 6 measurements of particle size were carried out at different time intervals from the addition of the second solution. The time gap between one measurement and the next was of approximately 4 minutes.

The tests lasted between 15 and 22 minutes in all. For all the runs, particle size decreased between the first and third measurement and then stabilized with values of D[4,3] after the third measurement within 2% of each other. The decrease in particle size could be due to phenomena of local aggregation occurring between the newly formed particles in the early stages of precipitation. The results reported here all refer to the third measurement of particle size, carried out after approximately 10 minutes from the addition of the reagents.

Two total volumes of suspensions were considered: a 100 cm^3 batch and a 20 cm^3 batch and the same magnetic stirrer was used in both cases to keep the solutions mixed. Figure 4.21 shows the particle size distributions obtained for the two different volumes for S = 2000 and S = 4000. As expected, the smaller volume batches gave lower particle size in both cases, as the mixing efficiency provided was higher. The data relative to the smallest volume batches were used for benchmarking purposes, so as to use data obtained in conditions of relatively high mixing efficiency. However, as the amount of energy transferred to the solutions in the batch experiments was not quantified, the results of the benchmarking tests should not be considered as exhaustive for the comparison between a batch system and the NCRs. At the same time, they can be regarded as very useful for a preliminary assessment of the performance of the NCRs versus a simplified form of a traditional batch system.

The smallest volume for the batch tests was equal to the total outlet volume of one of the experiments carried out with the 10 cm^3 syringes. The data reported here for benchmarking purposes and relative to the narrow channel reactors were obtained without using the surfactant in the particle size analysis procedure (more details can be found in Appendix B). This was because samples from the batch runs were taken from the product and analyzed directly, without adding the surfactant. This implied that aggregation of the particles might have had a higher occurrence than shown normally and this could be detectable in the particle size distributions. Figure 4.22 shows PSDs for the batch and two samples relative to reactor A and B respectively for S = 4000. Figure 4.23 instead shows a benchmarking plot between reactor A and the batch for S = 2000. In all cases the narrow channels gave smaller particle size, as PSDs for the batch are shifted towards higher dimensions when compared to those from the narrow channels. This is confirmed by the particle size data reported in Table

4.3. The results of these tests show that the narrow channel reactors were able to produce smaller particle size than an agitated system.

When taking into account these data, the characteristic time scales of the two types of equipment, as well as the energy input considerations reported above, should be taken into account. In fact, the measurements for the batch tests were taken after 10 minutes from the mixing of the reagents, whereas the characteristic residence times of the narrow channels were of the order of a few seconds or lower. This shows one of the differences of the two systems and how various parameters should be taken into account when comparing two types of equipment. It could be observed for example, that running the narrow channels in a mode so as to have characteristic residence times of minutes would probably lead to much higher particle size than that obtained in this case because the velocities of the reagents in the channels would be very low. At the same time, it could be observed that the difference in time scales between the two types of equipment could show another advantage for the narrow channels, as a much higher volume of slurry than that of the batch system could be generated in ten minutes by operating at the flow rates used in this case.

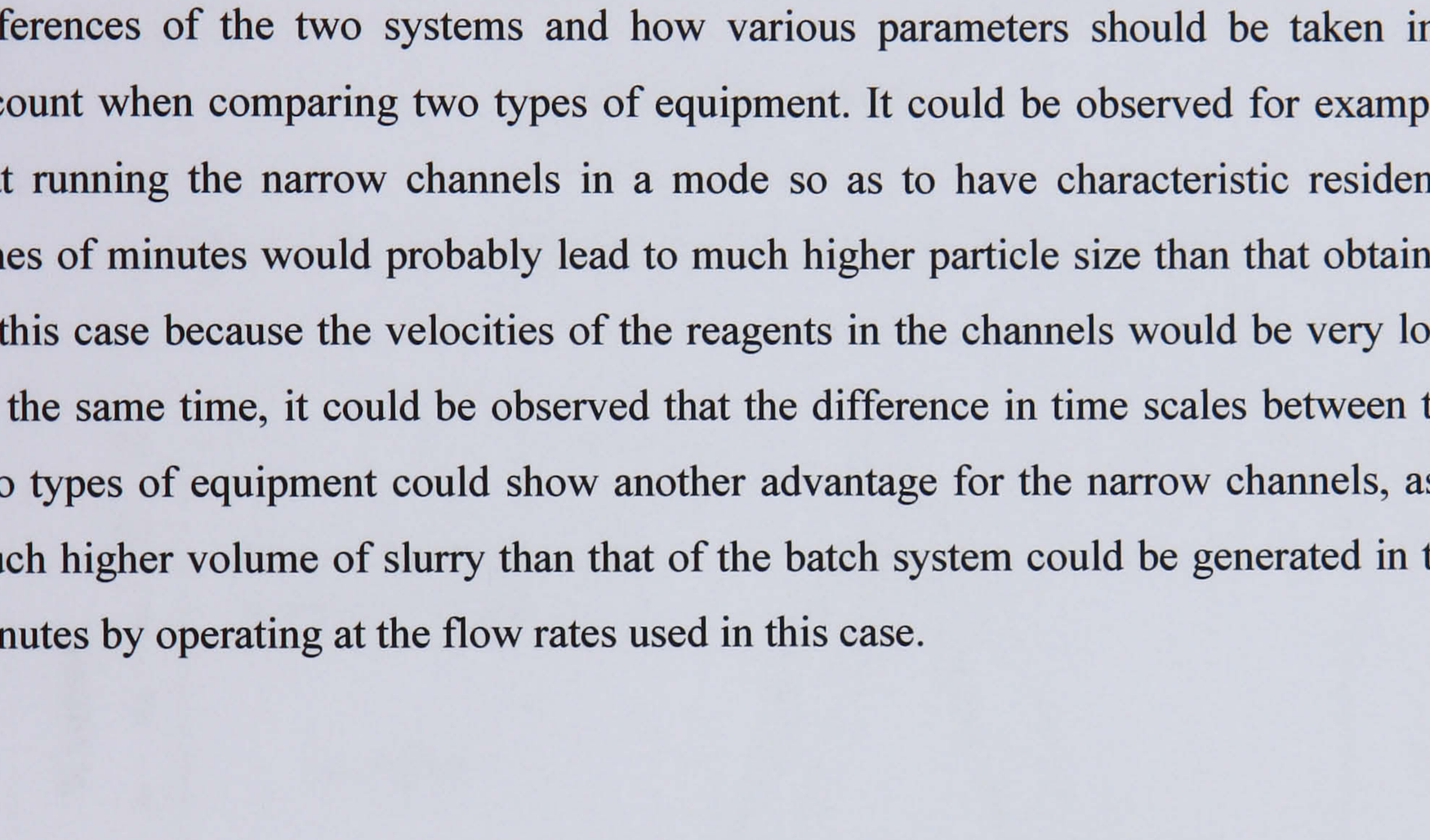

Figure 4.21. PSDs for the batch experiments.

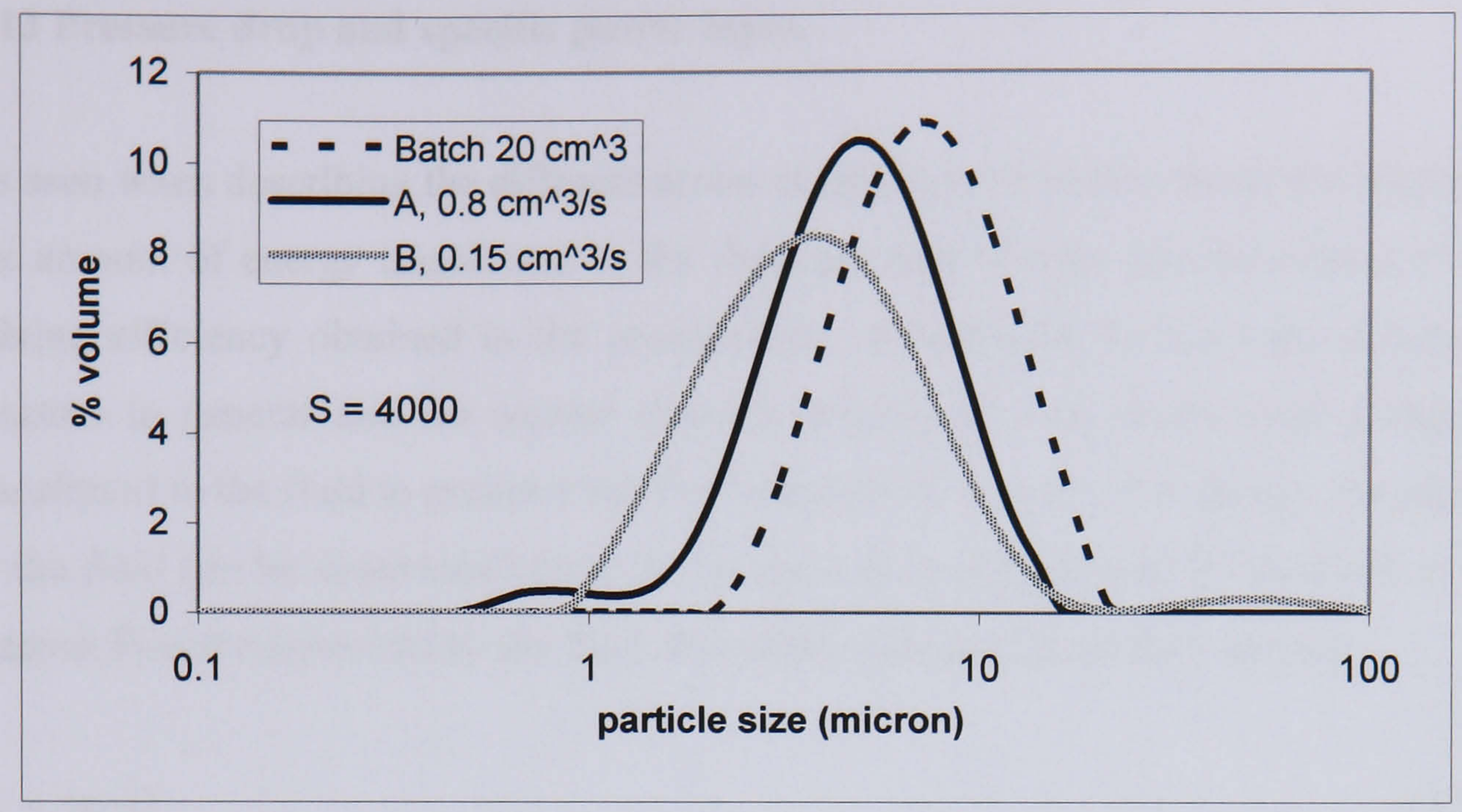

Figure 4.22. Benchmarking plot in terms of PSD for S = 4000.

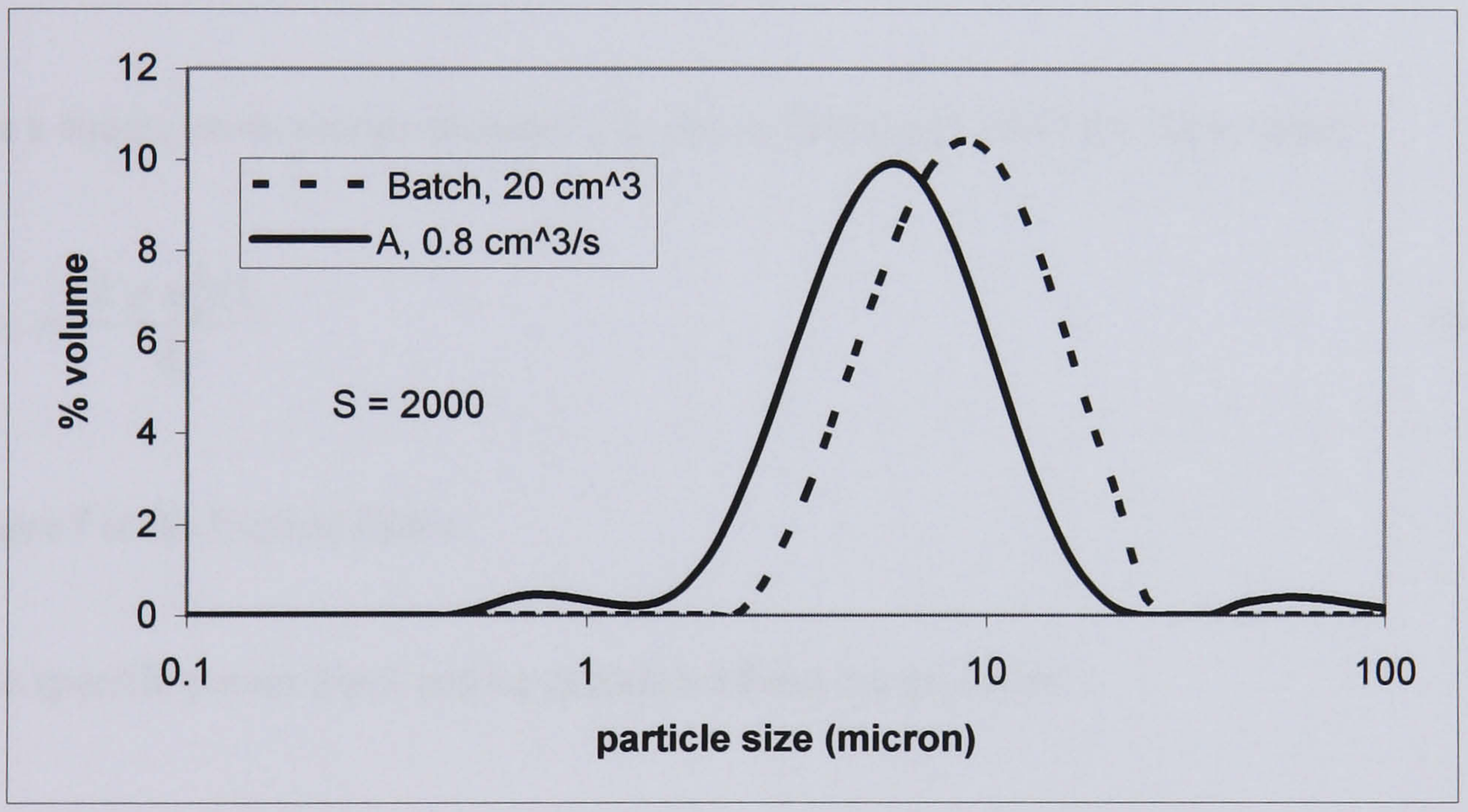

Figure 4.23. Benchmarking plot in terms of PSD for S = 2000.

Table 4.3. Mean particle size for NCRs and the batch tests.

Reactor	**S**	**D[4,3] (μm)**
20 cm^3 batch	4000	7.90
NCR A (Q_{out} = 0.80 cm^3/s)	4000	5.34
NCR B (Q_{out} = 0.15 cm^3/s)	4000	5.62
20 cm^3 batch	2000	9.58
NCR A (Q_{out} = 0.80 cm^3/s)	2000	7.73

4.13 Pressure drop and specific power input

As seen when describing the different scales of mixing in a stirred vessel in Chapter 2, the amount of energy transferred to the fluid per unit of mass can be related to the mixing efficiency obtained in the precipitation environment. In the case of tubular reactors in general and for narrow channel reactors as well, mechanical energy is transferred to the fluid to generate the flow through the reactor. The energy transferred to the fluid can be determined from the pressure drop experienced by the fluid in the reactor. Power transmitted to the fluid, P_f can be calculated from the equation:

$$P_f = \Delta p \cdot Q \tag{4.33}$$

where Δp (Pa) is the pressure drop and Q the volumetric flow rate of the fluid.

For a square cross section channel, Δp can be calculated from the expression:

$$\Delta p = \frac{2 \rho u_L^2 f L}{d_h} \tag{4.34}$$

where f is the friction factor.

The specific power input can be calculated from the equation:

$$\varepsilon = \frac{P_f}{Q \rho \tau} \tag{4.35}$$

where τ is the residence time.

If for a square cross section geometry and laminar flow the following relationship is considered (Darby, 2001, p.199):

$$f = \frac{14.2}{Re} \tag{4.36}$$

then combining equations 4.31, 4.32, 4.33 gives:

$$\varepsilon = 28.4 \frac{\mu Q^2}{\rho d_h^6} \tag{4.37}$$

which shows that the specific power input is independent of the considered reactor length.

Similarly, the pressure drop can be expressed as a function of the geometric characteristics of the reactor and the flow rate, so as to be used as a design equation:

$$\Delta p = 28.4 \mu \frac{Q}{d_h^4} L \tag{4.38}.$$

Similar expressions can be found for circular tubing, for the inlet and outlet capillary, with the factor 28.4 substituted by another value taking into account the different geometry.

Considering the reactor inlet and using the density and viscosity of water at 20°C as a first approximation, most of the energy is dissipated in the capillary tubing, with 1.3 % of the total pressure drop at the inlet (capillary and Y mixer) dissipated in the Y mixer for reactor A and about 10 % of the total in reactor B. In these calculations, the flow rate used was the inlet flow rate, as each solution determines a certain pressure drop on one of the sides of the inlet (tubing and Y mixer). The two values are the same if a 1:1 flow rate ratio between the solutions is assumed. Considering instead the total flow rate for the part in the Perspex block and the outlet tubing, the pressure drop in the Perspex block is around 18 % of the total for reactor A and around 76 % of the total for reactor B. Total pressure drops in the reactor and in the outlet tubing vary between 1300 Pa and 8500 Pa for reactor A and 5000 Pa and 21000 Pa for B. Figure 4.24 shows the pressure drop at the inlet and in the reactor (including the Perspex block and the outlet tubing) versus flow rate for both channels A and B. These calculations did not take into account the change in direction of the fluid from the inlet to the Perspex block and from the block to the outlet tubing.

Considering the specific power input, reactor B gives values of ε which are about 60 times higher than those for reactor A. The 1 mm capillary gives intermediate values between the two. Figure 4.25 shows the calculated specific power input at varying flow rate for both reactors and the capillary. Values as high as 100 W/kg are obtained in reactor B.

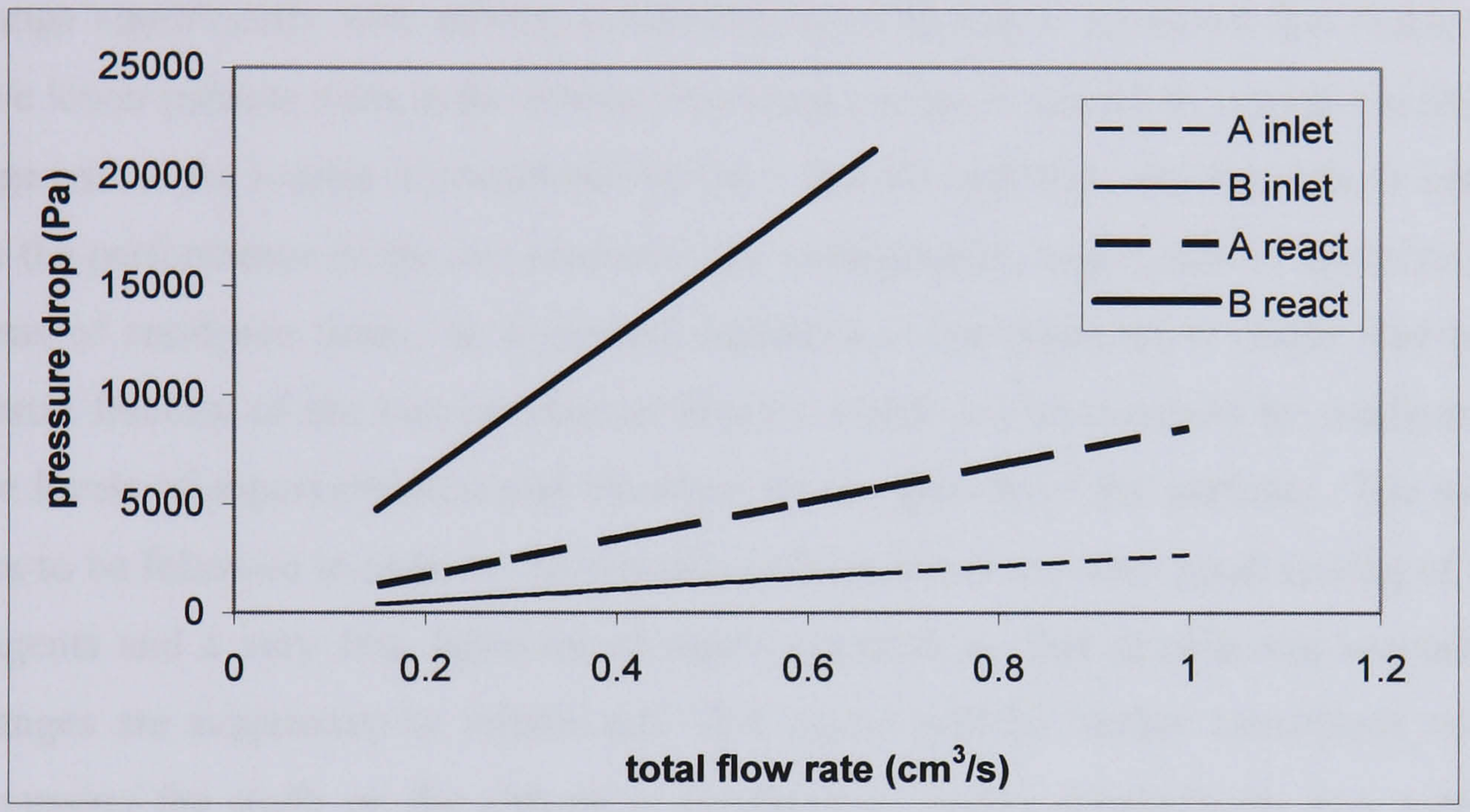

Figure 4.24. Pressure drop at the inlet and in the reactor for both channels.

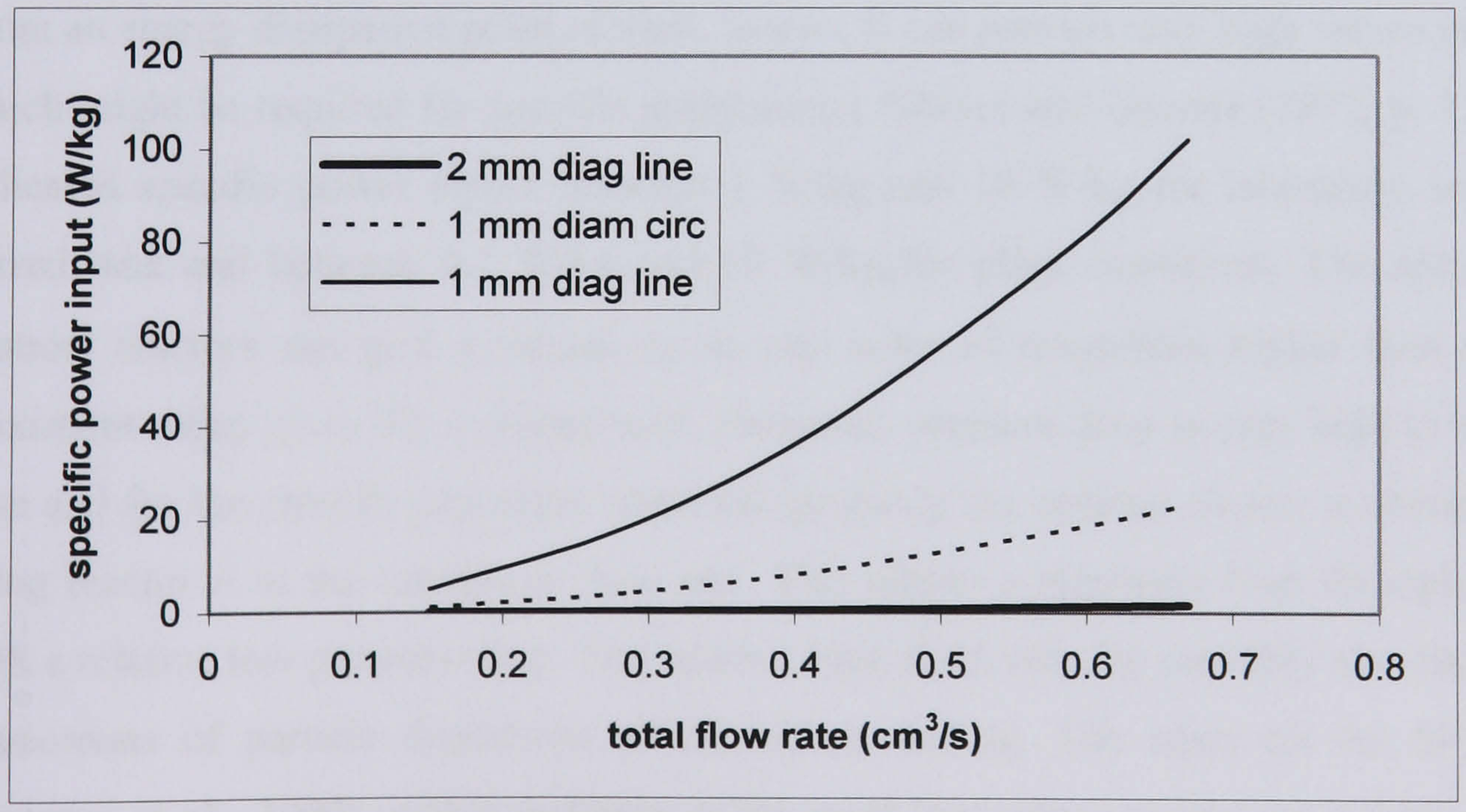

Figure 4.25. Specific power input at varying flow rate.

4.14 Conclusions

The investigation on liquid phase precipitation has shown that better product quality in terms of size and size distribution, compared to batch reactors, can be achieved in narrow channels. The mixing efficiency study showed that the prevailing mechanism for mixing is convection, thus giving interest in using higher flow rates for equal channel diameter to improve the mixing performance. Particle size did not seem to change significantly with mixing conditions, even though it appeared that reactor B gave lower particle sizes in the lowest flow rates region. It should be considered that a large part of the reactor is constituted by the 1 mm ID capillary, which probably evens out the performance of the two reactors. The configuration might also be optimized in terms of residence times, as a gradual depletion of supersaturation might lead to a greater fraction of the narrow channel reactor which is characterized by medium to low levels of supersaturation and therefore favour growth of the particles. The main idea to be followed in order to have small particles is to have very good mixing of the reagents and a very fast depletion of supersaturation, so that growth and secondary changes are suppressed or minimized. This aspect will be further considered when discussing the study on the change in conductivity during precipitation in a narrow channel (Chapter 6).

From an energy dissipation point of view, reactor B can provide very high values of ε, which might be required for specific applications. Söhnel and Garside (1992, p. 179) indicated specific power inputs between 1 W/kg and 10 W/kg for laboratory scale stirred tank and between 0.1 W/kg and 10 W/kg for plant conditions. The narrow channel reactors can give ε values up to one order of magnitude higher than the maximum value given for a stirred tank. However, pressure drop is very high in this case and for the particle properties obtained, probably the optimal choice is obtained using reactor A at the maximum flow rate. This allows a relatively high throughput with a relative low pressure drop. The relative high fluid velocity probably also limits phenomena of particle deposition which initiate scaling. The study on the SFTR (Vacassy et al., 2000), which probably is the most innovative equipment introduced for precipitation in recent years, indicated flow rates of each reactant between 100 cm^3/h and 700 cm^3/h which approximately correspond to the range 0.056 cm^3/s to 0.390 cm^3/s as a total outlet flow rate. As seen earlier, similar values of particle size

were obtained in the narrow channel reactors and the segmented flow tubular reactor. A higher flow rate with the same performance in terms of particle size can then be obtained with a narrow channel reactor. Replications of the single channel would allow to further increase the achievable throughput.

CHAPTER 5

Gas-liquid mass transfer and precipitation of calcium carbonate in a narrow channel reactor

5.1 Introduction

Calcium carbonate is produced industrially from the carbonation of concentrated calcium hydroxide suspensions (milk of lime). This reactive crystallization involves gas-liquid mass transfer, solid dissolution and the precipitation reaction. The operation of this process in batch stirred vessels is very common and well known in terms of effect of operating conditions on product properties. The aim of the study on the use of a narrow channel reactor for the gas-liquid precipitation of calcium carbonate was to characterize different steps of the process in this type of equipment and the product properties.

A square cross section 2 mm diagonal line narrow channel reactor was used. The NCR had a similar configuration to the one used for the liquid phase study. In all the investigations pure carbon dioxide was used as the gas phase. Flow patterns obtained in the narrow channel reactor for the mixture water-carbon dioxide were visually characterized. Absorption of carbon dioxide in water was characterized by reacting the water-CO_2 mixture at the NCR outlet with a sodium hydroxide solution. The final part of this investigation concerned the precipitation of calcium carbonate from calcium hydroxide solutions and suspensions. Volumetric mass transfer coefficients for the case of precipitation from solution were experimentally determined. Comparison with other gas-liquid contactors in terms of mass transfer performance was carried out. Selected calcium carbonate samples were characterized in terms of particle size and morphology.

5.2 Experimental set-up

The narrow channel reactor used in this investigation was designed with some modifications from the ones used in the liquid phase study. Like reactor A described in Chapter 4, it had a square cross section with a 2 mm diagonal line. The main requirement of the new configuration was that it had to allow the use of a different pumping system rather than a syringe pump in order to have a continuous operation for longer times. Moreover, the 1 mm capillary at the outlet was replaced with a larger one so as not to have most of the mass transfer performance at the outlet of the reactor.

The reactor used in the gas-liquid study was machined in Perspex by precision milling. Each side of the Perspex block was 15 mm thick and threads were machined in the top side in order to use Swagelok fittings with the feed tubes. After machining the two sides, diffusion bonding was used to seal the reactor, as for the module described in Chapter 4. This was carried out by placing about 5 kg of metal weights on top of the two sheets of Perspex in an atmospheric oven which was slowly heated to 150°C. The reactor was kept at this temperature in the oven for about 5 hours, after which the heating was switched off and the NCR was left to cool down. It was then checked for leaks before use. After the end of the experiments, the reactor was opened and the length of the diagonal line was measured. The measured distance was 2 mm, indicating that neither the bonding nor the use of the reactor had altered its cross section.

A schematic of the narrow channel reactor used in the gas-liquid investigation is shown in Figure 5.1. The distance between the beginning of the Y mixer and the channel was 3 cm whereas the distance between the two sides of the Y mixer was 2 cm. The other segments of the channel in the Perspex block had the same lengths as in the liquid phase module. The fittings used were all in stainless steel with ISO 228 parallel threads for tubing with 1/8 inch OD (outside diameter). The reactor in this case was not provided with an intermediate feed on the Y mixer, but it had a third feed at the beginning of the last straight segment of the channel.

Gas (CO_2 from BOC, stored in a cylinder) was fed to the channel through one side of the Y mixer using a digital flow controller (Bronkhorst F201 C mass flow controller).

PTFE (Poly Tetra Fluoro Ethylene) capillary with 1/8 inch OD was used in this case. The liquid was fed to the NCR by means of a peristaltic pump (Masterflex 7519-05 from Cole-Parmer). A pulse dampener (from Cole-Parmer, 190 cm^3 in volume) was used on the liquid feed line between the pump and the reactor. The tubing used for the liquid was 1/8 inch ID clear C-Flex tubing from Cole-Parmer which was connected to a short segment (about 5 cm) of 1/8 inch OD capillary and the Swagelok fitting. The liquid side capillary was in stainless steel for the visualization and mass transfer study and in PTFE for the precipitation study. PTFE allowed a better seal with the pump tubing. The outlet tubing was constituted by 15 cm of stainless steel 1/8 inch OD capillary and 5 cm of 1/8 inch ID PTFE tubing. A picture of the reactor can be seen in Figure 5.2, whereas Figure 5.3 shows a picture of the set-up.

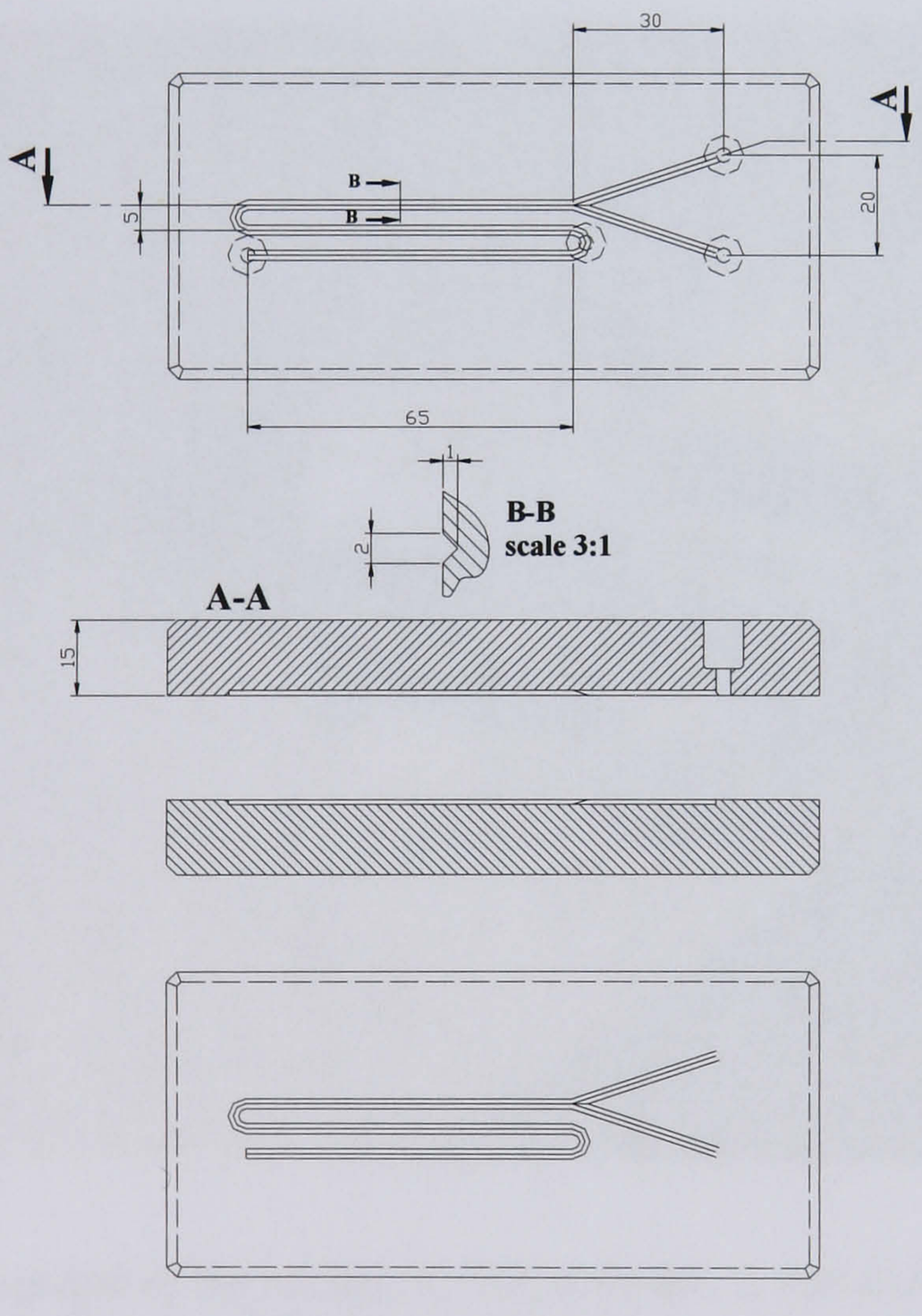

Figure 5.1. Schematic of the narrow channel reactor used for the gas-liquid investigation.

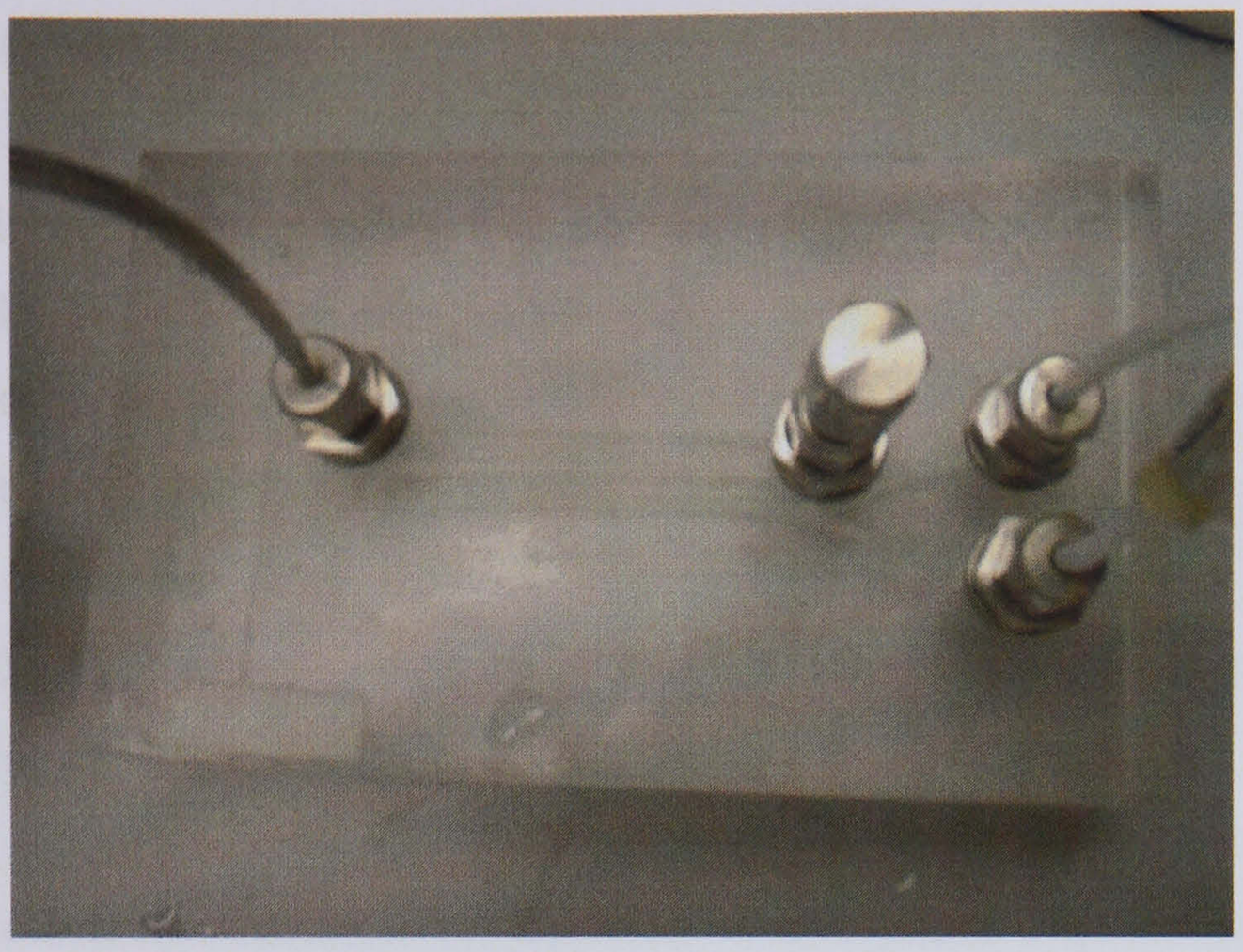

Figure 5.2. Photograph of the NCR.

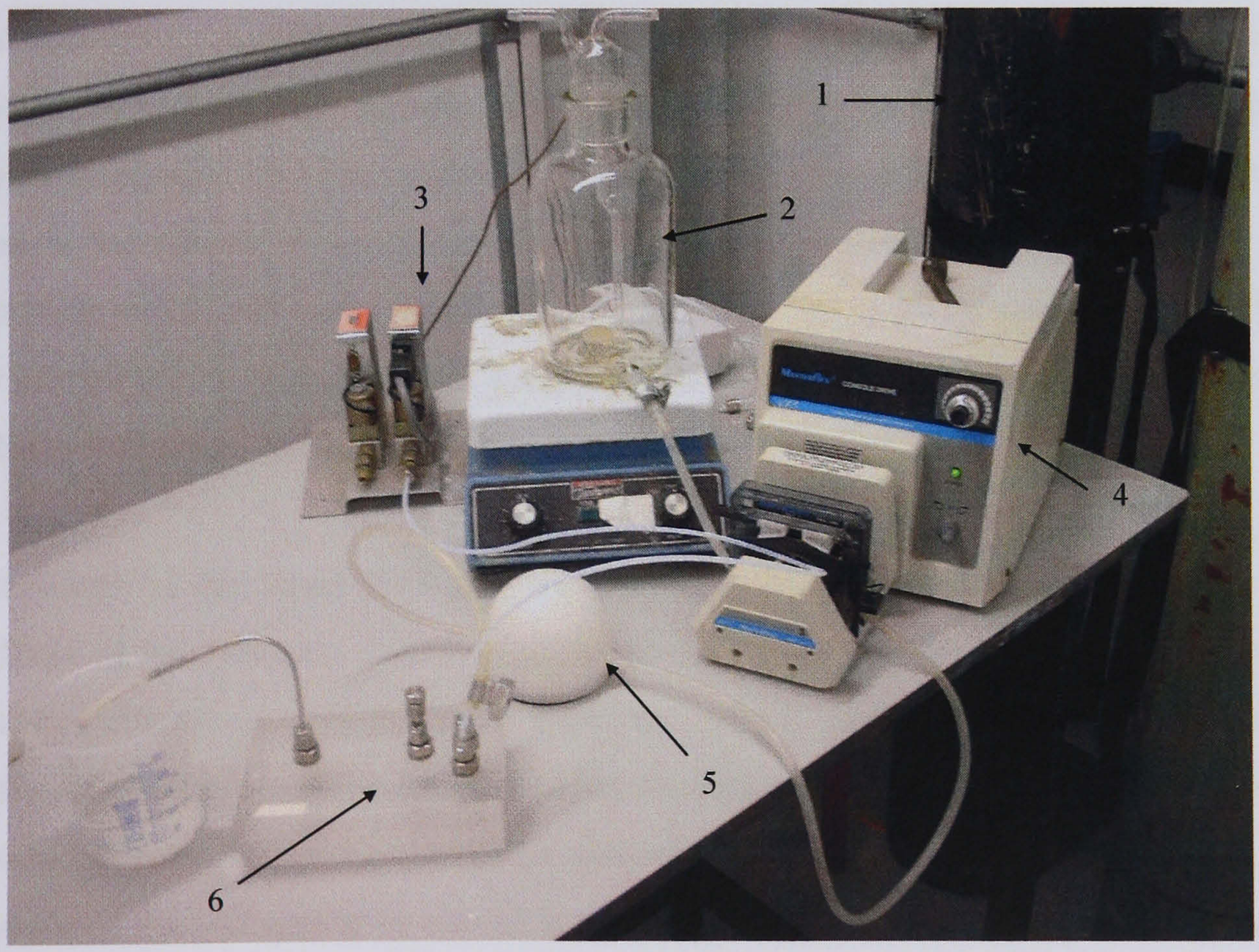

Figure 5.3. Photograph of the set-up: 1. CO_2 cylinder, 2. liquid feed bottle, 3. gas flow controller, 4. peristaltic pump, 5. pulse dampener, 6. narrow channel reactor.

5.3. Flow rate calibrations

The nominal gas flow rate declared by the flow controller manufacturer was verified experimentally for a limited number of settings of the flow controller. The values obtained, considered with the uncertainties, led to accepting the theoretical values as accurate. The maximum nominal flow rate for the gas was 50 l/h referring to nitrogen at 20°C. A correction factor equal to 0.74, as indicated by the manufacturer, was considered for the carbon dioxide flow rate, giving a maximum value of 37 l/h (corresponding to approximately 10.28 cm^3/s).

The liquid used for the calibration of the pump was deionised water and the tests were carried out at ambient conditions, with temperatures between 20°C and 23°C. For each value of pump speed considered (8 in total) at least 4 gas flow rate values were tested to ensure that the gas flow did not affect the velocity of the liquid in the channel. Gas flow rates considered generally varied between 5 % and 25 % of the maximum flow rate. The flow rate was calculated from the measurement of the volume collected in a certain amount of time and of the time itself. A measuring cylinder was used to measure the volume of the collected water and a stop clock was used to measure the time over which the liquid was collected. For each set of pump speed and gas flow rate measurements were repeated at least three times. Average values were considered as the best estimate of the flow rate.

Uncertainty in the liquid flow rate depended on the uncertainties introduced in the readings of the collected volume and the elapsed time and uncertainty analysis was used to estimate uncertainty of the flow rate values. This technique is described in Appendix A and provides a method for estimating uncertainty from the uncertainties introduced in the single measurements carried out to determine the required value. An example of the estimation of uncertainty with this technique is shown for the present case.

The water flow rate was calculated with the equation:

$$Q = \frac{V_c}{t} \tag{5.1}$$

where V_c (m^3) was the collected volume and t (s) the time over which the water was collected. Uncertainty in the flow rate depends on the uncertainty of the volume and the time through the following expression (of which equation A2 represents the general case):

$$w_Q = \left[\left(\frac{\partial Q}{\partial V_c} w_{V_c} \right)^2 + \left(\frac{\partial Q}{\partial t} w_t \right)^2 \right]^{1/2} \tag{5.2}$$

were w_i is the uncertainty for the generic variable i. Calculating the derivatives:

$$w_Q = \left[\left(\frac{1}{t} w_{V_c} \right)^2 + \left(-\frac{V_c}{t^2} w_t \right)^2 \right]^{1/2} \tag{5.3}.$$

The measuring cylinder had a precision of ± 1 ml, whereas the minimum time interval that could be measured with the stop clock was 1 s. In the calculations $w_{V_c} = 2\ cm^3$ and $w_t = 2\ s$ were considered. For the highest flow rates larger volumes of water were collected, the precision of the measuring cylinder was in this case ± 2 cm^3. For these data $w_{V_c} = 4\ cm^3$ was considered. Uncertainties were calculated for all the data and the average of all uncertainties at one flow rate was taken as the uncertainty of the result. Flow rates obtained ranged approximately between 0.35 cm^3/s and 1.48 cm^3/s with uncertainties between 0.75 % and 1.6 % of the flow rate. A plot of the experimental flow rate values versus pump speed is reported in Figure 5.4 together with the calibration line used in the study.

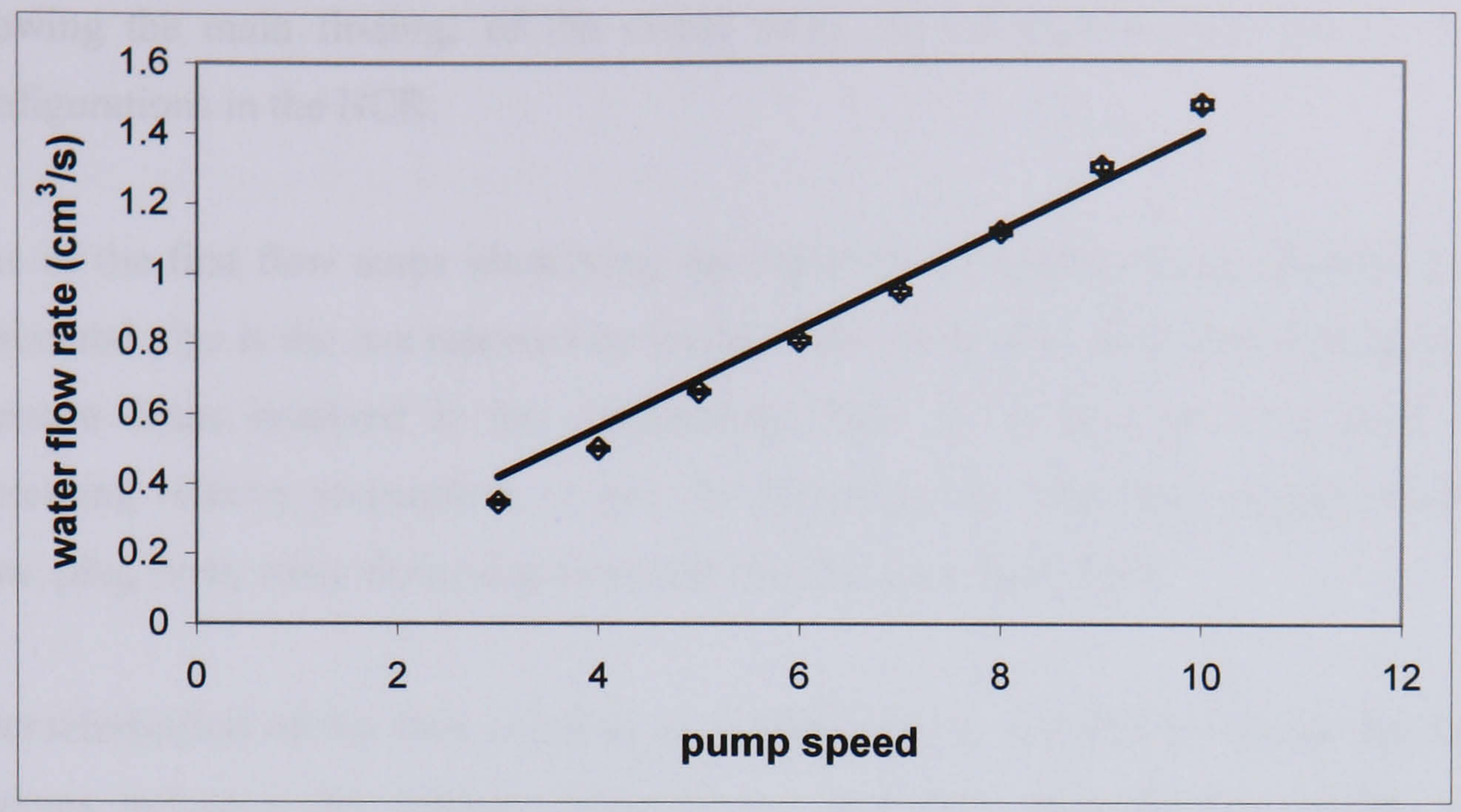

Figure 5.4. Calibration data for the water flow rate vs. pump speed.

5.4 Flow pattern for the water-carbon dioxide system in the NCR

5.4.1 Introduction and previous studies on gas-liquid flow regimes

Flow regimes for different gas-liquid systems have been the object of numerous studies, in relation with the various applications of multiphase flow through pipes. Flow regimes in vertical and horizontal channels have different characteristics, particularly in industrial scale pipes. For decreasing characteristic dimension of the channel, gravity becomes relatively less important than surface tension and channel orientation tends to become irrelevant. Different criteria have been proposed to identify this transition area in terms of characteristic dimension of the pipes and Ghiaasiaan and Abdel-Khalik (2001) briefly described them in their review on two-phase flow in microchannels. The transition to a surface tension dominated regime (for which flow patterns are not affected by channel orientation) appears to occur for the air-water system for diameters between 1 and 2 mm.

This case was concerned with the use of a horizontal square channel. The characteristics of gas-liquid flow patterns in industrial scale horizontal channels are preliminary described. The results of some of the numerous recent studies on flow patterns in micro channels and mm scale channels are then summarized before

showing the main findings of the visual study on the water-carbon dioxide flow configurations in the NCR.

One of the first flow maps identifying gas-liquid flow regimes in an industrial scale horizontal pipe is the one reported by Baker (1954) who was concerned with the high pressure drops involved in the simultaneous flow of oil and gas in a pipe. For increasing relative proportions of gas, he identified the following regimes: bubble flow, plug flow, wavy flow, slug flow, annular flow and spray flow.

Characterization of the flow patterns is fundamental in two phase flow as the flow regimes influence the characteristics of heat and mass transfer, the contact area between the phases and pressure drop. Many applications in recent years have driven the attention towards the study of gas-liquid flow patterns in micro channels and narrow channels. These include two phase heat transfer in miniaturized systems, reacting systems in micro scale channels and hollow fibre ultrafiltration. Flow patterns in mm scale channels and micro channels are morphologically similar to the ones in larger scale channels.

Barnea et al. (1983) carried out probably one of the first studies on millimetre scale pipes. The ID of the tubes studied varied between 4 and 12.3 mm and the work focused on the air-water system. The authors found that the transition between stratified and slug flow in the smaller channels did not follow the prediction of a model valid for larger scale pipes. They modified the model to include surface tension contributions.

Mishima et al. (1993) studied the flow patterns of an air-water mixture in narrow rectangular ducts with a high width to depth aspect ratio. The channels they studied were 4 cm wide with depths of 1, 2, 4 and 5 mm. They observed the occurrence of bubble, slug, churn and annular flow. Churn flow is a transition regime between slug and annular flow. It occurs when, at increasing gas flow rates, the slugs are disrupted and the gas is more dispersed in the liquid. Similar results were found by Wilmarth and Ishii (1994) who studied the two-phase flow of air and water in narrow rectangular gaps with channel widths of 15 and 20 mm and depths of 1 and 2 mm. Xu (1999) studied flow patterns for an air-water mixture for smaller gaps, with channels 12 mm wide and 1.0, 0.6 and 0.3 mm deep. The main finding of his study was that, for

the smallest channel, bubble flow was never observed, whereas similar flow patterns as the ones for larger tubes were observed for the other two channels. The results of these studies show that the geometry of the channel does not influence the type of flow pattern encountered for the two-phase system. It might affect the transition regions between regimes marginally as well as the shapes of the gas bubbles or slugs because of geometrical constraints.

Laborie et al. (1999) characterized flow patterns and flow parameters for air-water mixtures in 1, 2, 3 and 4 mm capillaries. Their operating conditions corresponded to the occurrence of slug flow. They characterized the slug length and velocity from visual observations. Triplett et al. (1999a) studied flow regimes for the system air-water in circular capillaries with 1.1 and 1.45 mm ID and in semi-triangular channels with hydraulic diameters equal to 1.09 and 1.49 mm. Flow regimes identified in the semi-trangular cross section channels were similar to those observed in the circular capillaries. They could be classified as bubble, slug, churn, annular-slug and annular flows. Cheng and Lin (2001) studied the flow patterns occurring in 2 to 8 mm ID capillaries with air and a dextran aqueous solution as the two fluids. Effect of tube inclination was also studied. They found the occurrence of slug flow for a wide range of gas and liquid velocities for all tube inclinations. Slug shape was dependent on inclination for the larger diameters whereas it was independent of it for the 2 mm channel.

Akbar et al. (2003) compared the results of different studies on millimetre scale and micro scale channels. They found general agreement between the data on the flow regimes collected in various studies and they observed that the flow transition regions seemed to be consistent across the different investigations. They also observed that triangular channels, studied by Triplett et al. (1999a) might present different flow properties and transition boundaries. This is in agreement with what was reported earlier about narrow rectangular gaps.

As the occurrence of slug flow is particularly relevant for this work, as it will be shown later, a short review on slug flow hydrodynamics is reported in the next section, before illustrating the results of the flow visualization study for the narrow channel reactor.

5.4.2 Slug flow hydrodynamics

An accurate definition of slug flow has recently been given by Ghiaasiaan and Abdel Khalik (2001) who describe it as being characterized by bullet-shaped (Taylor) bubbles with diameters close to the diameter of the channel. The slugs are separated from the wall by a thin liquid film and they can have various lengths reaching more than 15 times the channel diameter. The Taylor bubbles are separated by liquid slugs (or plugs) that often contain small entrained gas bubbles.

Taylor (1961) probably carried out one of the first experimental studies characterizing slug flow. The author examined the flow of air in a tube filled with viscous liquids and determined the relationship between the velocity of the liquid and that of the air column in the tube.

More recently, Chen (1986) measured the thickness of the film surrounding a slug for a wide range of slug velocities by using electrical resistance measurements. The author used a 0.4 mm bore glass capillary and studied slug flow for air and oils of different viscosities. He found that the wetting film thickness between the slug and the capillary decreased as the bubble speed decreased, until it approached a constant value dependant on the roughness of the tube wall.

Irandoust and Andersson (1989) characterized slug flow by solving numerically the flow and mass transfer equations for the case of air slugs in water. They considered a capillary ID of 2 mm and both the lengths of the gas slugs and that of the liquid plugs between two slugs was set to 4 mm. The fluid velocity used was 0.1 m/s. The authors found that for the absorption of oxygen with chemical reaction most of the mass transfer occurred in the liquid film between the slugs and the walls, for their set of operating conditions.

Elperin and Fominykh (1995) modelled liquid side controlled mass transfer in vertical gas-liquid slug flow at low Reynolds numbers. They took into account equal lengths of gas and liquid slugs. Their model applies to the case of relatively long slugs and allows the prediction of the mass transfer rate from the n-th gas slug in a series of n slugs.

Thulasidas et al. (1995) characterized slug flow inside a 2 mm circular capillary and a 2 mm square capillary using water and silicone oil as liquids and air as the gas. The use of silicone oil allowed the test of a large range of viscosities of the liquid phase, ranging between 0.0046 and 0.971 Pa·s. The authors experimentally determined length, velocity and diameter of the slugs. These experimental determinations allowed the calculation of other parameters characterizing slug flow. Considering their range of viscosities, gas velocities between $0.34 \cdot 10^{-2}$ and 0.442 m/s and liquid velocities between $0.15 \cdot 10^{-2}$ and $1.7 \cdot 10^{-2}$ m/s, they obtained specific interfacial areas between 700 and 1500 m^2/m^3 and film thicknesses between slugs and the wall varying between 47 and 332 μm.

Other studies on hydrodynamic characterization of slug flow include that from Kawaji et al. (1997) who used a photochromic dye activation method to investigate velocity profiles in the liquid in vertical slug flow inside a 25.4 mm ID pipe and the study carried out by Shemer (2003) on the use of statistical methods for an accurate description of slug flow.

5.4.3 Results for this investigation

For the flow visualization work, a Philips ToUcam USB PC camera was used. Videos of the flow of water and carbon dioxide were recorded and then images were taken from them. The camera used allowed a regulation of shutter speed up to 60 frames per second. As a high speed video camera was not used, the range of operating conditions in terms of fluid velocities that could be investigated was limited. In fact, at high gas and liquid velocities the camera did not allow the visualization of the flow pattern obtained. Most of the data have been collected over a limited range of gas and liquid flow rates. The videos were recorded in an almost dark environment.

Nearly all of the images obtained showed the occurrence of slug flow, with transition and annular flow corresponding to a limited set of gas and liquid flow rates. Figures 5.5 and 5.6 show images of slug flow in the NCR for a liquid flow rate equal to 0.42 cm^3/s and two different gas flow rates respectively. From the length of the channel sections it was estimated that in the two cases the lengths of the gas slugs were 3.7 and 9.8 mm respectively and those of the liquid plugs between them were 1.8 and 3.2 mm

respectively. Similarly, Figures 5.7 and 5.8 refer to two different gas flow rates with a water flow rate equal to 0.91 cm^3/s. For these two cases the lengths of the gas slugs were estimated to be 4 and 8.1 mm and that of the liquid plugs 2 and 2.7 mm respectively. In both cases it can be observed that, for a fixed liquid flow rate, slug length increases with increasing gas flow rate. This is consistent with the conclusions of previous studies, as indicated for example by Laborie et al. (1999).

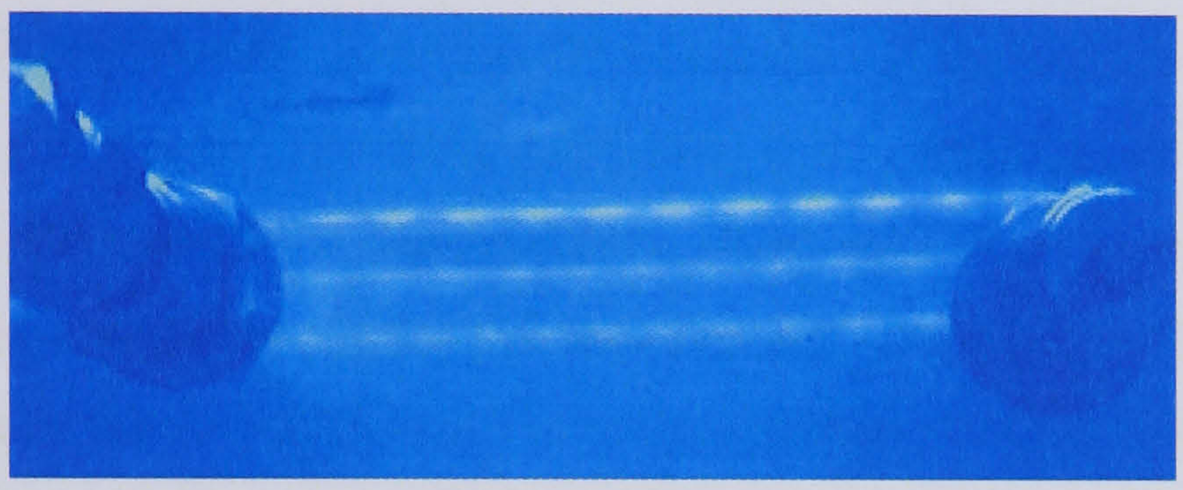

Figure 5.5. Gas-liquid flow in the NCR for $Q_G = 0.36\ cm^3/s$, $Q_L = 0.42\ cm^3/s$.

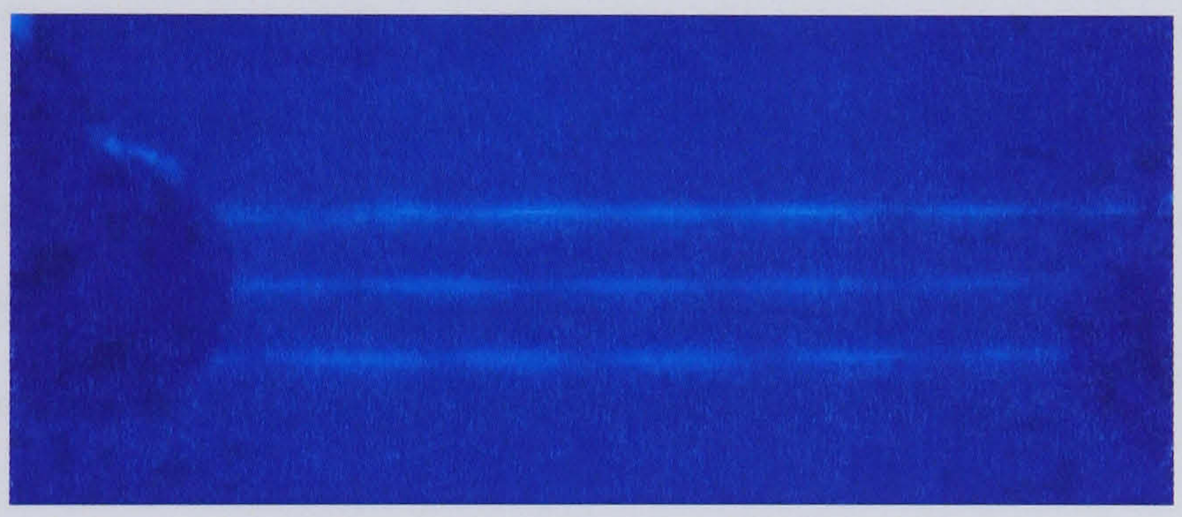

Figure 5.6. Gas-liquid flow in the NCR for $Q_G = 0.82\ cm^3/s$, $Q_L = 0.42\ cm^3/s$.

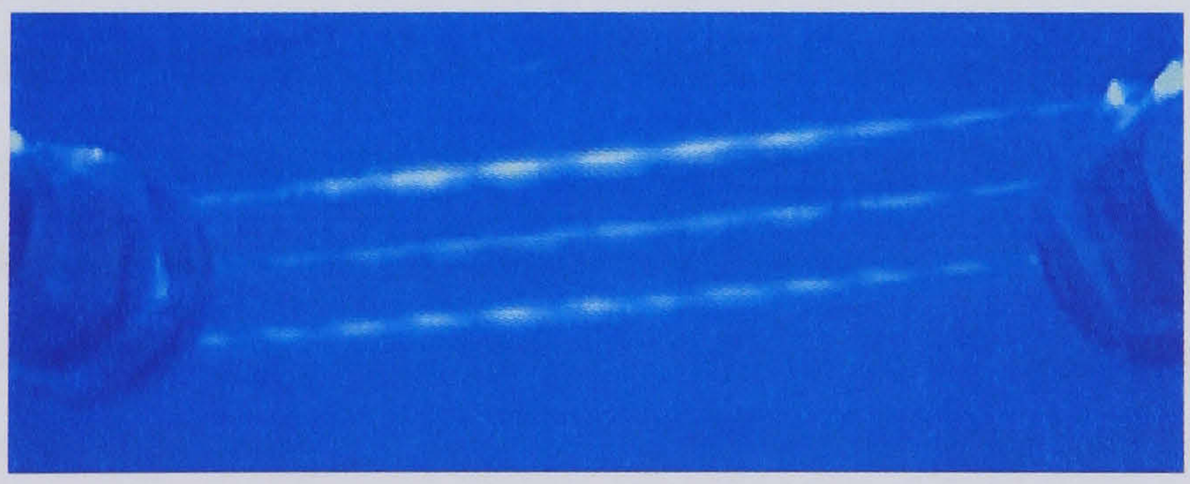

Figure 5.7. Gas-liquid flow in the NCR for $Q_G = 1.03\ cm^3/s$, $Q_L = 0.91\ cm^3/s$.

Figure 5.8. Gas-liquid flow in the NCR for $Q_G = 2.06\ cm^3/s$, $Q_L = 0.91\ cm^3/s$.

The occurrence of slug flow is reported by Laborie et al. (1999) for gas injection ratios between 0.17 and 0.67. This parameter is defined by the equation:

$$\varepsilon_G = \frac{u_{GS}}{u_{LS} + u_{GS}} \tag{5.4}$$

where u_{GS} (m/s) and u_{LS} (m/s) are the gas and liquid superficial velocities respectively, calculated as if each phase would occupy the channel as a one phase system. The authors also indicated that the transition from slug flow to annular flow occurs around the value $\varepsilon_G = 0.9$. For the operating conditions in this case the gas injection ratios varied between 0.09 and 0.95 approximately. Flow patterns that were identified as corresponding to a transition regime between slug and annular flow were obtained for gas injection ratios between 0.80 and 0.88 approximately. Annular flow was identified for three sets of operating conditions corresponding to gas injection ratios between 0.90 and 0.95. It appears that the results for this study are in accordance with the transition criterion between slug and annular flow given by Laborie et al. (1999). These authors also suggested that low values of the gas injection ratio ($\varepsilon_G < 0.2$) should lead to the occurrence of bubble flow. This was not valid in the present case, as only slug flow was observed for gas injection ratios lower than 0.80.

Results of investigations on characterization of flow patterns are normally reported in graphs containing the velocities of the two phases, or derived variables, as coordinates. Günther et al. (2004) studied gas-liquid flow patterns in 150 μm deep and 400 μm wide rectangular cross section microchannels fabricated in poly dimethylsiloxane with different configurations. They investigated a wide range of liquid and gas flow rates and reported in a flow map the occurrence of bubble, slug and annular flow for increasing gas velocity, as well as wavy annular and churn flow. They used gas velocities between 0.01 and 100 m/s and liquid velocities between $1 \cdot 10^{-4}$ and 10 m/s, although it is not clear which were the gas and liquid phases used for the flow visualization study.

As previously mentioned, Akbar et al. (2003) compared results of recent studies on flow patterns in micro scale and millimetre scale channels. They proposed a flow map to describe transition between regimes, generalizing the results of the different

investigations on the flow of air and water in both circular and non-circular channels. The transition regimes studied referred to channels with $d_h < 1$ mm or $d_h \approx 1$ mm for which the flow patterns should be independent of channel orientation and dependent on inertia and surface tension effects only. The transition functions are expressed in terms of Weber numbers of the two phases. The Weber dimensionless number represents the ratio between inertial forces and surface tension forces and is defined by the following equations, for gas and liquid respectively:

$$We_{GS} = \frac{u_{GS}^2 d_h \rho_G}{\sigma} \tag{5.5}$$

$$We_{LS} = \frac{u_{LS}^2 d_h \rho_L}{\sigma} \tag{5.6}$$

where the variables are defined in respect to the superficial velocities. To compare the results of this study with the transition map proposed by Akbar et al. (2003), Figure 5.9 shows in one graph the results for the NCR and the proposed transition functions. In this case $d_h \cong 1.4$ mm and the density of the gas was higher than in the case of air. If the ideal gas law is used to calculate the gas density, the following result is obtained at a temperature of 20°C:

$$\rho_{CO_2} \cong 1.53 \rho_{air} \tag{5.7}$$

and the Weber number varies accordingly. Figure 5.9 shows the Weber number for the gas phase versus the Weber number for the liquid phase from the results of this investigation for the CO_2-water system together with the transition map derived for the air-water system. All the data that corresponded to slug flow lie in the region identified as surface tension dominated, where slug and bubble flow are expected to occur. All of the data identified as belonging to a transition regime between slug and annular flow also lie in the same region. Data identified as relative to annular flow lie instead in the transition area according to the proposed map. It can be concluded that probably using transition areas rather than single curves could allow the inclusion of effects such as channel cross section. This is consistent with the results of the studies taken into account by Akbar et al. (2003) to draw the map, for which transition data lie within a certain distance from the transition curves. In fact, it can be expected that the

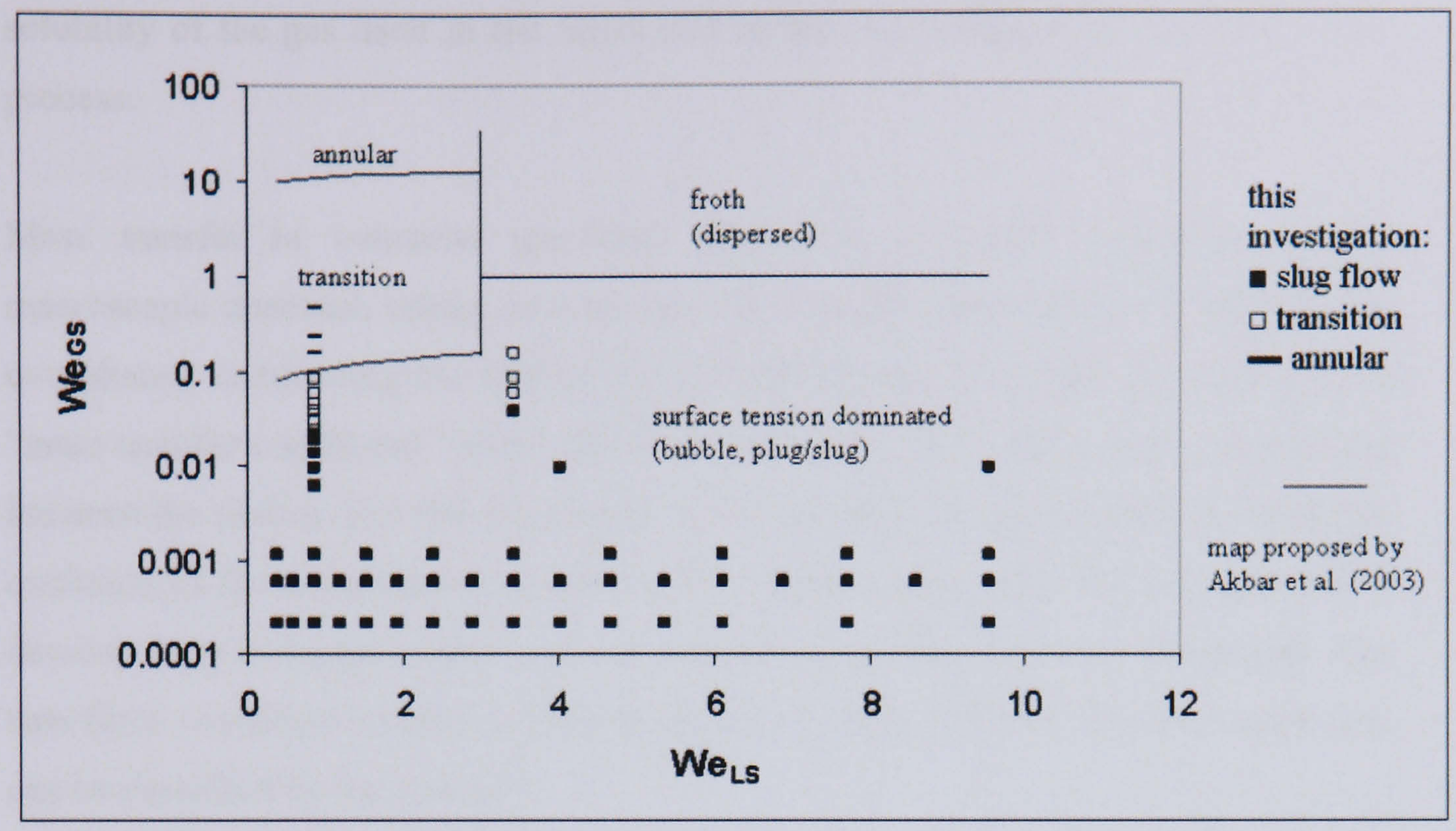

Figure 5.9. Results of the flow pattern study and transition map proposed by Akbar et al. (2003).

corners of a square cross section might favour the formation of a more stable thin film of liquid adjacent to the channel walls in respect to a circular channel. This would cause the onset of annular flow to occur at lower gas velocities than in a circular channel, as the results for the NCR seem to confirm. The same cross section properties might explain why no bubble flow was observed for the narrow channel, even at relatively low gas velocities. The influence of gas density does not seem to influence the discrepancies with the map, in fact if the transition curves were plotted taking into account the change in density, multiplying We_{GS} by 1.53, the transition curves would be shifted upwards.

5.5 Fundamentals of gas-liquid mass transfer

5.5.1 Physical absorption

Absorption of a gas in a liquid requires the gas molecules to be transferred from the bulk of the gas phase across the interface between the two phases to the bulk of the liquid phase. The final concentration of the solute in the liquid depends firstly on the

solubility of the gas itself in the liquid and on the mass transfer performance in the process.

Mass transfer in industrial gas-liquid contactors is usually described with a macroscopic approach taking into account the concentration difference between the two phases, constituting the driving force of the process, and what is defined as the "mass transfer coefficient" which describes the rate at which the solute is transferred between the phases. The two film model is the one most commonly used to depict the evolution of the concentration gradients. The concentration gradients are supposed to develop in two stagnant films on each side of the interface between the phases. The two films constitute a series of two resistances to mass transfer. The absorption rate can be described by the equation:

$$N = K_G A_{mt}(p - p_{bl}) = K_L A_{mt}(c_{bg} - c) \tag{5.8}$$

where K_G (mol/(s m^2 atm)) and K_L (m/s) are the overall mass transfer coefficients referred to the gas and liquid phase respectively (Cussler, 1997, p. 240) and A_{mt} (m^2) is the mass transfer area between the phases. The variable c_{bg} is the hypothetic value of the concentration in the liquid that would be in equilibrium with the gas at partial pressure p. Similarly, p_{bl} is the hypothetic value of the gas pressure in equilibrium with the concentration of the bulk of the liquid. The equation describing the equilibrium condition is Henry's law:

$$p = Hc \tag{5.9}$$

here written for the generic system, where H is the Henry's constant, in this case expressed in (atm m^3/mol). Considering the representation in respect to the overall liquid side mass transfer coefficient, K_L will have the expression:

$$K_L = \frac{1}{\frac{1}{k_L} + \frac{1}{k_G H}} \tag{5.10}$$

where k_L (m/s) and k_G (mol/(s m^2 atm)) are the mass transfer coefficients on the liquid side and on the gas side respectively. In many cases equation 5.10 can be simplified considering whether one of the resistances controls mass transfer. Usually for sparingly soluble gases, like in the absorption of CO_2 or O_2 in water, H has a relatively high value and therefore the approximation $K_L \cong k_L$ can be used. In this investigation no gas side mass transfer resistance was present as pure carbon dioxide was used. However the results of this study could be extended to the case of a gas phase not containing only carbon dioxide for the fact that the mass transfer resistance would be concentrated on the liquid side.

Other models have been proposed to describe mass transfer across interfaces, the most known are Higbie's penetration theory and Danckwerts' surface renewal model, both described by Sherwood et al. (1975). They have the advantage of being non stationary models and therefore to be more realistic, in respect to the mechanism of mass transfer between the phases. However, the film model will be taken into account for this investigation as it is the most widely used.

5.5.2 Mass transfer with chemical reaction

The rate of absorption of a gas in a liquid can be enhanced by using a liquid that can react with the gas and therefore increase the driving force for absorption. In addition to this, mass transfer combined with chemical reaction can occur in those processes for which the final product of the reaction is of main interest. The carbonation reaction to produce PCC falls in this last category. One of the main problems in conducting the reaction is making the gaseous reagent available in the liquid phase. This problem is parallel to the need of guaranteeing mixing efficiency in liquid phase precipitation. In order to understand more about the mass transfer characterization carried out, the fundamentals of the theory on combined mass transfer and chemical reaction are reviewed.

The kinetics of absorption in a reacting system depends on the relative rate of the reaction itself and mass transfer, in the general case both in the gas and in the liquid phase. As described by Levenspiel (1999, p. 527) there are eight cases to consider, going from infinitely fast reaction (mass transfer controlled kinetics) to extremely

slow reaction (negligible mass transfer resistance). For instantaneous and fast reaction in respect to mass transfer, the reaction occurs in the liquid film, rather than in the bulk of the liquid and the rate of mass transfer is enhanced by the chemical reaction. This phenomenon is usually quantified with the introduction of the enhancement factor E_f defined by the ratio between the mass transfer rate in presence of chemical reaction and the mass transfer rate for physical absorption (Levenspiel, 1999, p. 529). The enhancement factor is a function of two quantities:

$$E_f = E_f(E_{f,inf}, Ha) \tag{5.11}$$

the enhancement factor for infinitely fast reaction and the Hatta number. The Hatta number is a parameter that identifies the controlling regime and is given by the following expression:

$$Ha^2 = \frac{k_r c_L D_{G,L}}{k_L^2} \tag{5.12}$$

where k_r ($m^3/(mol\ s)$) is the kinetic constant for the reaction, which is assumed to have a second order rate. In equation 5.12 the gas phase resistance is considered negligible, c_L is the concentration of the reagent in the liquid phase and $D_{G,L}$ (m^2/s) is the diffusivity of the gas in the liquid. The following cases apply, in respect to the values of the Hatta number:

1. If $Ha > 2$ the reaction occurs in the liquid film (mass transfer controlled kinetics).
2. If $0.02 < Ha < 2$ the reaction occurs partially in the liquid film and in the bulk of the liquid (the rate depends both on mass transfer and on the kinetics of the reaction).
3. If $Ha < 0.02$ the reaction is infinitely slow and it occurs entirely in the bulk of the liquid, the rate is determined by the chemical kinetics alone.

5.6 Experimental procedures and operating conditions for the mass transfer and the precipitation studies

5.6.1 Mass transfer for the water-carbon dioxide system

Gas-liquid mass transfer performance for physical absorption in the NCR was characterized by contacting water and carbon dioxide in the channel and by reacting the mixture obtained at the reactor outlet with a batch of sodium hydroxide solution. This procedure was adopted in order to avoid de-absorption of carbon dioxide from the deionised water during the collection time that lasted several minutes. It was considered that in the short distance (about 2 cm) between the end of the outlet tubing of the NCR and the solution in the vessel no significant variation of CO_2 concentration in the water occurred. From a point of view of the reaction with the NaOH solution, the operation took place in a semi-batch mode, as the water-CO_2 mixture from the NCR went to gradually increase a certain volume of solution. The pH of the solution decreased with increasing volumes of water containing the absorbed carbon dioxide, forming in the general case either a mixed sodium hydroxide and sodium carbonate solution or a mixed sodium carbonate and sodium bicarbonate solution. Below pH 8.3-8.4 only sodium bicarbonate was present in solution (Hargis, 1988, p.181) and the amount of sodium bicarbonate formed could be determined by titration with hydrochloric acid until the methyl red end point (approximately pH = 4.2-4.6). This allowed the determination of the number of carbon dioxide moles absorbed per unit number of sodium hydroxide moles, considering that the overall stoichiometry of the reactions was:

$$NaOH + CO_2 \rightarrow NaHCO_3 \qquad (5.13).$$

Preliminary experiments were carried out to determine a concentration of the sodium hydroxide solution that would be suitable for this study. For each experiment a 0.04 M sodium hydroxide solution was prepared dissolving NaOH solid pellets (from BDH, analar grade, 99 % purity) in deionised water. The collecting vessel was filled with 200 ml of the solution. The liquid feed bottle (which can be seen in Figure 5.3) was filled with deionised water. The water was sparged with nitrogen before and during the experiment to remove the pre-existing absorbed carbon dioxide and to prevent any

significant absorption of carbon dioxide in the feed bottle. This was in case the increased carbon dioxide partial pressure in the environment could significantly enhance the absorption rate. Another aspect to be considered in order to have a correct characterization of the mass transfer performance of the NCR was the need to prevent any significant absorption from occurring in the water volume contained in the pulse dampener. This was achieved by connecting the gas feed pipe to the narrow channel reactor only just before starting the flow of water and by disconnecting it immediately after the end of the experiment.

Before starting each experiment, fresh deionised water was pumped to the reactor in order to replace the existing volume of water in the pulse dampener. The pH and temperature of the sodium hydroxide solution and deionised water were recorded. The gas flow rate was then set to the desired value and the pump speed setting was chosen. When the water and absorbed carbon dioxide started collecting in the vessel with the NaOH solution, a stop clock was started. This was to check that the liquid flow rate corresponded to the nominal flow rate. The pH of the solution was continually monitored during the collection time. After the pH had dropped to a value lower than 8.3, the water flow was stopped and pH and temperature of the solution were recorded. A few drops of 0.01 % methyl red solution in ethanol (from Fisher) were added to the sodium bicarbonate solution. The colour of the solution was at this point yellow. The solution was then titrated with 0.5 M HCl (volumetric solution, from Fisher) until the methyl red end point, which corresponded to the colour of the solution turning to bright pink. This occurred around pH 4.2, as declared by the manufacturer. The pH was continually monitored during the titration and at the end pH and temperature readings were taken. The final volume of the solution after titration was measured with a measuring cylinder.

A total of 19 different sets of operating conditions were considered. This was obtained by using 4 liquid flow rates and 5 gas flow rates for all liquid flow rates except one, for which 4 gas flow rates were considered. Liquid flow rates considered varied between 0.5 cm^3/s and 1.48 cm^3/s and gas flow rates varied between 1 cm^3/s and 8.2 cm^3/s. In all cases the gas phase used was pure carbon dioxide. All experiments were repeated at least three times. Ambient temperature during the experiments ranged between 14° C and 16° C.

A limited number of experiments were carried out by using two inlets for the gas, the one normally used on one side of the Y mixer and the feed point located at the beginning of the last straight segment of the channel in the Perspex block. In this case the main gas feed tube was provided with a T union which allowed the distribution of the gas feed. The same 1/8 inch OD PTFE tubing was used for both inlets so, theoretically, the gas flow rate should have been equally distributed between the two feed points. This series of runs was carried out both in the physical mass transfer investigation and in the one on precipitation from solution and it had the aim of evaluating possible influence of feed location on mass transfer performance and particle properties.

5.6.2 Precipitation from the carbonation of calcium hydroxide solutions and suspensions

The experimental procedure for the precipitation studies was similar to the one for the absorption study, except for the fact that a calcium hydroxide solution or suspension constituted the liquid feed. Experiments were carried out with one concentration of calcium hydroxide giving a solution (1.2 g/dm^3) and two values giving a suspension (5 g/dm^{3}and 7 g/dm^3). Calcium hydroxide solutions and suspensions were prepared by dissolving solid $Ca(OH)_2$ (GPR, 95% purity, from BDH) in water. For the experiments with the calcium hydroxide solution the operating conditions of the absorption study were replicated.

The aim of the tests with the suspensions was to evaluate the maximum concentration of the feed that could give total conversion to calcium carbonate in the NCR. In all cases the carbon dioxide flow rate used was the highest (8.2 cm^3/s) amongst the ones of the absorption study and 3 flow rate values for the liquid feed were tested. The double gas feed was not used for these experiments and the feed suspension was kept stirred during the reaction time.

For all the precipitation experiments the reaction time was recorded and the final volume of the calcium carbonate suspension was measured, similarly to the absorption study. Ambient temperature during the experimental study ranged between 17 °C and 20 °C.

The carbonation reaction of calcium hydroxide can be represented by the overall stoichiometry:

$$Ca(OH)_2 + CO_2 \rightarrow CaCO_3 \downarrow + H_2O \qquad (5.14).$$

After the reaction reaches total conversion, if carbon dioxide is still present in the reaction environment it further reacts with the carbonate ion to give bicarbonate ion:

$$CO_2 + CO_3^{2-} + H_2O \rightarrow 2HCO_3^- \qquad (5.15)$$

which, as previously seen, can be determined by titration to the methyl red end point.

For the studies in the NCR, if the conversion of calcium hydroxide to calcium carbonate was completed (this occurs for pH = 8.3 approximately), the outlet calcium carbonate solid was separated from the mother liquor by micro filtration. The apparatus used was the same as in the liquid phase study. A fixed amount of the remaining solution was then titrated to the methyl red end point with the 0.5 M HCl volumetric solution. This procedure had the aim of quantifying the total absorbed carbon dioxide. This allowed the calculation of the mass transfer coefficient in the presence of chemical reaction for the case of precipitation from solution. The solid collected was dried in an oven at a temperature of 110 °C. Selected samples of the dried powder were kept for particle size analysis (to be carried out after re-dissolution in water) and for SEM and X-ray diffraction.

When the conversion to calcium carbonate was not completed, as it happened in some cases in the precipitation from suspension, the outlet mixed calcium carbonate and calcium hydroxide slurry was titrated with the 0.5 M HCl volumetric solution to neutralize the residual calcium hydroxide. The extent of the neutralization was followed by recording the pH of the suspension. This determination allowed the calculation of the amount of carbon dioxide absorbed for this case. The remaining calcium carbonate slurry was then filtered in the micro filtration unit and the solid collected was dried at a temperature of 110 °C to collect the powder for the different analyses.

For the experiments with the calcium hydroxide solution, conversion was completed in all cases and runs were repeated at least twice for determination of the absorbed carbon dioxide and the collection of the calcium carbonate powder. In some cases experiments were repeated again only to collect the calcium carbonate slurry to analyze directly by laser diffraction. When the slurry was collected for analysis, small volumes of a sodium hexamethaphosphate solution were added to it to limit aggregation phenomena between the collection and the analysis. Typically 1 cm^3 of solution for 10 cm^3 of slurry were used, as in the liquid phase study, and the concentration of the surfactant solution was 0.1 % in weight.

As with the experiments that gave total conversion, for the experiments when conversion was not complete at least two repetitions were carried out for the titration procedure. When slurry samples were kept for particle size analysis, the surfactant solution was added to the calcium carbonate slurry after the neutralization of calcium hydroxide.

5.7 Mass transfer results

5.7.1 Absorption of carbon dioxide in water

As previously explained, the quantification of the amount of carbon dioxide absorbed in this case depends on the concentration of the sodium hydroxide solution used to react with the carbon dioxide itself. However, as the same concentration of sodium hydroxide was used in all the experiments, the results obtained at different operating conditions can be compared in terms of carbon dioxide absorption rate. This is defined by the equation:

$$N_{CO_2} = \frac{Q_L n(CO_2)_{abs}}{V_{H_2O}} \tag{5.16}$$

where $n(CO_2)_{abs}$ is the number of moles of absorbed carbon dioxide which, according to the stoichiometry of reaction 5.13, corresponds to the number of moles of sodium bicarbonate in the final solution as determined by the titration. V_{H_2O} is the volume of deionised water added to the volume of sodium hydroxide solution over the duration

of the experiment. It was determined by subtracting the initial volume of NaOH solution and the HCl titration volume from the total final volume measured after titration. In all the calculations regarding mass transfer, in this case and for the precipitation study, the liquid flow rate was calculated from the calibration line showed in Figure 5.4. This was to be consistent with the flow pattern study, where some flow rate values had to be calculated from the linear function as no experimental data where available for the specific speed settings. Errors introduced by using the correlation were taken into account in the uncertainty analysis carried out on the value of the absorption rate calculated from equation 5.16. Other than from the flow rate, uncertainty derived from the HCl titration volume and from the water volume which depended on the uncertainty of the measurements of the total final volume, the HCl volume and the NaOH solution volume.

Figure 5.10 shows the carbon dioxide absorption rate versus liquid flow rate for the various gas flow rates used. The results shown are averages of the different repetitions and average uncertainties vary between 2 % and 6 % of the average absorption rate. Figures 5.11 and 5.12 show the same data, for the first two gas flow rates and the remaining ones respectively, together with linear regression lines. The absorption rate varies linearly with the liquid flow rate with a limited influence of gas flow rate, which is more evident for the highest gas flow rates. If the gas injection ratio criterion for discriminating flow patterns described in section 5.4.2 is considered and the conclusions of the visual study are taken into account, 5 sets of operating conditions out of 19 would give transition or annular flow. However, from the results no influence of flow pattern on the mass transfer performance seems to be noticeable. Figure 5.13 shows the absorption rates for a liquid flow rate value of 0.84 cm^3/s when using one and two feed points. The absorption rate values obtained are very close in the two cases. The difference between the absorption rates are of the order of magnitude of the uncertainty itself for most gas flow rates. For the lowest flow rate value it appears that distributing the feed gave an advantage in terms of mass transfer performance. The absorption rate obtained in the case of distributed feed is about 16 % higher than in the case of one feed point.

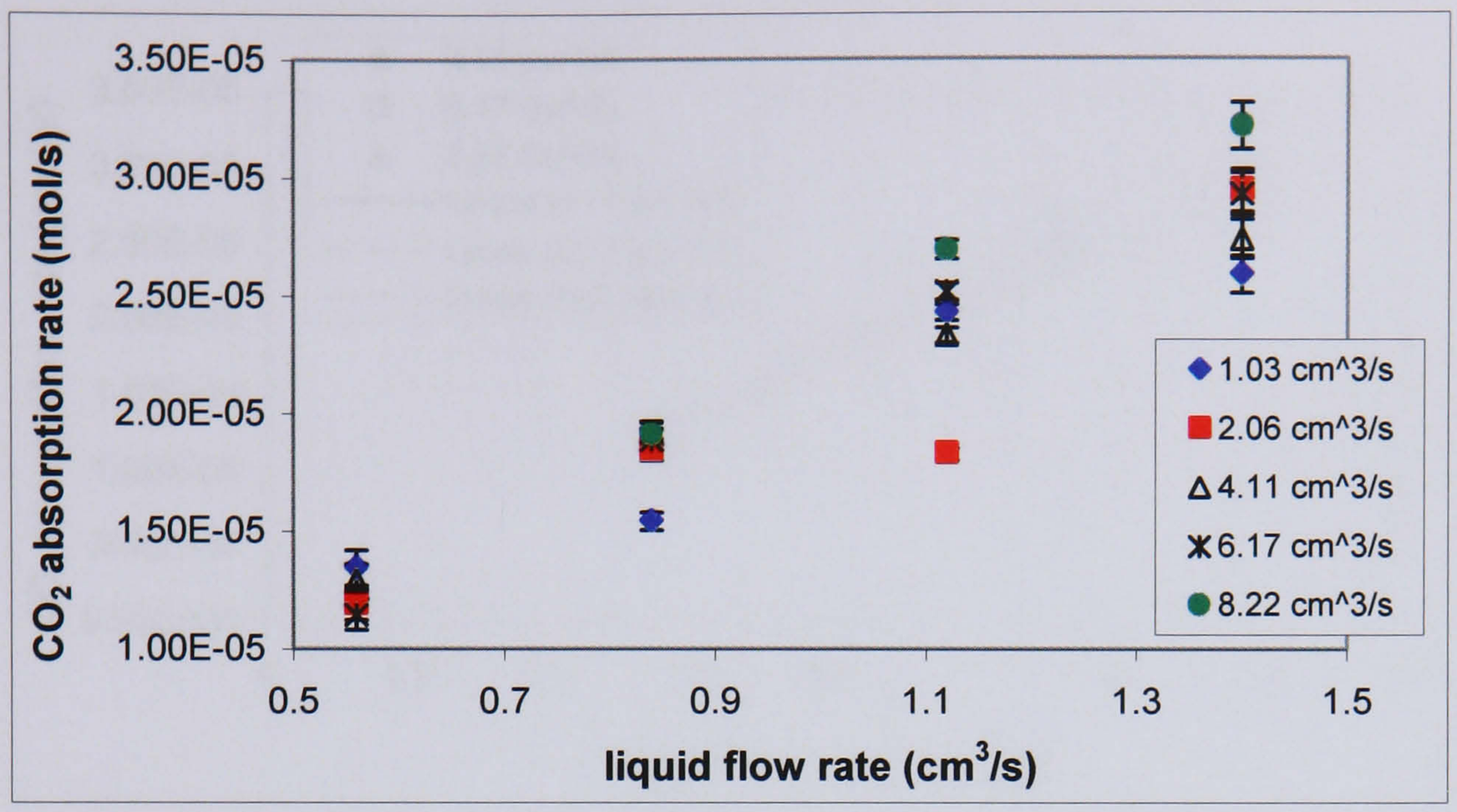

Figure 5.10. Carbon dioxide absorption rate vs. liquid flow rate at different gas flow rates.

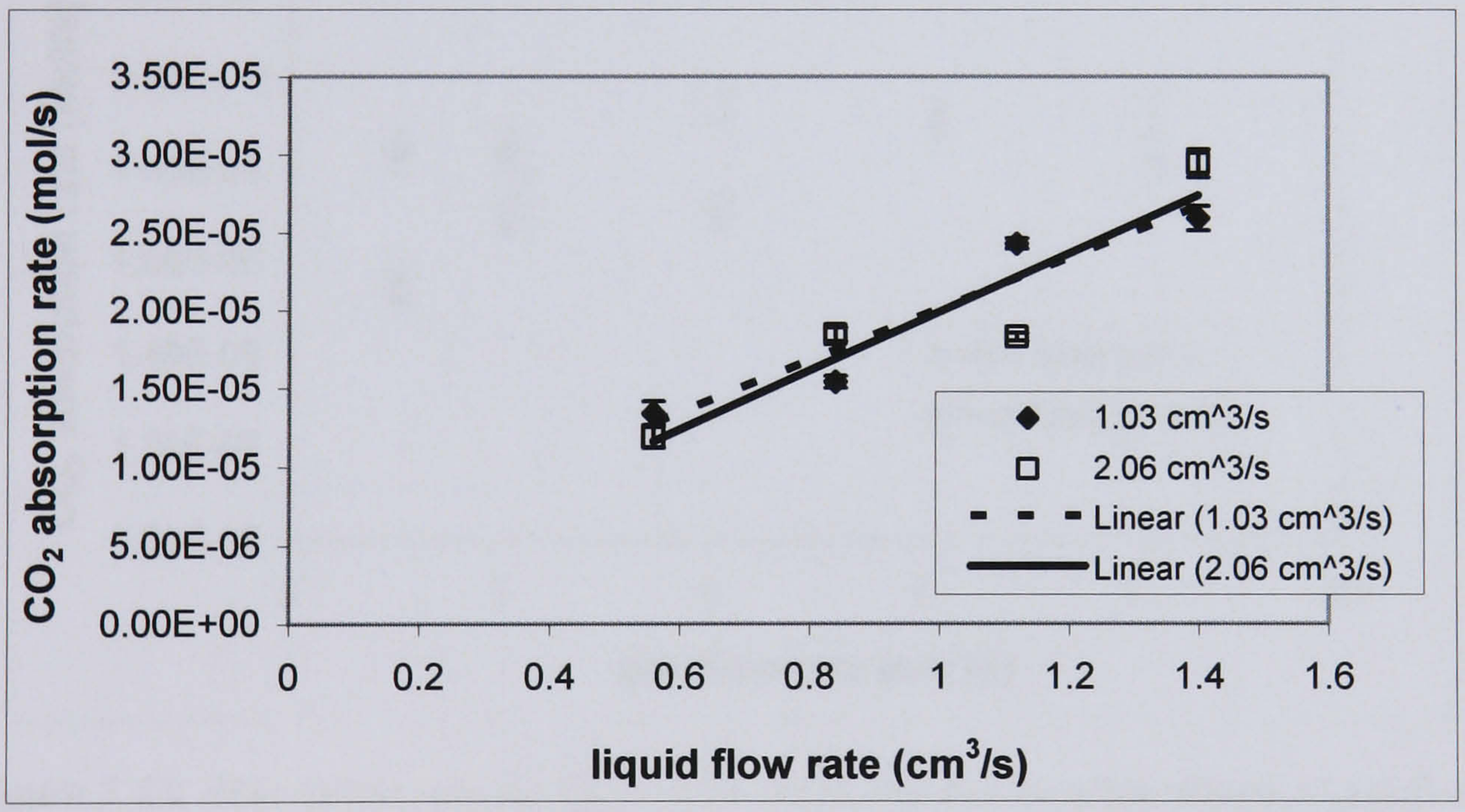

Figure 5.11. Carbon dioxide absorption rate vs .liquid flow rate for the lowest two gas flow rates and linear regression lines.

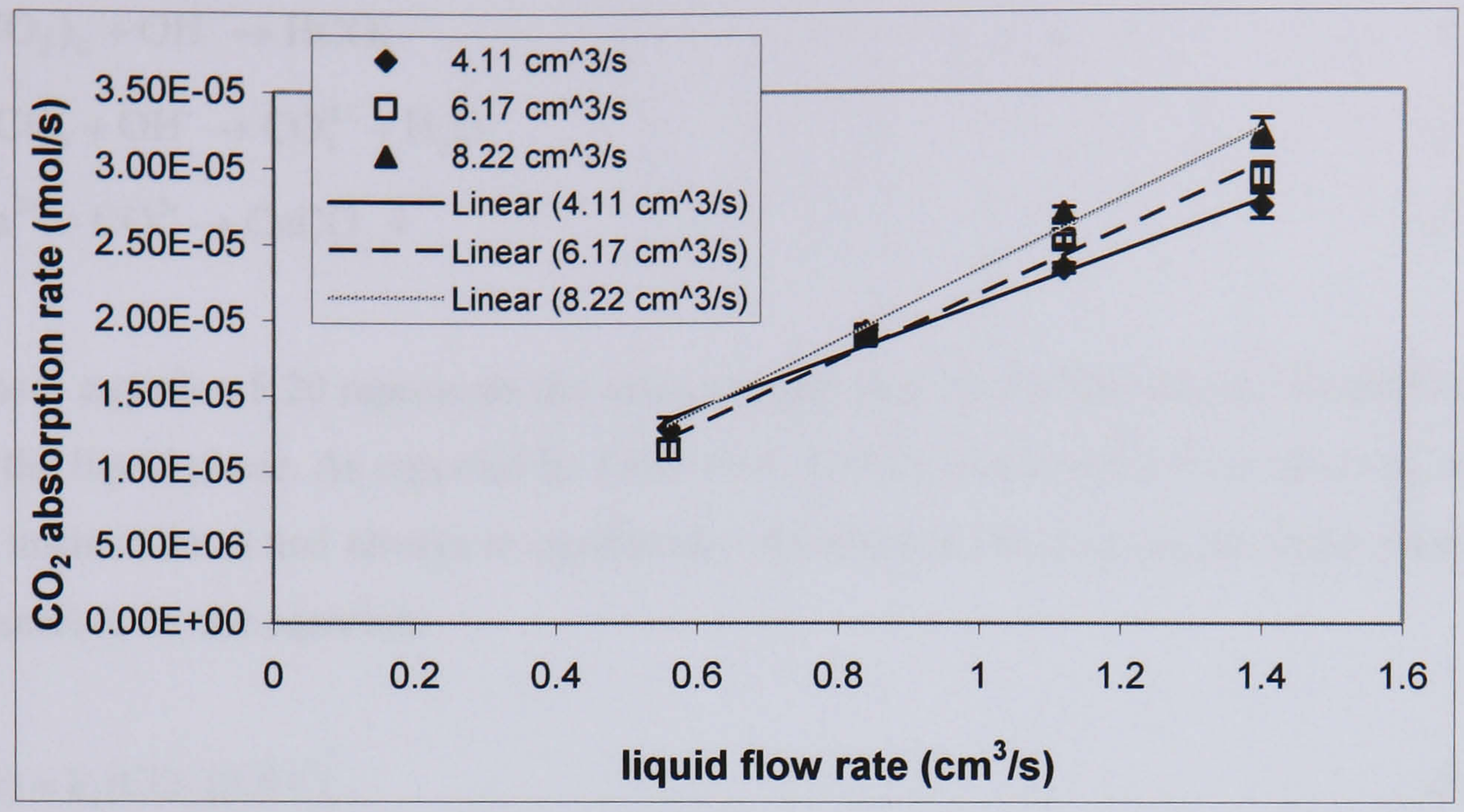

Figure 5.12.Carbon dioxide absorption rate vs. liquid flow rate for the three highest gas flow rates and linear regression lines.

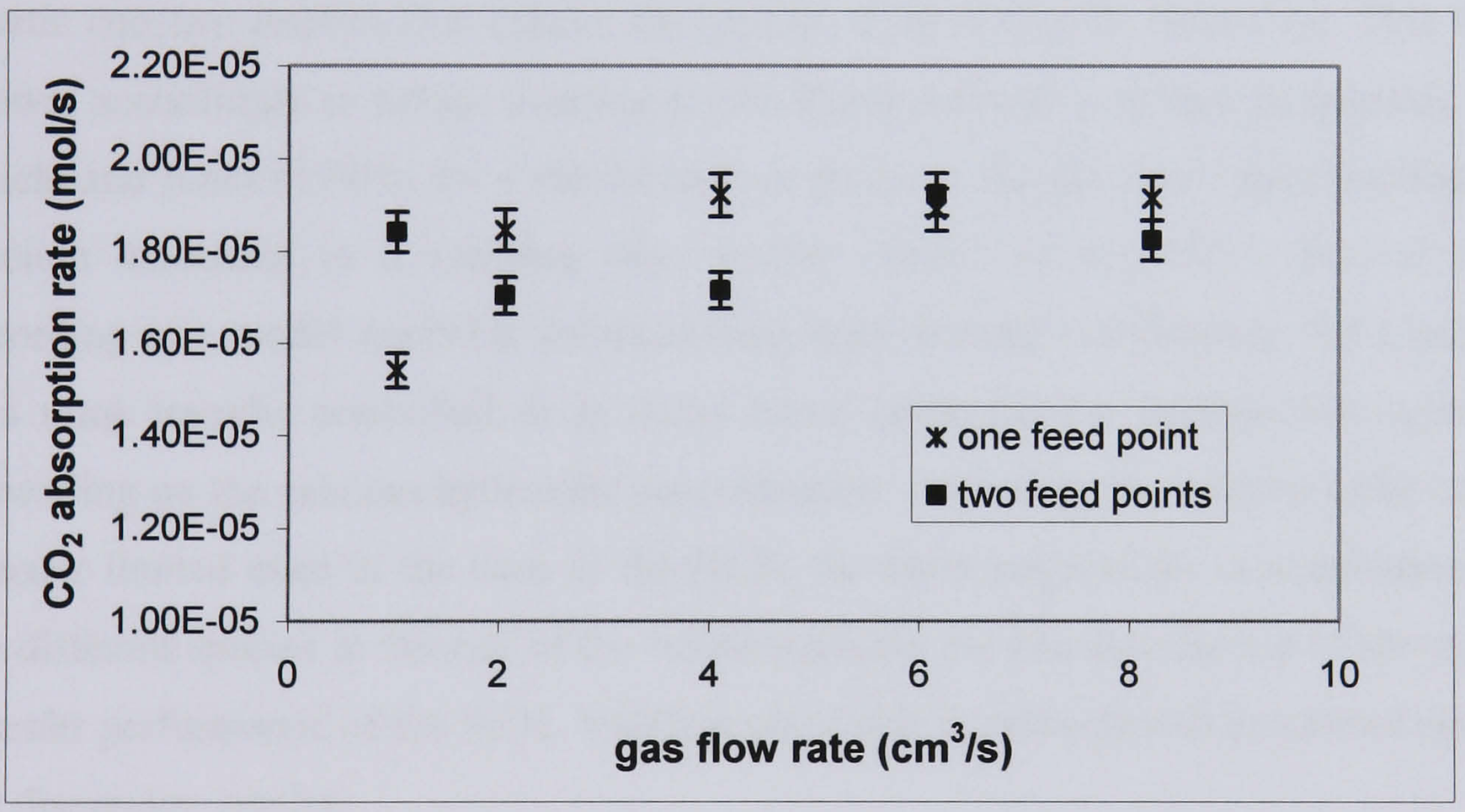

Figure 5.13. Absorption rate for Q_L = 0.84 cm^3/s and two configurations of gas feed.

5.7.2 Mass transfer and chemical reaction in the precipitation from solution

The carbonation reaction of calcium hydroxide solutions, represented overall by equation 5.14 is constituted by the following steps:

$$(CO_2)_G \rightarrow (CO_2)_L \qquad (5.17)$$

$$(CO_2)_L + OH^- \rightarrow HCO_3^- \quad (5.18)$$

$$HCO_3^- + OH^- \rightarrow CO_3^{2-} + H_2O \quad (5.19)$$

$$Ca^{2+} + CO_3^{2-} \rightarrow CaCO_3 \downarrow \quad (5.20)$$

where equation 5.20 represents the mass transfer step for carbon dioxide from the gas to the liquid phase. As reported by Jones et al. (1992), reaction 5.19 can be considered as instantaneous and always at equilibrium. Reaction 5.18 has a second order kinetics described by the equation:

$$(-r) = k_r[CO_2][OH^-] \quad (5.21)$$

where k_r = 12.4 $m^3/(s\ mol)$. The reaction rate will therefore be given by the slower of the two steps between mass transfer and reaction 5.18. The relatively high value of its kinetic constant implies that usually the process is mass transfer controlled. This was shown, accordingly to values assumed by the Hatta number or related parameters, by Wachi and Jones (1991b) for a stirred tank. A study on the gas-liquid precipitation of calcium carbonate in a spinning disc reactor (Trippa et al., 2002) showed that according to a model available for describing mass transfer coefficients, the reaction was mass transfer controlled or in some cases falling in the intermediate regime, depending on the calcium hydroxide concentration. Assuming the reaction to be mass transfer limited even in the case of the NCR, the knowledge of the concentration of the different species at the end of the reaction allows the characterization of the mass transfer performance of the NCR. Verification of this hypothesis will be carried out in the discussion section.

As mentioned earlier, for all cases of precipitation from solution the reaction went beyond completion, with some of the calcium carbonate re-dissolved to give bicarbonate ions. In this case the total amount of carbon dioxide absorbed was given, according to the stoichiometries of reactions 5.14 and 5.15, by the following expression:

$$n(CO_2)^*_{abs} = 0.5(n^i(OH^-) + n^f(HCO_3^-)) \quad (5.22).$$

In equation 5.22 the initial concentration of hydroxyl ions was considered to be equal to double the concentration of calcium hydroxide as this was considered to be fully dissociated. The concentration of bicarbonate ion was determined by titration, as illustrated in the description of the experimental procedure.

The carbon dioxide absorption rate in the presence of chemical reaction was calculated with the equation:

$$N^*_{CO_2} = Q_L [CO_2]^*_{abs} \tag{5.23}$$

where the asterisk indicates the presence of chemical reaction.

The mass transfer coefficient was calculated from the equation (Gaddis, 1999):

$$N^*_{CO_2} = k^*_L a V_r \Delta c \tag{5.24}$$

where a (m^2/m^3) is the specific interfacial area per unit volume and V_r (m^3) is a reference volume that can be either the volume of the liquid or the volume of the gas-liquid mixture in the gas-liquid contactor (Gaddis, 1999). The corresponding specific surface area is defined accordingly.

In practice, it is very difficult to estimate the values of a and the parameter more frequently used is $k_L a$, which is the volumetric mass transfer coefficient. In this case $k^*_L a$ is considered because of the presence of the chemical reaction. Δc is the generic concentration gradient which depends on the kinetic regime and on the way in which the two phases are contacted. In this case the reaction rate was assumed to be mass transfer controlled and, representing the kinetics according to the film theory, the reaction was considered to be entirely completed within the liquid film. The concentration gradient was then approximated as constant in the entire length of the reactor and equal to the concentration of carbon dioxide at the interface, $[CO_2]_i$. For the reference volume, the internal volume of the NCR, constituted by the part in the Perspex block and the outlet tubing, was considered. This would correspond to the total volume occupied by the gas-liquid mixture. The equation giving the mass transfer coefficient (in the case of chemical reaction) was:

$$k_L^* a = \frac{Q_L [CO_2]^*_{abs}}{V [CO_2]_i} \qquad (5.25).$$

Uncertainty was given by the measurement of the absorbed carbon dioxide and by the uncertainty on the flow rate value, which was taken into account in the same way as in the physical absorption study. This was justified considering that the measurement of the final volume of suspension and of the reaction time in each experiment lead to the conclusion that no significant variation in the flow rates obtained was noticed if comparing to the physical absorption study. Averages of the values obtained in the different repetitions were considered as the best result and average uncertainties varied between 1% and 6% of the average $k^*_L a$ values.

The mass transfer coefficients showed the same type of trend obtained for the carbon dioxide absorption rate in the previous section. Volumetric mass transfer coefficients were between 0.1 and 1 s^{-1}, with values ranging between 0.33 and 0.80 s^{-1} approximately. Figure 5.14 shows $k^*_L a$ versus liquid flow rate for the different gas flow rate values. Similarly to that reported earlier, Figures 5.15 and 5.16 show the same data for the two lowest and the three highest gas flow rates together with linear regression lines. In Figure 5.17 the mass transfer data versus gas flow rate with liquid flow rate as a parameter are reported. Mass transfer coefficients at 0.56 cm^3/s liquid flow rate are practically equal for all gas flow rates. Gas flow rate has a greater influence in increasing mass transfer coefficients for the highest liquid flow rates.

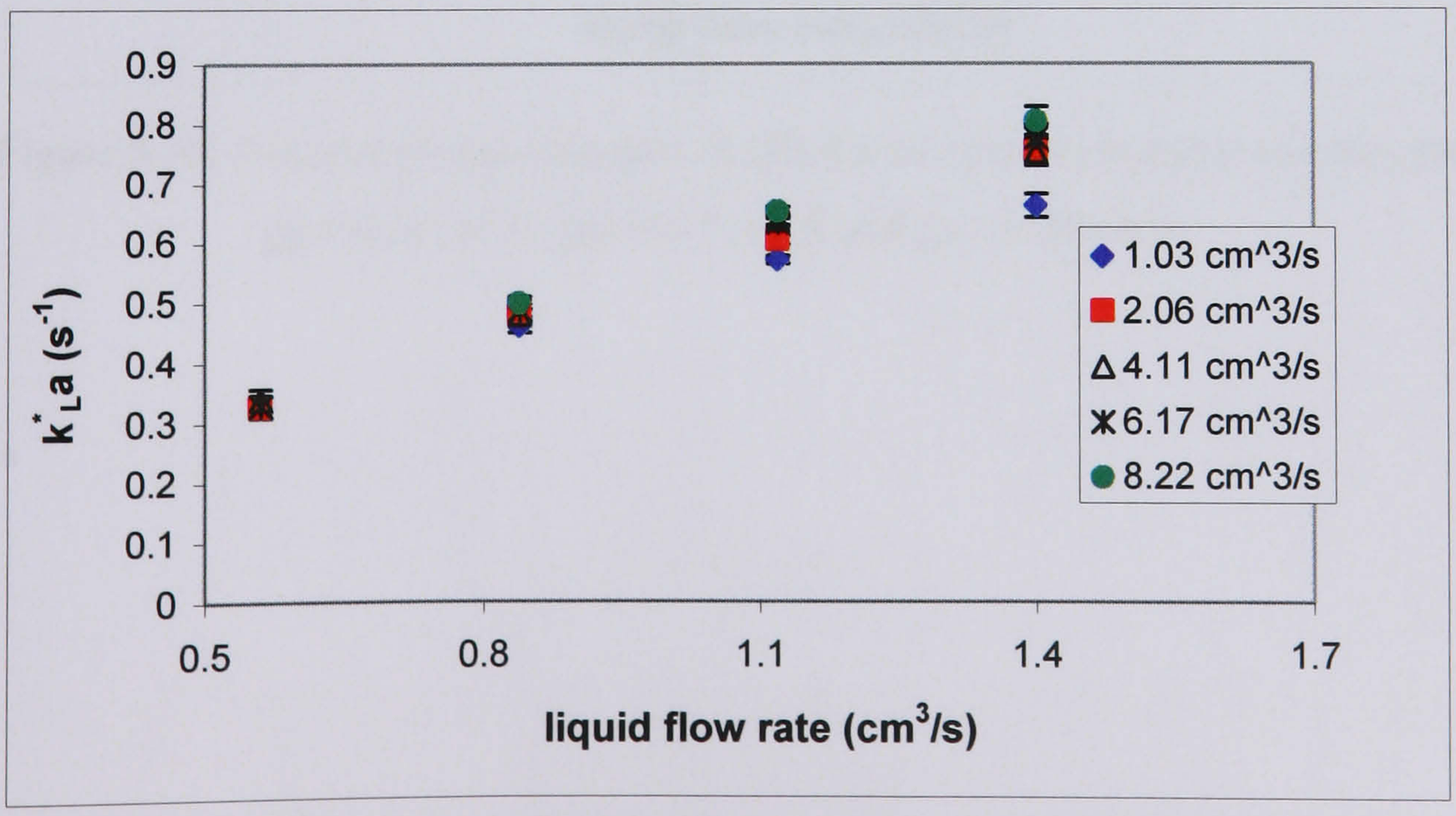

Figure 5.14. $k^*_L a$ vs. liquid flow rate.

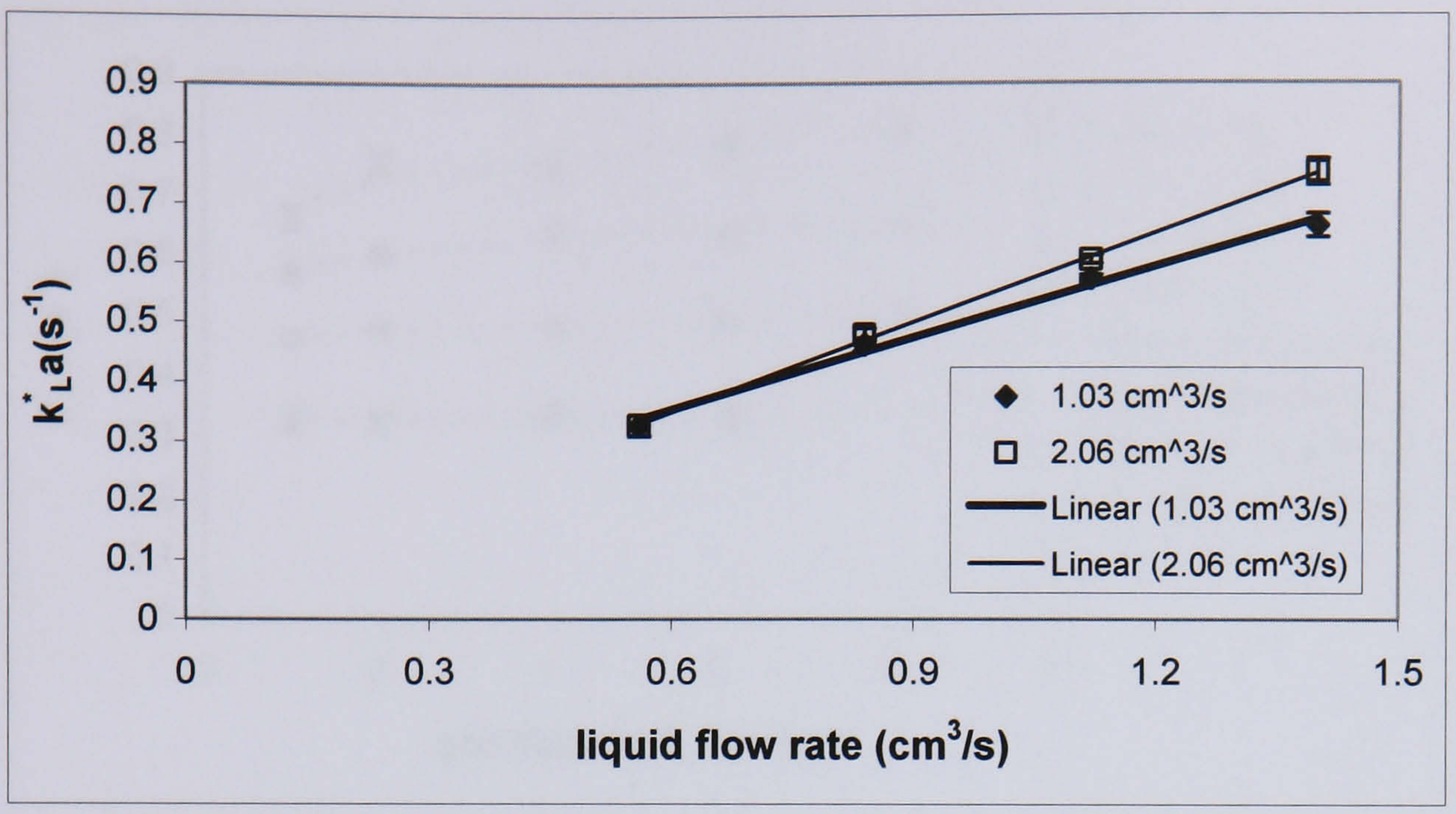

Figure 5.15. Volumetric mass transfer coefficient in case of chemical reaction for Q_G=1.03 cm^3/s and Q_G=2.06 cm^3/s.

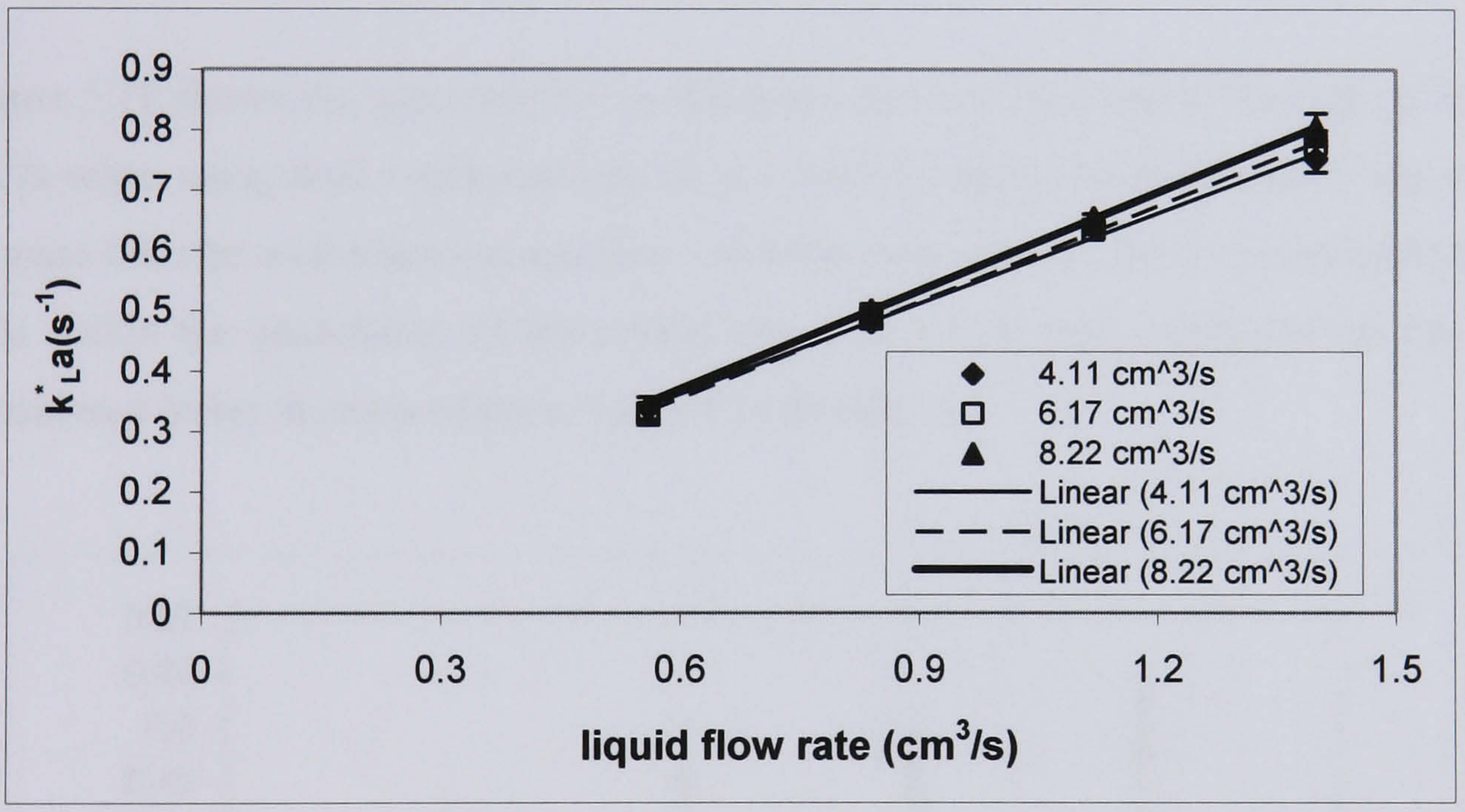

Figure 5.16. Volumetric mass transfer coefficient in case of chemical reaction for Q_G=4.11 cm^3/s, Q_G=6.17 cm^3/s and Q_G=8.22 cm^3/s.

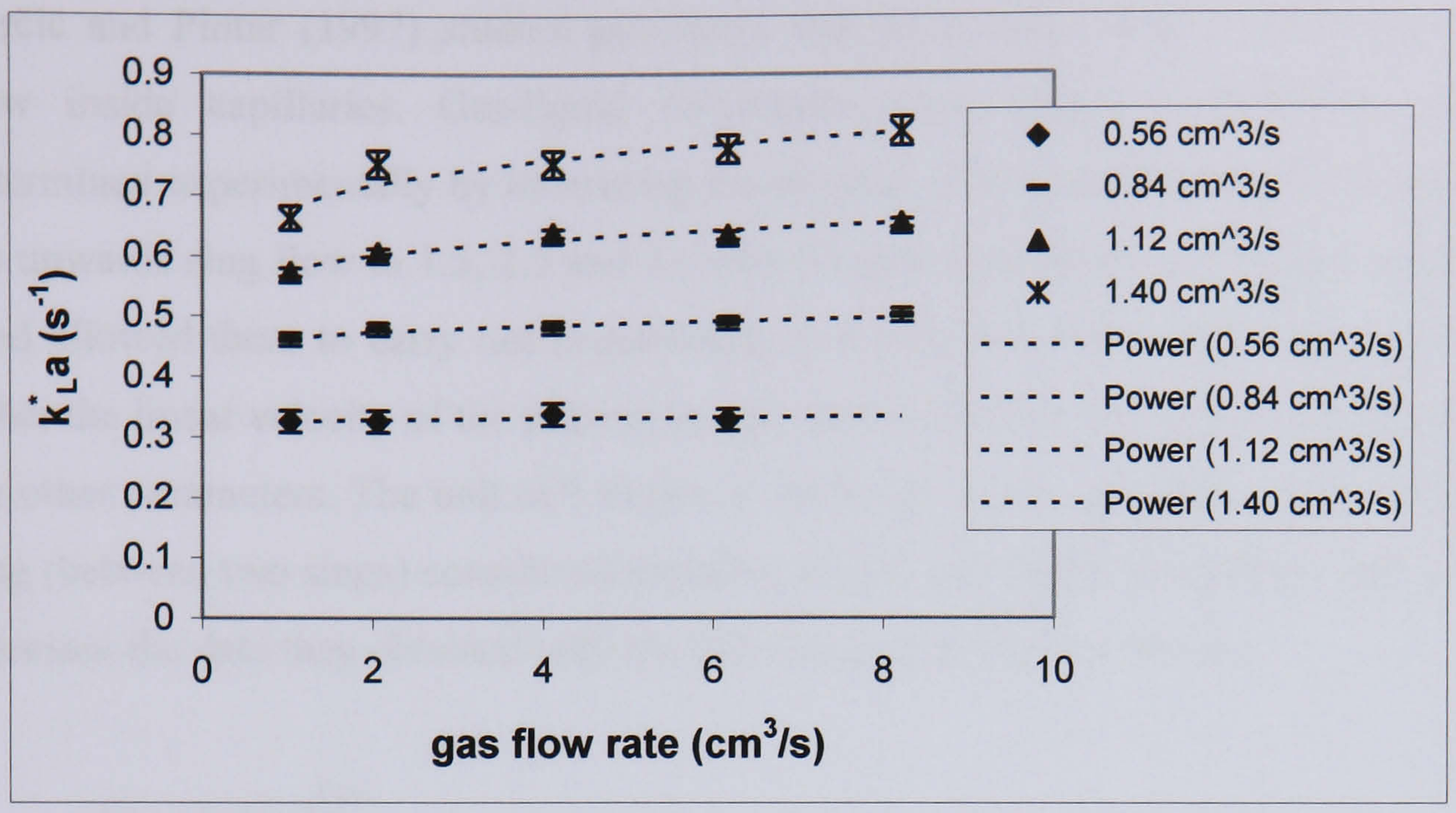

Figure 5.17. Volumetric mass transfer coefficient in case of chemical reaction vs. gas flow rate with liquid flow rate as a parameter.

Figure 5.18 shows the mass transfer coefficients obtained for a liquid flow rate of 0.84 cm^3/s when using both configurations of gas feed. It can be observed that in the case of mass transfer with chemical reaction the difference between the two configurations falls within the uncertainty of the results and none of the two configurations can be considered better in terms of mass transfer performance.

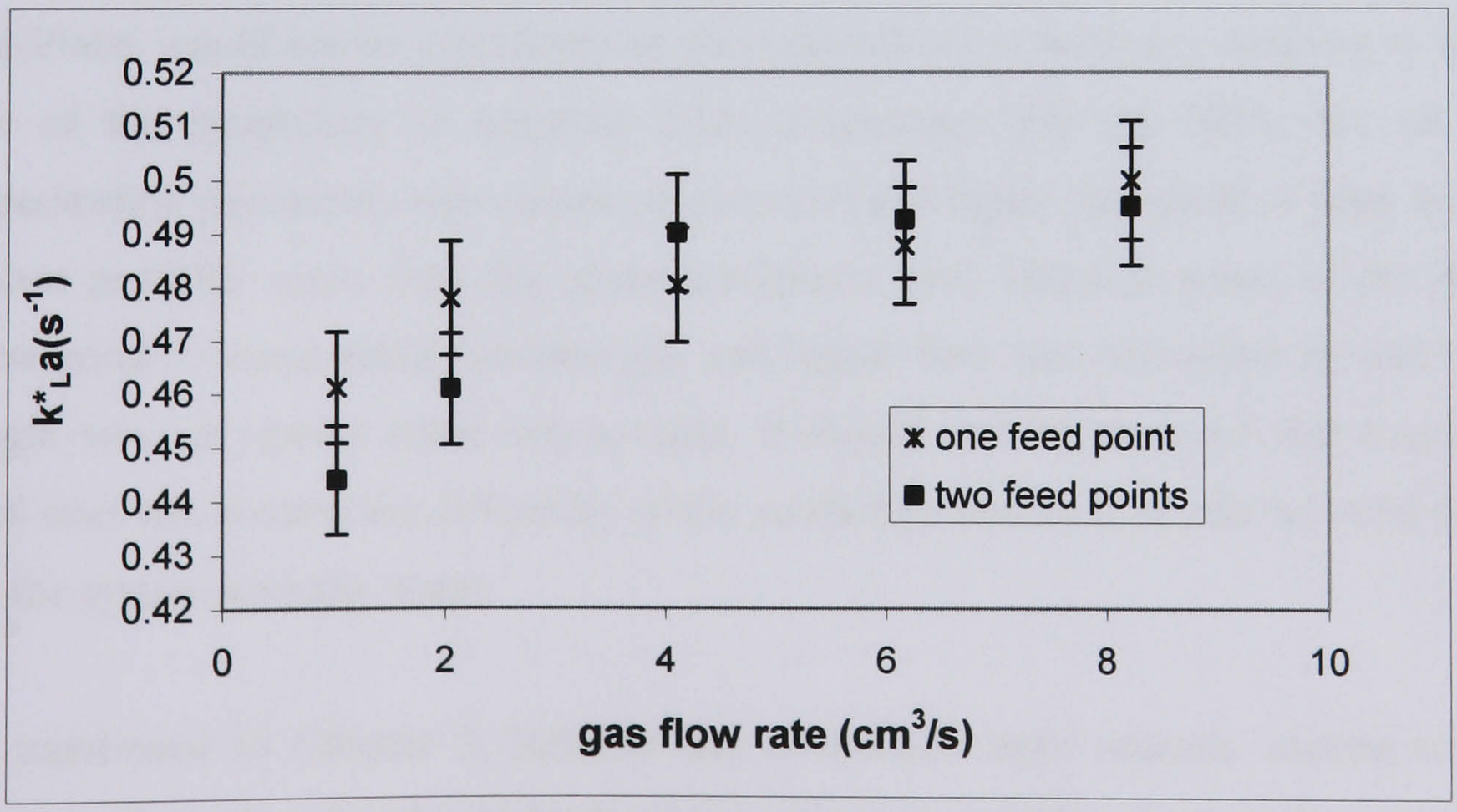

Figure 5.18. Volumetric mass transfer coefficient in case of chemical reaction for the two configurations of gas feed.

Berčič and Pintar (1997) studied gas-liquid and liquid-solid mass transfer for slug flow inside capillaries. Gas-liquid volumetric mass transfer coefficients were determined experimentally by measuring the amount of methane dissolved in water in the upwards slug flow in 1.5, 2.5 and 3.1 mm ID glass capillaries. The apparatus they used allowed them to carry out experiments in a way that they could keep constant either the linear velocity of the phases, the gas hold-up or the unit cell length and vary the other parameters. The unit cell length is the length of one gas slug and one liquid plug (between two slugs) considered together. Berčič and Pintar found that they could represent the data they obtained with the following empirical correlation:

$$k_L a = \frac{(u_{GS} + u_{LS})^{1.19}}{((1 - h_G)L_{UC})^{0.57}} \tag{5.26}$$

where L_{UC} (m) and h_G are the unit cell length and the gas hold up respectively. The authors considered velocity values, in terms of $u_{GS} + u_{LS}$ up to 0.5 m/s and obtained volumetric mass transfer coefficients between 0.01 and 0.2 s^{-1}. In the case of the NCR, as seen from the graphs versus flow rates, the mass transfer coefficients varied linearly with liquid velocity with a limited dependence on gas velocity. The maximum liquid velocity was around 0.7 m/s and the maximum gas velocity around 4 m/s, thus giving a wider range of linear velocities than for the experiments carried out by Berčič and Pintar. A more direct comparison of the data obtained for the NCR and those of Berčič and Pintar would not be significant as they carried out experiments keeping in turn one of the parameters in equation 5.26 as constant. For the NCR, the set of experimental parameters was chosen so as to vary the liquid and gas flow rates in the widest possible range with the given equipment and, although some of the data correspond to equal ratios between gas and liquid flow rate, the effect of unit cell length was not openly taken into account. It should also be observed that equation 5.26 does not contain the diffusivity of the studied system so it should be valid only for the system methane-water.

As mentioned in Chapter 3, Krishna and co-workers have recently carried out a number of studies for the hydrodynamic and mass transfer characterization of a monolith reactor operating in slug flow regime (Vandu et al., 2004, Vandu et al., 2005a, van Baten and Krishna, 2004). A monolith reactor is composed of an array of

uniformly structured parallel square or circular cross section channels with characteristic dimensions of the order of a few mm. One of the latest studies (Vandu et al., 2005b) took into account the experimental measurement of volumetric mass transfer coefficients for the oxygen-water system in circular capillaries of 1, 2 and 3 mm diameter. The authors observed a dependence of mass transfer coefficient on channel diameter, which did not appear explicitly in equation 5.26. They also observed that, at relatively high gas and liquid velocities and relatively low slug lengths, as used in their work, the dominant part of the mass transfer process would occur in the liquid film between the slug and the capillary wall. The liquid plugs between the slugs would have a negligible contribution to mass transfer in this case.

Vandu et al. (2005b) used $u_{GS} + u_{LS}$ values up to 0.65 m/s and found volumetric mass transfer coefficients to vary linearly with $u_{GS}^{1/2}$. The values reported in their graph are as high as about 0.7 $m^{1/2}$ $s^{1/2}$in terms of $u_{GS}^{1/2}$ which would translate to a maximum gas velocity of 0.49 m/s. In the case of the NCR this strong influence of gas velocity on volumetric mass transfer coefficients was not obtained, this could be due to the fact that much higher gas velocities were used when comparing to the operating conditions of the study by Vandu et al. (2005b). The range of variation of liquid velocity in their study is not explicitly given, however data reported for a limited number of cases suggest the liquid velocities to be of the same order of the gas velocities. The fact that the mass transfer coefficients were not strongly dependent on gas velocity for the NCR could also be due to the fact that higher ratios between gas and liquid velocities were used in this case if compared to the operating conditions for the study of Vandu et al. (2005b).

5.7.3 Absorption of carbon dioxide in the precipitation from suspension

For precipitation from calcium hydroxide suspensions it had to be considered that a mass transfer resistance to the solid dissolution also existed and therefore only the overall absorption rate could be quantified instead of the liquid side mass transfer coefficient. For both concentrations, the three highest pump settings amongst the ones used in the study on precipitation from solution were considered. The correspondent flow rates were in this case lower than in the previous absorption studies with close values obtained for both concentrations of calcium hydroxide suspension. Figure 5.19 shows the flow rate values for the suspensions versus the flow rates obtained for the

precipitation from solution or by using water (nominal flow rate). Uncertainty was calculated from statistical analysis of the data (described in Appendix A).

Precipitation from 5 g/dm^3 calcium hydroxide suspensions lead to total conversion to calcium carbonate, for all three liquid flow rate values used (these experiments were only carried out with a carbon dioxide flow rate of 8.22 cm^3/s). In this case, as in the case of precipitation from solution, part of the PCC further reacted with CO_2 leading to an amount of absorbed carbon dioxide exceeding the amount of precipitated calcium carbonate in terms of number of moles. The absorption rate was calculated again using equations 5.22 and 5.23.

For the experiments carried out with the concentration of 7 g/dm^3 the conversion to calcium carbonate was not complete. The titration allowed the determination of the calcium hydroxide left in the suspension. In this case the moles of precipitated calcium carbonate corresponded to the moles of absorbed carbon dioxide. Considering the overall stoichiometry of the carbonation reaction (equation 5.14), for this case the number of moles of absorbed carbon dioxide was calculated from the equation:

$$n(CO_2)_{abs} = n^i(Ca(OH)_2) - n^f(Ca(OH)_2) \qquad (5.27).$$

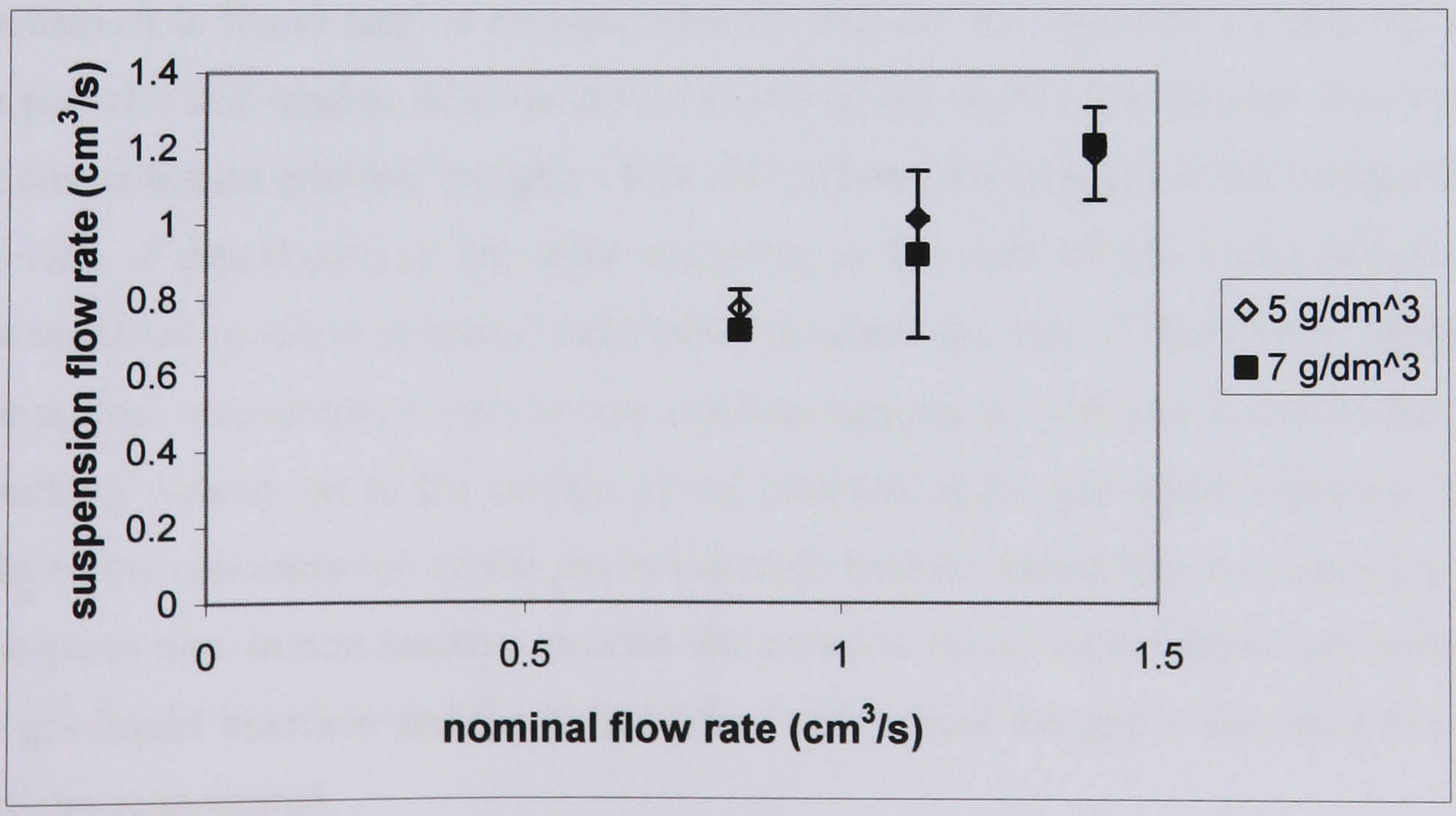

Figure 5.19. Suspension flow rates vs. nominal flow rate.

The final amount of calcium hydroxide was given by:

$$n^f(Ca(OH)_2) = 0.5\,V_{HCl}[HCl] \tag{5.28}$$

where V_{HCl} (m^3) is the titration volume.

The carbon dioxide absorption rate was then calculated from equation 5.23. Uncertainty was again determined from statistical analysis. Figure 5.20 shows the absorption rates at both concentrations of 5 g/dm^3 and 7 g/dm^3 together with the absorption rate for the precipitation from solution (1.2 g/dm^3). It can be observed that absorption rate increases with increasing concentration, implying that the enhancement to physical absorption is increased in respect to the reaction from solution by the presence of the solids in suspension. A similar behaviour has been reported for the absorption of SO_2 in calcium hydroxide and magnesium hydroxide slurries in a stirred reactor (Dagaonkar et al., 2001).

An overview of the mechanisms that can cause enhancement to gas-liquid mass transfer due to the presence of suspended solid particles in the liquid was given by Beenackers and Van Swaaij (1993). The enhanced absorption rates observed for the narrow channel can be due to two mechanisms: enhanced dissolution rate of the solid and adsorption of the gas on the solid particles at the gas-liquid interface. The first mechanism is found only in reacting systems and can be explained considering that the particles will tend to dissolve preferentially in the liquid mass transfer film where the concentration gradient is higher. This will enhance the absorption rate compared to the case of dissolution of the solid occurring in the bulk of the liquid, where the concentration gradient is lower, and further promote the rate of dissolution of solid. The second mechanism occurs in non reacting systems as well and is due to the gas adsorbing directly on to the surface of the particles at the gas-liquid interface. This reduces the concentration of the gas in the mass transfer liquid film and increases the absorption rate. In non reacting systems the particles would repeatedly travel between the gas-liquid interface and the bulk of the liquid where the gas is desorbed and the particles regenerated.

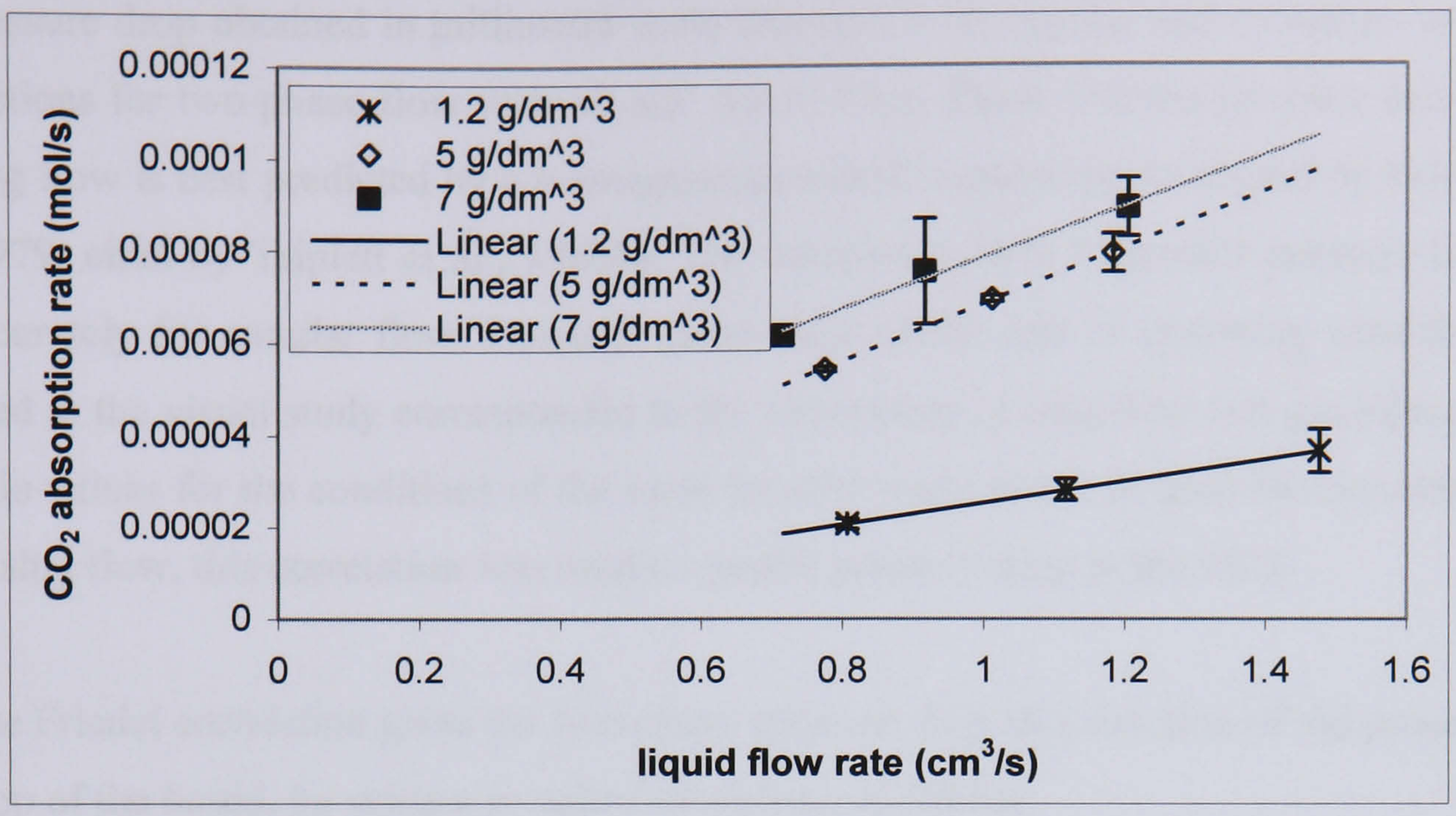

Figure 5.20. Absorption rates vs. flow rate for the precipitation from solution and suspensions.

5.7.4 Energy dissipation and discussion of the mass transfer results

In the previous sections the quantification of mass transfer coefficients in the gas-liquid precipitation of calcium carbonate for the NCR has been described. In this section a comparison of the narrow channel reactor to other gas-liquid contactors in terms of mass transfer performance is carried out. As seen for the mixing of two liquids, the choice of one type of equipment is highly dependent on the product quality combined with the energy costs associated to it. In relation to this, the calculation of the pressure drop associated with the gas-liquid flow in the narrow channel will be shown before carrying out a comparison of the mass transfer data for this study with the ones reported in the literature.

Several models are used for calculating pressure drops in two-phase flow through channels, a review of them is presented by Darby (2001, p.462). The homogeneous gas-liquid models assume that the two phases move at the same velocity (no-slip condition) and calculate the pressure drop as a single term. The separated flow models assume instead that each phase occupies a specific fraction of the flow cross section and take into account the possible difference in velocity between the two phases. Pressure drop models used for micro channels and narrow channels usually are the same used in large scale tubes. Triplett et al. (1999b) investigated experimentally the

pressure drop obtained in millimetre scale channels with circular and triangular cross sections for two-phase flow with air and water. They found that the pressure drop in slug flow is best predicted by a homogeneous model correlation developed by Friedel (1979, cited by Triplett et al., 1999b). The correlation fails to predict pressure drop accurately for annular flow. However since most of the sets of operating conditions used in the visual study corresponded to the occurrence of slug flow and gas injection ratio values for the conditions of the mass transfer study also indicated the occurrence of slug flow, this correlation was used to predict pressure drop in the NCR.

The Friedel correlation gives the two-phase pressure drop as a function of the pressure drop of the liquid, by using a so called two-phase multiplier:

$$\Delta p_{TP} = \Phi_{Lo}^2 \Delta p_L \tag{5.29}$$

where Δp_{TP} (Pa) is the two-phase pressure drop and Φ_{Lo}^2 is the all liquid two-phase flow multiplier.

All the equations defining the model are reported by Ould Didi et al. (2002). The pressure drop of the liquid is given by the equation:

$$\Delta p_L = \frac{4 f_L L \dot{m}_{tot}^2 (1-\chi)^2}{d_h} \frac{1}{2\rho_L} \tag{5.30}$$

where the hydraulic diameter was used to refer to the case of square cross section.

In this equation $\dot{m}_{tot}$ (Kg/(m^2 s)) is the total mass flux, which is calculated from the expression:

$$\dot{m}_{tot} = \frac{(\rho_G Q_G + \rho_L Q_L)}{S_{NCR}} \tag{5.31}$$

here written referring specifically to the cross section of the narrow channel reactor. χ is the mass fraction of the gas, which is generally referred to as the vapour quality for vapour-liquid systems, and is calculated with the equation:

$$\chi = \frac{\rho_G Q_G}{\rho_G Q_G + \rho_L Q_L} \tag{5.32}.$$

The all liquid two-phase multiplier is given by the expression:

$$\Phi_{Lo}^2 = A_{TP} + 3.24\chi^{0.78}(1-\chi)^{0.224}\left(\frac{\rho_L}{\rho_G}\right)^{0.91}\left(\frac{\mu_G}{\mu_L}\right)^{0.19}\left(1-\frac{\mu_G}{\mu_L}\right)^{0.7} Fr_{TP}^{-0.0454} We_{TP}^{-0.035} \tag{5.33}$$

where Fr_{TP} and We_{TP} are the Froude and Weber two-phase dimensionless numbers defined by the following equations:

$$Fr_{TP} = \frac{\dot{m}_{tot}^2}{g d_h \rho_{TP}^2} \tag{5.34}$$

$$We_{TP} = \frac{\dot{m}_{tot}^2 d_h}{\sigma \rho_{TP}} \tag{5.35}$$

where g (m/s^2) is the acceleration due to gravity and ρ_{TP} is the two-phase density:

$$\rho_{TP} = \left(\frac{\chi}{\rho_G} + \frac{1-\chi}{\rho_L}\right)^{-1} \tag{5.36}.$$

In equation 5.33 A_{TP} is the dimensionless parameter defined by the equation:

$$A_{TP} = (1-\chi)^2 + \chi^2 \frac{\rho_L f_G}{\rho_G f_L} \tag{5.37}.$$

The Reynolds numbers to be used in the calculation of the friction factors are given by the equations:

$$Re_L = \frac{\dot{m}_{tot} d_h}{\mu_L} \tag{5.38}$$

$$Re_G = \frac{\dot{m}_{tot} d_h}{\mu_G} \tag{5.39}$$

for the liquid and the gas respectively.

In this case Re_L varied approximately between 400 and 1000 whereas Re_G varied approximately between 27000 and 40000. For calculating the friction factor of the liquid, equation 4.35 for laminar flow in square channels was used and the Blasius equation (Tilton, 1997, p. 6-10) was used for the gas. This equation, normally used for turbulent flow, is valid for Reynolds numbers between $4 \cdot 10^3$ and 10^5 and has the following expression:

$$f = \frac{0.079}{Re^{0.25}} \qquad (5.40).$$

In the calculation of the two-phase pressure drop the physical and transport properties of carbon dioxide and water were taken into account, considering negligible the change in properties due to the presence of calcium hydroxide in solution. The proposed model is valid for $\mu_L/\mu_G < 1000$, which in this case was approximately equal to 70. Pressure drops varying between 4000 and 20000 Pa approximately were found for the NCR. For the calculations the length of the reactor in the Perspex chip was considered. The values obtained are about ten times higher than the corresponding one phase pressure drops calculated for reactor A in the Perspex chip as reported in section 4.13. It has to be considered that the maximum liquid flow rate is about 50% higher in the case of the gas-liquid study.

The main interest was to relate the pressure drop and the energy dissipation to the mass transfer performance of the narrow channel reactor. Gaddis (1999), in a review on gas-liquid contactors, reported a series of correlations expressing mass transfer coefficients as a function of the dissipated power or related variables for various types of equipment. These expressions usually contain a parameter representing the gas hold-up or some other function of the ratio between gas and liquid volumes. Types of equipment covered are stirred vessels and jet reactors. Similarly, Zhu et al. (1992) presented a review of the most common high intensity gas-liquid contactors such as static mixers and ejectors. Other parameters used to correlate mass transfer coefficients include the phases velocities and Reynolds numbers.

In this case, the reactor was operated in a continuous mode for both phases. Pressure drops and mass transfer coefficients were correlated for constant values of the ratio between the gas and liquid flow rate. Amongst all operating conditions used, three sets of data correspond to constant values of the ratio between Q_G and Q_L. The first set corresponds to $Q_G/Q_L = 7.34$ and is composed of three data points. Mass transfer coefficients plotted against pressure drop show a linear trend for this case, as shown in Figure 5.21. This is consistent with the fact that the volumetric mass transfer coefficient varies linearly with liquid flow rate and that the liquid is in laminar flow, which implies that the two-phase pressure drop varies linearly with the liquid flow rate. The sets of data correspondent to $Q_G/Q_L = 3.67$ and $Q_G/Q_L = 1.83$ have also been taken into account. Each of them contain two data and the three sets considered together allowed the derivation of a correlation for mass transfer coefficients as a function of pressure drop. If the following expression is considered:

$$k_L^* a = \varphi\left(\frac{Q_G}{Q_L}\right) \cdot \Delta p_{TP} \tag{5.41}$$

where $\varphi\left(\frac{Q_G}{Q_L}\right)$ is a function of the ratio between gas and liquid flow rate which

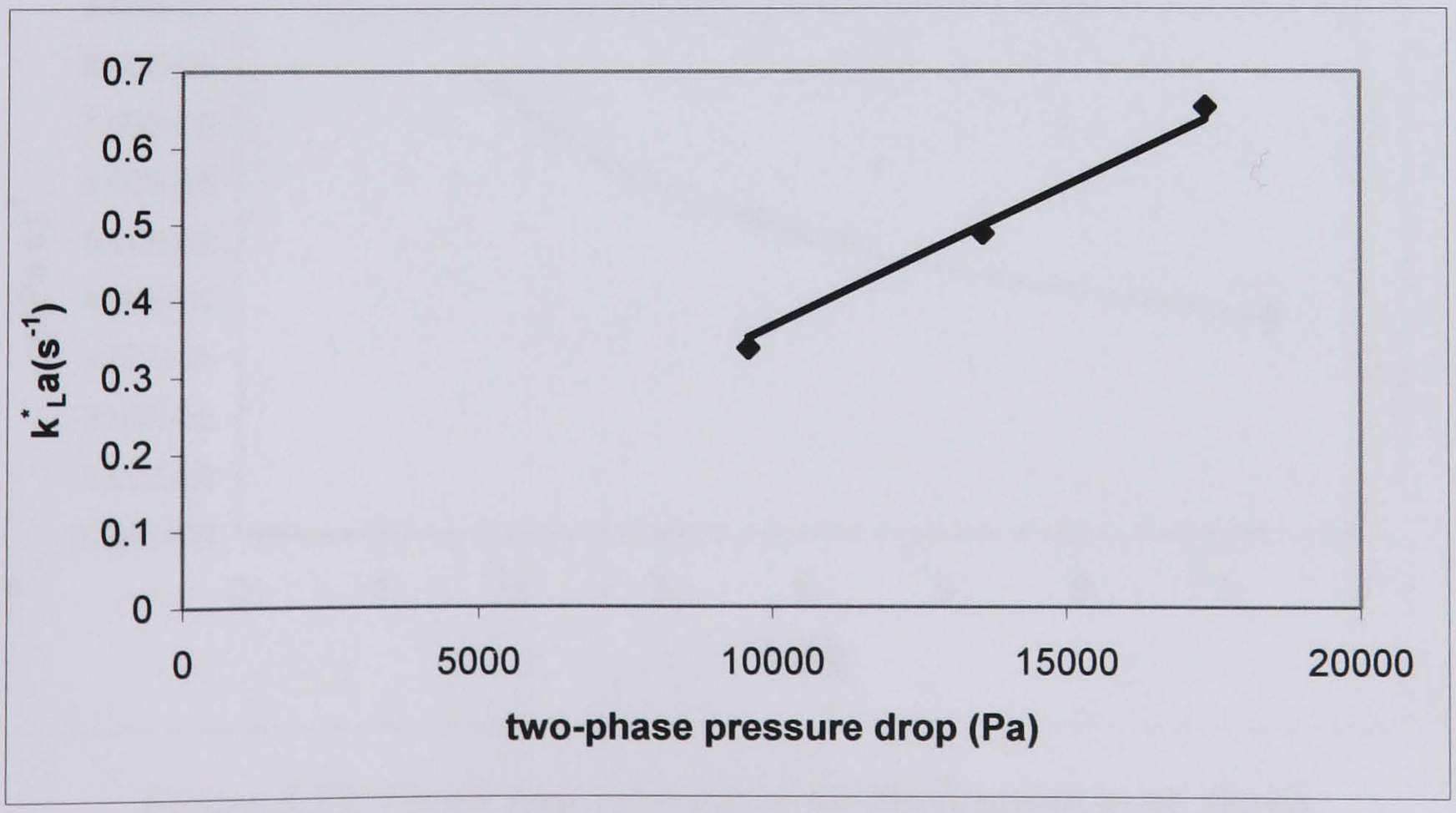

Figure 5.21. Volumetric mass transfer coefficient vs. pressure drop for $Q_G/Q_L = 7.34$.

would have the dimensions of $(s\ Pa)^{-1}$ and the equations obtained in this case are considered:

$$k_L^* a = 7.640481 \cdot 10^{-5} \Delta p_{TP} \qquad \text{for } \frac{Q_G}{Q_L} = 1.83 \tag{5.42}$$

$$k_L^* a = 5.389466 \cdot 10^{-5} \Delta p_{TP} \qquad \text{for } \frac{Q_G}{Q_L} = 3.67 \tag{5.43}$$

$$k_L^* a = 3.669238 \cdot 10^{-5} \Delta p_{TP} \qquad \text{for } \frac{Q_G}{Q_L} = 7.34 \tag{5.44}$$

then an expression for the function φ can be derived.

Figure 5.22 shows φ versus Q_G/Q_L and a power type correlation curve for the data reported. From this the following correlation for mass transfer data for the NCR is obtained:

$$k_L^* a = 1.057715 \cdot 10^{-4} \left(\frac{Q_G}{Q_L} \right)^{-0.528035} \Delta p_{TP} \tag{5.45}.$$

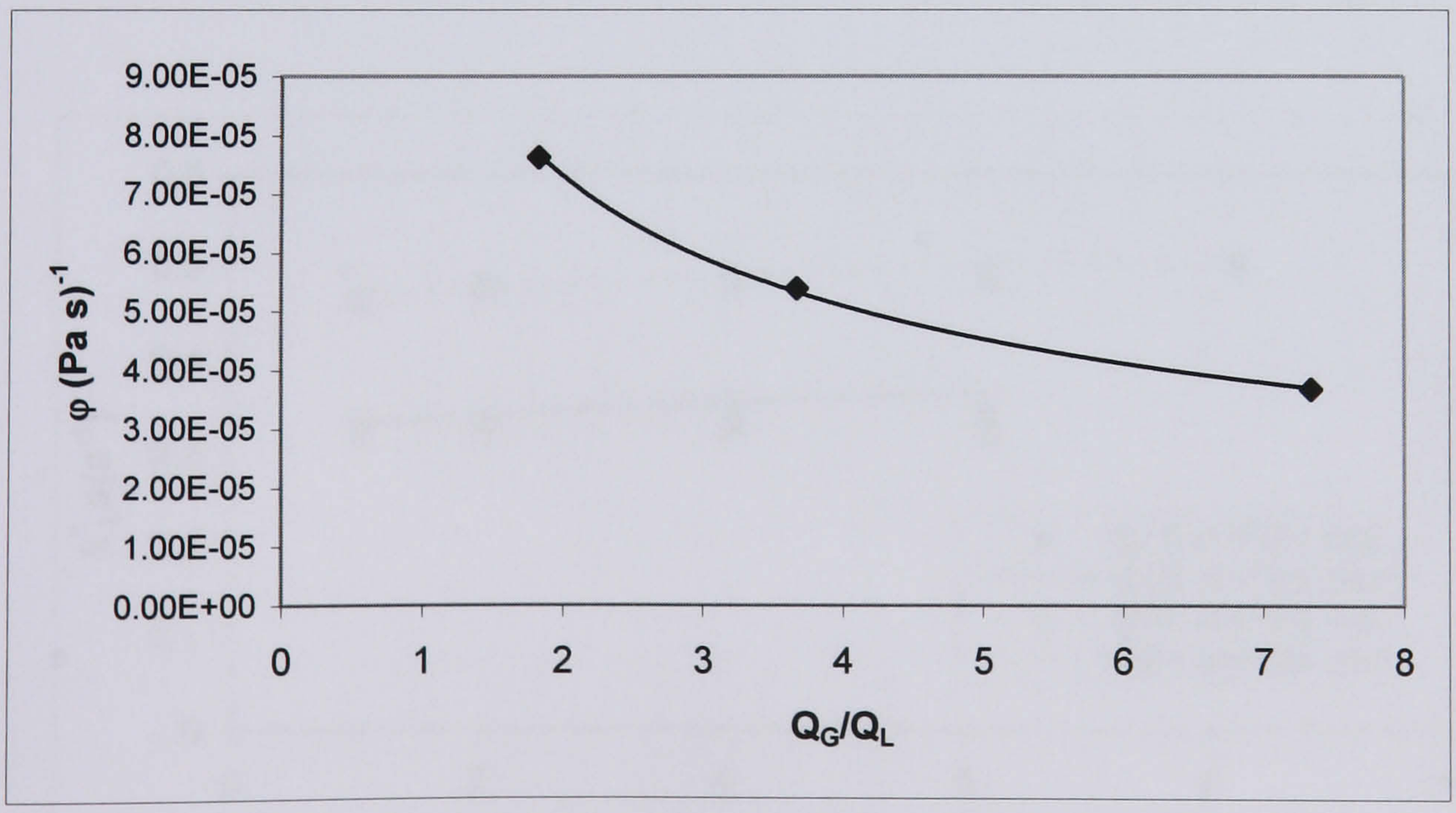

Figure 5.22. Power type correlation for the function φ vs. Q_G/Q_L.

Figure 5.23 shows the experimental mass transfer coefficients together with values predicted by the correlation for liquid flow rates of 0.56 and 0.84 cm^3/s, whereas Figure 5.24 shows the same type of data for liquid flow rates of 1.12 and 1.40 cm^3/s. It can be seen that in most cases the difference between the correlation and the experimental data falls within the uncertainty. The highest errors correspond to values of the ratio between gas and liquid flow rates not considered to derive the correlation. The maximum error in predicting mass transfer coefficients in the range of considered gas to liquid flow rate ratios is 5%. To express the mass transfer coefficients as a function of the dissipated power equation 4.31 can be considered again. The dissipated power per unit volume of the reactor is given by:

$$\frac{P_f}{V} = \frac{Q_L \Delta p_{TP}}{V} \tag{5.46}$$

where the volume of the reactor was considered as it is the one in respect to which the mass transfer coefficients were calculated.

In this case the specific dissipated power varies between 2 and 24 kW/m^3. Figure 5.25 shows mass transfer coefficients versus specific dissipated power at varying ratios between the gas flow rate and the volume of the reactor (Q_G/V). The performance in terms of volumetric mass transfer coefficients versus dissipated power appears to be

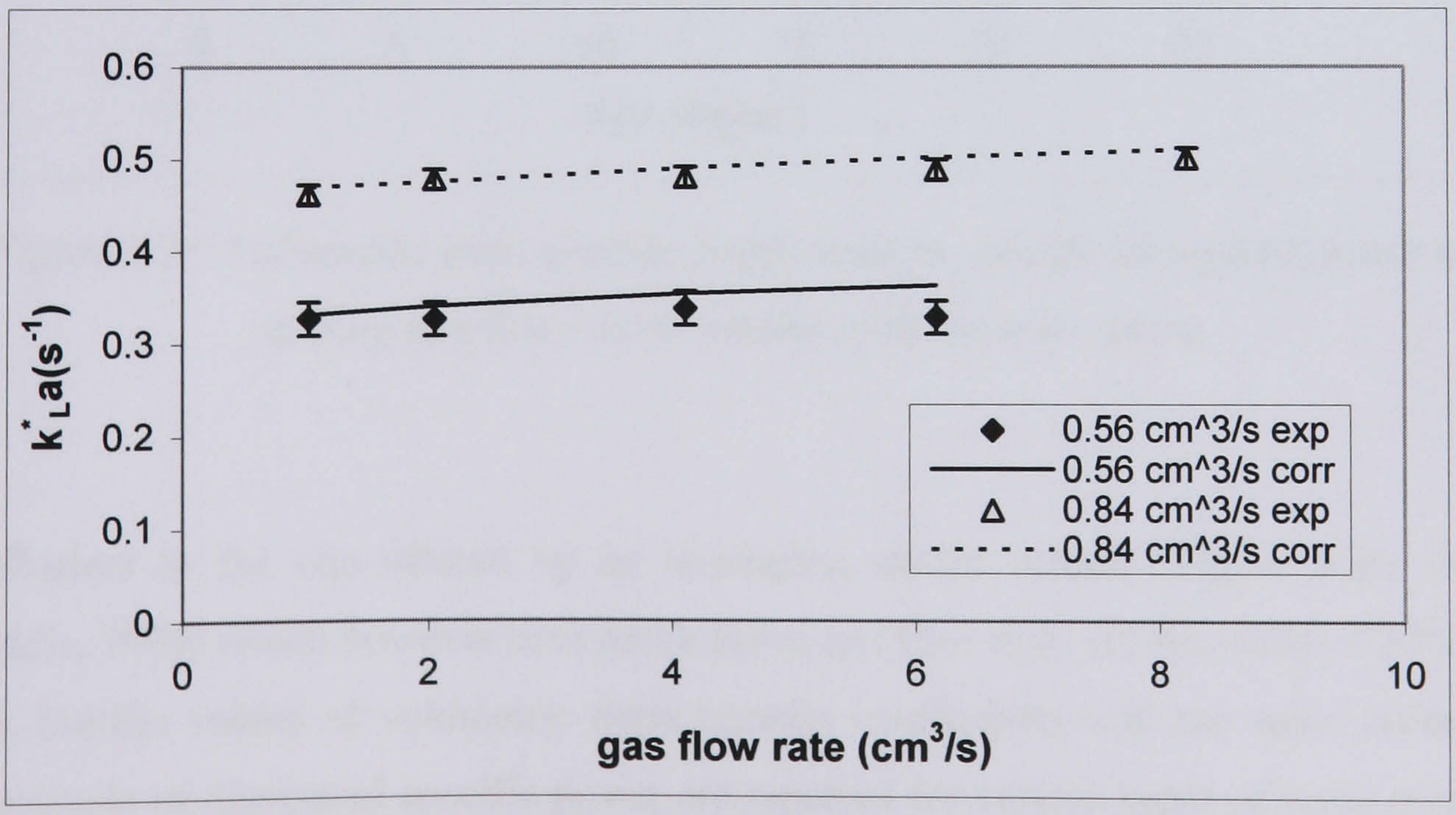

Figure 5.23. Comparison between mass transfer coefficient predicted by the correlation and experimental data (liquid flow rates of 0.56 and 0.84 cm^3/s).

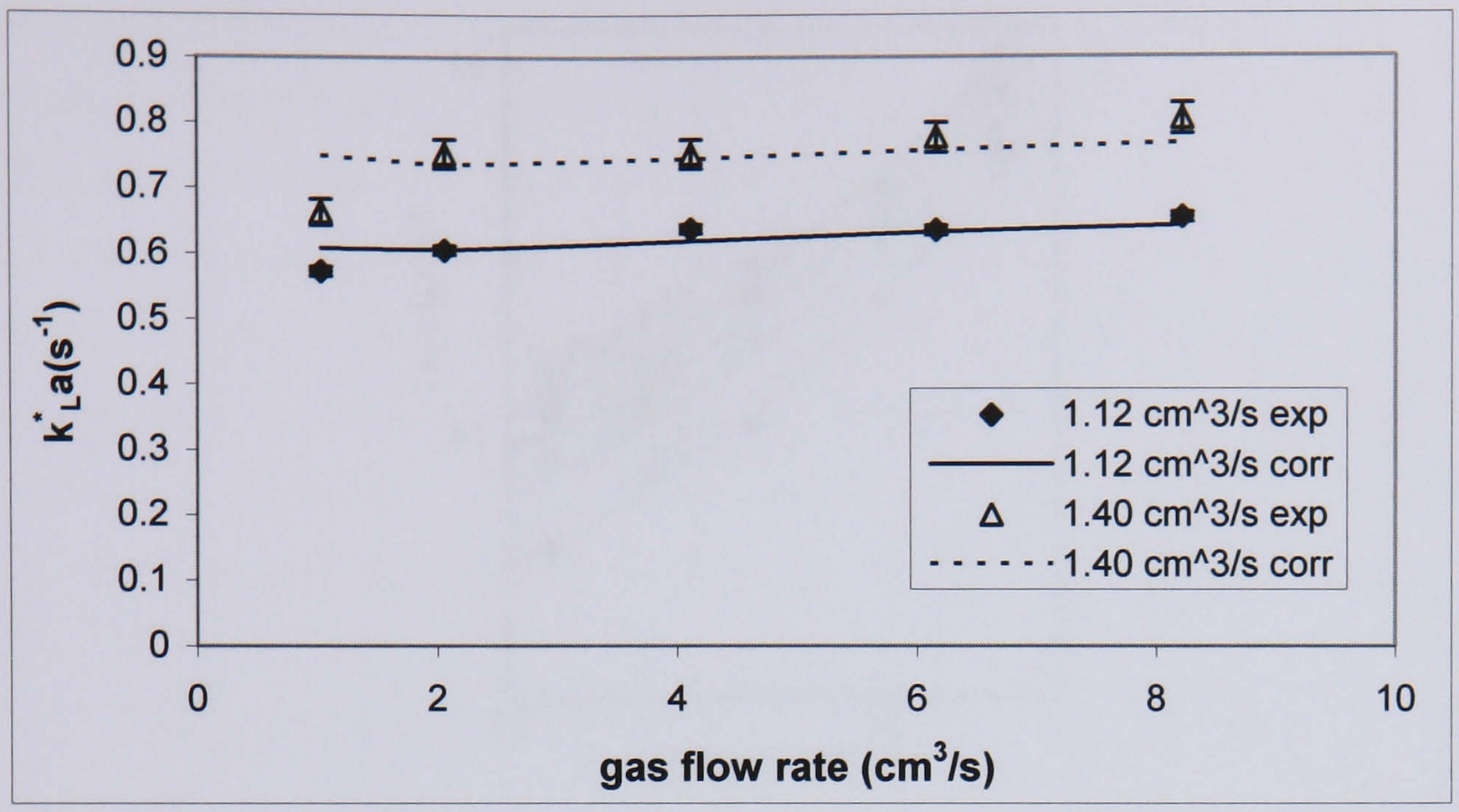

Figure 5.24. Comparison between mass transfer coefficient predicted by the correlation and experimental data (liquid flow rates of 1.12 and 1.40 cm^3/s).

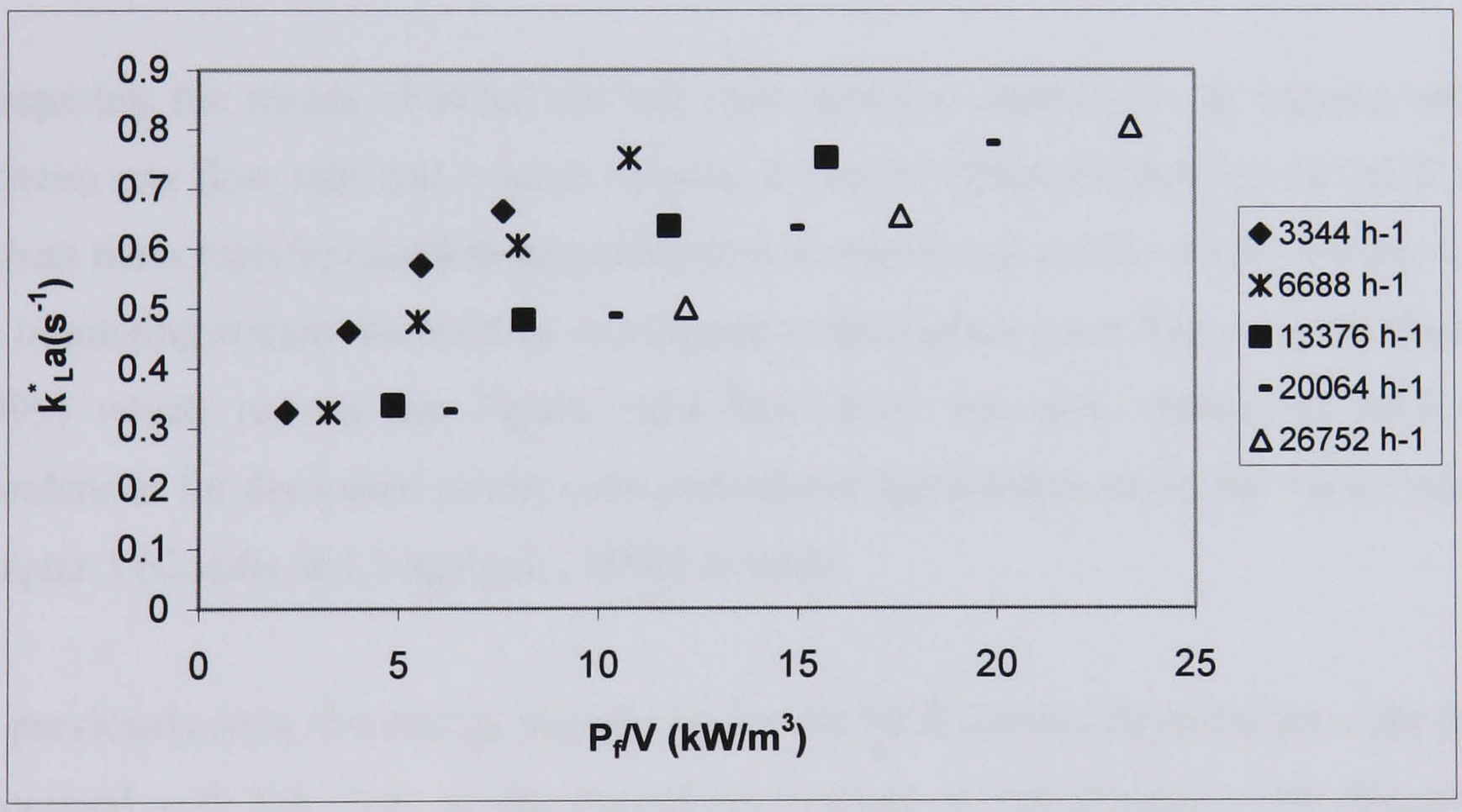

Figure 5.25. Volumetric mass transfer coefficients vs. specific dissipated power at varying gas flow rate to volume of the reactor ratios.

equivalent to the one offered by an impinging stream reactor (Figure 5.26, from Gaddis, 1999) which however uses much lower gas flow rates (of the order of 10^1-10^2 h^{-1}). Similar values of volumetric mass transfer coefficients with the same order of magnitude of dissipated specific power are reported for various types of static mixers (Zhu et al., 1992). Stirred vessels usually are characterized by volumetric mass transfer coefficients of the order of 10^{-2} s^{-1} (Gaddis, 1999).

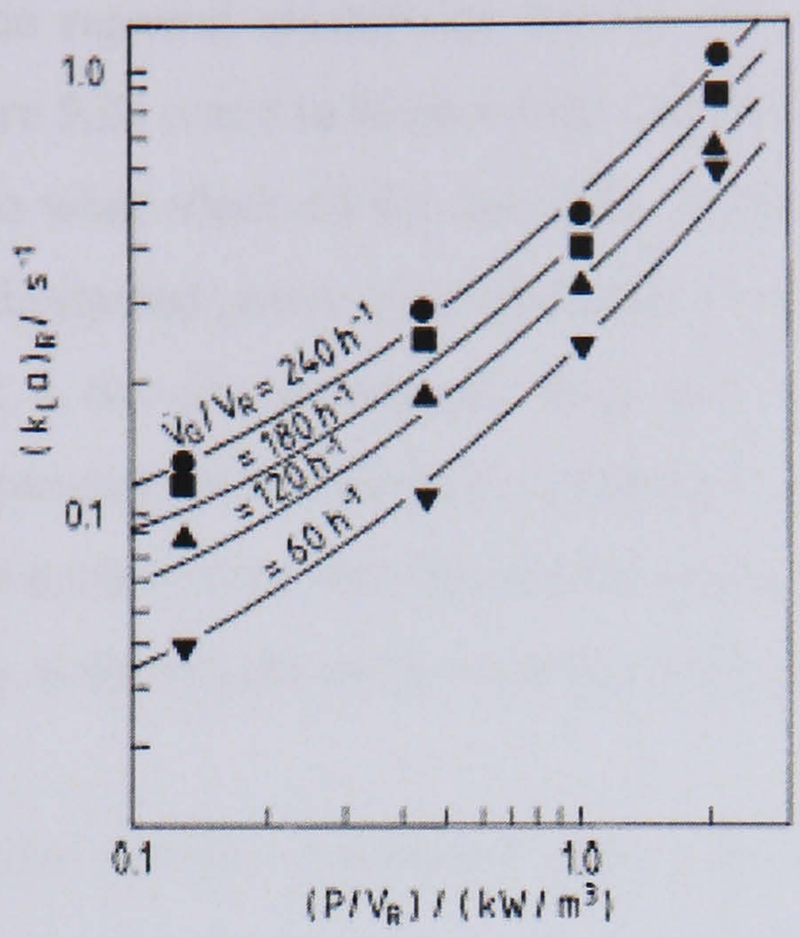

Figure 5.26. Mass transfer performance for the impinging stream reactor (from Gaddis, 1999).

Comparing the trends obtained for the mass transfer coefficients at varying ratios between gas flow rate and reactor volume, it can be observed that for the NCR the highest mass transfer coefficients correspond to the lowest gas flow rates whereas for the impinging stream reactor they correspond to the highest ones. The study by Gaddis (1999) which reports the Figure used here does not give details on how the calculations for dissipated power were carried out, but a reference to the work cited in Chapter 3 (Gaddis and Vogelpohl, 1992) is made.

As previously seen, the energy dissipation for the NCR derives from the pressure drop associated with the flow of the two-phase mixture in the channel. The dissipated energy for the impinging stream reactor is instead considered to derive from kinetic losses in the nozzles in which the two phases pre-mix before contacting in the impinging zone. It is calculated referring to the jet velocity at the outlet of the nozzle and the liquid density. This probably leads to underestimating the dissipated power in the entire system. For the narrow channel reactor, at equal specific dissipated power values, the highest mass transfer coefficients correspond to the lowest gas flow rates because mass transfer coefficients are mostly dependent on liquid flow rate, so increasing the fraction of the energy transferred to the liquid is more beneficial in terms of achieving a high mass transfer performance. The impinging stream reactor has a totally different way in respect to the NCR of achieving the contact between the

phases and the surface renewal mechanism behind the mass transfer process. The trend obtained in Figure 5.26 could indicate a high dependence of mass transfer on gas flow rate in contrast to what observed for the NCR. However it might also be due to the way in which the dissipated power was calculated for the impinging stream reactor. In fact, for the NCR a two-phase pressure drop term was included, whereas the expression for the impinging stream reactor considered only the liquid density. This implies that it does not entirely take into account the presence of the gas, other than by assuming a jet velocity at the nozzle as the velocity of the gas-liquid pre-mixture.

5.7.5 Estimation of the specific interfacial area and of physical mass transfer coefficients

In the previous section mass transfer data which include the contribution of chemical reaction for the NCR have been compared to physical mass transfer data reported in the literature. In order to have an estimate of physical mass transfer coefficients for the NCR, the mass transfer enhancement by chemical reaction would have to be quantified. As a first step, a certain value for the specific interfacial area a (m^2/m^3), which is the active area for mass transfer between the phases, can be assumed. The specific interfacial area depends on the way the two phases are contacted, for this case of flow in a small scale channel it can be imagined to be proportional to the surface to volume ratio of the NCR. Hessel et al. (2000) studied flow patterns and mass transfer performance of various micro bubble columns and they found experimentally that a 1100 μm × 170 μm cross section column was characterized by a specific interfacial area equal to 8700 m^2/m^3 for slug flow. In that case the surface to volume ratio of the column was approximately equal to 13600 m^2/m^3.

In this case the surface to volume ratio of the part of the channel in the perspex module was around 2800 m^2/m^3. If a specific surface area of 2000 m^2/m^3 is considered, regardless of the different operating conditions, k^*_L values between $1.6 \cdot 10^{-4}$ and $4.0 \cdot 10^{-4}$ m/s are obtained. If the expression for the enhancement factor relative to the case of infinitely fast reaction in respect to mass transfer (Levenspiel, 1999, p. 532) applied to reaction 5.18 is used:

$$E_{f,\,inf} = \frac{[OH^-]D_{OH^-,sol}}{[CO_2]_i D_{CO_2,sol}} + 1 \qquad (5.47)$$

then an enhancement factor approximately equal to 3.13 is obtained, when referring to the initial hydroxyl ion concentration.

This condition implies that a factor of around 3 differentiates physical mass transfer coefficients from mass transfer coefficients with the contribution of chemical reaction and the same conclusions can be assumed to be valid for the corresponding volumetric mass transfer coefficients. This means that the discussion on the mass transfer performance of the NCR can be considered valid even though it was carried out referring to the volumetric mass transfer coefficients with the contribution of chemical reaction.

Calculating the Hatta number from equation 5.12, values of Ha^2 values ranging between 40 and 240 approximately are obtained. This shows that the kinetics is actually mass transfer controlled and that equation 5.46 can be used to estimate the enhancement factor, at least as a first approximation.

5.8 Particle properties

5.8.1 Particle size and size distribution

Particle size analysis was carried out on slurry samples a few hours after the experiments and on dry powder dissolved in deionised water, as the particle size analyzer was not available to use at the same time as the experiments were carried out. As in the liquid phase study, the instrument used was a Malvern Mastersizer 2000.

For the precipitation from suspension, both slurry and powder samples were analyzed. As the concentration of solids was in this case relatively high, an ultrasonic probe was used for limiting aggregation phenomena both for the slurry collected from the reactor and the one obtained dispersing the calcium carbonate in water. The time during which the slurry was exposed to ultrasound was different in the two cases. Several preliminary tests were carried out to find what was believed to be a suitable time for

the exposure of the samples to ultrasound. This was done by checking that the amount of fines created was not too high and by making sure that the slurry and powder samples gave consistent results. More details on these procedures are given in Appendix B. The results presented here were obtained considering averages of the results of the single measurements.

Table 5.1 shows mean particle size (D[4,3] is considered again) for the experiments with calcium hydroxide suspensions. Mean particle size is around 4 μm in all cases and no significant influence of flow rate is noticeable. Figures 5.27 and 5.28 show calcium carbonate particle size distributions for $Ca(OH)_2$ initial concentrations equal to 5 g/dm^3 and 7 g/dm^3 respectively. The size distributions are similar in the two cases and for all flow rates.

Table 5.1 Mean particle size for the precipitation from $Ca(OH)_2$ suspensions.

$[Ca(OH)]^i$ (g/dm^3)	**Flow rate (cm^3/s)**	**D[4,3] (μm)**
5	0.78	4.1
5	1.01	3.7
5	1.18	3.8
7	0.72	3.7
7	0.92	4.1
7	1.20	4.2

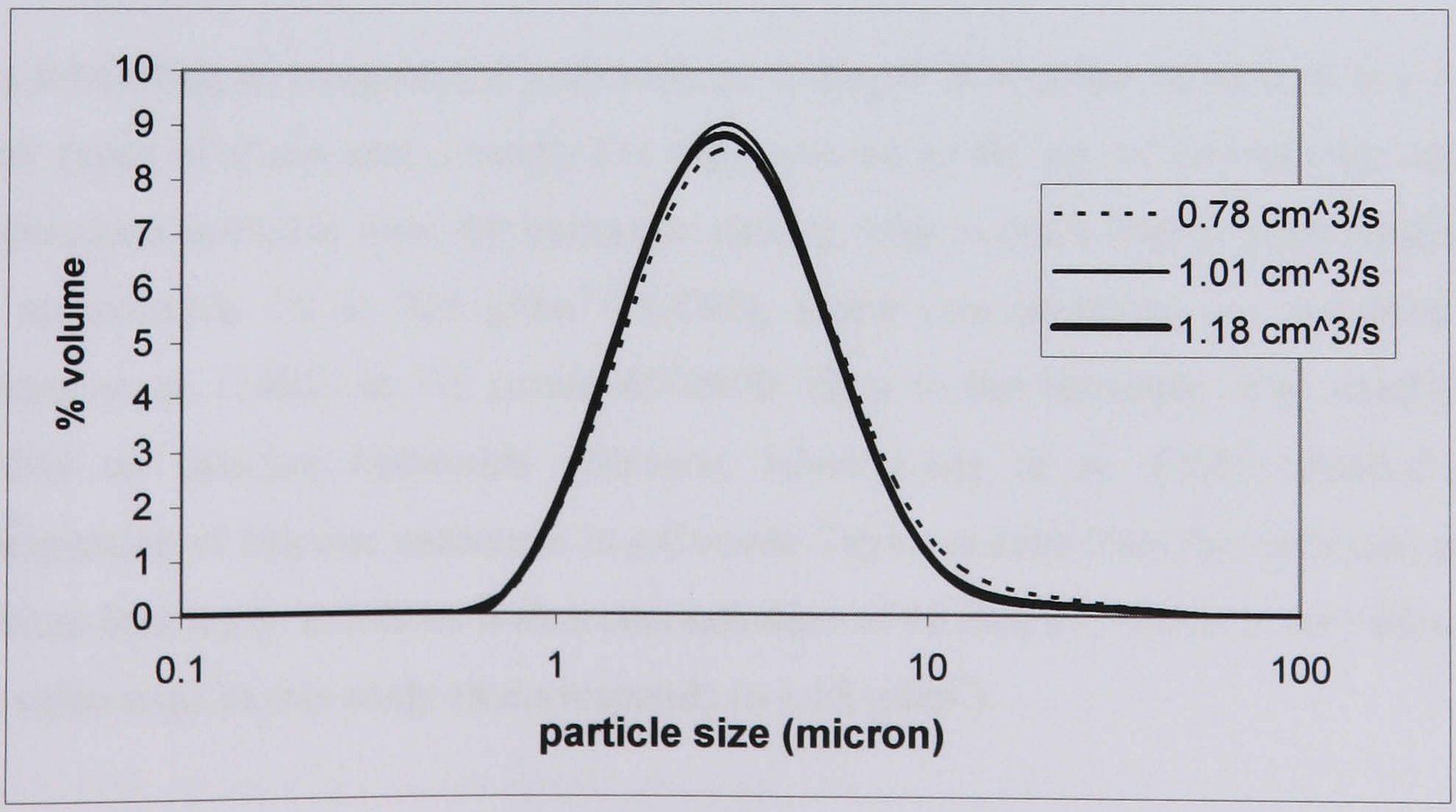

Figure 5.27. Particle size distributions for the experiments with $[Ca(OH)_2]^i$=5 g/dm^3.

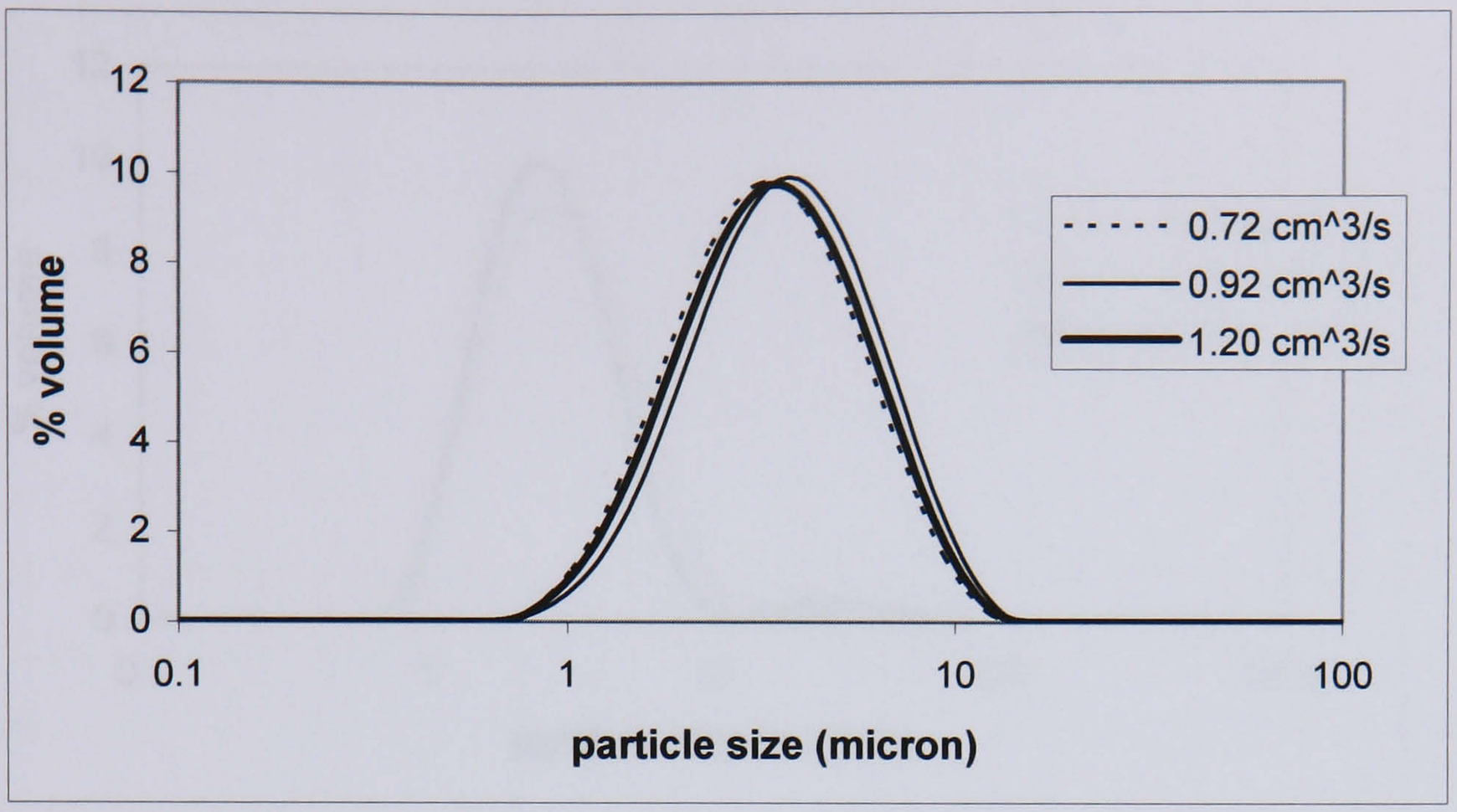

Figure 5.28. Particle size distributions for the experiments with $[Ca(OH)_2]^i$=7 g/dm^3.

For the study on precipitation from a calcium hydroxide solution the samples correspondent to a liquid flow rate of 0.84 cm^3/s were analyzed. Particle size analysis was carried out on slurry samples. Mean particle size varied between 3.7 and 5.3 μm, when considering the experiments at the different gas flow rates. Particle size distributions were very similar in all cases, as shown for 3 gas flow rates in Figure 5.29. Considering all the results, it can be observed that the change in carbon dioxide absorption rate and mass transfer coefficient at varying operating conditions does not influence particle size significantly.

It is interesting to compare the performance of the NCR in terms of particle size with other types of equipment. Usually the data relevant to the use of calcium hydroxide suspensions available from the numerous patents refer to much higher concentrations. As an example, 70 to 220 g/dm^3 $Ca(OH)_2$ initial concentrations are indicated by Kinnen et al. (2002) in US patent 6500400. Data in the literature refer usually to studies on calcium hydroxide solutions. Hoon Kang et al. (2003) studied the precipitation of calcium carbonate in a Couette-Taylor reactor from the carbonation of calcium hydroxide solutions with a concentration of 16 mol/m^3, which is very close to the value used in this study (it corresponds to 1.18 g/dm^3).

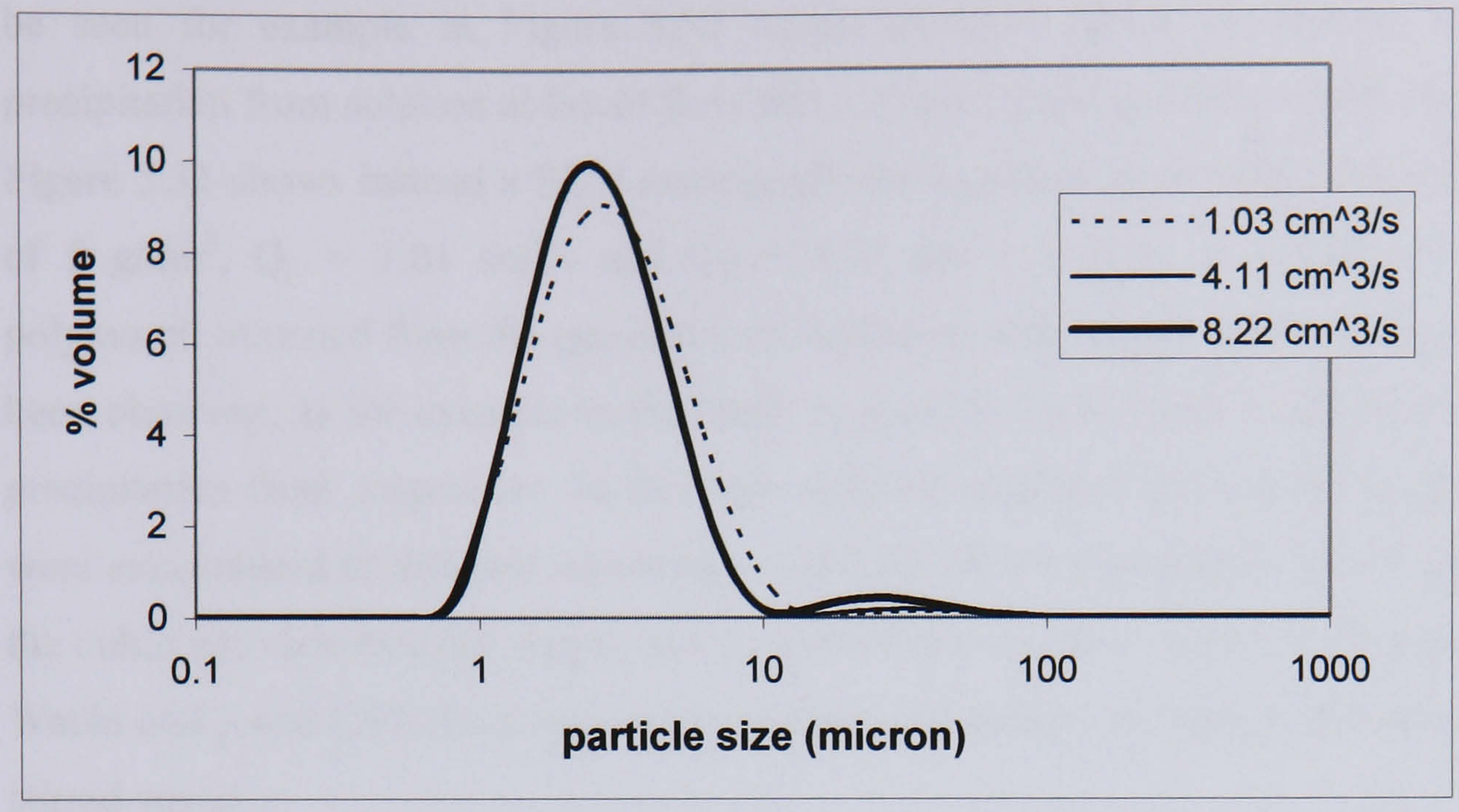

Figure 5.29. Particle size distributions for the experiments with a [$Ca(OH)_2$] solution at different gas flow rates(Q_L = 0.84 cm^3/s).

They found mean particlesizes (D[4,3]) ranging between 3 and 8 μm at varying operating conditions. The particles had a bimodal type size distribution, with a consistent amount of largeparticles in some samples and generally broader particle size distributions than for the NCR. In the cited work on the spinning disc reactor (Trippa et al., 2002) larger particle sizes that in the case of the narrow channel reactor were obtained and it was shown that the SDR could give a narrower particle size distribution than a stirred batch. It must be observed though that the techniques used in that investigation and in the present one for particle size analysis were different. The comparison between the two types of equipment might therefore have limited validity.

5.8.2 Calcium carbonate morphology

Selected powder samples were analyzed by X-ray diffraction and viewed with a SEM both for the precipitation from solution and suspensions. The instruments used were a Philips XPert MPD diffractometer and a FEI 30 XL ESEM respectively. Five samples in all were analyzed, two for the precipitation from solution and three for the precipitation from suspension. The X-ray diffraction patterns can be seen in Appendix D. Results of the X-ray diffraction showed that all samples corresponded to pure calcite without any other phase significantly present. Particle shape was in all cases cubic or rhombohedral, as for the calcite particles in the liquid phase study. This can

be seen for example in Figure 5.30 which shows a SEM micrograph for the precipitation from solution at liquid flow rate 1.12 cm^3/s and gas flow rate 8.22 cm^3/s. Figure 5.31 shows instead a SEM micrograph for a calcium hydroxide concentration of 5 g/dm^3, Q_L = 1.01 cm^3/s and Q_G = 8.22 cm^3/s. Calcite is usually the only polymorph obtained from the gas-liquid precipitation and various crystal shapes have been observed, as for example in the study by García Carmona et al. (2003a) on the precipitation from suspension. In this case scalenohedral and rhombohedral particles were encountered at different operating conditions. In the precipitation from solution the cubic and rhomboedral shapes are the most common, as reported for example by Wachi and Jones (1991b) in their study on the precipitation of calcium carbonate in a stirred vessel.

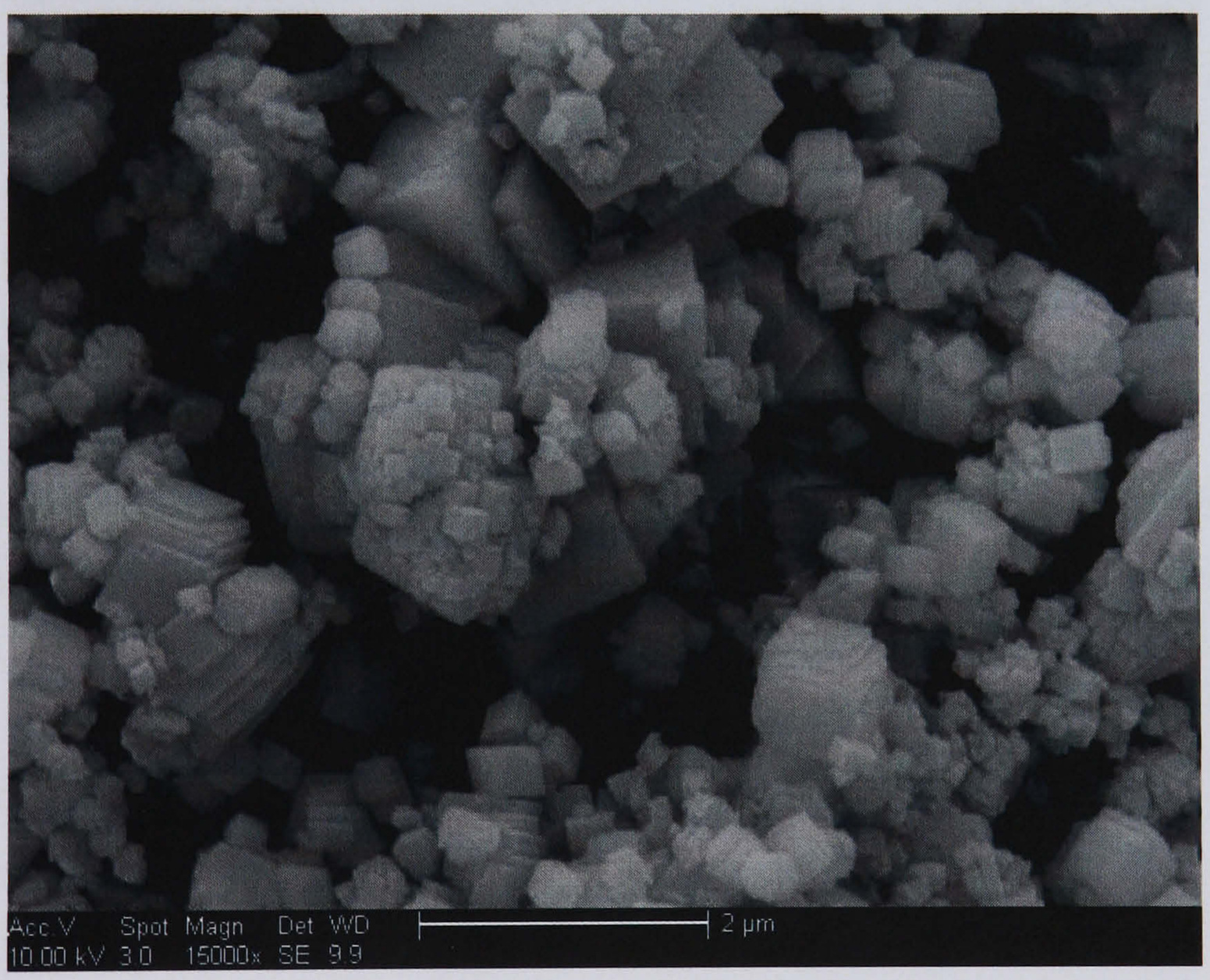

Figure 5.30. SEM micrograph for the precipitation from solution (Q_L = 1.12 cm^3/s and Q_G = 8.22 cm^3/s).

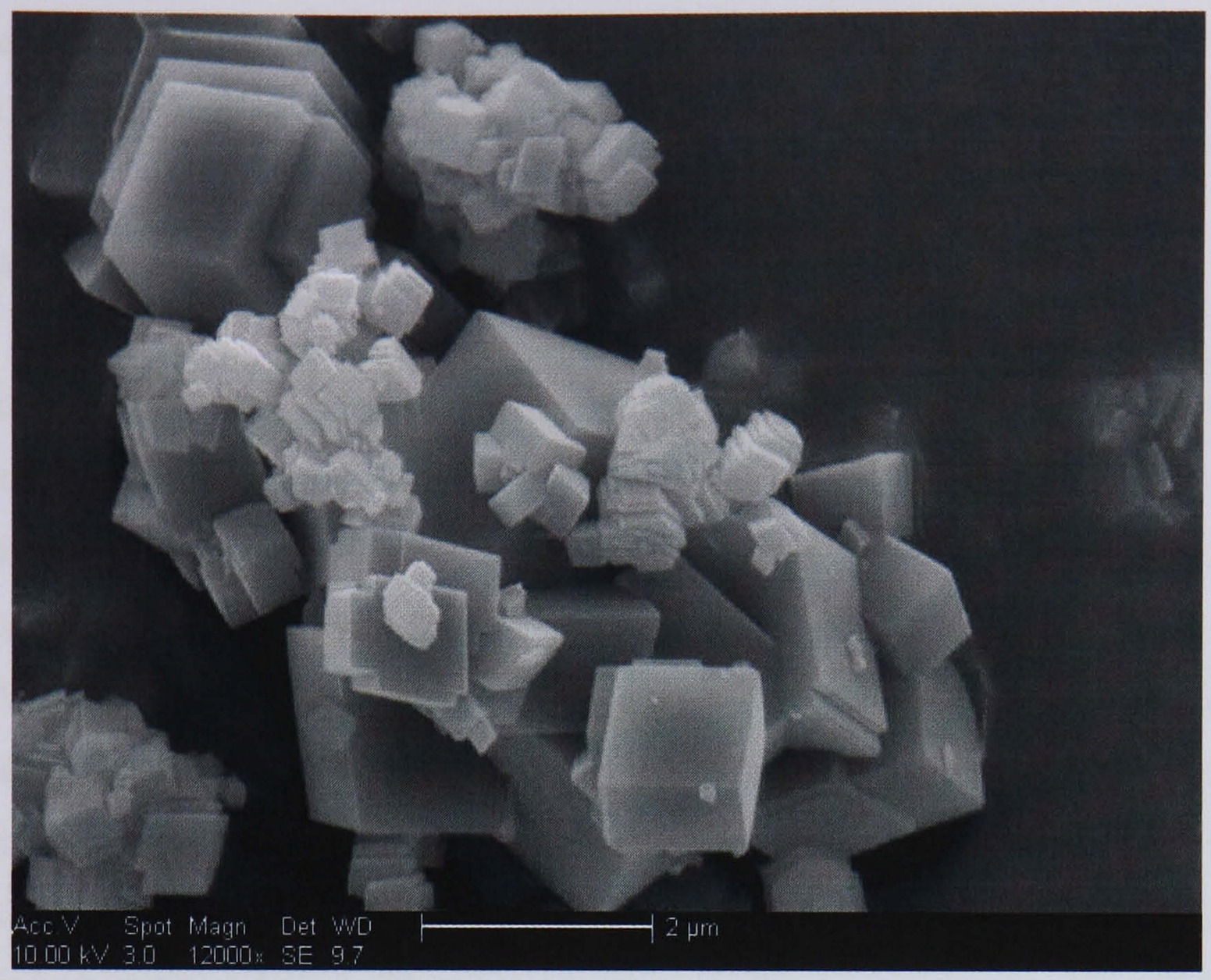

Figure 5.31. SEM micrograph for the precipitation from a 5 g/dm^3 calcium hydroxide suspension (Q_L = 1.01 cm^3/s and Q_G = 8.22 cm^3/s).

5.9 Scaling

For the gas-liquid investigation specific scaling tests were not carried out. However some information on scaling could be obtained from the duration of the experiments carried out for characterizing mass transfer. The necessity to limit uncertainty in the results lead in fact to collecting relatively high volumes of suspensions. For the precipitation from solution, the duration of the experiments was between 5 and 17 minutes approximately and, as previously seen, no relevant decrease in flow rate in respect to the nominal values was observed. At the end of each experiment no significant build up of solid was visually detected. However the NCR was rinsed with hydrochloric acid and deionised water after each experiment, so these conclusions would have to be limited to the duration of one experiment. For the precipitation from suspensions experiments lasted between 5 and 12 minutes approximately. In this case it is more difficult to draw any conclusion as the concentration of the calcium hydroxide slurry influenced the flow rate that could be obtained at different pump speeds. Repeatable flow rate values were obtained, considering a certain margin of uncertainty, however it is difficult to separate the effect of pressure drop due to the

increase in feed concentration to the one of possible scaling due to both the reagent and the product. A more targeted study should be carried out to analyze this aspect.

5.10 Conclusions

Precipitation of calcium carbonate from the carbonation reaction in a 2 mm diagonal line square cross section narrow channel reactor was studied. Mass transfer and precipitation of calcium carbonate in the reaction from calcium hydroxide solutions and suspensions were characterized in different investigations. Liquid flow rates used varied between 0.35 and 1.48 cm^3/s and gas flow rates varied between 1 and 8.2 cm^3/s. Flow patterns for the water-carbon dioxide system in the NCR were visually observed and were found to correspond to slug flow for most of the gas and liquid flow rates used. Absorption of carbon dioxide in water was characterized by reacting the water-CO_2 mixture at the NCR outlet with a sodium hydroxide solution. Absorption rates were found to vary linearly with liquid flow rate with a limited influence of gas flow rate. Volumetric mass transfer coefficients in the case of precipitation from a calcium hydroxide solution were experimentally determined. It was found that values of k^*_La showed the same type of trends versus flow rates as the carbon dioxide absorption rates and that they ranged between 0.33 and 0.80 s^{-1}. Performance in terms of mass transfer was found to be equivalent to high efficiency gas-liquid contactors such as the impinging stream reactor.

Precipitation from calcium hydroxide suspensions with $Ca(OH)_2$ concentrations of 5 g/dm^3 and 7 g/dm^3 was also studied for a limited set of gas and liquid flow rates. Carbon dioxide absorption rates for the precipitation from calcium hydroxide suspensions were found to increase with increasing concentrations and to be higher than in the case of precipitation from solution. For all experiments with the calcium hydroxide suspensions and for the case of precipitation from solution, mean particle size was in all cases of approximately 4-5 μm. The precipitated calcium carbonate particles were found to correspond to pure calcite and to have generally a rhombohedral shape.

CHAPTER 6

Conductivity change in the liquid phase precipitation of calcium carbonate in a narrow channel reactor

6.1 Introduction

This chapter describes the application of a narrow channel reactor with embedded electrodes for detecting the conductivity change during the liquid phase precipitation of calcium carbonate. The information obtained in this study in terms of kinetics, pressure drop and scaling is discussed in relation to gaining a greater knowledge about precipitation in narrow channel reactors.

The reactor machined for this study had the same configuration as the one described in Chapter 5, except for the fact that it had a 1 mm diagonal line. The change in conductivity during precipitation was measured by using a Wheatstone bridge technique, where the unknown resistance was the one offered by the reacting system in the NCR. Experiments were carried out at two different concentrations and three flow rates, replicating operating conditions reported in Chapter 4.

6.2 Conductivity of electrolyte solutions

Electrical conductivity κ (S/m) is defined as the electrical current flowing in the unit area when the unit potential is applied. Conductivity of electrolyte solutions is related to the dissociations of the solutes and it increases with increasing temperature (Koryta et al., 1993, p.89). Unlike metals, electrical conductivity is not an intrinsic property of the material and it depends on concentration of the electrolyte solutions.

Strong electrolytes exhibit a much higher conductivity than weak electrolytes, since they are completely ionized. For strong electrolytes, at low concentrations the plot of the molar conductivity Λ (S m^2/mol) is proportional to the square root of the concentration (Hibbert and James, 1984, p.52):

$$\Lambda = \Lambda_o - C\sqrt{c} \qquad (6.1)$$

where Λ_o is the molar conductivity at infinite dilution and C is a constant.

This expression has a theoretical basis in the interionic attraction theory that can be represented by Coulomb's law and has been confirmed by experimental data. Equation 6.1 is valid for 1:1 electrolytes at concentrations up to 2 mol/m^3 (Hibbert and James, 1984, p.45). A number of modifications of equation 6.1 have been introduced to take into account the increase in concentration (Hine, 1985, p. 82 and Hibbert and James, 1984, p.47). These expressions usually contain one of more corrective terms dependent on concentration.

The conductivity of mixtures of electrolytes usually is lower than the value that would be obtained by simply following the mixture rule (Hibbert and James, 1984, p.52). Models predicting conductivity of mixtures usually contain empirical parameters, fitted from experimental data, and are polynomial functions of concentration and temperature (Cortazar et al., 2002).

6.3 Conductivity change in precipitation reactions

The change in conductivity of a solution during precipitation has been used in many cases to follow the extent of the reaction. In fact, the precipitation of the solid is usually related to a change in conductivity, as some of the ions originally present in the reacting system are not in solution at the end of the reaction. Measurements of conductivity taken at different time intervals from the beginning of the reaction can be used to detect the induction time of precipitation. If a plot of conductivity versus reaction time is reported, the induction time can be determined as the time at which the slope of the curve conductivity-time starts to change (Söhnel and Handlířová, 1984, cited by Söhnel and Garside, 1992, p.206). The possibility of detecting the induction time depends on the refinement of the technique used to measure conductivity. Söhnel and Mullin (1978) developed a precipitation apparatus that allowed determinations of induction times within different orders of magnitude.

For this study, the aim was to increase knowledge of the kinetics of precipitation in narrow channel reactors while carrying out the process itself at the same time. A non-invasive technique was needed, as in the study carried out by Burns and Jachuck (2005) who used a Perspex rotating disc with embedded electrodes to monitor gas-liquid mass transfer in the precipitation of calcium carbonate in a spinning disc reactor. For this study a narrow channel reactor with embedded electrodes that could allow measurement of conductivity at various distances from the point in which the two reagent mix was designed. The characteristics of the set-up and the procedure used for measuring conductivity are described in the following sections.

6.4 Experimental set-up

The narrow channel reactor used for this study had the same configuration as that for the gas-liquid investigation, except that the cross section had a 1 mm diagonal line. Brass screws with an M3 (3 mm) thread and 30 mm long purchased from RS were used as electrodes. Before machining the channel, 14 electrodes were embedded in the lower part of the Perspex block keeping the heads of the screws on the outside. The first screw was located at 5 mm distance from the Y mixer, with all the others at 15 mm from the previous one considering the distances taken on the straight segments only. If two adjacent electrodes were separated by a U bend, the distance between the

two would be 10 mm to be added to the length of the U bend (which had a diameter of 5 mm) to give a total of 17.85 mm. Distances are considered from the centre of the screws. The screws were cut accordingly to the thickness of the Perspex in such a way that the end of the screw would be levelled with the Perspex. The channel was then machined on the two sides and bonded following the same procedure described in Chapter 5 for the diffusion bonding of the 2 mm channel. A schematic of the reactor can be seen in Figure 6.1.

In order to be able to connect the narrow channel reactor to an electrical circuit without interfering with the reaction, a second Perspex module with embedded electrodes was manufactured. It had the function of creating electrical continuity between the narrow channel reactor and the external circuit. The block had screws embedded in the same configuration as in the narrow channel reactor, as can be seen in Figure 6.2. The ends of the screws in the external Perspex module were put in contact with the heads of the screws of the narrow channel reactor. The narrow channel reactor was connected to the circuit by wiring between the screws in the external module and the circuit itself. A photograph of the final set-up can be seen in Figure 6.3.

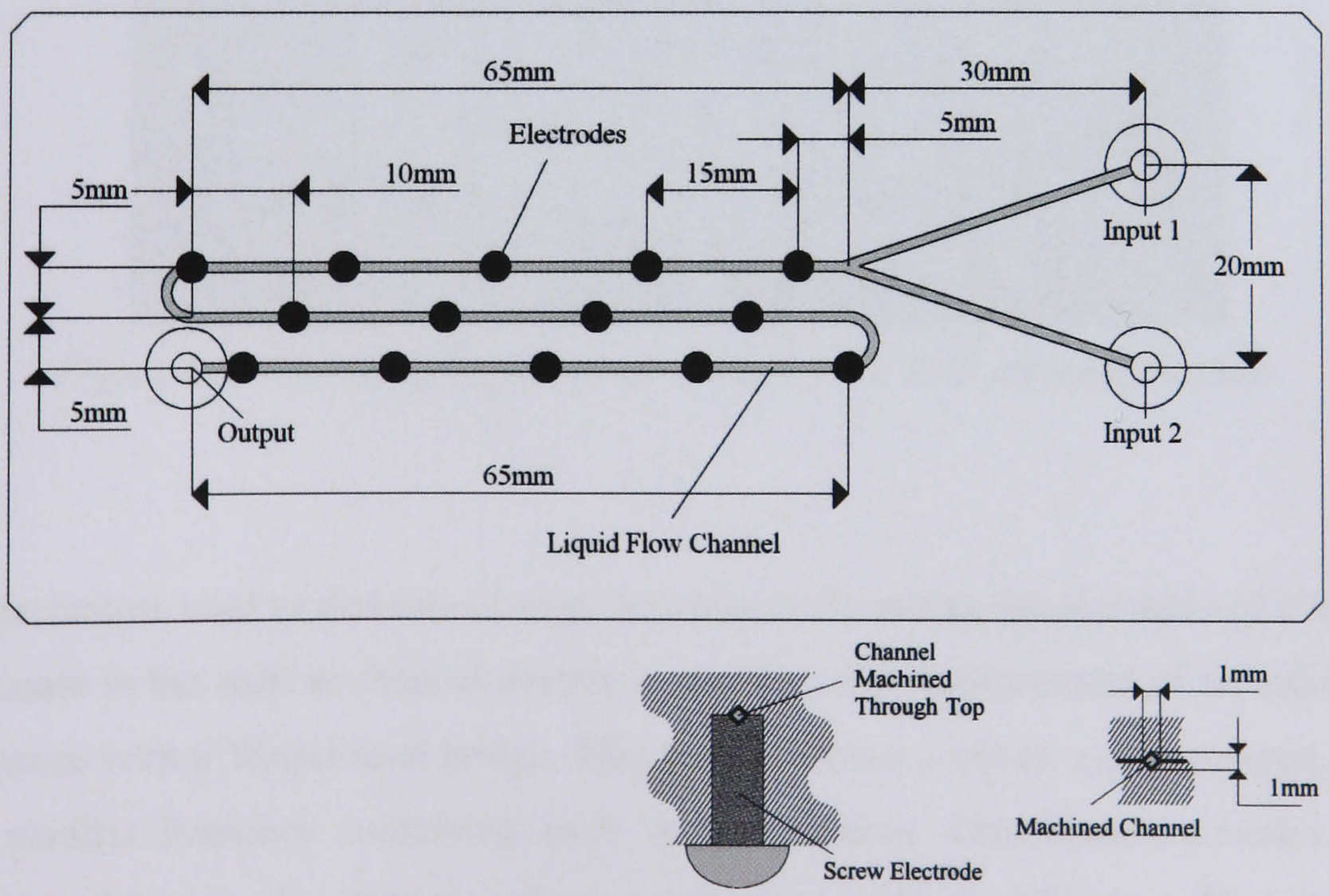

Figure 6.1. Schematic of the NCR with embedded electrodes.

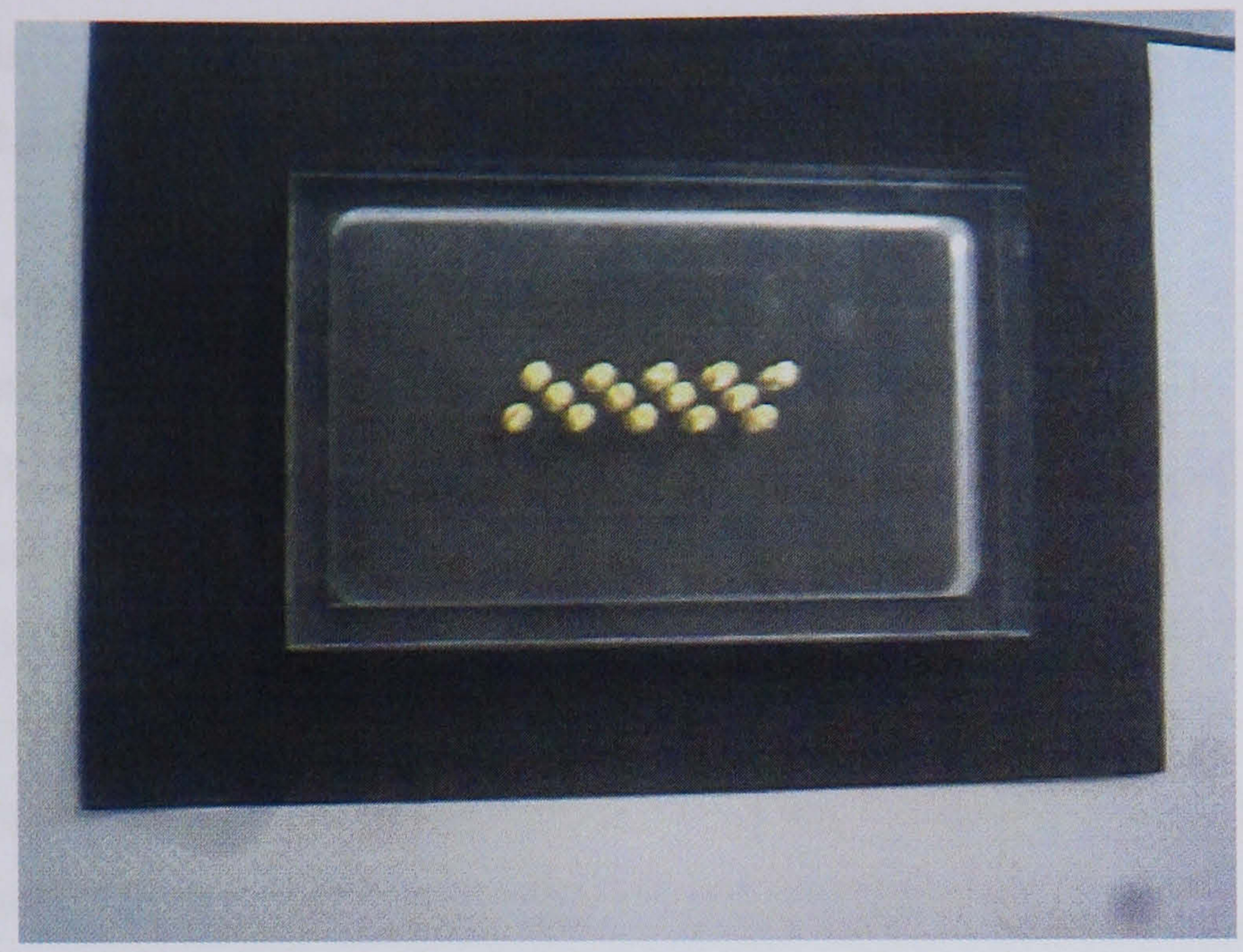

Figure 6.2. External Perspex module.

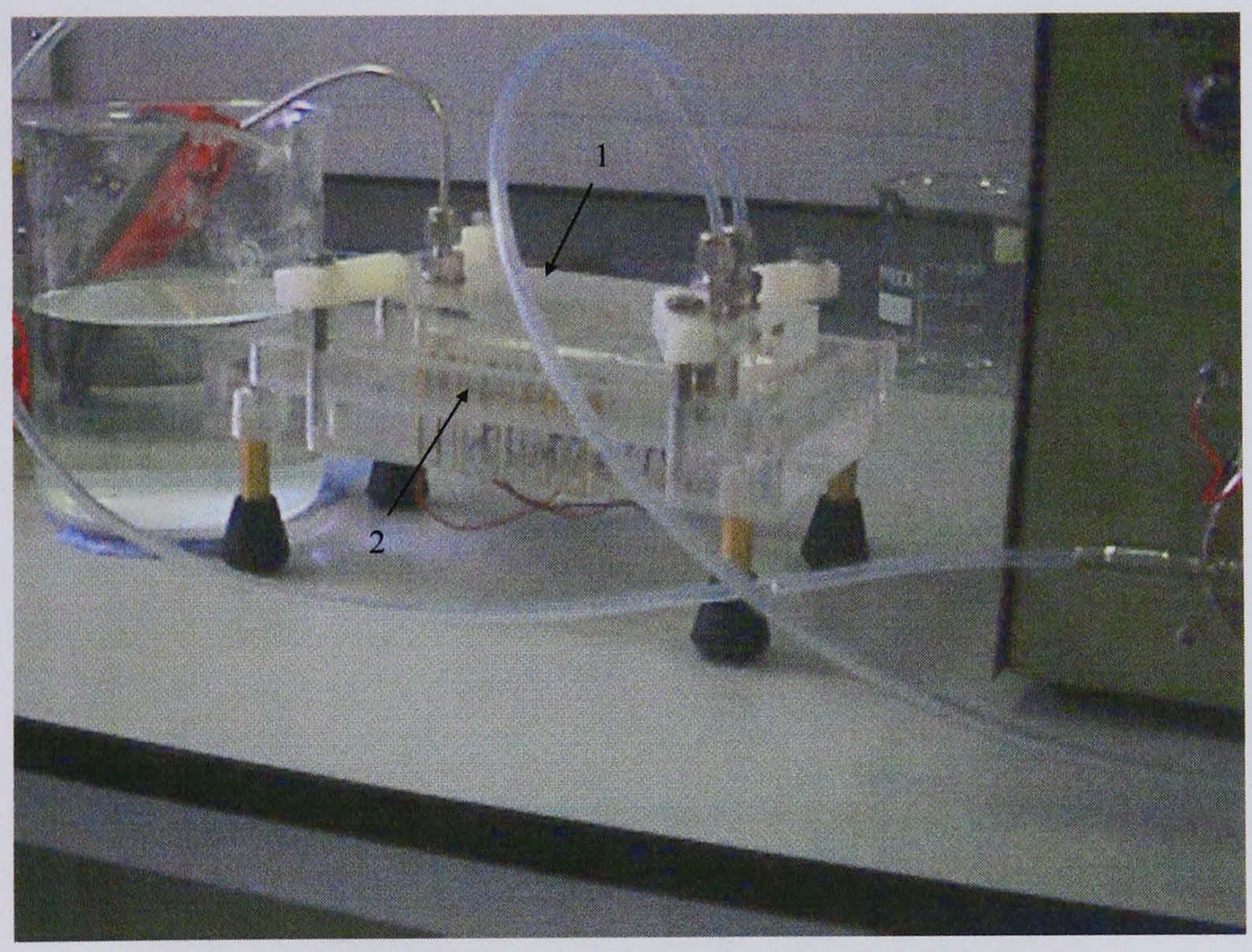

Figure 6.3. Photograph of the final set-up: 1. NCR, 2. external module.

The technique used to measure change in conductivity during precipitation of calcium carbonate in the narrow channel reactor is based on the measurement of an unknown resistance with a Wheatstone bridge. This type of circuit contains a power supply and two parallel branches containing each two resistances. One branch contains two known resistances, the other an unknown resistance and a variable one. The variable resistance is used to balance the two branches of the circuit, this allows the determination of the unknown resistance from the values of the other three resistances.

A schematic of a Wheatstone bridge can be seen in Figure 6.4 (http://civil.colorado.edu/courseware/struct_labs/wheatstone.html).

In this case the unknown resistance was the reacting system in the narrow channel reactor. Measurements used an AC power supply, with a Thurlby Thandar Instruments TG 120 20 MHz function generator. The input voltage used had a frequency of 12 kHz. The volt meter used to check that the bridge was balanced was a Iso-tech IVM 100 1 Mhz AC Volt meter. The bridge was balanced by using 10 kΩ and 50 kΩ variable resistances and the value of the resistance that balanced the bridge was measured with a Iso-tech IDM63N hand held resistance meter. Exclusion of one of the resistances from the circuit was achieved with a switch.

The variable resistance values to be used in the circuit were determined by carrying out some preliminary tests on calcium carbonate precipitation and measuring the conductivity at the inlet and the outlet of the reactor. The reaction system:

$$Na_2CO_3 + Ca(NO_3)_2 \rightarrow CaCO_3 \downarrow + 2NaNO_3 \qquad (6.2)$$

leads to the production of calcium carbonate, which precipitates and gives a negligible

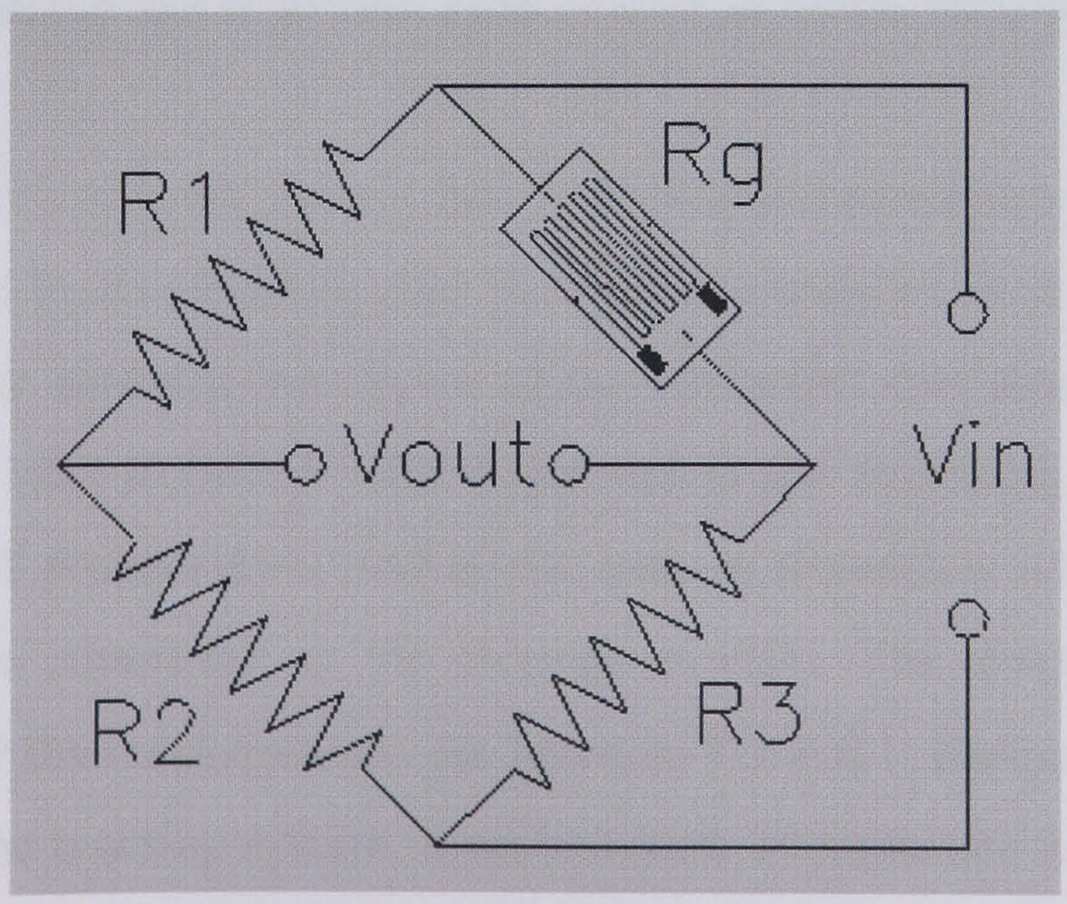

Figure 6.4. Schematic of a Wheatstone bridge (from http://civil.colorado.edu/courseware/struct_labs/wheatstone.html).

contribution to the conductivity of the final solution, and sodium nitrate, which gives a relatively high conductivity. Preliminary measurements showed that a negligible increase of conductivity was obtained dispersing calcium carbonate in deionised water. Conductivity measurements at the beginning and at the end of the reaction gave values in terms of resistance between two electrodes varying between 5 kΩ and 30 kΩ.

Solutions were fed to the reactor by using two gear pumps with digital flow controllers. Calibration of the pumps was carried out for one value of the flow rates used (0.67 cm^3/s) and results of the calibration were found to be consistent with the readings indicated by the controller. The solutions were fed to the reactor with a 4 mm OD clear C-Flex tubing from Cole-Parmer. The outlet tubing was a 14 cm long, 1/8 inch OD stainless steel capillary. Swagelock fittings with ISO 228 parallel threads were used to connect the inlet and outlet tubing to the reactor.

A digital pressure meter (Digitron 2084P) was connected to the calcium nitrate feed line to measure the pressure drop between one side of the inlet and the outlet of the reactor.

6.5 Experimental procedure

Concentrations and flow rates of the solutions were chosen to replicate operating conditions in the study described in Chapter 4. Supersaturation ratios S = 2000 and S = 4000 were considered and total flow rates of 0.15, 0.43 and 0.67 cm^3/s were used.

As previously mentioned, the reactor had 14 embedded electrodes, of which only 11 could be connected to the circuit to give 10 resistance measurements. Preliminary tests were carried out to optimize the choice of the electrodes that should be considered. The main interest was to follow what happened at the beginning of the reactor, to detect the onset of precipitation, and at the end, to determine whether most of the reaction would be completed in the Perspex module. The distances between the electrodes used for the measurements are listed in Table 6.1. Before carrying out each experiment with the reacting system, measurements of resistance were taken with the calcium nitrate solution to be used in the reaction. This procedure was followed to

Table 6.1. Distances between the couples of electrodes used for measurement.

Electrode couple	Distance (mm)
1-2	15
2-3	15
3-4	15
4-5	15
5-6	17.85
6-7	30
7-8	32.85
8-9	15
9-10	30
10-11	15

have conductivity data for the reaction in dimensionless form. This would allow the elimination of uncertainty related to the geometry of the system, in aspects such as the distance between the electrodes or the extension of the cross section of the reactor. Data obtained in terms of resistance with the calcium nitrate solution also allowed an estimate of this uncertainty. This was possible by comparison with measurements of the conductivity of calcium nitrate taken outside the NCR, as explained in the results section.

For each experimental run, solutions were prepared by dissolving solid reagents in water, as for the study described in Chapter 4. The conductivity and the temperature of the solutions were measured using a Hanna Instruments HI 8733 conductivity meter and a Digitron T 228 thermometer respectively. Then the calcium nitrate solution was fed to the reactor. During the experiments, the resistance between couples of adjacent electrodes was measured by using a switch that excluded all the other electrodes from the circuit. The same procedure was then repeated for all remaining couples of adjacent electrodes.

For each run, usually two sets of measurements with the calcium nitrate solution were taken. The reactor was then flushed with deionised water for times ranging between 30 s for the highest flow rate and 2 minutes for the lowest one. Solutions of sodium carbonate and calcium nitrate were fed to the reactor and no measurement of resistance was taken for the same time intervals indicated for the deionised water. At least three sets of resistance measurements were taken for each experiment and

readings of pressure drop were recorded at the beginning and/or at the end of each set of conductivity readings. Each set of conductivity readings lasted approximately between 4 and 6 minutes and the overall duration of each run was around 15 to 25 minutes. The conductivity at the outlet of the NCR was also recorded.

6.6 Results

6.6.1 Evaluation of uncertainty

For this study about 20 experiments were carried out, using the operating conditions mentioned above. No specific trend was found when looking at the different sets of measurements of conductivity taken within a single experiment. Usually three sets of data for each experiment were collected. In limited cases, a fourth set of conductivity measurements was taken.

Of all the data collected, only information about a limited number of experiments could actually be used. For each experiment, averages of the first three sets of data were considered and the conductivity in dimensionless form in respect to the conductivity of the calcium nitrate solution was calculated. Standard deviation of the data was also calculated, using the equation reported in Appendix A for a small number of data (equation A6). Uncertainty was then considered to be equal to $\pm 2\sigma_d$ which gives a confidence of 95.4%, as described in Appendix A.

Data sets were not considered if one or more data had a relatively high standard deviation. Particularly, if the ratio between the standard deviation and the average of the data x_m multiplied by 100 is considered:

$$B = \frac{\sigma_d}{x_m} \cdot 100 \qquad (6.3)$$

then all sets of data for which more than two values of B were higher than 7 % were not considered.

The sets of data obtained for the highest flow rate (0.67 cm^3/s) were those affected by the highest amount of error. For the sets of data that were considered, average values of B varied between 3.3 % and 5.8 %.

6.6.2 Initial conductivity of calcium nitrate and calibration measurements

The resistance measurements taken for the calibration solution can be compared to the initial measurements of conductivity to estimate the uncertainty in the geometry of the system. In fact, the screws have a finite diameter and therefore the distance considered between the electrodes is higher than the real one. Moreover, the tolerance of the manufacture of the channel contributes to an error in the extension of the cross section. Resistance offered by the solution is related to its resistivity by the equation:

$$R_s = \frac{\rho_s d_e}{S_{NCR}} \qquad (6.4)$$

where d_e (m) is the distance between the electrodes, S_{NCR} (m^2) is the cross section of the narrow channel reactor and ρ_s (Ω m) is the resistivity of the solution.

The resistivity is the reciprocal of the conductivity:

$$\rho_s = \frac{1}{\kappa_s} \qquad (6.5).$$

For the resistance measurements of the calcium nitrate solution, data considered in terms of conductivity gave a normal frequency distribution and indicated that the errors were randomly distributed and no systematic error was present in the system (Appendix A). Standard deviation was around 3 - 4% of the average value. Table 6.2 lists the average conductivities, obtained calculating the conductivity from equations 6.4 and 6.5 at the different operating conditions used. The results reported refer to those runs for which the data of the change in conductivity were considered acceptable. Table 6.2 also contains values of conductivity of the calcium nitrate solution, measured before the test in the NCR, and the ratio between the two. The average of the ratio between the calculated value and the measured one is 2.34, with a

Table 6.2. Calculated average conductivity and experimental measurement for calcium nitrate solutions.

Supersaturation ratio, S	Q_{out} (cm^3/s)	Calculated average κ (S/m)	Experimental κ (S/m)	Calculated average κ / Experimental κ
2000	0.15	5.20	2.04	2.55
2000	0.43	4.96	2.08	2.39
2000	0.67	4.79	2.05	2.34
4000	0.15	8.32	3.58	2.33
4000	0.43	8.62	3.67	2.35
4000	0.67	7.92	3.70	2.14

standard deviation of 5.5% of the average. The resistance deriving from balancing the Wheatsone bridge is then more than two fold lower than expected from the conductivity of the solution. This indicates that the real geometric factor of the set-up G (m^{-1}):

$$G = \frac{d_e}{S_{NCR}} \tag{6.6}$$

is lower than the theoretical one.

This confirms that by not considering the dimension of the electrodes the distance between them is overestimated and it might also indicate that the actual cross section of the NCR is higher than the theoretical one. In fact, if the thickness of the screws is taken into account and the distance between the electrodes is considered to be 12 mm instead of 15 mm, then equation 6.6 gives a ratio between the calculated geometric factor and the real one equal to 1.25. Moreover, if in addition to a shorter distance between electrodes, a cross section with a 1.2 mm diagonal line instead of the 1 mm nominal one is considered, equation 6.6 gives a ratio between the calculated geometric factor and the real one equal to approximately 1.8. This value is close to the average of the values reported in Table 6.2. As for the reactor used in the gas-liquid study, the NCR used in this investigation was opened at the end of its use and the diagonal line was measured. The diagonal line was 1 mm long both on the Perspex and on the brass screws (the reactor was viewed under an optical microscope). However, it is possible that because the channel was machined through two different materials at the same

time, some irregularities on the surface of the channel might be present in correspondence of the brass screw (the channel surface looked smoother on the Perspex that on the brass screws). This could account for the deviation from the theoretical cross section which is considered to partly determine the discrepancy between the real and calculated geometric factor. The calculation of the geometric factor allows the manipulation of the results in terms of real resistance or conductivity measurements for this set-up and gives an estimate of the overall uncertainty in the manufacturing technique.

6.6.3 Change in conductivity during precipitation

The initial conductivity of the solutions and the final conductivity of the suspensions collected at the reactor outlet are listed in Table 6.3 for the different operating conditions. The temperatures varied between 21°C and 25°C. It can be seen that the two solutions had very similar conductivities and the conductivity at the outlet was generally lower than the conductivity of each of the solutions.

Figure 6.5 shows a plot of the ratio between the conductivity during the reaction and the conductivity of the calcium nitrate solution for S = 2000. The dimensionless conductivity κ^* was obtained calculating the ratio:

$$\frac{R_s}{R_p} = \kappa^* = \frac{\kappa_p}{\kappa_s} \tag{6.7}$$

where R_p (Ω) and κ_p (S/m) are the resistance and the conductivity during precipitation respectively. For complete conversion at S = 4000 the solids concentration would be around 1.25 % in weight. Hence, it was considered that the precipitating calcium carbonate did not significantly increase the effective resistance of the solution as the solids concentration was low in all cases.

Table 6.3. Initial and final conductivity values (measured with the conductivity meter).

Supersaturation ratio, S	Q_{out} (cm^3/s)	κ ($Ca(NO_3)_2$) (S/m)	κ (Na_2CO_3) (S/m)	Final κ (S/m)
2000	0.15	2.04	1.93	1.05
2000	0.43	2.08	1.89	1.28
2000	0.67	2.05	1.89	1.43
4000	0.15	3.58	3.40	1.46
4000	0.43	3.67	3.36	3.30
4000	0.67	3.70	3.41	2.58

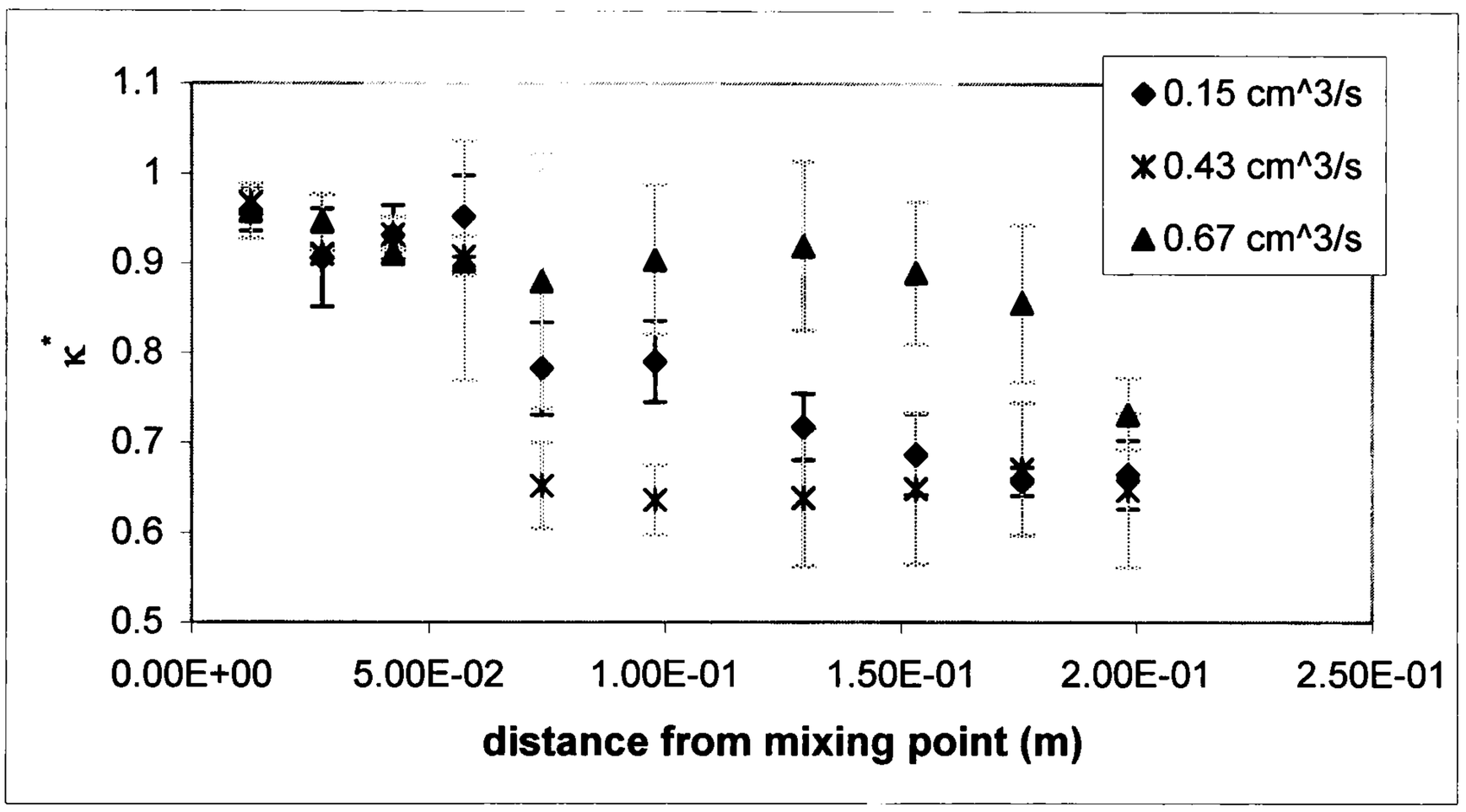

Figure 6.5. Dimensionless conductivity vs. distance from the Y mixer for S = 2000.

The dimensionless conductivity is plotted against the distance from the Y mixer. As the dimensionless conductivity between couples of adjacent electrodes is considered, the abscissa value used is the distance of the mean point between the two electrodes from the Y mixer, where the two solutions start mixing. Conductivity at the last electrode is between 65% and 75% of the initial one. The highest fall in conductivity and therefore the highest precipitation rate appears to be obtained for 0.43 cm^3/s. Taking into account the uncertainty in the data, it can be considered that the conductivity is almost constant between the first and fourth electrode, whereas a relatively high change occurs between the fourth and sixth electrode. This seems to occur for all flow rates, although uncertainty in the data might imply that this is not true for 0.67 cm^3/s. The high change in conductivity corresponds to distances between 5 cm and 8.3 cm from the Y mixer. As each straight segment of the reactor is 6.5 cm

long, the onset of precipitation occurs before the end of the first segment and extends into the second one. It can be considered that the induction time corresponds to the residence time between the Y mixer and the point where precipitation starts. The resolution of the technique used allows only the indication of a time interval for the onset of precipitation. The observations on the change in conductivity can be considered equivalent to the condition for the change in slope for a continuous curve given by Söhnel and Handlířová (1984, cited by Söhnel and Garside, 1992, p.206).

Figure 6.6 shows the dimensionless conductivity versus distance from the mixing point for S = 4000. In this case the data for different flow rates are very close for almost all electrodes and the relative high amount of uncertainty does not allow drawing any conclusion. Moreover the range of variation of κ^* is narrower than in the case of S = 2000, so it is difficult to distinguish the different phases of the process. This is also seen in the data reported relative to the two different concentrations, for one flow rate in the same graph. The flow rate 0.67 cm^3/s is not considered because of the high uncertainty, as previously mentioned. Figure 6.7 shows κ^* for 0.15 cm^3/s, and Figure 6.8 shows κ^* for 0.43 cm^3/s. Precipitation rate is expected to be higher for S = 4000, as seen in Chapter 2, which seems to be confirmed in the results. For the highest concentration what seems to be identifiable is a very rapid depletion of conductivity for the precipitation itself combined with a fast increase of conductivity due to the ions remaining in solution.

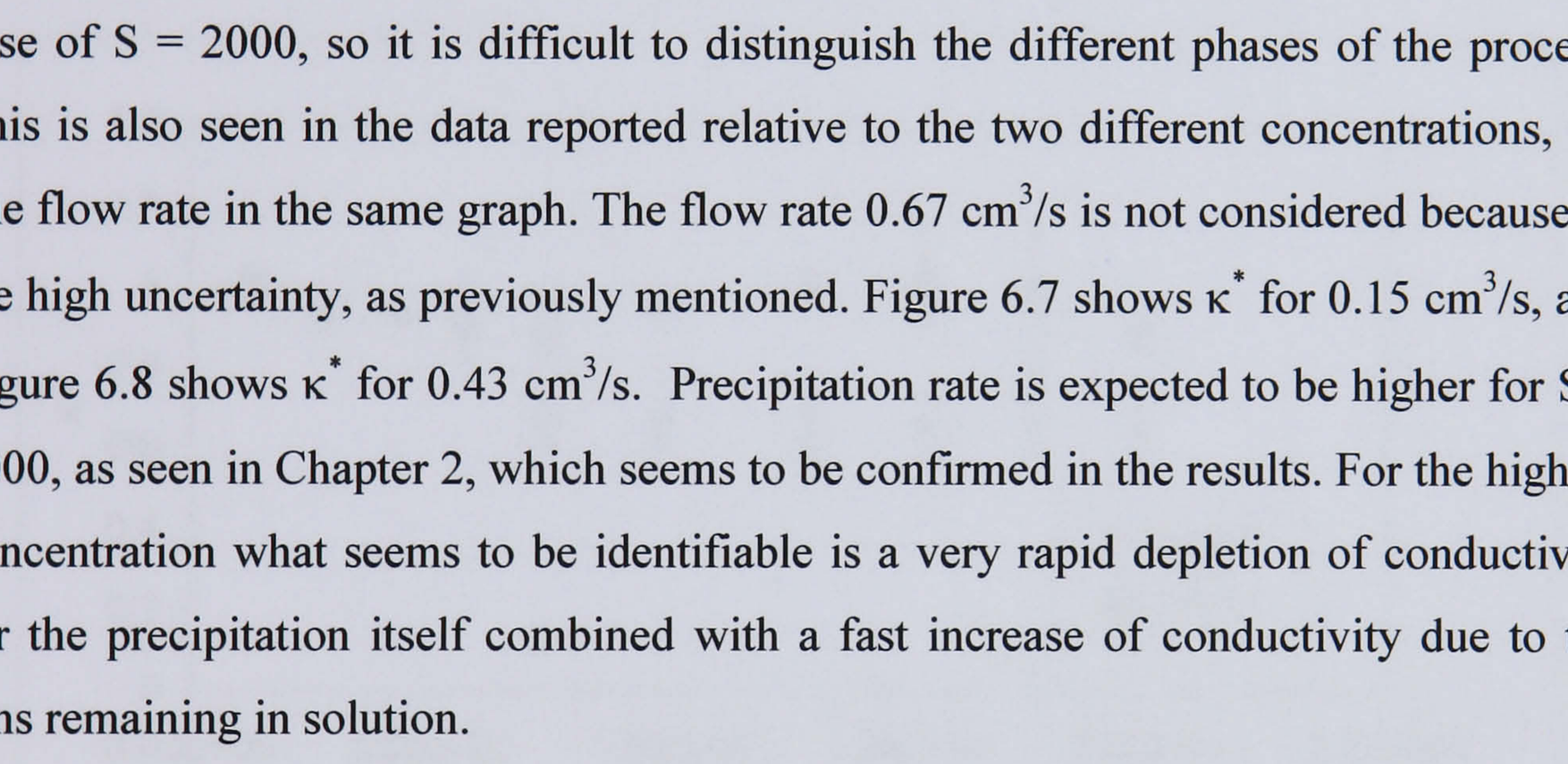

Figure 6.6. Dimensionless conductivity vs. distance from the Y mixer for S = 4000.

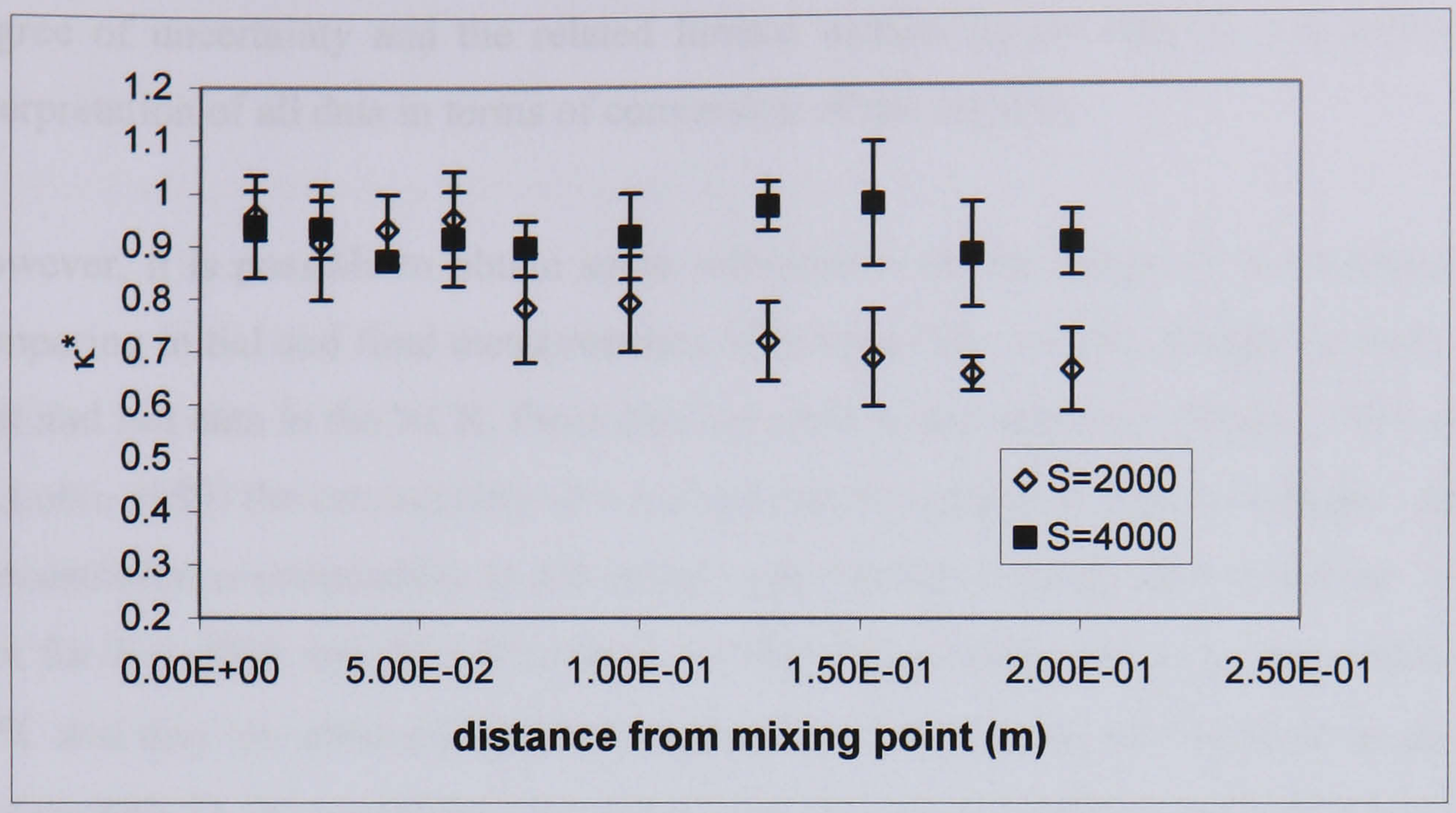

Figure 6.7. Dimensionless conductivity for 0.15 cm^3/s.

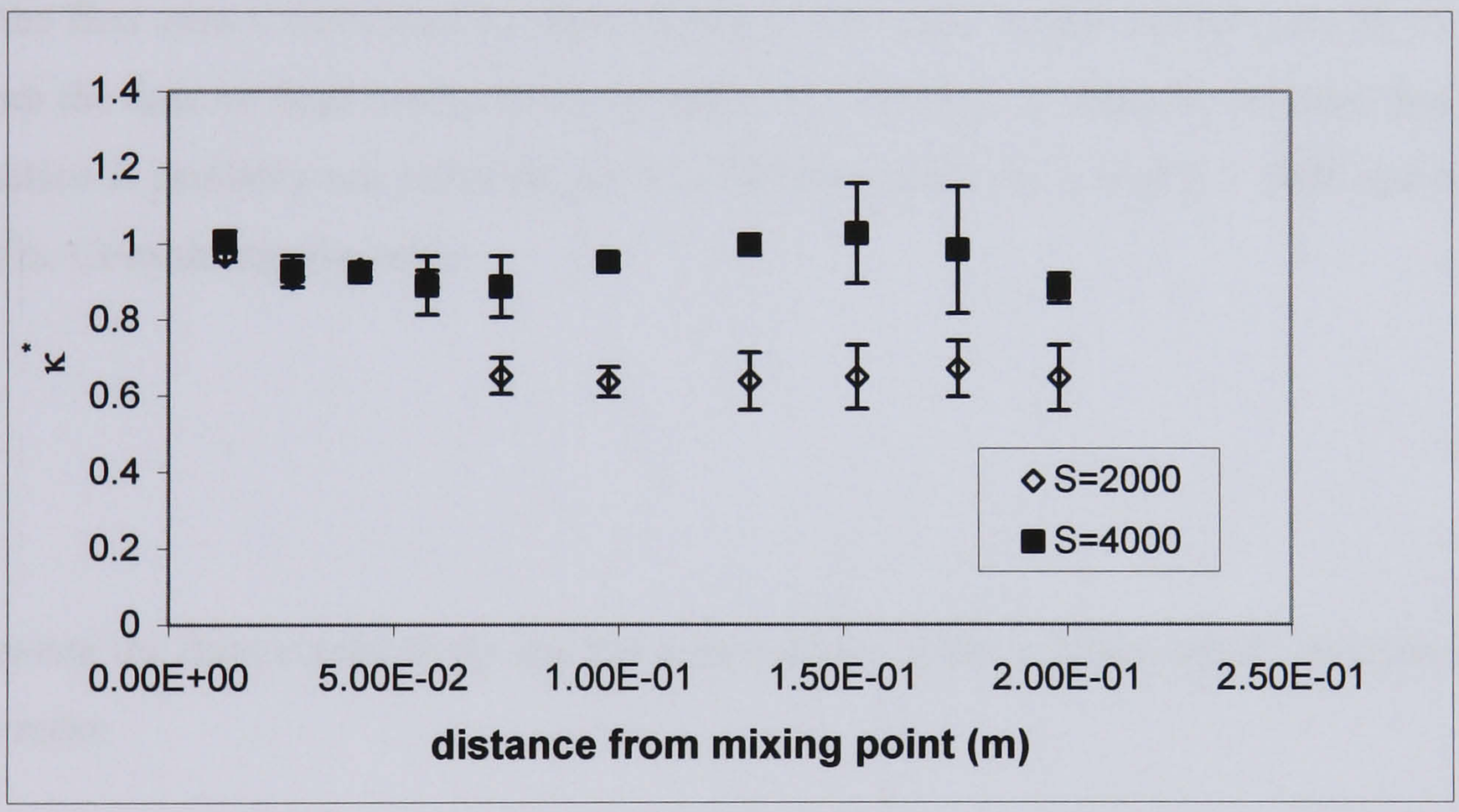

Figure 6.8. Dimensionless conductivity for 0.43 cm^3/s.

6.6.4 Extent of the reaction in the NCR

As previously mentioned, one of the aspects of interest was the evaluation of the conversion in the narrow channel reactor. In the work described in Chapter 4, the reactors had an outlet channel constituted by a 1 mm ID capillary with a length of the same order of magnitude as the channel in the Perspex chip. It was found that the conversion was very similar in the case of the two reactors and close to completion. To optimize the design of NCRs for precipitation, an analysis of the results of this study in terms of conversion within the Perspex module can be carried out. The high

degree of uncertainty and the related limited availability of data do not justify an interpretation of all data in terms of conversion of the reaction.

However, it is possible to obtain some information on the extent of the reaction by comparing initial and final measurements of conductivity and the change between the first and last data in the NCR. From data reported in the literature (Postler, 1970 cited by Lobo, 1989) the conductivity of a sodium nitrate solution at total conversion with a concentration corresponding to the initial supersaturation ratios used would be 1.075 S/m for S = 2000 and 2.15 S/m for S = 4000. These data refer to a temperature of 25°C and they are obtained by linear regression of the data in the literature as shown in Appendix D. By considering an initial conductivity of 2.06 S/m and 3.65 S/m for S = 2000 and S = 4000 respectively for the calcium nitrate solution, it can be seen that in the first case κ decreases by approximately 50 % and in the second case by 40 %. From the data on final conductivity, reported in Table 6.3, it might be inferred that the reaction is probably not complete for S = 2000 and 0.67 cm^3/s and S = 4000 and 0.43 cm^3/s. Considering the ratio:

$$\frac{\kappa^{f}}{\kappa_{s}} \tag{6.8}$$

between the final conductivity and the conductivity of the calcium nitrate solution and the ratio:

$$\frac{\kappa^{*}_{last}}{\kappa^{*}_{first}} \tag{6.9}$$

between the dimensionless conductivity obtained between the last couple of electrodes and the first one, the degree of completion of the reaction occurring in the NCR can be quantified.

Figures 6.9 and 6.10 show these two parameters for S = 2000 and S = 4000 respectively. In both cases except for the lowest flow rate, the two ratios have relatively close values, indicating that most of the depletion of conductivity is achieved in the narrow channel reactor. It should be considered that in this case the

outlet capillary has and ID which is approximately double than the one used in the study described in Chapter 4. This determines a residence time 4 times higher, if equal lengths for the capillary are considered in the two cases, which should give a higher conversion. In an optimized configuration a shorter outlet capillary than the one used for reactor B could be used for obtaining similar conversions to the ones reported in Chapter 4. This would also reduce pressure drop and therefore energy costs. This aspect would have particular relevance when scaling out using a high number of channels. A shorter reactor length could also be beneficial in terms of final PSD as the particles would be in contact with a depleted solution for shorter times. The growth process would then be less favoured and better control of the final particle size could be achieved.

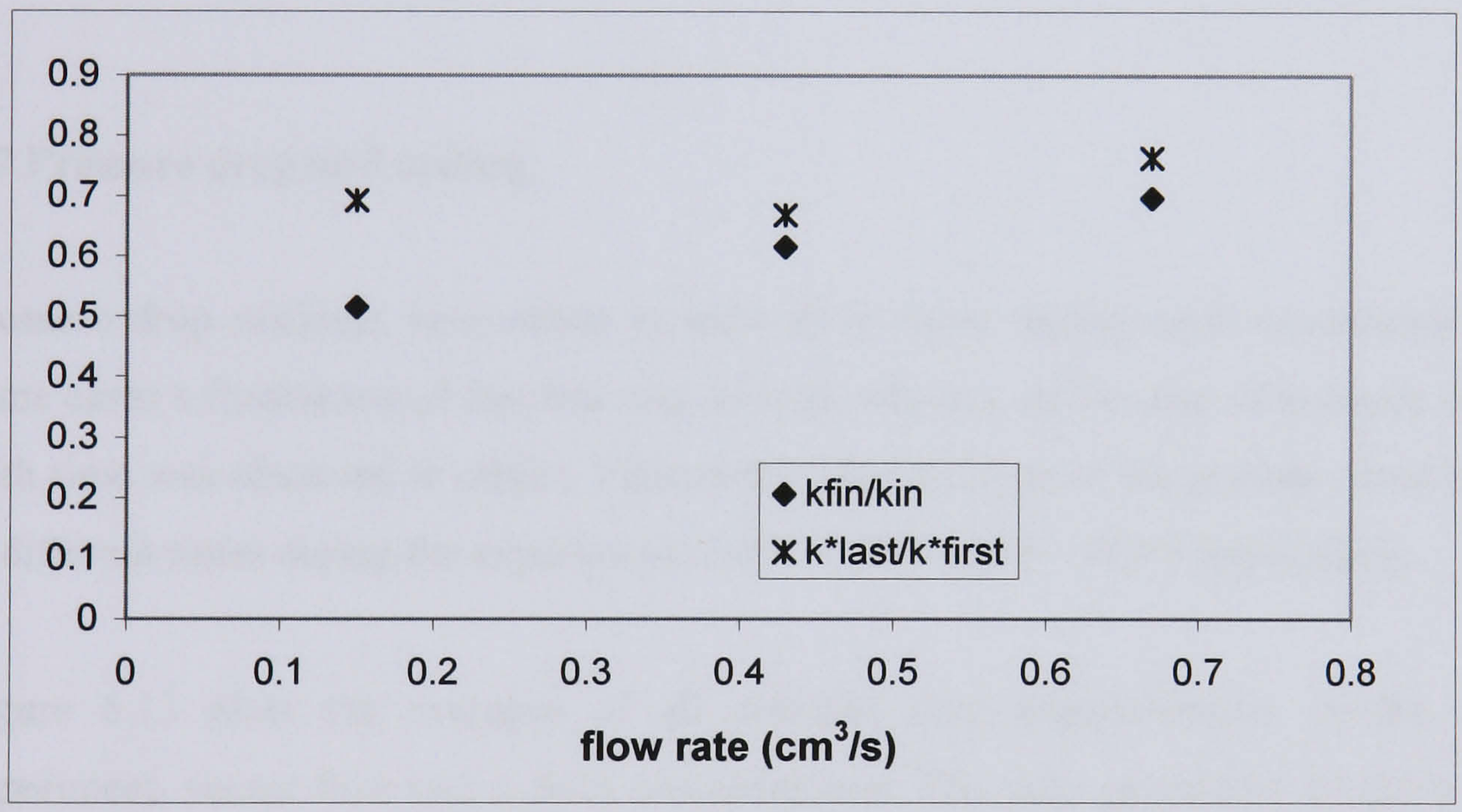

Figure 6.9. Comparison of ratios of conductivities at the beginning and end of the reaction and between the first and last electrode for S = 2000.

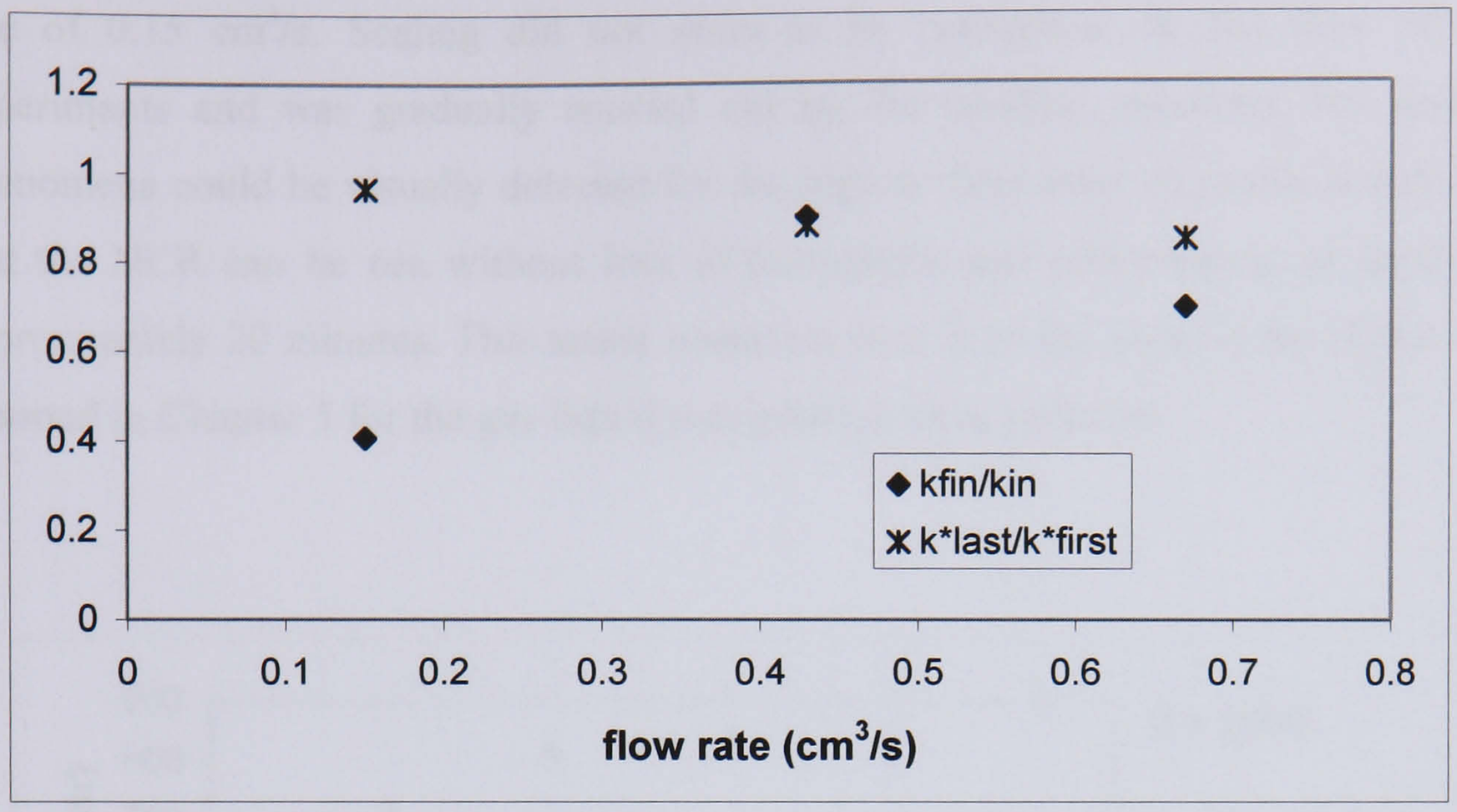

Figure 6.10. Comparison of ratios of conductivities at the beginning and end of the reaction and between the first and last electrode for S = 4000.

6.7 Pressure drop and scaling

Pressure drop readings were taken at least three times during each experiment. In some cases a fluctuation of the data was noticed, whereas an increase of pressure drop with time was observed in others. Figures 6.11 and 6.12 show the pressure drop data at different times during the experiments for S = 2000 and S = 4000 respectively.

Figure 6.13 plots the averages of all pressure drop measurements, within one experiment, versus flow rate at both concentrations. The same graph also contains the theoretical pressure drop, obtained considering the properties of water at 20°C, as in Chapter 4. In both cases measured pressure drop values are higher than the values predicted for water and the influence of the rheology of the suspensions on pressure drop should be investigated in further studies. For Q = 0.15 cm^3/s and Q = 0.43 cm^3/s the pressure drop at S = 4000 is more than double than the one at S = 2000. The highest flow rate seems instead to give very similar pressure drop values in both cases.

No significant scaling was noticed in our experiments as no increase of the electrical resistance at the electrodes could be detected after a certain period from the beginning of the experiment. Visual observations during the experiments showed temporary formation of localized scale build-up (for example around the U bends) for the flow

rate of 0.15 cm^3/s. Scaling did not seem to be permanent for the time of the experiments and was gradually washed out by the reacting solutions. No scaling phenomena could be visually detected for the highest flow rates. It can be concluded that the NCR can be run without loss of throughput and performance; at least for approximately 20 minutes. This tested operating time is of the same order of the one reported in Chapter 5 for the gas-liquid precipitation from solution.

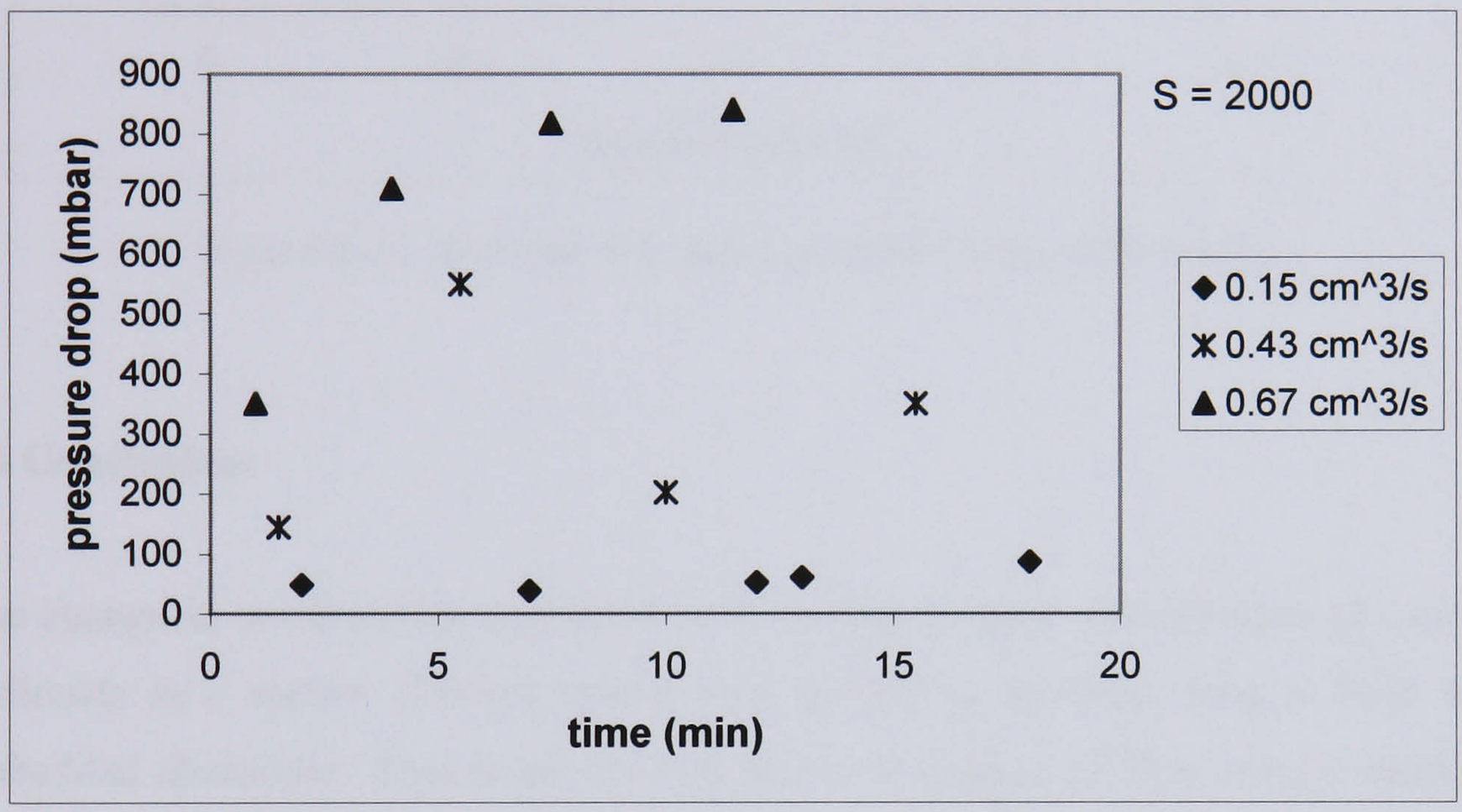

Figure 6.11. Measured pressure drop vs. time for S = 2000.

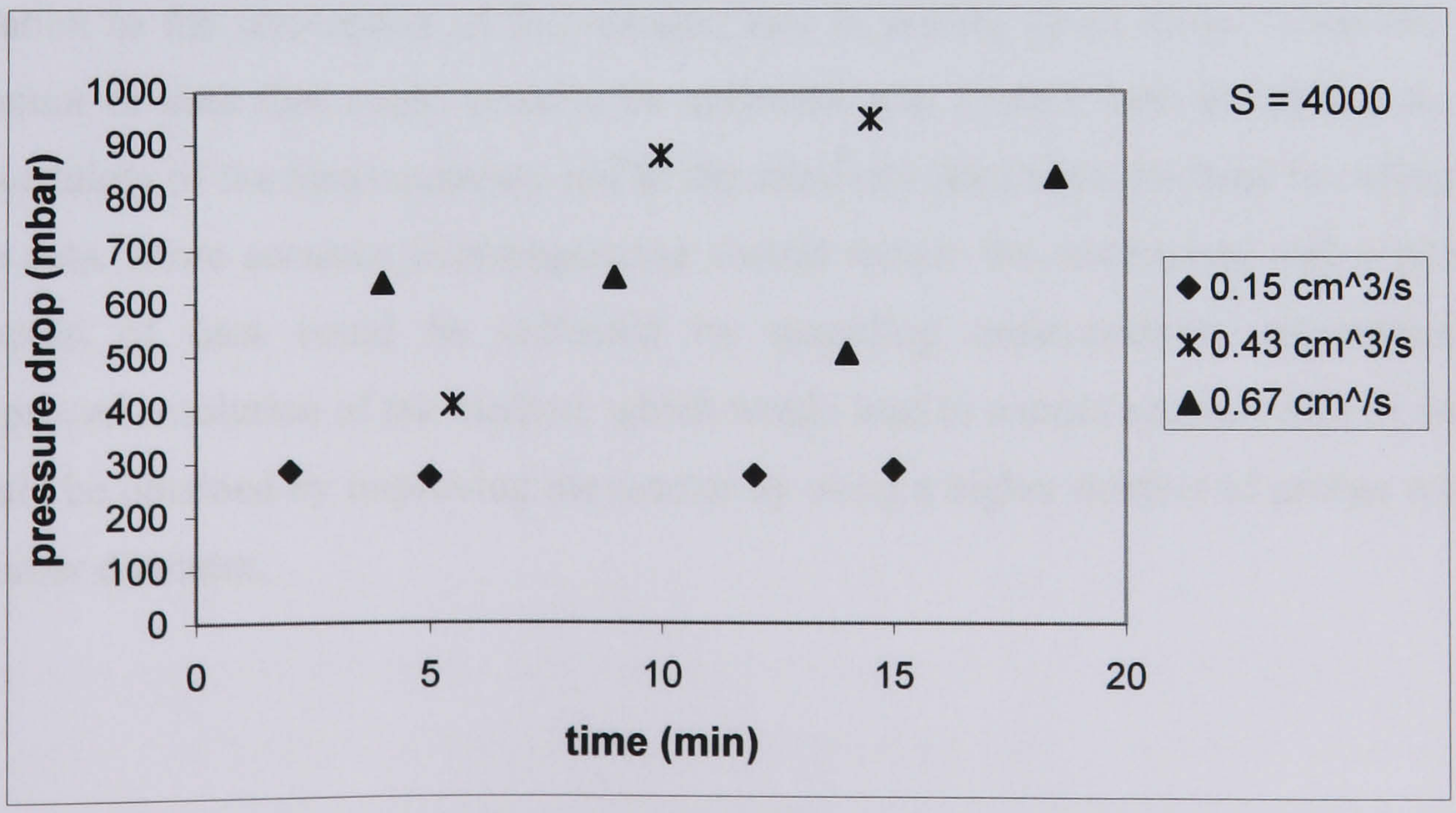

Figure 6.12. Measured pressure drop vs. time for S = 4000.

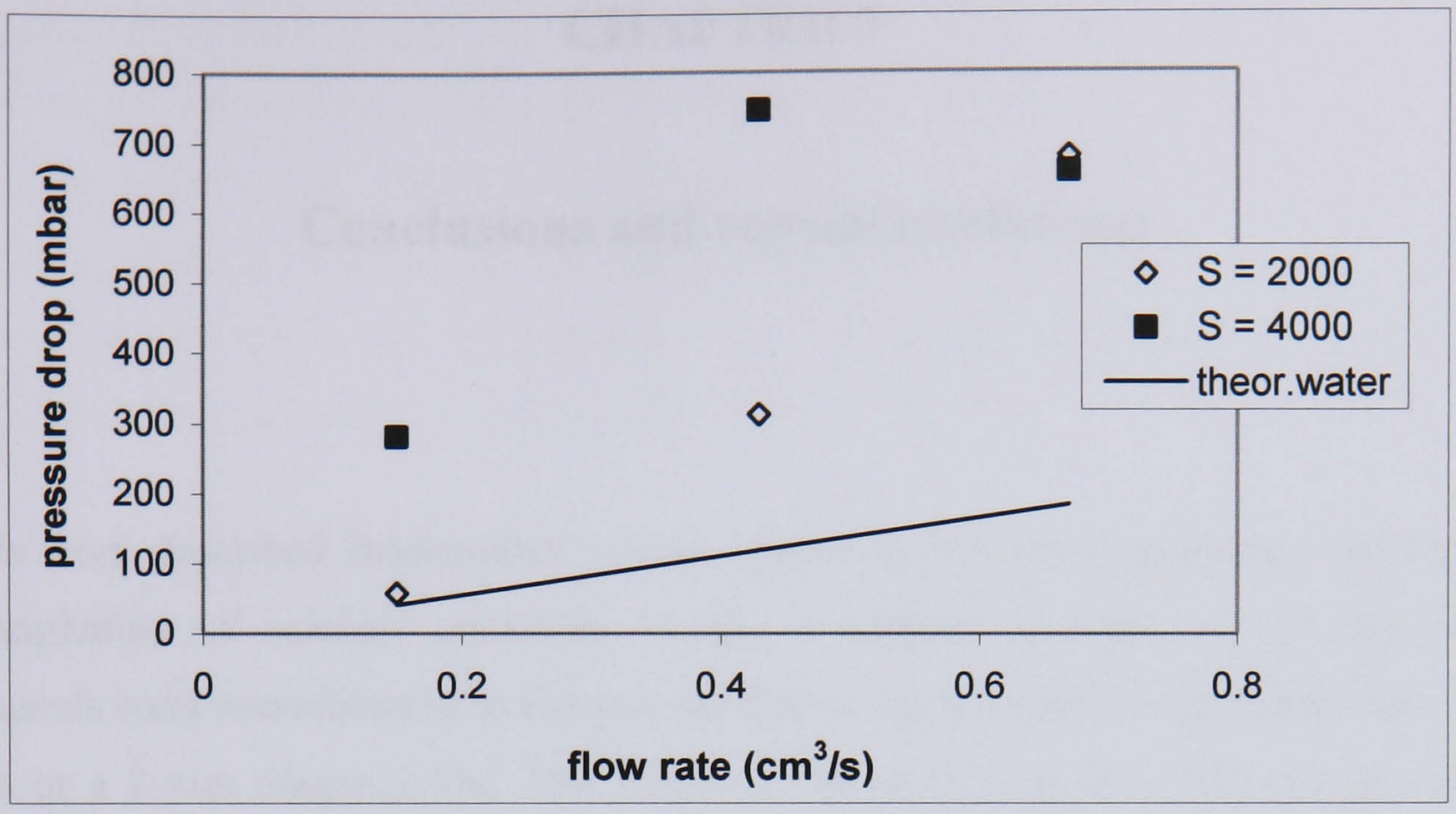

Figure 6.13. Average measured pressure drop vs. flow rate.

6.8 Conclusions

The change in conductivity associated with the liquid phase precipitation of calcium carbonate in a narrow channel reactor was studied by manufacturing a NCR with embedded electrodes. This work showed that in the range of flow rates considered (0.15 – 0.67 cm^3/s) there is a variation in the rate of precipitation and therefore optimal operating conditions in terms of rate of the process can be chosen. Other information obtained relates to what could be an optimized length of the NCR in relation to the conversion of the reaction and to scaling phenomena. However, the amount of data that could actually be collected was limited both in relation to the uncertainty of the measurements and to the relatively long time involved in collecting the data. More accurate instrumentation should reduce the uncertainty and a greater amount of data could be collected by recording measurements automatically. Improved resolution of the method, which would lead to a more accurate kinetic study, could be obtained by improving the reactor by using a higher number of probes with a smaller diameter.

CHAPTER 7

Conclusions and recommendations

This work described fundamental studies related to the liquid phase and gas-liquid precipitation of calcium carbonate in narrow channel reactors. In all cases the channels were manufactured in Perspex and had a square cross section, either with a 1 mm or a 2 mm diagonal line. The length of the reactors in the Perspex block was approximately 20 cm and a stainless steel capillary tube completed the reactor length.

Liquid phase precipitation of calcium carbonate was studied using aqueous solutions of calcium nitrate and sodium carbonate as reagents. Two different concentrations were used, corresponding to supersaturation ratios S = 2000 and S = 4000. The reaction was investigated in a module with both a 1 mm and a 2 mm diagonal line reactor. Results showed that mixing efficiency increased with increasing Reynolds number for both reactors. Calculation of pressure drop in the channels and of the specific power input transferred to the fluid showed that changes in channel size and flow rate determine the variation in the amount of energy transferred to the fluid. For the 2 mm reactor values of the specific power input varied between 0.08 and 3.5 W/kg and for the 1 mm reactor between 5 and 100 W/kg.

Particle size was largely unaffected by varying operating conditions, although the 1 mm reactor seemed to give lower particle size than the 2 mm one in the lowest flow rate region. Mean diameter was found to range between 3.4 and 5.3 μm for S = 4000 and between 3.0 and 8.0 μm for S = 2000 for both reactors and all flow rates.

Particle morphology was investigated on selected samples and it was found to be correspondent, for both reactors, to a mixture of spherical and cubic particles. X-ray diffraction indicated that the samples were composed of a mixture of calcite and vaterite. Further work on particle morphology could be targeted to identify possible differences between the two reactors in terms of the relative amount of polymorphs formed and how to control the transition to calcite, if this is the desired product.

Benchmarking tests carried out with a well stirred batch reactor, showed that the narrow channel reactors can give lower mean particle size than the batch. Taking into account particle size, achievable throughput and energy dissipation, in terms of pressure drop, it was concluded that the optimal choice of configuration and parameters for narrow channel reactors would correspond to using the 2 mm reactor at the highest flow rate investigated, 1 cm^3/s.

Liquid phase precipitation was further investigated by studying the change in conductivity associated with the precipitation reaction in solution. A narrow channel reactor with a 1 mm diagonal line containing embedded electrodes was used. The electrodes were evenly spaced in the length of the channel in the Perspex block, so as to follow change in conductivity during the residence time in the reactor. Results for S = 2000 indicated that precipitation rate appears to be higher for a flow rate of 0.43 cm^3/s. The relatively high amount of error found in the results showed that the conclusions of this study could not be considered exhaustive and further work should be carried out. However, the advantage of using this type of NCR was shown as it allowed monitoring of the reaction with a non-invasive technique. This narrow channel reactor could also be used to investigate other phenomena related to precipitation such as scaling.

Gas-liquid precipitation of calcium carbonate was studied in a 2 mm diagonal line narrow channel reactor. A visual investigation of the flow patterns of the water-carbon dioxide system in the narrow channel reactor showed the occurrence of slug flow for nearly all flow rates. This was found to be in agreement with results of studies on two-phase flow on similar sized channels.

Precipitation of calcium carbonate from a calcium hydroxide solution was characterized. This was quantified in terms of mass transfer performance in the presence of the carbonation reaction for the narrow channel reactor. Volumetric mass transfer coefficients were found to range between 0.33 and 0.80 s^{-1}. Calculation of two phase pressure drop allowed evaluation of the results in terms of energy dissipation. It was shown that the NCR presented mass transfer performance of the same order of high efficiency gas-liquid contactors. Estimation of the specific interfacial area between the phases and of the enhancement factor for the carbonation reaction

allowed the conclusions on mass transfer performance in the presence of chemical reaction for the NCR to be extended to physical mass transfer coefficients.

Limited concentrations of calcium hydroxide suspensions were used to carry out the carbonation reaction. Absorption rate of carbon dioxide was found to increase with increasing solid concentration. Particle size and morphology were characterized for selected samples obtained from the calcium hydroxide solution and suspensions. Particle size was found to range between 3.7 and 5.3 μm. Precipitated calcium carbonate was found to correspond to rhombohedral/cubic calcite particles.

Further work on the gas-liquid system could include more detailed studies on the flow patterns at high gas and liquid velocities and the measurement of the specific interfacial area between the phases. The maximum concentration used in this case of 7 g/dm^3 calcium hydroxide did not give total conversion, so it would be interesting to study the effect of various channel lengths on the conversion to calcium carbonate.

No significant scaling phenomena were detected in the experiments conducted in the narrow channel reactors. The conductivity study also showed that no appreciable build-up of material with higher resistance could be detected over the time scales of the experiments. Further investigations should evaluate the time limits for efficient operation of narrow channel reactors without scaling. In this context a wider series of slurry concentrations should be taken into account.

Another aspect for further work is related to the scaling up of narrow channel reactors. Scaling up by replication or scale out is considered by many authors as the main route for extending the use of small scale systems for industrial production. A detailed feasibility study on the manufacture and the operation of more than one channel running in parallel should be carried out.

The aim of the study was to define basic characterization and understanding of precipitation in narrow channel reactors with the aim of introducing NCRs for the manufacturing of slurries/powders by precipitation. However, it must be considered that calcium carbonate is a product employed in very large amounts and with a low

cost. Where narrow channel reactors would probably find their best application is in the production of limited amounts of slurries/powders with higher added values.

APPENDIX A

Experimental errors and estimation of uncertainty

A.1 Introduction

Experimental work always involves a certain amount of error on the final values that are determined. As suggested by Holman (1992, p.49), it is more appropriate to speak about *uncertainty* rather than *error*, as the amount of error involved in a measurement cannot be known exactly, otherwise it could be eliminated. Every experimental determination carries a certain amount of uncertainty. Uncertainty can be defined as the possible value the error may have. When determining the results, the experimenter must provide an estimate of their uncertainty in order to draw significant conclusions from the data. In the following sections two methods for the estimation of uncertainty are illustrated. The techniques shown as general cases are the ones to which references have been made in the description of the experimental results.

A.2 Uncertainty analysis

This method is based on the specification of the uncertainty in the single primary measurements carried out to calculate the final result. If the result is calculated from n primary experimental measurements then it will be a function of n independent variables $x_1, x_2, \ldots, x_n$:

$$R = R(x_1, x_2, \ldots x_n) \qquad \text{(A1).}$$

If w_R is the uncertainty in the result and $w_1, w_2, \ldots w_n$ are the uncertainties of the single measurements stated by the experimenter with the same probability in each case, the following functional dependence exists (Holman, 2001, p.52):

$$w_R = \left[\left(\frac{\partial R}{\partial x_1} w_1 \right)^2 + \left(\frac{\partial R}{\partial x_2} w_2 \right)^2 + ... + \left(\frac{\partial R}{\partial x_n} w_n \right)^2 \right]^{1/2} \qquad \text{(A2).}$$

Indicating with R_b the best approximation that can be obtained for the result, the degree of accuracy will be given by $R_b \pm w_R$. R_b is usually obtained by calculating the average of the results of repetitions of the same experiment carried out each time in the same (as much as possible) conditions. Uncertainty analysis can be used to estimate the accuracy of the results as well as to improve it. Expression A2 shows that if one of the uncertainties is much larger than all the others, than that will be the predominant in affecting the uncertainty of the overall result. The experimenter can then take action so as to make that specific measurement more accurate.

A.3 Statistical analysis of experimental data

Uncertainty analysis can only be carried out if the uncertainty related to each single measurement is known. In some circumstances, the reading of one measurement involves the use of more than one instrument, so that the origin and the entity of the uncertainty on the reading cannot be predicted. In cases like this, a statistical approach can be used to analyze the results of the measurements and the uncertainty of the results can be estimated from this analysis.

If a number n of measurements of the same variables are taken, the arithmetic mean or average can be calculated from the expression:

$$x_m = \frac{1}{n} \sum_{i=1}^{n} x_i \qquad \text{(A3).}$$

The deviation d_i for each reading is defined by:

$$d_i = x_i - x_m \qquad \text{(A4)}$$

and the standard deviation σ_d by the equation:

$$\sigma_d = \left[\frac{1}{n} \sum_{i=1}^{n} (x_i - x_m)^2 \right]^{1/2} \qquad \text{(A5).}$$

In order to be able to use equation A5 a large number of data, at least 20 readings (Holman, 2001, p.63) should be available. If this is not the case, a reliable estimate of the standard deviation can not be obtained. If a small number of data is available, the following expression should be used:

$$\sigma_d = \left[\frac{\sum_{i=1}^{n} (x_i - x_m)^2}{n-1} \right]^{1/2} \qquad \text{(A6).}$$

All these parameters serve to characterize the set of measurements considered. If for a set of measurements the probability density function approximates a normal distribution, then it can be assumed that the errors occur randomly.

If the average is considered as the best approximation of the result, the standard deviation can be used to estimate the confidence interval of the result itself. Particularly, considering σ_d as the uncertainty will give 65 % confidence, $2\sigma_d$ will give 95.4 % confidence and $3\sigma_d$ will give 99.7 % confidence (Galyer and Shotbolt, 1990, p.8).

APPENDIX B

Particle size characterization by laser diffraction

B.1 Operating principles of laser diffraction instruments

Particle size analysis was carried out with a Malvern Mastersizer 2000 which uses laser diffraction or, more correctly, Low Angle Laser Light Scattering (LALLS) (Rawle). This has in the last few years become one of the most common methods for characterizing particle size and a description of the principles on which it is based and of a series of general guidelines on its application is given in the ISO standard 13320.

LALLS relies on the fact that diffraction angle is inversely proportional to particle size. Instruments using this technique consist of (Rawle):

- A laser as a source of light of fixed wavelength. He-Ne gas lasers are the most common.
- A suitable detector. Usually this is a slice of photosensitive silicon with a number of discrete detectors. It can be shown that there is an optimum number of detectors (16-32), increasing the number above this range does not lead to increased resolution.
- A device that allows the particles to be illuminated by the beam. This can vary depending on the type of sample, for example if the analysis has to be carried out on dry powder or a suspension.

Some instruments rely only on the Fraunhofer approximation which assumes that the particle is much larger than the wavelength of the light employed, that particles of all sizes scatter with equal efficiency and that they are opaque and transmit no light. These assumptions introduce a variable amount of error, especially for very small particles, for which errors can reach up to 30%. The Mie theory provides rigorous solution of the scattering phenomena in the interaction between the light and the particles which allows very accurate results over a wide range of sizes (typically 0.02-

2000 μm). The Mastersizer 2000 uses the Mie theory and instruments like this require the knowledge of the refractive index of the particles to carry out particle size analysis.

B.2 Definitions of average particle size

If we consider a spherical particle, its size will be uniquely identified by its diameter. Similarly, one dimension will be sufficient to characterize a cubic particle. Particles with a more complex geometry will need more than one dimension in order to be fully characterized. If the size of a particle of general geometry has to be characterized with only one parameter, equivalent diameters relative to the spherical geometry can be used (Allen, 1997, p.45). Equivalent diameters can be defined considering a sphere that has the same surface area as the particle or the same volume as the particle considered, for example. The two determinations will in general give different results and the parameter chosen to characterize particle size will depend on the specific application the particle has. This means that many definitions of particle size can be introduced.

Similar concepts apply when considering a sample with a number of particles. In the general case a sample will be composed of particles of different shapes and sizes. The size distribution can be represented in different ways. A number distribution can be used, in this way the fraction of the number of particles lying in a certain size range is plotted versus the correspondent size range. Once again the size can be identified by different parameters.

The most common way of representing a size distribution is however with a volume distribution, as this is the type of characterization laser diffraction gives. In volume distributions the fraction of the volume of the entire sample correspondent to a certain size range is represented versus the size range itself. Size distributions can be characterized by different parameters, these are used to identify particle size for a sample. For a number distribution, if we assume the distribution to be discrete, the average or number mean will have the following expression:

$$D[1,0] = \frac{1}{n}\sum_{i=1}^{n} D_i \qquad \text{(B1)}$$

this is the same type of expression seen in Appendix A for the average value of a series of measurements. The variable D_i is the generic value of particle size and the average is defined as D[1,0] because it contains a first order dependence on top of the equation and a zero order dependence on bottom (Rawle). For a volume distribution the average will be D[3,0], as the volume varies with the third power of the size. In this case the expression to use will be (Allen, 1997, p.53):

$$D[3,0] = \left(\frac{\sum_{i=1}^{n} D_i^3}{n} \right)^{1/3} \qquad \text{(B2).}$$

The calculation of D[1,0] and D[3,0] require the knowledge of the number of particles.

The use of moment means does not require this knowledge and allows the characterization of a sample regardless of the number of particles contained in it. The surface area moment mean (or Sauter mean diameter) is defined by the equation (Allen, 1997, p.53):

$$D[3,2] = \frac{\sum_{i=1}^{n} D_i^3}{\sum_{i=1}^{n} D_i^2} \qquad \text{(B3).}$$

The volume moment mean or D[4,3] is instead defined by the equation:

$$D[4,3] = \frac{\sum_{i=1}^{n} D_i^4}{\sum_{i=1}^{n} D_i^3} \qquad \text{(B4)}$$

and this is the main parameter obtained when particle size is analyzed by laser diffraction.

Particle size distributions, number and volume based, can be characterized by other parameters, for example the median diameter or D_{50} and the mode (Allen, 1997, p.50). The median diameter represents the size value that divides the size distribution in two equal parts, it can also be described as the value corresponding to 50% in the

cumulative distribution curve. The mode is instead the size value correspondent to the maximum of the particle size distribution curve and it represents the most occurring size value in the sample.

B.3 Sample preparation and analysis procedure

Sample preparation and particle size analysis were carried out following the guidelines given in the ISO standard 13320 of which the main principles are reported in the Malvern Mastersizer 2000 instructions for use.

The first work to be carried out in this investigation was the one on the liquid phase precipitation and in this case the slurry was analyzed within 2 minutes of the completion of the reaction in the NCR, as seen in Chapter 4. Preliminary measurements carried out by adding a few drops of the calcium carbonate slurry to the Mastersizer dispersion unit filled with deionised water gave results which were often inconsistent with each other and with limited repeatability. It was then necessary to stop any change occurring between the end of reaction and the analysis itself.

Two techniques were tested separately: small amounts of sodium hexametaphosphate solutions were added to the outlet slurry and the slurry was kept in a mixed status by using a magnetic stirrer before it was added to the dispersion unit of the instrument were stirring would continue. Both techniques led to improved repeatability of the results. A limited number of surfactant solution concentrations was tested and the concentration used in the end, 0.1 % in weight, was the one that gave the best results in terms of preventing aggregation after the reaction for all the reagents concentrations used. For this reason the same concentration was used for the calcium carbonate slurry samples analyzed for the gas-liquid study.

The volume used for the sodium hexametaphosphate solution was determined empirically from a limited number of tests. Particularly, it was found that increasing of 5 times the volume of the surfactant solution led to an increasing relevance of aggregation in the final particle size distribution. A similar effect was obtained by diluting the calcium carbonate suspension in deionised water before adding it to the dispersion unit. These trials led to the definition of the procedure reported in Chapter 4.

As seen in Chapter 4, results for particle size analysis all referred to the use of the finalized procedure except for the data used for benchmarking with a stirred vessel. Reaction in the stirred vessel was carried out by keeping the reagents stirred and to avoid any delay in the measurement, particle size analysis was carried out by adding the calcium carbonate suspension to the dispersion unit directly from the stirred vessel itself. In order to compare consistent type of data, the data for the narrow channel reactors used for benchmarking are obtained from analyses carried out on suspensions that were kept in a mixed status without the use of the surfactant.

For the precipitation from $Ca(OH)_2$ suspensions, the sample preparation procedure involved the use of ultrasound to disperse the aggregates. As seen in Chapter 5, this was due to the fact that the particle size analyzer was not available for use immediately after the reaction and because the slurry concentration was relatively high. The samples were exposed to ultrasound by using a Branson 2000 ultrasonic probe. Various intensities and exposure times were tested before determining the final procedure. As seen in Chapter 5, this was determined by ensuring that the slurry and dry powder samples for a single experiment gave consistent results. The final procedure involved using the ultrasonic probe with 20 % intensity both for the slurry and the dry powder samples. For the powder samples 10 cm^3 of 1% in weight $CaCO_3$ suspensions were prepared to which 1 cm^3 0.1% in weight sodium hexametaphosphate solution was added. The suspension formed was then stirred for around 5 minutes with a magnetic stirrer and then exposed to the ultrasonic probe for 2 minutes. The slurry samples were instead directly exposed to the ultrasonic probe for 1 minute.

For the slurry samples obtained for the precipitation from solution, the concentration was very low and the best dispersion procedure was found to be obtained by stirring the slurry at a high stirring speed in the dispersion unit of the particle size analyzer.

In every case the particle size analysis was carried out by using a standard operating procedure (SOP) that can be set-up using the software provided with the Mastersizer and then used each time a new analysis is carried out. The use of a SOP allows to control the particle size procedure as this contains all the necessary information for the analysis and its use ensures that the same data are used all the time. The SOP contains the refractive indexes of the solvent and of the particles and limits on the concentrations to be used. A refractive index of 1.33 was used for water, whereas the

value 1.6 was used for calcium carbonate. This is approximately the mean value of the range indicated by the ISO standard for the various polymorphs of calcium carbonate (1.49-1.74). The ISO standard recommends operating with values of obscuration of the laser between 5 % and 15 % for particles smaller than 20 μm. This guidance was followed in the setting up the SOP.

APPENDIX C

X-ray diffraction patterns for the precipitated calcium carbonate samples

The X-ray diffraction patterns obtained with a Philips XPert MPD diffractometer for all the samples analyzed for this study are reported (Figures C3 to C9). Figures C3 and C4 refer to the liquid phase investigations, whereas Figures C5 to C9 are relative to the gas-liquid work. The operating conditions they refer to are listed separately in each case. The first two spectra shown are the standards used by the instrument to identify vaterite and calcite respectively (Figures C1 and C2). The intensity shown does not follow the same scale in all the graphs.

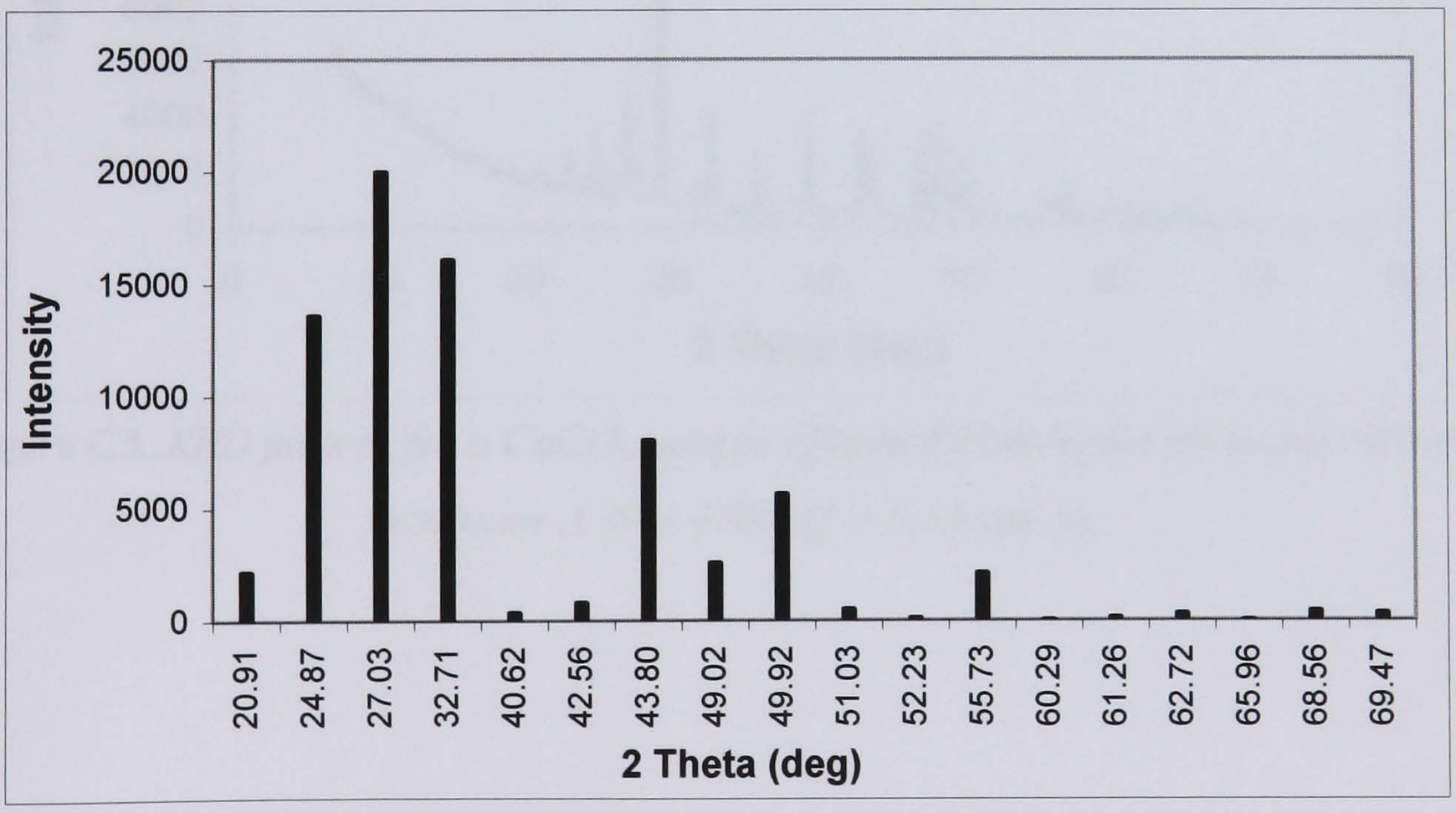

Figure C1. Characteristic peaks for the vaterite standard.

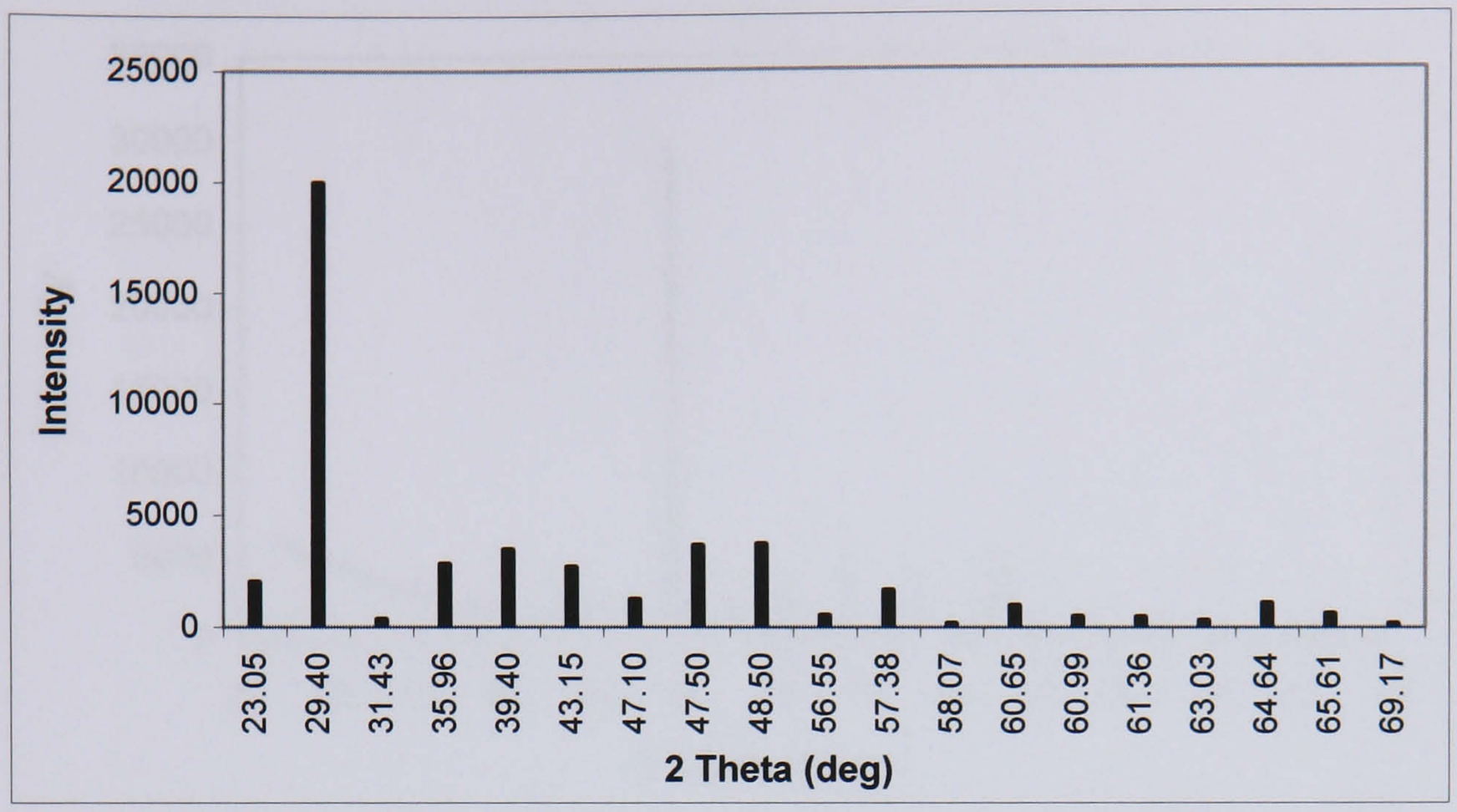

Figure C2. Characteristic peaks for the calcite standard.

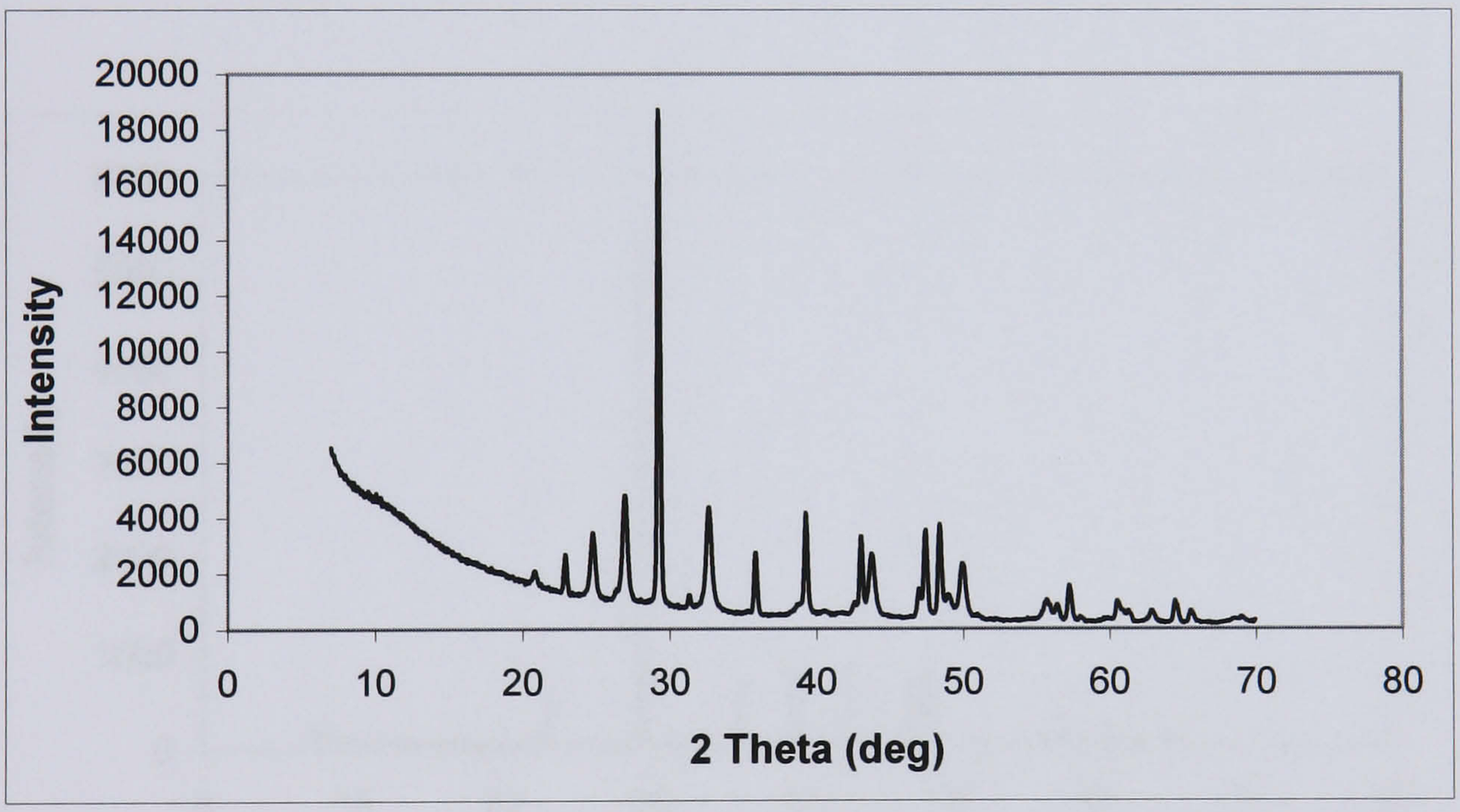

Figure C3. XRD pattern for a $CaCO_3$ sample obtained from liquid phase precipitation in reactor A (S = 4000, Q = 0.43 cm^3/s).

X-ray diffraction patterns

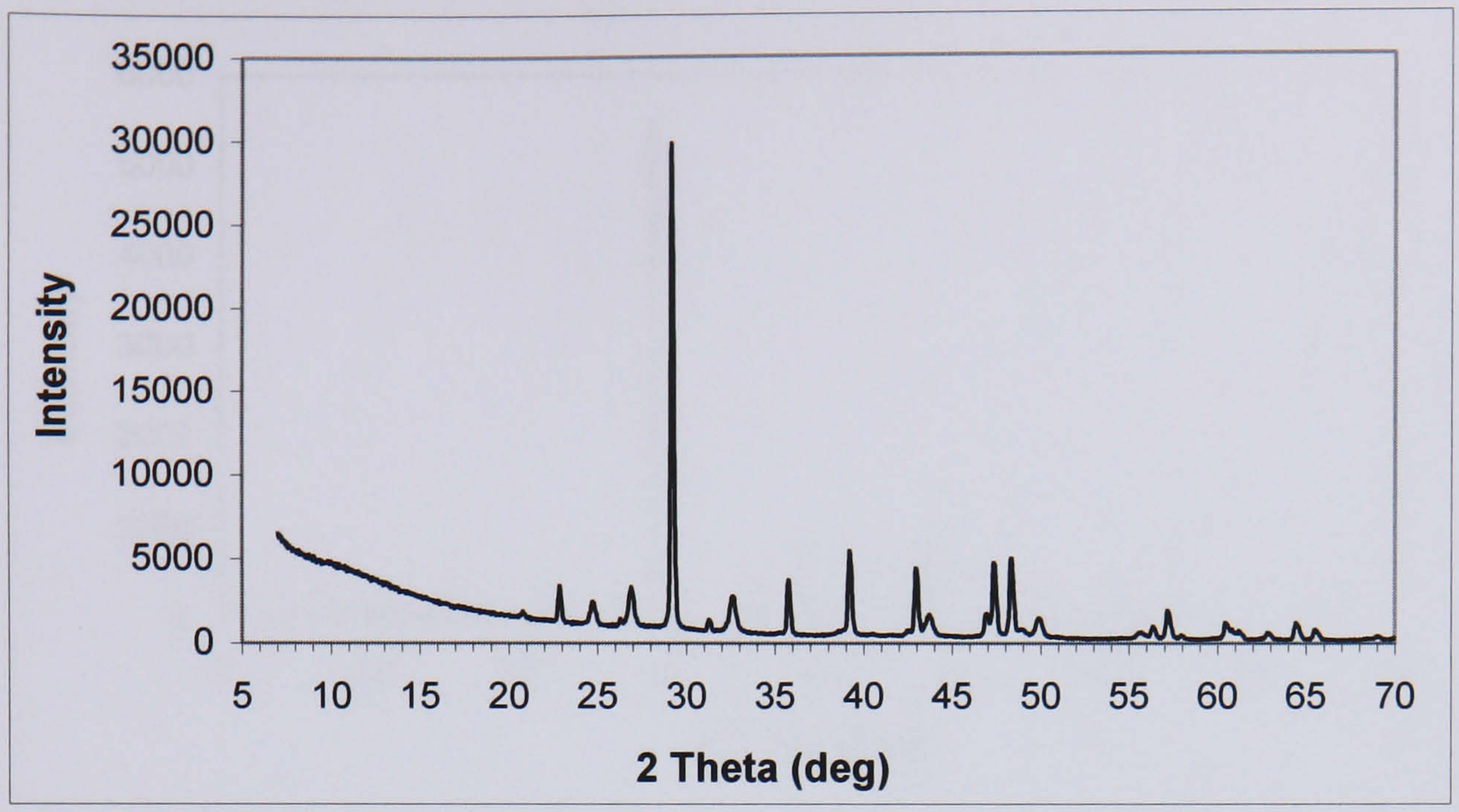

Figure C4. XRD pattern for a $CaCO_3$ sample obtained from liquid phase precipitation in reactor B ($S = 4000$, $Q = 0.43\ cm^3/s$).

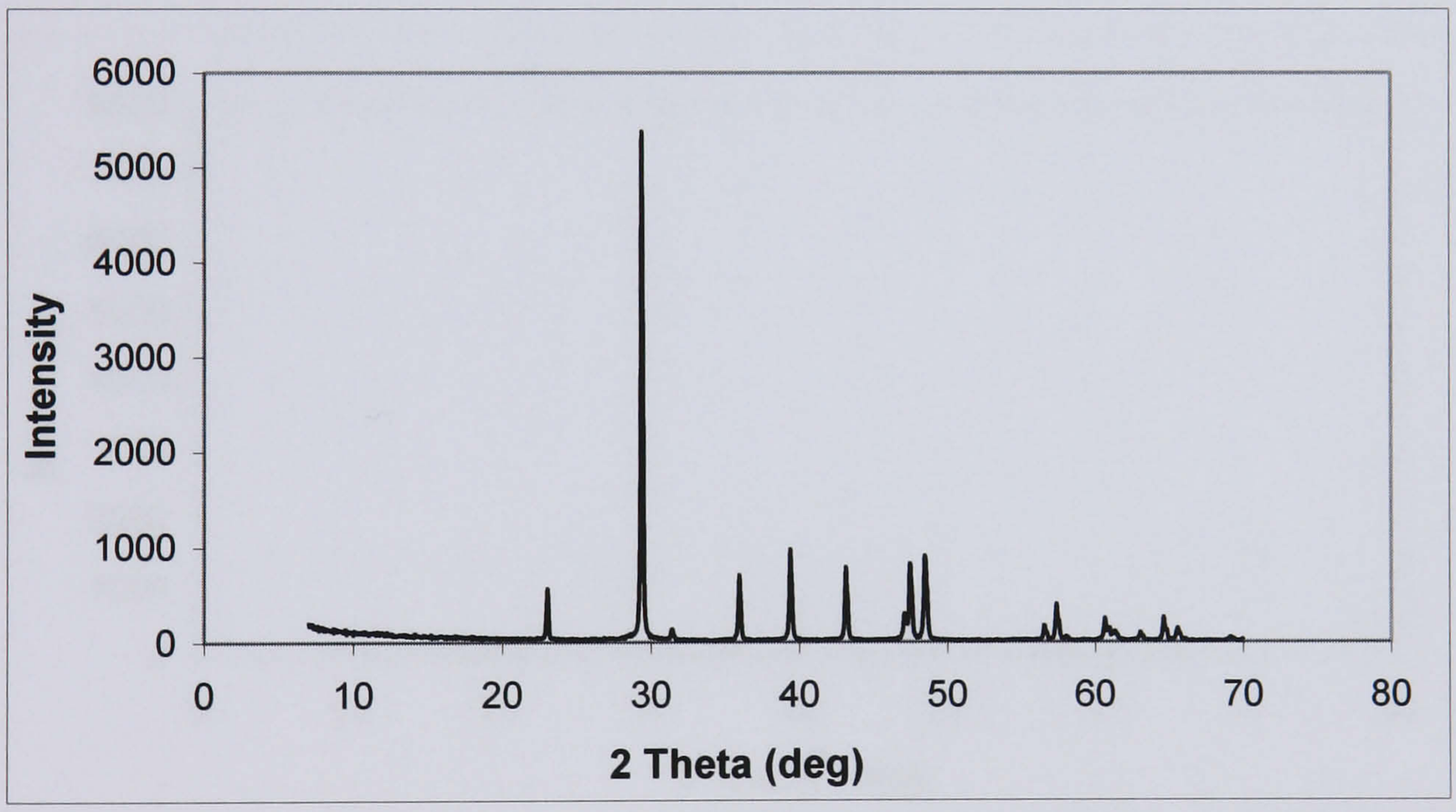

Figure C5. XRD pattern for a $CaCO_3$ sample obtained from gas-liquid precipitation from solution ($Q_G = 8.22\ cm^3/s$, $Q_L = 0.84\ cm^3/s$).

X-ray diffraction patterns

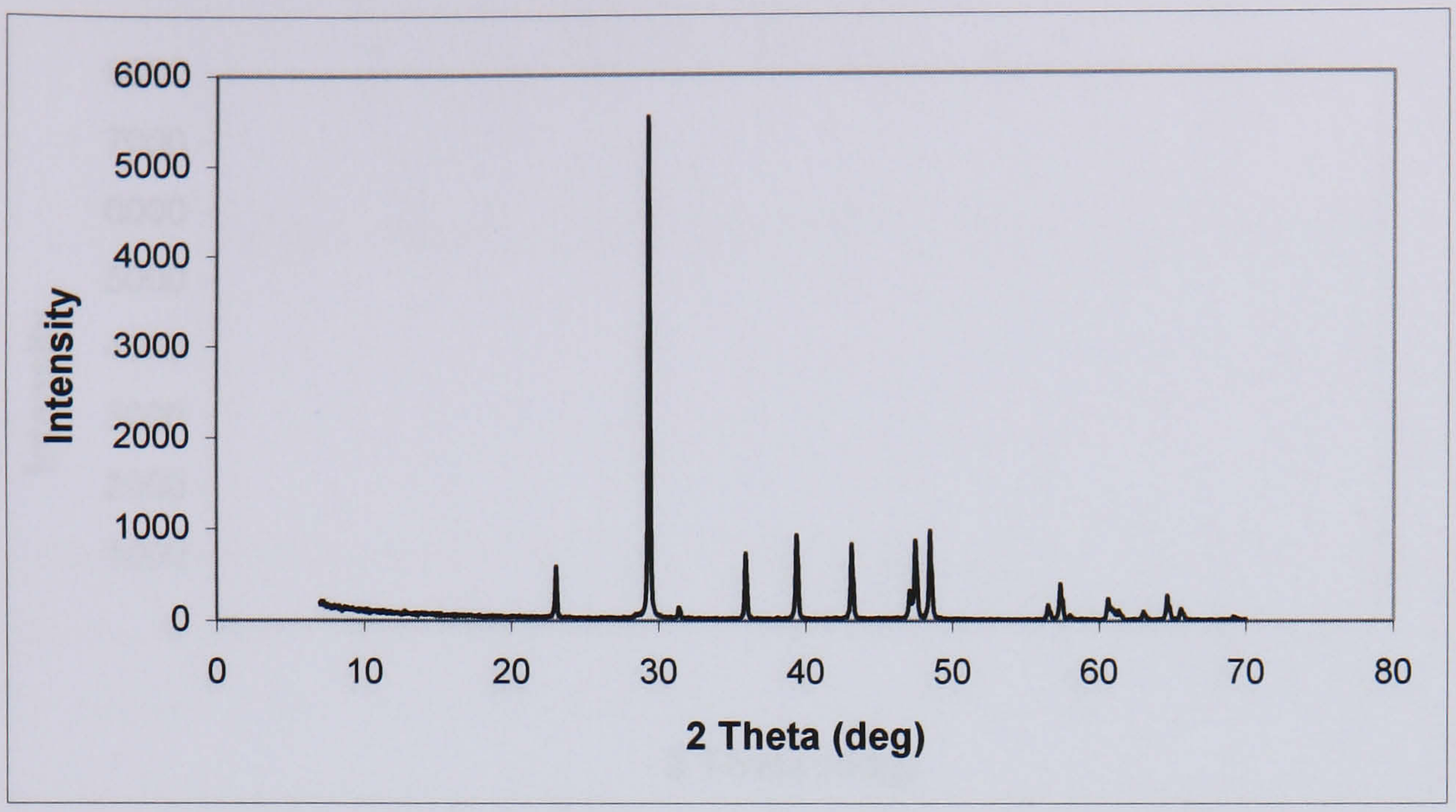

Figure C6. XRD pattern for a $CaCO_3$ sample obtained from gas-liquid precipitation from solution (Q_G = 8.22 cm^3/s, Q_L = 1.12 cm^3/s).

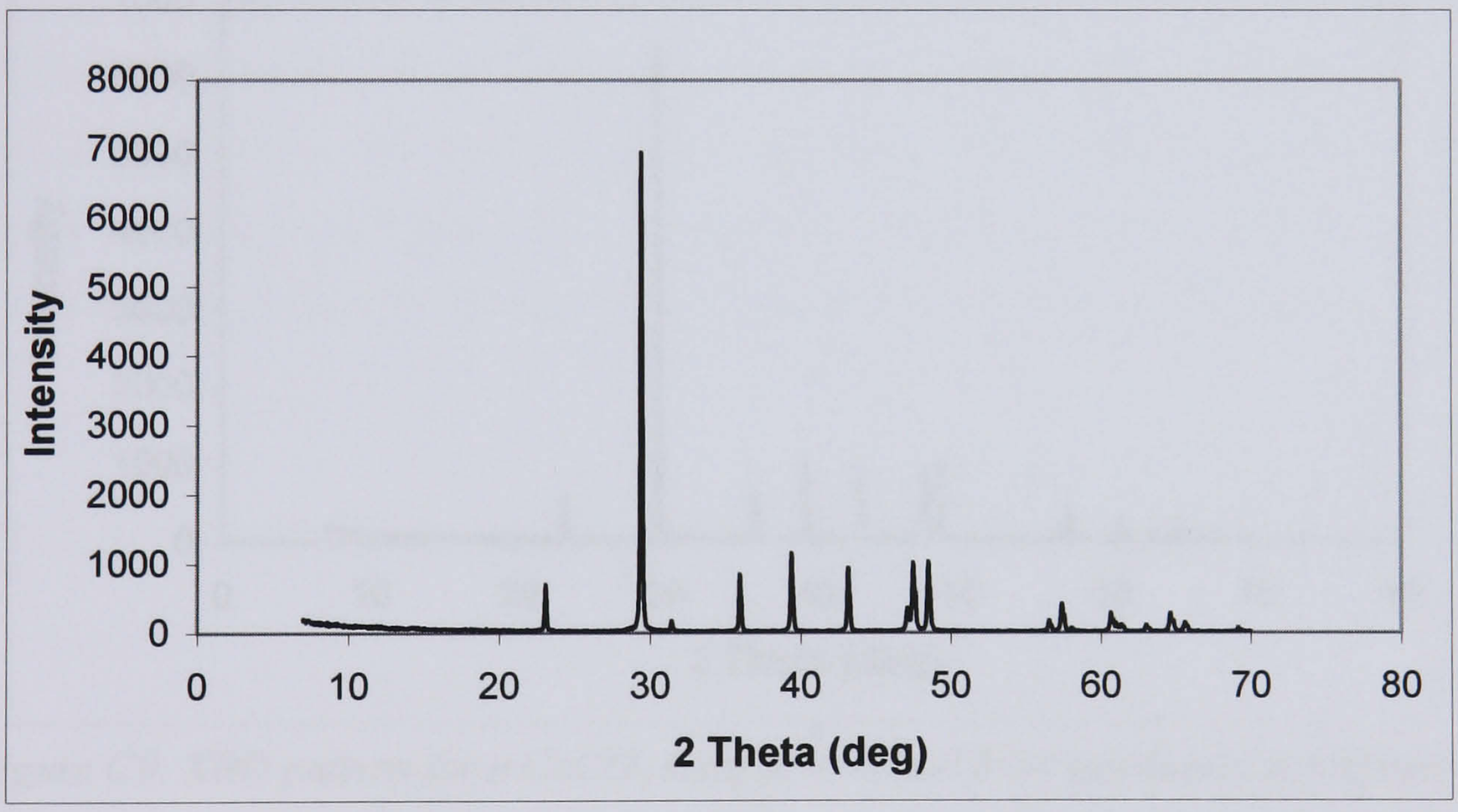

Figure C7. XRD pattern for a $CaCO_3$ sample obtained from gas-liquid precipitation from a 5 g/dm^3 $Ca(OH)_2$ suspension (Q_G = 8.22 cm^3/s, Q_L = 1.01 cm^3/s).

X-ray diffraction patterns

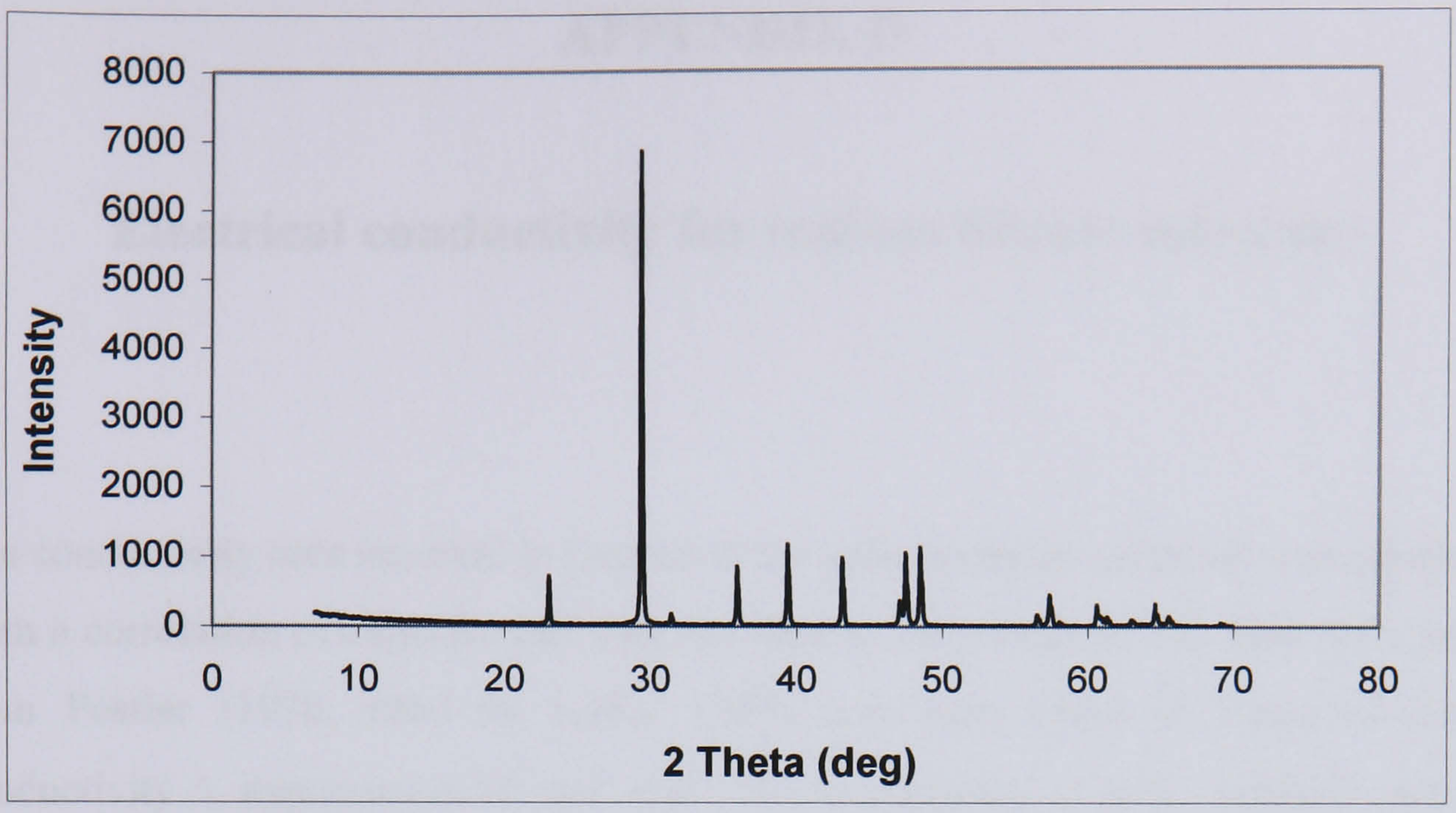

Figure C8. XRD pattern for a $CaCO_3$ sample obtained from gas-liquid precipitation from a 5 g/dm^3 $Ca(OH)_2$ suspension (Q_G = 8.22 cm^3/s, Q_L = 1.18 cm^3/s).

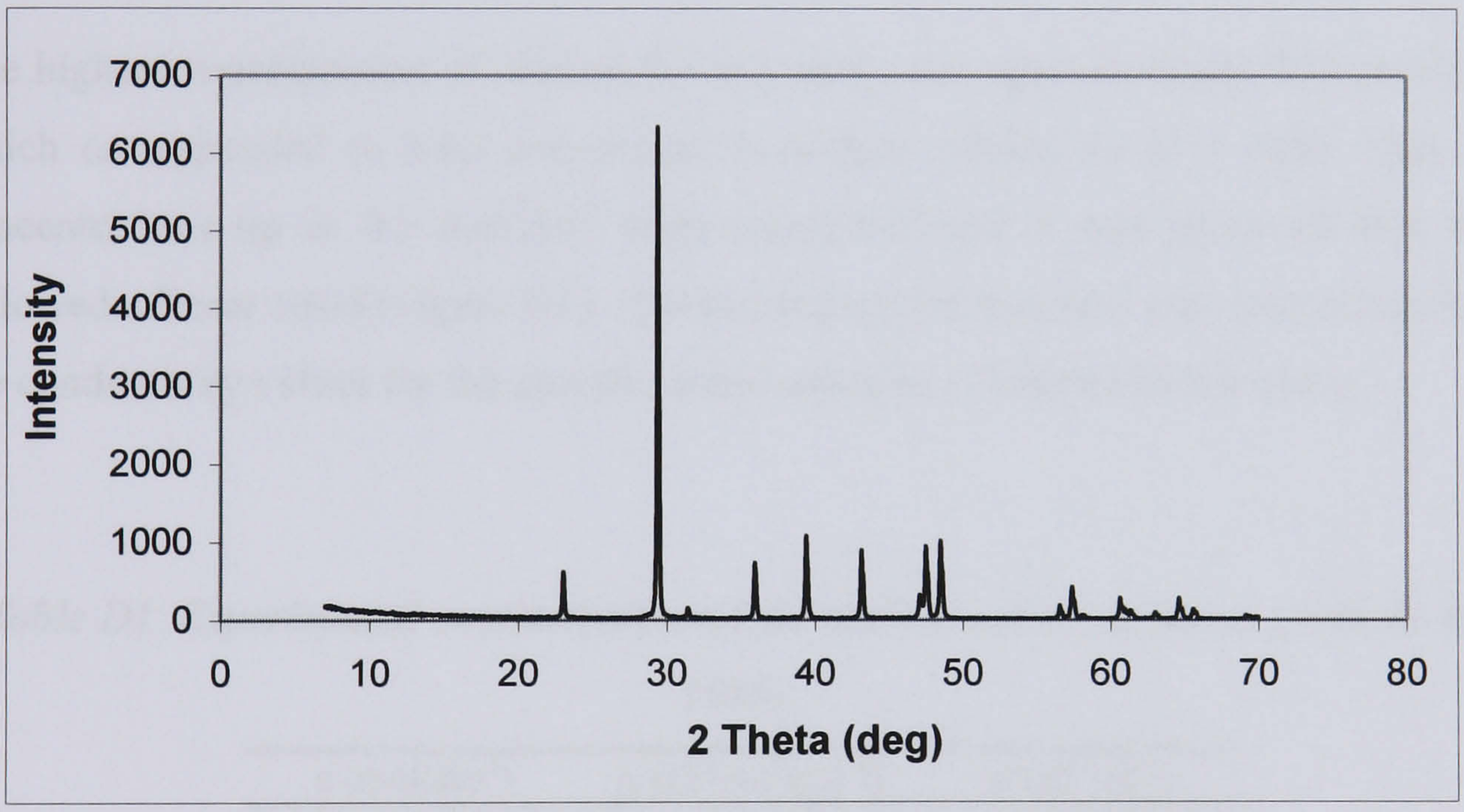

Figure C9. XRD pattern for a $CaCO_3$ sample obtained from gas-liquid precipitation from a 7 g/dm^3 $Ca(OH)_2$ suspension (Q_G = 8.22 cm^3/s, Q_L = 0.92 cm^3/s).

APPENDIX D

Electrical conductivity for sodium nitrate solutions

The conductivity data reported in Chapter 6 for sodium nitrate solutions were obtained from a correlation of experimental data reported in the literature. The data were taken from Postler (1970, cited by Lobo, 1989) and were listed in terms of molar conductivity Λ, expressed in Ω^{-1} cm^2 mol^{-1}, at a temperature of 25°C. Table D1 reports the data from Postler together with the data in terms of conductivity, obtained multiplying the molar conductivity by the concentration.

The highest concentration of interest for this study was approximately 0.25 mol/dm^3, which corresponded to total conversion to sodium nitrate for S = 4000. Data for concentrations up to 0.5 mol/dm^3 were considered and it was observed that they followed a linear trend (Figure D1). A linear regression function was used to calculate the conductivity values for the specific concentrations of interest in this study.

Table D1. Experimental conductivity data for sodium nitrate solutions (from Lobo, 1989).

c (mol/dm^3)	Λ (Ω^{-1}cm^{2}mol^{-1})	κ (Ω^{-1} m^{-1})
0.01	114.05	0.11405
0.05	105	0.525
0.1	98.9	0.989
0.5	84.14	4.207
1.0	75.16	7.516
2.0	62.95	12.59
3.0	53.99	16.197
4.0	46.4	18.56
5.0	39.81	19.905
6.0	33.96	20.376

Conductivity for sodium carbonate solutions

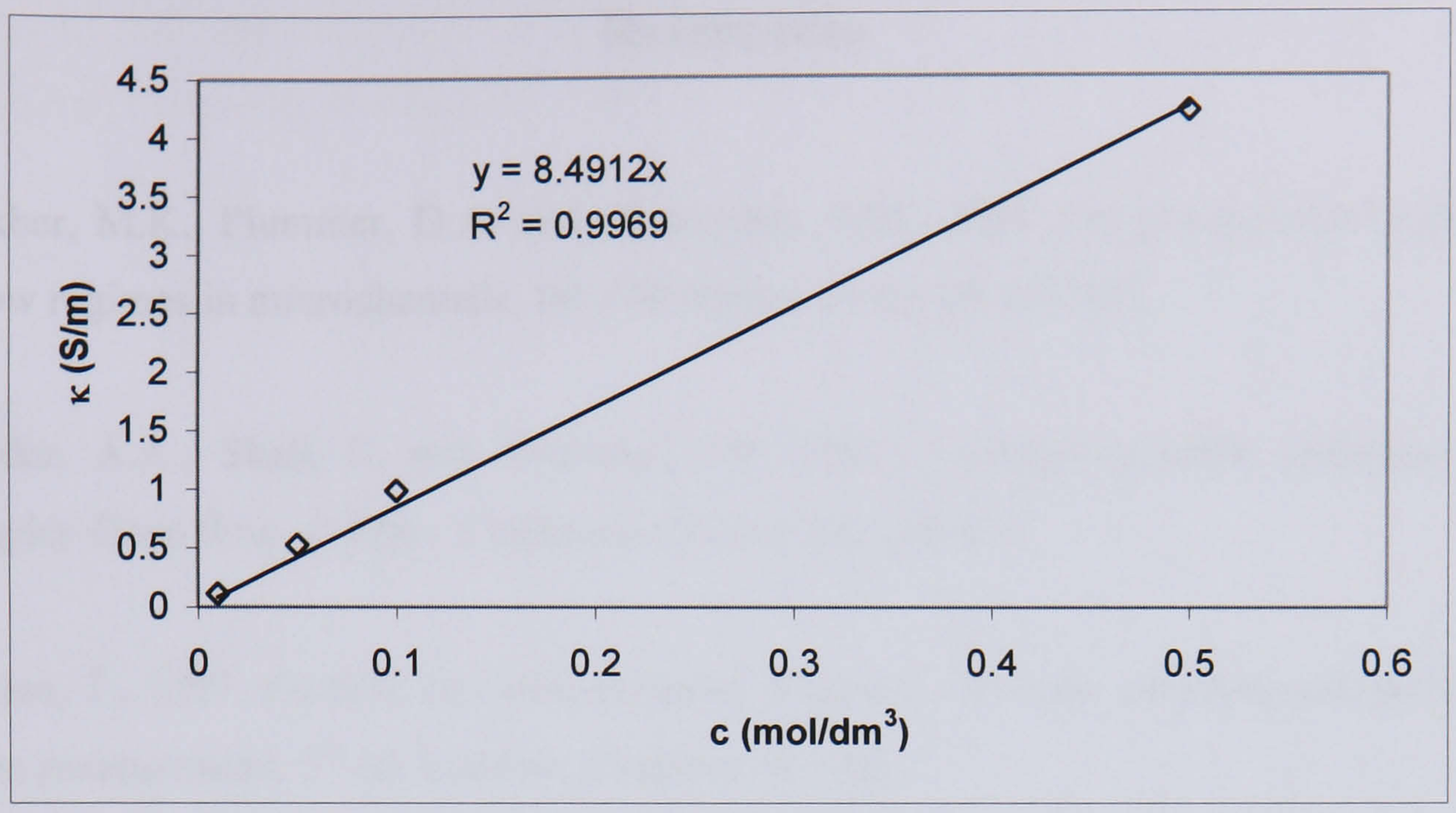

Figure D1. Experimental conductivity vs. concentration and linear regression function.

References

Akbar, M.K., Plummer, D.A. and Ghiaasiaan, S.M., 2003. On gas-liquid two-phase flow regimes in microchannels. *Int J Multiphas Flow*, 29, 855-865.

Aider, A.A., Skali, S. and Brancher, J.P., 2005. Laminar-turbulent transition in Taylor-Dean flow. *J. Phys: Conference Series,* 14, 118-127.

Allen, T., 1997. *Particle size measurement, Volume 1, Powder sampling and particle size measurement.* 5th ed. London: Chapman & Hall.

Baker, O., 1954. Simultaneous flow of oil and gas. *Oil Gas J*, 53, 185-195.

Barnea, D., Luninski, Y. and Taitel, Y., 1983. Flow pattern in horizontal and vertical two phase flow in small diameter pipes. *Can J Chem Eng*, 61, 617-620.

Barresi, A.A., Marchisio, D., Baldi, G., 1999. On the role of micro- and mesomixing in a continuous Couette-type precipitator. *Chem Eng Sci*, 54, 2339-2349.

Beenackers, A.A.C.M., Van Swaaij, W.P.M., 1993. Mass transfer in gas-liquid slurry reactors. *Chem Eng Sci*, 48, 3109-3139.

Bénet, N., Muhr, H., Plasari, E., Rousseaux, J.M., 2002. New technologies for the precipitation of solid particles with controlled properties. *Powder Technol*, 128, 93-98.

Berčič, G., Pintar, A., 1997. The role of gas bubbles and liquid slug lengths on mass transport in the Taylor flow through capillaries. *Chem Eng Sci,* 52, 3709-3719.

Boodhoo, K.V.K. and Jachuck, R.J., 2000. Process Intensification: spinning disk reactor for styrene polymerisation. *Appl Therm Eng*, 20, 1127-1146.

Bosshard, A.W. and Schlumpf, H.P., 1987. In Gächter, R. and Müller, H., eds. *Plastics Additives Handbook*. 2nd ed. Munich, Vienna, New York: Hanser.

Bourne, J.R. and Rohani, S., 1983. Micro-mixing and the selective iodination of l-tyrosine. *Chem Eng Res Des*, 61, 297-302.

Bourne, J.R., Kut, O.M., Lenzner, J. and Maire, H., 1990. Kinetics of the diazo coupling between 1-naphtol and diazotized sulfanilic acid. *Ind Eng Chem Res*, 29, 1761-1765.

Bourne, J.R., Kut, O.M., Lenzner, J., 1992. An improved reaction system to investigate micromixing in high intensity mixers. *Ind Eng Chem Res*, 31, 949-958.

Burns, J.R. and Ramshaw, C., 1996. Process Intensification: Visual study of liquid maldistribution in rotating packed beds. *Chem Eng Sci,* 51, 1347-1352.

Burns, J.R. and Ramshaw, C., 1999. Development of a microreactor for chemical production. *Trans IChemE Part A, Chem Eng Res Des,* 77, 206-211.

Burns, J.R. and Ramshaw, C., 2002. A microreactor for the nitration of benzene and toluene. *Chem Eng Comm,* 189, 1611-1628.

Burns, J.R. and Jachuck, R.J.J., 2005. Monitoring of gas-liquid mass transfer during $CaCO_3$ production on a spinning disc reactor using local conductivity measurements. *AIChE J.,* 51, 1497-1507.

Buscaglia, M.T., Buscaglia, V., Viviani, M., Testino, A., Nanni, P., Bowen, P., Donnet, M., Jongen, N., Schenk, R., Hessel, V., and Schoenfeld. F., 2002. Continuous precipitation of ultrafine (30-500 nm) $BaTiO_3$ particles in a segmented flow tubular reactor (SFTR). In Chianese, A. ed. *15th International Symposium on Industrial Crystallization*, 15-18 September 2002, Sorrento, Italy.

Carr, F.P. and Frederick, D.K., 2003. Calcium carbonate. In Kirk-Othmer Encyclopedia of Chemical Technology. New York: Wiley. Available from: http://www3.interscience.wiley.com/cgi-bin/home

Chen, J., 1986. Measuring the film thickness surrounding a bubble inside a capillary. *J Coloid Interf Sci,* 109, 341-349.

Chen, J., Wang, Y., Jia, Z. and Zheng, C., 1997. Synthesis of nano-particles of $CaCO_3$ in a novel reactor. In Semel, J. ed. *2nd International Conference on Process Intensification in Practice*, 21-23 October 1997, Antwerp, Belgium.

Chen, J., Zhou, M., Shao, L., Wang, Y., Yun, J., Chew, N.Y.K., and Chan, H.K., 2004. Feasibility of preparing nanodrugs by high-gravity reactive precipitation. *Int J Pharm*, 269, 267-274.

Cheng, T.W. and Lin, T.L., 2001. Characteristics of gas-liquid two-phase flow in small diameter inclined tubes. *Chem Eng Sci,* 56, 6393-6398.

Chiang, P.P. and Donohue, M.D., 1988. A kinetic approach to crystallization from ionic solution, I. Crystal growth. *J Colloid Interf Sci,* 122, 230-249.

Cortazar, E., Usobiaga, A., Fernández, L.A., de Diego, A., Madariaga, J.M., 2002. Automation of a procedure to find the polynomial which best fits (κ, c_1, c_2, T) data of electrolyte solutions by non-linear regression analysis using MATHEMATICA® software. *Comput Chem*, 26, 253-264.

Cramers, P.H.M.R., Smit, L., Leuteritz, G.M., van Dierendonck, L.L. and Beenackers, A.A.C.M., 1993. Hydrodynamics and local mass transfer characteristics of gas-liquid ejectors. *Chem Eng J,* 53, 67-73.

Cussler, E.L. *Diffusion, mass transfer in fluid systems.* 2nd ed. New York: Cambridge University Press.

Dagaonkar, M.V., Beenackers, A..A..C.M., Pangarkar, V.G., 2001. Gas absorption into aqueous reactive slurries of calcium and magnesium hydroxide in a multiphase reactor. *Catal Today*, 66, 495-501.

Darby, R., 2001. *Chemical Engineering Fluid Mechanics.* 2nd ed. New York: Marcel Dekker.

deMello, J. and deMello, A., 2004. Microscale reactors: nanoscale products, *Lab Chip*, 4, 11-15.

Donnet, M, Jongen, N., Lemaître, J., Bowen, P., 2000. New morphology of calcium oxalate triyydrate precipitated in a segmented flow tubular reactor. *J Mater Sci Lett,* 19, 749-750.

Donnet, M., Bowen, P., Jongen, N., Lemaître, J., Hofmann, H., Schreiner, A., Jones, A.G., Schenk, R., Hofmann, C., De Carlo, S., 2002. Successful scale-up from millilitre batch optimisation to a small scale continuous production using the segmented flow tubular reactor. Example of calcium carbonate precipitation. In Chianese, A. ed. *15th International Symposium on Industrial Crystallization*, 15-18 September 2002, Sorrento, Italy.

Ehrfeld, W., Golbig, K., Hessel, V., Löwe, H. and Richter, T., 1999. Characterization of mixing in micromixers by a test reaction: single mixing units and mixer arrays. *Ind Eng Chem Res,* 38, 1075-1082.

Ellenberger, J. and Krishna, R., 2003. Shaken, not stirred, bubble column reactors: Enhancement of mass transfer by vibration excitement. *Chem Eng Sci*, 58, 705-710.

Elperin, T., Fominykh, A., 1995. Liquid phase controlled mass transfer in gas-liquid slug flow at low Reynolds numbers. *Int Comm Heat Mass Transfer, 22, 741-750.*

Estrin, J., 1993. Precipitation processes. In Myerson, A.S. ed. *Handbook of industrial crystallization*. Boston: Butterworth-Heinemann.

Fang, J.Z. and Lee, D.J., 2001. Micromixing efficiency in static mixer. *Chem Eng Sci*, 56, 3797-3802.

Ferstl, W., Loebbecke, S., Antes, J., Krause, H., Haeberl, M., Schmalz, D., Muntermann, H., Grund, M., Steckenborn, A., Lohf, A., Hassel, J., Bayer, T., Kinzl, M., Leipprand, I., 2004. Development of an automated microreaction system with integrated sensorics for process screening and production. *Chem Eng J*, 101, 431-438.

Fournier, M.C., Falk, L. and Villermeaux, J., 1996a. A new parallel competing reaction system assessing micromixing efficiency – experimental approach. *Chem Eng Sci,* 51, 5053-5064.

Fournier, M.C., Falk, L. and Villermeaux, J., 1996b. A new parallel competing reaction system assessing micromixing efficiency – determination of micromixing time by a simple mixing model. *Chem Eng Sci,* 51, 5187-5192.

Galyer, J.F.W. and Shotbolt, C.R., 1990. *Metrology for Engineers.* 5th ed. London: Cassel Publishers.

Gaddis, E.S. and Vogelpohl, A., 1992. The impinging stream reactor: a high performance loop reactor for mass transfer controlled chemical reactions. *Chem Eng Sci,* 47, 2877-2882.

Gaddis, E.S., 1999. Mass transfer in gas-liquid contactors. *Chem Eng Process*, 38, 503-510.

García Carmona, J., Gómez Morales, J., and Rodríguez Clemente, R., 2003a. Rhombohedral–scalenohedral calcite transition produced by adjusting the solution electrical conductivity in the system $Ca(OH)_2$–CO_2–H_2O. *J Colloid Interf Sci*, 261, 434-440.

García Carmona, J., Gómez Morales, J., Fraile-Sainz, J. and Rodríguez Clemente, R., 2003b. Morphological characteristics and aggregation of calcite crystals obtained by bubbling CO_2 through a $Ca(OH)_2$ suspension in the presence of additives. *Powder Technol,* 130, 307-315.

Gavriilidis, A., Angeli, P., Yeong, K.K., and Wan, Y.S.S., 2002. Technology and applications of microengineered reactors. *Trans IChemE Part A, Chem Eng Res Des*, 80, 3-30.

Ghiaasiaan, S. M., and Abdel-Khalik, S.I., 2001. Two-phase flow in microchannels. *Adv Heat Transfer*, 134, 145-255.

Guichardon, P. and Falk, L. 2000a. Characterisation of micromixing efficiency by the iodide-iodate reaction system. Part I: experimental procedure. *Chem Eng Sci,* 55, 4233-4243.

Guichardon, P., Falk, L., Villermaux, J., 2000. Characterisation of micromixing efficiency by the iodide-iodate reaction system. Part II: kinetic study. *Chem Eng Sci,* 55, 4245-4253.

Guillemet-Fritsch, S., Aoun-Habbache, M., Sarrias, J., Rousset, A., Jongen, N., Donnet, M., Bowen, P., Lemaître, J., 2004. High-quality nickel manganese oxalate powders synthesized in a new segmented flow tubular reactor. *Solid State Ionics,* 171, 135–140.

Günther, A., Khan, S.A., Thalmann, M., Trachsel, F., Jensen, K.F., 2004. Transport and reaction in microscale segmented gas-liquid flow. *Lab Chip*, 4, 278-286.

Hamid, S.N.S. and Jones, A.G., 2002. Scale-up of gas-liquid precipitation of calcium carbonate crystals in draft tube bubble columns. In Chianese, A. ed. *15th International Symposium on Industrial Crystallization*, 15-18 September 2002, Sorrento, Italy.

Hargis, H., 1988. *Analytical chemistry.* Prentice-Hall International.

Harvey, A.P., Mackley, M.R. and Stonestreet, P., 2001. Operation and Optimization of an Oscillatory Flow Continuous Reactor. *Ind Eng Chem Res,* 40, 5371-5377.

Harvey, A.P., Mackley, M.R. and Seliger, T., 2003. Process intensification of biodiesel production using a continuous oscillatory flow reactor. *J Chem Technol Biotechnol,* 78, 338–341.

Hemrajani, R.R., 1995. Mixing and blending. In Kirk-Othmer Encyclopedia of Chemical Technology. New York: Wiley. Available from: http://www3.interscience.wiley.com/cgi-bin/home

Hessel, V., Ehrfeld, W., Herweck, Th., Haverkamp, V., Löwe, H., Schiewe, J., Wille, Ch., Kern, Th., Lutz, N., 2000. *Gas/Liquid Microreactors: Hydrodynamics and Mass*

Transfer, IMRET 4: Proceedings of the 4th International Conference on Microreaction Technology, 174-186.

Hessel, V., Hardt, S., Löwe, H., Schönfeld, F., 2003. Laminar mixing in different interdigital micromixers: I. Experimental characterization, *AIChE J*, 49, 566-577.

Hessel, V., Löwe, H., Schönfeld, F., 2005. Micromixers-a review on passive and active mixing principles, *Chem Eng Sci,* 60, 2479-2501.

Hessel, V. and Löwe, H., 2003a. Microchemical engineering: components, plant concepts, user acceptance – Part I. *Chem Eng Technol, 26,* 13-24.

Hessel, V. and Löwe, H., 2003b. Microchemical engineering: components, plant concepts, user acceptance – Part II. *Chem Eng Technol, 26,* 391-408.

Hessel, V. and Löwe, H., 2003c. Microchemical engineering: components, plant concepts, user acceptance – Part III. *Chem Eng Technol, 26*, 531-544.

Hibbert, D.B. and James, A.M., 1984. *Dictionary of electrochemistry.* 2nd ed. London: Macmillan.

Hine, F., 1985. *Electrode processes and electrochemical engineering.* New York: Plenum Press.

Holman, J.P., 2001. *Experimental methods for engineers.* 7th ed. Singapore: McGraw-Hill.

Hoon Kang, S., Goo Lee, S., Mo Jung, W., Chan Kim, M., Kim, W., Kyun Choi, C. Feigelson, R.S., 2003. Effect of Taylor vortices on calcium carbonate crystallization by gas–liquid reaction. *J Cryst Growth*, 254, 196-205.

Hostomský, J. and Jones, A.G., 1991. Calcium carbonate crystallization, agglomeration and form during continuous precipitation from solution. *J Phys D Appl Phys*, 24, 165-170.

Hostomský, J. and Jones, A.G., 1995. A penetration model of the gas-liquid reactive precipitation of calcium carbonate crystals. *Trans IChemE Part A, Chem Eng Res Des*, 73, 241-245.

Iransdoust, S., Andersson, B., 1989. Simulation of flow and mass transfer in Taylor flow through a capillary. *Comput Chem Eng,* 13, 519-526.

Jachuck, R.J., Lee, J., Kolokotsa, D., Ramshaw, C., Valachis, P. and Yanniotis, S., 1997. Process Intensification for energy saving. *Appl Therm Eng*, 17, 861-867.

Jachuck, 2002. Process Intensification for responsive processing. *Trans IChemE Part A, Chem Eng Res Des*, 80, 233-238.

Jones, A.G., Hostomsky, J and Li, Z., 1992. On the effect of liquid mixing rate on primary crystal size during the gas-liquid precipitation of calcium carbonate. *Chem Eng Sci*, 47, 3817-3824.

Judat, B., Racina, A. and Kind, M., 2004. Macro- and micromixing in a Taylor-Couette reactor with axial flow and their influence on the precipitation of barium sulphate. *Chem Eng Technol*, 27, 287-292.

Kabasci, S., Althaus, W. and Weinspach, P.M., 1996. Batch-precipitation of calcium carbonate from highly supersaturated solutions. *Trans IChemE Part A, Chem Eng Res Des*, 74, 765–772.

Kakuta, M., Bessoth, F.G. and Manz, A., 2001. Microfabricated devices for fluid mixing and their application for chemical synthesis. *Chem Rec,* 1, 395-405.

Kawaji, M., DeJesus, J.M., Tudose, G., 1997. Investigation of flow structures in vertical slug flow. *Nucl Eng Des,* 175, 37-48.

Kawano, J., Shimobayashi, N., Kitamura, M., Shinoda, K. and Aikawa, N., 2002. Formation process of calcium carbonate from highly supersaturated solution. *J Cryst Growth*, 237-239, 419-423.

Keoschkerjan, R., Richter, M., Boskovic, D., Schnüner, F., Löbbecke, S., 2004. Novel multifunctional microreaction unit for chemical engineering, *Chem Eng J*, 101, 469-475.

Kinnen, A., Dillenburg, H., Schinninger, K., Nover, C., 2002. Solvay Soda Deutschland GmbH. Process for preparing precipitated calcium carbonates. *US Patent 6500400.*

Kitamura, M., 2001. Crystallization and transformation mechanism of calcium carbonate polymorphs and the effect of magnesium ion. *J Colloid Interf Sci*, 236, 318-327.

Klein and David, 1995. Reaction crystallization. In Mersmann A. ed. *Crystallization technology handbook.* New York: M.Dekker.

Kleingeld, A.W., Lorenzen, L. and Botes, F.G., 1999. The development and modelling of high-intensity impinging stream jet reactors for effective mass transfer in heterogeneous systems. *Chem Eng Sci*, 54, 4991-4995.

Koryta, J., Dvořák, J and Kavan, L., 1993. *Principles of Electrochemistry.* 2nd ed. Chichester: John Wiley.

Kotaki, Y. and Tsuge, H., 1990. Reactive crystallization of calcium carbonate by gas-liquid and liquid-liquid reactions. *Can J Chem Eng*, 68, 435-442.

Laborie, S., Cabassud, C., Durand-Bourlier, L. and Lainé, J.M., 1999. Characterisation of gas-liquid two-phase flow inside capillaries. *Chem Eng Sci,* 54, 5723-5735.

Levenspiel, O., 1999. *Chemical reaction engineering.* 3rd ed. New York: John Wiley.

Ligrani, P.M., and Niver, R.D., 1988. Flow visualization of Dean vortices in a curved channel with 40 to 1 aspect ratio. *Phys. Fluids,* 31, 3605-3617.

Liu, C.I. and Lee, D.J., 1999. Micromixing effects in a Couette flow reactor. *Chem Eng Sci,* 54, 2883-2888.

Lobo, V.M.M. and Quaresma, J.L., 1989. *Handbook of electrolyte solutions.* Amsterdam: Elsevier.

Löwe, H. and Ehrfeld, W., 1999. State-of-the-art in microreaction technology: concepts, manufacturing and applications., *Electrochim Acta,* 44, 3679-3689.

McCreedy, T., 2000. Fabrication techniques and materials commonly used for the production of microreactors and micro total analytical systems. *Trends anal chem*, 19, 396-401.

Mengeaud, V., Josserand, J., Girault, H.H., 2002. Mixing processes in a zigzag microchannel: finite element simulations and optical study. *Anal Chem,* 74, 4279-4286.

Mersmann, A., 1995. in Mersmann, A. ed. *Crystallization technology handbook.* New York: M.Dekker.

Meyer, T., David R., Renken, A. and Villermaux, J., 1988. Micromixing in a static mixer and an empty tube by a chemical method. *Chem Eng Sci,* 43, 1955-1960.

Mishima, K., Hibiki, T., and Nishihara, H., 1993. Some characteristics of gas-liquid flow in narrow rectangular ducts. *Int J Multiphas Flow*, 19, 115-124.

Moore, S.R., 1986. *Mass transfer to thin liquid films on rotating surfaces, with and without chemical reaction.* PhD thesis. University of Newcastle upon Tyne.

Mullin, J.W., 2002. Crystallization and precipitation. In *Ullmann's Encyclopedia of Industrial Chemistry*. New York: Wiley. Available from: http://www3.interscience.wiley.com/cgi-bin/home

Mudimu, A.O., Gaddis, E.S. and Vogelpohl, A., 2000. Gas holdup in an impinging-stream reactor. *Chem Eng Technol,* 23, 661-663.

Murphy, J., 1996. *Additives for plastics handbook*. Oxford: Elsevier.

Myerson, A.S. and Ginde, R., 1993. Crystals, crystal growth and nucleation. In Myerson, A. S. ed. *Handbook of Industrial Crystallization*. Boston: Butterworth-Heinemann.

Ogino, T., Suzuki, T. and Sawada, K., 1987. The formation and transformation mechanism of calcium carbonate in water. *Geochim et Cosmochim Acta*, 51, 2757-2767.

Ould Didi, M.B., Kattan, N. and Thome, J.R., 2002. Prediction of two-phase pressure gradients of refrigerants in horizontal tubes. *Int J Refrig*, 25, 935-947.

Palmer, D.A., Ramette, R.W. and Mesmer, R.E., 1984. Triiodide ion formation equilibrium and activity coefficients in aqueous solution. *J Sol Chem* 13, 673-683.

Ramshaw, C., 1993. The opportunities for exploiting centrifugal fields. *Heat Recov Syst CHP*, 13, 493-513.

Rawle, A. Basic principles of particle size analysis. Available from: www.malvern.co.uk.

Rebrov, E.V., de Croon, M.H.J.M. and Schouten, J.C., 2001. Design of a microstructured reactor with integrated heat exchanger for optimum performance of a highly exothermic reaction, *Catal Today*, 69, 183-192.

Schaer, E., Guichardon, P., Falk, L. and Plasari, E., 1999. Determination of local energy dissipation rates in impinging jets by a chemical reaction method. *Chem Eng J*, 72, 125-138.

Shemer, L., 2003. Hydrodynamic and statistical parameters of slug flow. *Int J Heat Fluid Flow*, 24, 334-344.

Sherwood, T.K., Pigford, R.L. and Wilke, C.R., 1975. *Mass transfer*. New York: McGraw- Hill.

Shestopalov, I., Tice, J.T. and Ismagilov, F., 2004. Multi-step synthesis of nanoparticles performed on millisecond time scale in a microfluidic droplet-based system, *Lab Chip*, 4, 316-321.

Skoog, D.A., West, D.M. and Holler, F.J., 1992. *Analytical Chemistry.* 6th ed. Fort Worth: Saunders College Publishing.

Söhnel, O. and Garside, J., 1992. *Precipitation, Basic Principles and Industrial Applications.* Oxford: Butterworth-Heinemann.

Söhnel, O. and Mullin, J.W., 1978. A method for the determination of precipitation induction periods. *J Cryst Growth*, 44, 377-382.

Sue, K., Kazuhito,K., Arai, K., 2004. Hydrothermal synthesis of ZnO nanocrystals using microreactor, *Mat Lett*, 58, 3229-3231.

Takagi, M., Maki, T., Miyahara, M., Mae, K., 2004. Production of titania nanoparticles by using a new microreactor assembled with same axle dual pipe, *Chem Eng J,* 101, 269-276.

Taylor, G.I., 1961. Deposition of a viscous fluid on the wall of a tube. *J Fluid Mech,* 10, 161-165.

Thulasidas, T.C., Abraham, M.A., Cerro, R.L., 1995. Bubble-train flow in capillaries of circular and square cross section. *Chem Eng Sci*, 50, 183-199.

Tilton. J.E., 1997. Fluid and particle dynamics. In Perry, R.H. ed. *Chemical Engineers' Handbook*, 7th ed. New-York: McGraw-Hill

Triplett, K.A., Ghiaasiaan, S.M., Abdel-Khalik, S.I. and Sadowski, D.L., 1999a. Gas-liquid two-phase flow in microchannels Part I: two-phase flow patterns. *Int J Multiphas Flow*, 25, 377-394.

Triplett, K.A., Ghiaasiaan, S.M., Abdel-Khalik, S.I., LeMouel, A. and McCord, B.N, 1999b. Gas-liquid two-phase flow in microchannels Part II: void fraction and pressure drop. *Int J Multiphas Flow*, 25, 395-410.

Trippa, G., Hetherington, P. and Jachuck, R.J.J., 2002. Process Intensification: precipitation of calcium carbonate from the carbonation reaction of lime water using a spinning disc reactor. In Chianese, A. ed. *15th International Symposium on Industrial Crystallization*, 15-18 September 2002, Sorrento, Italy.

Trippa, G. and Jachuck, R.J.J., 2003. Process Intensification, precipitation of calcium carbonate using narrow channel reactors. *Trans IChemE Part A, Chem Eng Res Des*, 81, 766–772.

Vacassy, R., Lemaître, J, Hofmann, H. and Gerlings, J.H., 2000. Calcium carbonate precipitation using segmented flow tubular reactor. *AIChE J*, 46, 1241-1252.

Van Baten, J.M., and Krishna, R., 2004. CFD simulations of mass transfer from Taylor bubbles rising in circular capillaries. *Chem Eng Sci*, 59, 2535-2545.

Vandu, C.O., Ellenberger, J. and Krishna, R., 2004. Hydrodynamics and mass transfer in an upflow monolith loop reactor. *http://ct-cr4.chem.uva.nl/Monolith/*

Vandu, C.O., Ellenberger, J. and Krishna, R., 2005a. Hydrodynamics and mass transfer in an upflow monolith loop reactor. *Chem Eng Process,* 44, 363-374.

Vandu, C.O., Liu, H., Krishna, R., 2005b. Mass transfer from Taylor bubbles rising in single capillaries. *Chem Eng Sci,* 60, 6430-6437.

Villermeaux, J., Falk, L., Fournier, M.C. and Detrez, C., 1992. Use of parallel competing reactions to characterize micromixing efficiency. *AIChE Symp Ser* 286, 6-10.

Wachi, S. and Jones, A.G., 1991a. Mass transfer with chemical reaction and precipitation. *Chem Eng Sci*, 46, 1027-1033.

Wachi, S. and Jones, A.G., 1991b. Effect of gas-liquid mass transfer on crystal size distribution during the batch precipitation of calcium carbonate. *Chem Eng Sci*, 46, 3289-3293.

Walton, A.G., 1967. *The formation and properties of precipitates.* New York: Interscience Publishers.

Wagner, J, Kirner, T., Mayer, G., Albert, Köhler, J.M., 2004. Generation of metal nanoparticles in a microchannel reactor, *Chem Eng J,* 101, 251-260.

Watts, P. and Haswell, S.J., 2003. Continuous flow reactors for drug discovery. *Drug Discov Today,* 8, 586-593.

Wilmarth, T. and Ishii, M., 1994. Two-phase flow regimes in narrow rectangular vertical and horizontal channels. *Int J Heat Mass Transfer*, 37, 1749-1758.

Wörz, O., Jäckel, K.P., Richter, Th. and Wolf, A., 2001. Micoreactors, a new efficient tool for optimum reactor design. *Chem Eng Sci,* 56, 1029-1033.

Xu, J., 1999. Experimental study on gas-liquid two-phase flow regimes in rectangular channels with mini gaps. *Int J Heat Fluid Fl,* 20, 422-428.

Zauner, R. and Jones, A.G., 2000. Mixing effects on product particle characteristics from semi-batch crystal precipitation. *Trans IChemE Part A, Chem Eng Res Des*, 78, 894–902.

Zhang Lin, X., Terepka, A.D. and Yang, H., 2004. Synthesis of silver nanoparticles in a continuous flow tubular microreactor, *Nano Lett,* 11, 2227-2232.

Zhu, Z.M., Hannon, J. and Green, A., 1992. Use of high intensity gas-liquid mixers as reactors. *Chem Eng Sci* 47, 2847-2852.